Chemo-rheological Characterization of Asphalt Binders Using Different Aging Processes

by

Aditi Sharma

A thesis
presented to the University of Waterloo
in fulfillment of the
thesis requirement for the degree of
Doctor of Philosophy
in
Civil Engineering

Waterloo, Ontario, Canada, 2025

© Aditi Sharma 2025

Examining Committee Membership

The following served on the Examining Committee for this thesis. The decision of the Examining Committee is by majority vote.

External Examiner	**Dr. Eyad Masad** Civil and Environmental Engineering, Hamad bin Khalifa University
Supervisor	**Dr. Hassan Baaj** Civil and Environmental Engineering, University of Waterloo
Supervisor	**Dr. Pejoohan Tavassoti** Civil and Environmental Engineering, University of Waterloo
Internal Member	**Dr. Anh Pham** Civil and Environmental Engineering, University of Waterloo
Internal Member	**Dr. Christine Moresoli** Chemical Engineering, University of Waterloo
Internal Member	**Dr. Hervé Di Benedetto** Civil and Environmental Engineering, University of Waterloo (Adjunct)

Author's Declaration

I hereby declare that I am the sole author of this thesis. This is a true copy of the thesis, including any required final revisions, as accepted by my examiners.

I understand that my thesis my may be made electronically available to the public.

Abstract

The performance and longevity of asphalt pavements depend heavily on the properties of asphalt binders, which are affected by aging, binder modifications, and the incorporation of reclaimed asphalt pavement (RAP) materials. However, significant gaps exist in understanding the long-term chemical and rheological changes induced by aging processes (particularly with respect to differences between thermo-oxidative aging and UV exposure), and in the use/standardization of chemical analytical techniques such as Fourier Transform Infrared (FTIR) and Nuclear Magnetic Resonance (NMR) spectroscopy for binder characterization. Furthermore, the behaviour in RAP-virgin binder blends, along with the influence of bio-based rejuvenators and anti-aging additives under different aging conditions, remains underexplored. Addressing these gaps are crucial to developing more durable, sustainable pavements. This thesis bridges these research gaps through comprehensive investigation of chemo-rheological binder characterization, combining experimental testing with advanced analytical tools and varying aging methods. The findings offer essential insights into binder aging, rejuvenation strategies, and modification techniques, with significant implications for pavement durability and environmental sustainability.

The first chapter presents an evaluation of Attenuated Total Reflection-Fourier Transform Infrared (ATR-FTIR) spectroscopy combined with functional group and multivariate analysis techniques to characterize asphalt binders. The research identifies challenges in repeatability across binder sources and aging states demonstrating the importance of standardized protocols for improving reliability. Repeatability as described by AASHTO standards is listed in the precision and bias statement as single operator precision. This is the allowable difference in two test results measured under the repeatability conditions (same asphalt binder, measured by the same operator, on the same piece of equipment in the same lab). Principal Component Analysis (PCA) and k-means clustering successfully classified binder types and aging states, with large quantity (LQ) sample preparation yielding more consistent results than small quantity (SQ) preparation. These findings underscore the need for uniform procedures in binder analysis, addressing inconsistencies prevalent in the current literature.

The second part of the thesis investigates the impact of Styrene-Butadiene-Styrene (SBS) polymer modification on binder performance and oxidative resistance. Using Nuclear Magnetic Resonance (NMR) and ATR-FTIR spectroscopy, along with PCA and Partial Least Squares Regression (PLSR), the research highlights the ability of SBS to enhance high-temperature performance and slow thermo-oxidative aging. This work not only confirms previous findings on SBS but also provides new insights into the molecular interactions contributing to aging resistance. The study fills a gap in understanding how SBS-modified binders behave under various aging scenarios, offering a deeper perspective on polymer-modified asphalt technologies.

The thesis also addresses a critical gap related to UV-induced aging, which has been underexplored in comparison to thermo-oxidative aging. A novel UV aging chamber was developed to simulate real-world environmental conditions, incorporating UV exposure, water spray cycles, and controlled heating at 70°C. Comparative analysis revealed that different additives exhibit varying effectiveness under UV and thermo-oxidative conditions. Zinc diethyldithiocarbamate (ZDC) showed strong resistance to thermo-oxidative aging but limited efficacy under UV aging, while ascorbic acid (Vit. C) accelerated aging under UV exposure, contrary to expectations. These findings emphasize the challenges involved in designing effective anti-aging strategies for asphalt binders, demonstrating the value of combining conventional rheological tests with spectroscopic techniques and further highlighting the need for more targeted approaches to additive selection and development.

This thesis advances the understanding of asphalt binder behaviour and aging processes by integrating chemical, rheological, and multivariate analysis techniques. It offers critical contributions to the standardization of binder characterization protocols, the optimization of polymer-modified asphalt technologies, and the development of more effective anti-aging strategies. The research also demonstrates the potential of machine learning and artificial intelligence (AI) in predicting binder performance from spectroscopic data using multivariate analysis, paving the way for future innovations in asphalt binder characterization.

In conclusion, the work in this thesis addresses significant gaps in the literature, providing new insights into aging mechanisms, additive/rejuvenation strategies, and RAP binder interactions. By combining chemical analysis, rheological testing, and multivariate techniques, this research contributes both to academic knowledge and practical pavement engineering, promoting the development of more sustainable, long-lasting asphalt pavements.

Acknowledgements

This thesis would not have been possible without the unwavering guidance, support, and encouragement of many remarkable individuals. First and foremost, I would like to express my deepest gratitude to Professor Hassan Baaj and Professor Pejoohan Tavassoti, my supervisors, for their invaluable expertise, patience, and mentorship throughout this journey. Your insights and encouragement have been instrumental in shaping both my research and personal growth over the years, and for that, I am profoundly grateful.

I am sincerely thankful to my committee members—Professor Christine Moresoli, Professor Hervé Di Benedetto, Professor Anh Pham, and Professor Eyad Masad—for your thoughtful feedback, guidance, and support. A very special acknowledgment goes to Dr. Roberto Aurilio. Your unwavering advice, support, and friendship have been a source of strength, and without you, this accomplishment would not have been possible.

I am also grateful to the following partners and individuals who have made this work possible:

- The Centre for Pavement and Transportation Technology (CPATT), Norman W. McLeod Chair, University of Waterloo.
- The Civil and Environmental Engineering Department's technical staff: Isabelle Graansma and Rob Kaptein, for your technical expertise and assistance.
- My colleagues in the CPATT research group, both past and present: Dr. Saeid Salehi, Dr. Hui (Daniel) Liao, Hana Fissiha Hailu, Leila Miri, Elahe Nasiriamiri, and Anahita Diyanoush—thank you for the camaraderie, collaboration, and support along the way.
- Mike Aurilio, Terminal Manager at Yellowline Asphalt Products Limited, for the technical support and collaborative efforts that contributed to this research.
- Dr. Blossom Yan, NMR Lab Manager at the University of Waterloo, for technical and professional guidance/support.
- Professor Alexander Penlidis, for his support and guidance with intellectual feedback

A heartfelt thank you to my best friend and companion, Sidhi (my dog), whose presence and comfort helped me get through the most challenging moments.

Finally, to my friends and family, your unwavering encouragement, emotional support, and belief in me have been my greatest source of strength throughout this demanding but rewarding process. I am deeply grateful to each of you, for without your love and support, I would not have reached this point.

Table of Contents

Author's Declaration iii

Abstract iv

Acknowledgements vi

List of Figures x

List of Tables xvi

List of Abbreviations xvii

Chapter 1 1

Introduction 1

1.1 Background 1

1.2 Problem Statement and Objectives 2

1.3 Thesis Organization and Contribution 3

Chapter 2 6

Literature Review 6

2.1 Asphalt Binder Aging – Chemistry and Mechanisms 6

2.3 Techniques for Evaluating Rheological and Chemical Properties of Asphalt Binder Aging 21

2.3.1 Chemical Testing Methods 21

2.3.2 Rheological Testing Methods 27

2.3.3. Micro-characterization of asphalt binder structure 30

2.4 Common Approaches to Improve Sustainability and Combat Effects of Aging 31

2.4.1 RAP + Rejuvenators 31

2.4.2 SBS 35

2.4.3 Anti-aging additives 37

2.5 Summary of Literature Review 40

Chapter 3 42

Research Methodology 42

3.1 Scope 42

3.2 Materials and Methods 42
3.3 Overview of Material and Methodology 47
Chapter 4 48
Repeatability of FTIR in Characterizing Unmodified Binder Sources and Aging States 48
4.1 Introduction 48
4.2 Material Preparation and Methodology 49
4.2.1 FTIR Spectra Functional Group Analysis 50
4.2.2 FTIR Multivariate Analysis 50
4.3 Results and Discussion 54
4.3.1 FTIR Functional Group Analysis – Chemical Indices 55
4.3.2 Multivariate Analysis – PCA and k-means Cluster Analysis 60
4.4 Conclusions 67
Chapter 5 69
Chemical and Rheological Effects of Oxidative Aging on SBS-modified Asphalt Binders 69
5.1 Introduction 69
5.2 Motivation and Objectives 71
5.3 Methodology 71
5.3.1 Materials 71
5.3.1 SBS Modified Asphalt Binder Preparation 72
5.3.3 Rheological Testing 72
5.3.4 Chemical Testing 73
5.3.5 Multivariate Analysis Techniques 77
5.4. Results and Discussion 79
5.4.1 Rheological Testing Results 79
5.4.2 ATR-FTIR Analysis 81
5.4.3 ^{1}H NMR Analysis 85
5.4.4 Correlations Between Rheological and NMR Testing 89

5.4.5 Multivariate Analysis of Spectroscopic Data for SBS-modified Asphalt Binders A and B.....93
5.5 Conclusions.....106
Chapter 6.....108
Comparative Analysis of Thermo-Oxidative and UV Aging on Asphalt Binder Properties.....108
6.1 Introduction.....108
6.2 Methodology.....110
6.2.1 Materials.....110
6.2.2 UV Aging Chamber Construction.....111
6.2.3 Testing Methods.....117
6.3 Results and Discussion.....118
6.3.1 Rheological Testing Results.....118
6.3.2 NMR and FTIR Spectroscopic Analysis.....129
6.4. Conclusions.....138
Chapter 7.....140
Conclusions, Recommendations and Future Work.....140
7.1 Overall Summary.....140
7.2 Conclusions.....141
7.3 Recommendations and Future Work.....142
References.....145
A. Appendix A.....174
B. Appendix B.....186

List of Figures

Figure 2.1: Typical structure of SARA fractions. (Polo-Mendoza et al., 2022a) 8
Figure 2.2: Schematic of the colloidal structures in (a) sol- and (b) gel-type asphalt binders.(R. Hunter et al., 2015) 9
Figure 2.3: Different stages in the life cycle of asphalt binder.(Y. Li et al., 2022b) 11
Figure 2.4: Pathways involved aging process at different stages in asphalt life cycle. (Polo-Mendoza et al., 2022a) 12
Figure 2.5: Different chemical change occurring during oxidation. (Polo-Mendoza et al., 2022a) 13
Figure 2.6: Functional groups in asphalt binders (i) naturally occurring and (ii) formed upon aging. (Polo-Mendoza et al., 2022a) 14
Figure 2.7: Major processes involved in UV aging. (X. Sun et al., 2020) 16
Figure 2.8: Aging gradient asphalt binder experiences when exposed to UV radiation. (Cháves-Pabón et al., 2019a) 20
Figure 2.9: Typical FTIR spectrum for asphalt binder with SBS (adapted from (L. Ma et al., 2023)) 25
Figure 2.10: Effect of aging and rejuvenation on asphalt binders (Behnood, 2019) 34
Figure 3.1: Prepared ATR-FTIR samples before testing. 42
Figure 3.2:ATR-FTIR equipment and set up for data collection. 43
Figure 3.3:Asphalt binder sample placed on ATR-FTIR diamond crystal. 43
Figure 3.4: Asphalt binder sample being tested in DSR. 44
Figure 3.5: Asphalt binder beams prepared for testing in the BBR. 44
Figure 3.6: NMR spectroscopy equipment. 44
Figure 3.7:Anti-aging additives, Ascorbic Acid (Vit.C), (left) and Zinc Diethyldithiocarbamate (ZDC) (right). 45
Figure 3.8:Constructed UV aging Chamber. 45
Figure 3.9: (a) Metal pan with RTFO aged binder, (b) Sample rack, (c) Pressure vessel 46
Figure 3.10:Summary of the materials and methods used in each chapter throughout research. 47
Figure 4.1: Showing a quick mathematical overview of what PCA does. 51
Figure 4.2: ATR-FTIR Spectra for all binder samples presented in Table 4.1 including replicates. (n=16) 55
Figure 4.3: Carbonyl and Sulfoxide Indices for all 9 binder samples using both preparation methods SQ and LQ. (Error bars represent standard deviation, n = 16). 55
Figure 4.4: Aromatic Indices for all 9 binder samples using both preparation methods SQ and LQ. (Error bars represent standard deviation, n = 16). 56

Figure 4.5: Aliphatic Indices for all 9 binder samples using both preparation methods SQ and LQ. (Error bars represent standard deviation, n = 16) 56
Figure 4.6: Plot of PC_1 vs PC_2 after performing PCA analysis on ATR-FTIR Raw Data. Legend on the graph is of the following form Source_Ageing State_Preparation Method. 61
Figure 4.7: 3-D Plot of PC_1, PC_2 and PC_3 scores obtained from performing PCA analysis on ATR-FTIR Raw Data. 62
Figure 4.8:Showing centroid locations determined from k-means clustering superimposed onto 3-D PCA plot 64
Figure 4.9: Multiple Comparison of PC_1 means for different groupings identified using k-means cluster analysis 66
Figure 4.10: Multiple Comparison of PC_2 means for different groupings identified using k-means cluster analysis. 66
Figure 4.11: Multiple Comparison of PC_3 means for different groupings identified using k-means cluster analysis. 67
Figure 5.1: Overview of the steps involved in running 1H NMR spectroscopy. 74
Figure 5.2: Comparison of NMR spectral data before and baseline correction. 76
Figure 5.3: Comparison of NMR spectral data after baseline correction. 76
Figure 5.4: Representative Master Curves for Binder 58-28A with 0, 2 and 4% SBS at different aging levels. 80
Figure 5.5: Representative Master Curves for Binder 58-28B with 0, 2 and 4% SBS at different aging levels. 80
Figure 5.6: FTIR spectra for 58-28A with 0, 2 and 4% SBS at 20-, 40- and 60-Hour PAV Aging. 82
Figure 5.7: FTIR spectra for 58-28B with 0, 2 and 4% SBS at 20-, 40- and 60-Hour PAV Aging. 82
Figure 5.8: Changes in polybutadiene vinyl double bond and trans double bond-based indexes with aging and SBS modification. (Error bars represent standard deviation, n = 12). 83
Figure 5.9: Sulfoxide Index (SI) and Carbonyl Index (CI) at different aging conditions and SBS contents for PG 58-28A. (Error bars represent standard deviation, n = 12). 84
Figure 5.10: Sulfoxide Index (SI) and Carbonyl Index (CI) at different aging conditions and SBS contents for PG 58-28B. (Error bars represent standard deviation, n = 12). 84
Figure 5.11: Typical ^{1}H NMR spectrum obtained for neat asphalt binder. 85
Figure 5.12: Showing the ^{1}H NMR spectrum for asphalt binder with 2% SBS. 86
Figure 5.13: The structure of SBS with identification of the spatial locations of characteristic SBS peaks. 86

Figure 5.14: The area under H_β (1.25 ppm) and H_γ (0.9 ppm) Peaks for Binders A and B. (Error bars represent standard deviation, n = 3).....87
Figure 5.15: Area under Vinylic H (~5.4 ppm) peak vs SBS content for Binders A. 87
Figure 5.16: Area under Vinylic H (~5.4 ppm) peak vs SBS content for Binders B. 88
Figure 5.17: Area under Allylic H (~2ppm) peak vs SBS content for Binders A. 88
Figure 5.18: Area under Allylic H (~2ppm) peak vs SBS content for Binders B. 89
Figure 5.19: Relation between Crossover Temperature and H_γ at different SBS contents for A. 90
Figure 5.20: Relation between Crossover Temperature and H_β at different SBS contents for A. 90
Figure 5.21: Relation between Crossover Temperature and H_γ at different SBS contents for B. 90
Figure 5.22: Relation between Crossover Temperature and H_β at different SBS contents for B. 91
Figure 5.23: Relation between ΔT_c and H_γ at different SBS contents for A. 92
Figure 5.24: Relation between ΔT_c and H_β at different SBS contents for A. 92
Figure 5.25: Relation between ΔT_c and H_γ at different SBS contents for B.....92
Figure 5.26: Relation between ΔT_c and H_β at different SBS contents for B 93
Figure 5.27: Score Plots obtained from PCA Analysis on FTIR Data (after pre-processing) for Binder A. 94
Figure 5.28: Score Plots obtained from PCA Analysis on FTIR Data (after pre-processing) for Binder A. 95
Figure 5.29: Score Plots obtained from PCA Analysis on FTIR Data (after pre-processing) for Binder B. 96
Figure 5.30: Score Plots obtained from PCA Analysis on FTIR Data (after pre-processing) for Binders A and B. 96
Figure 5.31: Score Plots obtained from PCA Analysis on NMR Data (after pre-processing) for Binders A. 97
Figure 5.32: Score Plots obtained from PCA Analysis on NMR Data (after pre-processing) for Binders B. 98
Figure 5.33: Residual Plot for aging state obtained from PLSR on FTIR (left) and NMR Data (right). ..100
Figure 5.34: Residual Plot for SBS concentration obtained from PLSR on FTIR (left) and NMR Data (right). 100
Figure 5.35: Residual Plot for ΔTc obtained from PLSR on FTIR (left) and NMR Data (right). 100
Figure 5.36: Residual Plot for T_{cross} obtained from PLSR on FTIR (left) and NMR Data (right). 101
Figure 5.37: MSE vs Number of Components in PLSR model. 102
Figure 5.38: VIP Score Plot obtained from PLSR on FTIR Data. (Red points represent VIP > 1) 104
Figure 5.39: VIP Score Plot obtained from PLSR on NMR Data. (Red points represent VIP > 1).....104

Figure 6.1: Rejuvenator A (mixture of bio-oils) and rejuvenator B (derived from Tall Oil). 110
Figure 6.2: Binder Blending Set Up 111
Figure 6.3: Hybridization Oven used for modification into UV aging chamber. 112
Figure 6.4: UV lamp used in chamber construction. 112
Figure 6.5: Showing the mounted UV lamp on hybridization oven. 113
Figure 6.6: Iteration one of the UV aging chamber. 114
Figure 6.7: Aged binder obtained from the initial UV Chamber set up. 115
Figure 6.8: Iteration two of UV aging chamber. 115
Figure 6.9: Pitting pattern observed on surface of asphalt binder after aging trial 2. 116
Figure 6.10: Asphalt binder samples in final iteration of aging chamber. 117
Figure 6.11: Overall set-up for final iteration of Aging chamber. 117
Figure 6.12: Representative Master Curves for IO and RAP-Virgin-Rejuvenator binder blends at different aging states 119
Figure 6.13: Representative Master Curves for ZDC binder blends at different aging states. 119
Figure 6.14: Representative Master Curves for Vit. C binder blends at different aging states. 120
Figure 6.15: M-values obtained from BBR testing of (a) RAP-Virgin-Rejuvenator, (b) ZDC, and (c) Vit. C Blends. 125
Figure 6.16: Stiffness values obtained from BBR testing of (a) RAP-Virgin-Rejuvenator, (b) ZDC, and (c) Vit. C Blends. 126
Figure 6.17: Sample (a) FTIR and (b) NMR spectra for unaged binder blends. 130
Figure 6.18: Score Plot for RAP-Virgin-Rejuvenator Binder Blends and IO at all aging states from FTIR data. 131
Figure 6.19: Score Plot for ZDC Blends at all aging states from FTIR data. 133
Figure 6.20: Score Plot for Vit. C Blends at all aging states from FTIR data. 133
Figure 6.21: Score Plot for (a) RAP-Virgin-Rejuvenator, (b) ZDC, and (c) Vit. C Blends at all aging states from NMR data. 135
Figure 6.22: Evolution of MSE with Number of Components in PLSR models derived from NMR (top) and FTIR (bottom). 136
Figure 6.23: VIP Score Plots for (a)RAP-Virgin-Rejuvenator (b) ZDC and (c) Vit. C Blends obtained from FTIR. 137
Figure 6.24: VIP Score Plots for (a) RAP-Virgin-Rejuvenator (b) ZDC and (c) Vit. C Blends obtained from NMR. 138
Figure A-1: Residual Plot for aging state obtained from PLSR on NMR data for Binder A only. 174

Figure A-2: Residual Plot for SBS Concentration obtained from PLSR on NMR data for Binder A only. 174
Figure A-3: Residual Plot for ΔTc obtained from PLSR on NMR data for Binder A only. 175
Figure A-4: Residual Plot for Crossover Temperature obtained from PLSR on NMR data for Binder A only. 175
Figure A-5: MSE vs Number of Components in PLSR model using NMR data for Binder A.....176
Figure A-6: VIP Score Plot obtained from PLSR on NMR data for Binder A only. (Red points represent VIP > 1). 176
Figure A-7: Residual Plot for aging state obtained from PLSR on NMR data for Binder B only. 177
Figure A-8: Residual Plot for SBS concentration obtained from PLSR on NMR data for Binder B only. 177
Figure A-9: Residual Plot for ΔTc obtained from PLSR on NMR data for Binder B only. 178
Figure A-10: Residual Plot for Crossover Temperature obtained from PLSR on NMR data for Binder B only. 178
Figure A-11: MSE vs Number of Components in PLSR model using NMR data for Binder B.....179
Figure A-12: VIP Score Plot obtained from PLSR on NMR data for Binder B only. (Red points represent VIP > 1). 179
Figure A-13: Residual Plot for aging state obtained from PLSR on FTIR data for Binder A only. 180
Figure A-14: Residual Plot for SBS concentration obtained from PLSR on FITR data for Binder A only. 180
Figure A-15: Residual Plot for ΔTc obtained from PLSR on FTIR data for Binder A only.....181
Figure A-16: Residual Plot for Crossover Temperature obtained from PLSR on FTIR data for Binder A only. 181
Figure A-17: MSE vs Number of Components in PLSR model using FTIR data for Binder A. 182
Figure A-18: VIP Score Plot obtained from PLSR on FTIR data for Binder A only. (Red points represent VIP > 1) 182
Figure A-19: Residual Plot for aging state obtained from PLSR on FTIR data for Binder B only. 183
Figure A-20: Residual Plot for SBS concentration obtained from PLSR on FITR data for Binder B only. 183
Figure A-21: Residual Plot for ΔTc obtained from PLSR on FTIR data for Binder B only. 184
Figure A-22: Residual Plot for Crossover Temperature obtained from PLSR on FTIR data for Binder B only. 184
Figure A-23: MSE vs Number of Components in PLSR model using FTIR data for Binder B. 185

Figure A-24: VIP Score Plot obtained from PLSR on FTIR data for Binder B only. (Red points represent VIP > 1). 185
Figure B-1: Normalized FTIR Spectral Data for all RAP-IO-Rejuvenator Blends at all ageing states. ... 186
Figure B-2: Normalized FTIR Spectral Data for all Vit. C Blends at all ageing states..... 186
Figure B-3: Normalized FTIR Spectral Data for all ZDC Blends at all ageing states. 187
Figure B-4: Carbonyl Indices based on FTIR spectra for RAP-IO-Rejuvenator Blends. 187
Figure B-5: Sulfoxide Indices based on FTIR spectra for RAP-IO-Rejuvenator Blends..... 188
Figure B-6: Carbonyl Indices based on FTIR spectra for Vit C Blends..... 188
Figure B-7: Sulfoxide Indices based on FTIR spectra for Vit C Blends. 189
Figure B-8: Carbonyl Indices based on FTIR spectra for ZDC Blends. 189
Figure B-9: Sulfoxide Indices based on FTIR spectra for ZDC Blends. 190
Figure B-10: H_{γ} normalized peak area based on NMR spectra for RAP-IO-Rejuvenator Blends. 190
Figure B-11: H_{β} normalized peak area based on NMR spectra for RAP-IO-Rejuvenator Blends. 191
Figure B-12: H_{γ} normalized peak area based on NMR spectra for Vit. C Blends..... 191
Figure B-13: H_{β} normalized peak area based on NMR spectra for Vit. C Blends. 192
Figure B-14: H_{γ} normalized peak area based on NMR spectra for ZDC Blends. 192
Figure B-15: H_{β} normalized peak area based on NMR spectra for ZDC Blends. 193
Figure B-16: Normalized NMR Spectral Data for all RAP-IO-Rejuvenator Blends at all ageing states.. 193
Figure B-17: Normalized NMR Spectral Data for all Vit.C Blends at all ageing states. 194
Figure B-18: Normalized NMR Spectral Data for all ZDC Blends at all ageing states. 195

List of Tables

Table 2.1: Characteristics of SARA fractions in asphalt binders. (Polo-Mendoza et al., 2022a) 7
Table 2.2: Chemical reactions involved in photo-oxidative aging. (Polo-Mendoza et al., 2022a) 15
Table 2.3:Different UV light wavelengths and associated energy. (Y. Li et al., 2022a).....18
Table 2.4: Bond energies of common bonds found in asphalt binder molecules. (Y. Li et al., 2022a) 18
Table 2.5: Common functional groups in asphalt binders and corresponding wavenumber (adapted from Mirwald et al., 2020b) 23
Table 2.6: Summary of Rheological Parameters (adapted from Pipintakos et al., 2024).....30
Table 2.7:Summary of anti-aging additive used in literature (modified from Camargo et al., 2021).....39
Table 4.1: Different Asphalt Binder Types and Ageing States tested using ATR-FTIR 49
Table 4.2: ANOVA on CI with respect to Binder Source, Ageing State and Sample Preparation Method. 58
Table 4.3: ANOVA on SI with respect to Binder Source, Ageing State and Sample Preparation Method 59
Table 4.4: Percentage of Variability in the data explained by first four principal components 60
Table 4.5: ANOVA on PC_1 with respect to Binder Source, Ageing State and Sample Preparation Method 63
Table 4.6: ANOVA on significance of different clusters using PC 1 64
Table 4.7: ANOVA on significance of different clusters using PC 2 64
Table 4.8: ANOVA on significance of different clusters using PC 3 65
Table 5.1: Summary of different asphalt binder samples tested for binders A and B.....72
Table 5.2: Crossover temperature and ΔTc parameter for asphalt binder samples. (T_{cross}± 0.83, n = 3; ΔT_c± 1.01, n = 3).....81
Table 5.3: Percentage of Variability in the data explained by first three principal components with FTIR and NMR data.....98
Table 6.1: Different binder blends and aging states investigated. 118
Table 6.2: Summary of Rheological Parameters Obtain from BBR (ΔT_c) and DSR (Crossover Temperature) testing.....129

List of Abbreviations

AASHTO	American Association of State Highway and Transportation Officials
AFM	Atomic Force Microscopy
ASTM	American Society for Testing and Material
ATR	Attenuated Total Reflection
BBR	Bending Beam Rheometer
BRRC	Belgian Road Research Centre
C	Concentration
CAS	Chemical Abstracts Service
CB	Carbon Black
D	Diffusion Coefficient/Diffusivity
DOB	Degree of Blending
DOT	Department of Transportation
DSR	Dynamic Shear Rheometer
EPR	Electron Paramagnetic Resonance
FEA	Finite Element Analysis
FEEM	Fluorescence Excitation Emission Mapping
FTIR	Fourier Transform Infrared
G-R	Glover-Rowe
GPC	Gel Permeation Chromatography
HMA	Hot Mix Asphalt
HPLC	High Pressure Liquid Chromatography
HSQC	Heteronuclear Single Quantum Coherence
IR	Infrared
LAS	Linear Amplitude Sweep
LCPC	Laboratoire Central des Ponts et Chaussées
LDH	Layered Double Hydroxide
LQ	Large Quantity
LTA	Long-Term Aging
MD	Molecular Dynamics
MMT	Montmorillonite
MSCR	Multiple Stress Creep Recovery

MTO	Ministry of Transportation Ontario
NaCl	Sodium Chloride
NAPA	National Asphalt Pavement Association
NCHRP	National Cooperative Highway Research Program
NMR	Nuclear Magnetic Resonance
OAPC	Ontario Asphalt Pavement Council
OMMT	Organomontmorillonite
PAV	Pressure Ageing Vessel
PB	Polybutadiene
PCA	Principal Component Analysis
PDA	Photodiode Array
PG	Performance Grading
PLSR	Partial Least Squares Regression
PMAs	Polymer Modified Asphalts
PMMA	Polymethylmethacrylate
PS	Polystyrene
R%	Recovery Percentage
RAP	Reclaimed Asphalt Pavement
RBR	RAP Binder Ratio
RTFO	Rolling Thin Film Oven
SANS	Single Angle Neutron Scattering
SARA	Saturates, Aromatics, Resins, Asphaltenes
SAXS	Single Angle X-ray Scattering
SBS	Styrene-Butadiene-Styrene
SEE	Synchronous Excitation Emission
SHRP	Strategic Highway Research Program
SNV	Standard Normal Variant
SQ	Small Quantity
STA	Short-Term Aging
TGA	Thermogravimetric Analysis
THF	Tetrahydrofuran
TLC-FID	Thin Layer Chromatography - Flame Ionization Detection
TMS	Tetramethylsilane

TOF-SIMS	Time Of Flight - Secondary Ion Mass Spectroscopy
TTSP	Time-Temperature Superposition Principle
UV	Ultraviolet
VAPro	Viennese Aging Procedure
Vis	Visible
WCO	Waste Cooking Oil
WLF	William-Landel-Ferry
ZDC	Zinc Diethyldithiocarbamate

Chapter 1

Introduction

1.1 Background

Pavement infrastructure is a foundational part of modern society, enabling efficient transportation and economic growth (Y. Li et al., 2022a; Remisova & Briliak, 2023a). The vast network of roads, highways, and airfields that exist across the globe relies predominantly on asphalt as the primary material for construction and maintenance. Asphalt pavements have been extensively used due to their cost-effectiveness, durability, and relative ease of maintenance. The major components of asphalt pavements include aggregates, and asphalt binder (obtained from distillation of crude oil). However, with the growing demand for sustainable construction practices and the finite nature of raw materials, the asphalt industry faces challenges that necessitate continuous innovation and adaptation.

Asphalt binder, the key component that imparts viscoelastic properties to asphalt mixtures, plays a crucial role in determining the performance and longevity of pavements (Remisova & Briliak, 2023a; Rossi et al., 2018a). It serves as the glue that binds aggregates together, providing cohesion and ensuring structural integrity under traffic loads and environmental conditions. Over the years, significant advancements have been made in the understanding and enhancement of asphalt binder properties, driven by the need to improve pavement performance, extend service life, and reduce maintenance costs.

Some major techniques and strategies that have shown promise in the past thirty years include:

1) Introduction of Reclaimed Asphalt Pavements (RAP) into new asphalt mixtures, which sometimes requires the use of additives called rejuvenators when incorporating large amounts of RAP (Gulotta et al., 2019; Lo Presti et al., 2020; Rathore & Zaumanis, 2020).
2) Use of extenders and modifiers to improves overall performance and extend service life such as Styrene Butadiene Styrene (SBS) polymer (Aurilio et al., 2020a; Cong et al., 2013a; Hettiarachchi et al., 2020).
3) Incorporation of anti-aging additives into the asphalt mixes to prolong service life (J. Hu et al., 2017a; Y. Hu et al., 2022).

RAP, which is obtained from the milling or removal of existing pavements, offers a sustainable solution by recycling old materials and reducing the need for virgin aggregates and binders. The use of RAP not only conserves natural resources but also reduces the environmental footprint of pavement construction. However, the incorporation of RAP into new mixtures presents unique challenges, particularly related to the aging of the asphalt binder. The aged binder in RAP is often stiffer and more brittle, which can lead to reduced pavement durability if not properly addressed.

While aging in asphalt binders are impossible to reverse, in order to mitigate the adverse effects of aged binders, the industry has increasingly turned to rejuvenators—additives designed to restore the chemical, physical and rheological properties of aged asphalt binder to a level that closely resembles that of virgin binder. Rejuvenators work by diffusing into the aged binder, softening it, and improving its workability and overall performance. Typically, rejuvenators can be either petroleum-based or bio-based. The use of rejuvenators, especially those derived from bio-based sources, has gained significant attention as a sustainable approach to enhancing RAP mixtures. These bio-based rejuvenators offer the dual benefits of improving pavement performance and aligning with the global push toward greener construction practices. In addition to rejuvenators, other innovations in asphalt binder modification have emerged, aimed at enhancing pavement performance under varying traffic loads and environmental conditions. Polymer-modified asphalts (PMAs), specifically SBS, for example, have been widely adopted to improve the elasticity, stiffness, and resistance to deformation of asphalt binders. The incorporation of polymers into asphalt binders can significantly enhance pavement durability, particularly in regions with extreme temperature fluctuations or heavy traffic loads. However, the use of polymers also presents challenges, including increased costs and potential compatibility issues with specific virgin binders, RAP and other recycled materials. Anti-aging additives have also gained increasing attention in the past decade. Asphalt binders are susceptible to aging, which reduces their performance and increases vulnerability to deterioration. Anti-aging additives have different working mechanisms, but all attempt to slow or reduce aging in the asphalt binders/mixtures, which extent the service life and reduce the frequency at which maintenance and rehabilitation activities are required.

1.2 Problem Statement and Objectives

As the industry moves toward a circular economy model, the recycling of materials, reduction of greenhouse gas emissions, and the overall concept of sustainability have become central to the development of new technologies and materials in the pavement industry. The literature on asphalt binders and pavement performance is vast, reflecting the complexity of the subject and the diverse approaches taken to address the challenges faced by the industry. This thesis seeks to improve the current state of knowledge, focusing on key areas such as the aging of asphalt binders and aging methods including the use of RAP, the role of rejuvenators, the application of polymer modifications and anti-aging additives. In order to achieve the overall goal of this thesis several hypotheses were identified and are summarized below:

1) FTIR spectroscopy, when analyzed using multivariate statistical techniques, can reliably distinguish between different unmodified binder sources and aging states, with a high repeatability indicating consistency across different sample.

2) Increasing the concentration of SBS in asphalt binders can improve its overall performance in terms of rheological properties and chemical stability, with specific correlations existing between chemical properties and rheological behaviour.
3) UV aging induces distinct chemical changes in asphalt binders when compared to thermo-oxidative aging, leading to measurable differences in chemical characteristics that are not evident from only examining rheological properties.

After proposing the above hypothesis, several objectives were formulated to accomplish the overall objective of this thesis mentioned earlier. The identified objectives were as follows:

- To determine the repeatability of FTIR for identifying different unmodified binder sources and aging states using various statistical analysis and multivariate techniques
- To investigate the impact of increasing SBS concentration on the aging behaviour of asphalt binders through comprehensive rheological and chemical analysis, utilizing both NMR and FTIR spectroscopy alongside conventional rheological tests, while establishing correlations between the obtained parameters to enhance the understanding of oxidative aging behaviour in SBS-modified asphalt binders.
- To detail the construction of the novel ultraviolet (UV) aging chamber, including the challenges encountered during its development, while simultaneously investigating the effects of thermo-oxidative and UV aging on the chemical and rheological properties of asphalt binders.
- To identify differences between these two aging processes (UV and thermo-oxidative), which is essential for developing more effective anti-aging strategies and enhancing the long-term performance of asphalt pavements under varying environmental conditions.

1.3 Thesis Organization and Contribution

This thesis consists of seven chapters. The following list presents a brief overview of their contents and general contributions:

- Chapter 1: Introduction

  This chapter provides a concise introduction to the topic of interest, outlining the main hypotheses, objectives, and goals of the research. This overview establishes the foundational rationale for the subsequent discussions.

- Chapter 2: Literature Review

  This chapter presents an overview of the aging processes in asphalt pavements, accompanied by a thorough review of technologies aimed at enhancing performance and minimizing aging. It includes definitions, mechanisms, and characterization methods related to these technologies' ad processes.

- Chapter 3: Research Methodology

This chapter includes an overview of the materials and methodologies employed in this research. The focus of this thesis is on various aging processes in asphalt binders, along with an exploration of strategies to enhance pavement performance, extend service life, and minimize the rate at with overall aging occurs, from a chemo-rheological perspective. Detailed explanations of the theoretical foundations, adopted methods, and statistical analyses are provided in their respective chapters.

- Chapter 4: Assessing the Repeatability of FTIR in Characterizing Unmodified Binder Sources and Aging States

  This chapter makes significant contributions to the field of asphalt research by systematically evaluating the efficacy of Attenuated Total Reflection Fourier Transform Infrared (ATR-FTIR) spectroscopy combined with multivariate analysis techniques. By investigating asphalt binders from three different sources and at varying aging levels, it provides robust empirical evidence that underscores the analytical strength of ATR-FTIR in characterizing chemical compositions and distinguishing between binder sources and aging states. The comparison of Small Quantity (SQ) and Large Quantity (LQ) sample preparation methods reveals important insights into the variability and repeatability of results, emphasizing the critical need for standardized protocols in ATR-FTIR analysis. Furthermore, the application of Principal Component Analysis (PCA) and k-means clustering enhances the interpretation of complex spectral data, demonstrating the power of multivariate approaches in capturing the nuances of binder characteristics that traditional single-peak analyses may overlook. Overall, this chapter not only fills a gap in the current literature by addressing methodological inconsistencies but also lays the groundwork for future research aimed at refining analytical techniques and establishing standardized practices in the use of ATR-FTIR in the asphalt industry.

- Chapter 5: Chemical and Rheological Effects of Oxidative Aging on SBS-modified Asphalt Binders

  This chapter makes several significant contributions to the understanding of aging behaviour in Styrene Butadiene Styrene (SBS)-modified asphalt binders, particularly through the application of advanced spectroscopic techniques and a comprehensive analysis of the effects of SBS concentration and aging duration. By integrating conventional rheological tests with innovative methodologies such as Nuclear Magnetic Resonance (NMR) and Fourier Transform Infrared (FTIR) spectroscopy. The study offers a meticulous perspective on the molecular interactions and aging mechanisms at play in asphalt binders. Key findings demonstrate that increased SBS content enhances high-temperature performance and reduces oxidative aging, indicating the role of SBS as

a potential sacrificial component during aging processes. The chapter also establishes strong correlations between rheological parameters and NMR data, suggesting new avenues for performance prediction and characterization. Furthermore, it highlights the importance of binder compatibility, particularly in relation to the specific type of SBS used. Overall, these insights not only validate existing literature but also pave the way for future research aimed at optimizing SBS concentrations and developing more effective testing methodologies for polymer-modified asphalts.

- Chapter 6: Comparative Analysis of Thermo-Oxidative and UV Aging on Asphalt Binder Properties

  This chapter significantly contributes to the field of asphalt binder research by providing a comprehensive analysis of the effects of thermo-oxidative and UV aging on both the chemical and rheological properties of asphalt binders. By investigating the performance of a single base binder modified with two anti-aging additives at varying concentrations, the research revealed differences in the effectiveness of these additives under different aging conditions. Notably, the development of a novel UV aging chamber and documentation of challenges represents a methodological innovation, allowing for more realistic simulation of environmental conditions faced by pavements. The chapter also establishes a crucial link between chemical and rheological changes, employing advanced spectroscopic techniques such as FTIR and NMR alongside traditional rheological assessments. The findings highlight the distinct mechanisms of degradation associated with each aging mechanism, suggesting that while some additives may enhance resistance to thermo-oxidative aging, their efficacy against UV aging can vary significantly. This multifaceted approach not only enriches the understanding of asphalt binder behaviour under varying environmental conditions but also lays the groundwork for more effective anti-aging strategies, ultimately contributing to improved pavement longevity and performance.

- Chapter 7: Conclusions and Recommendations

  Finally, this chapter summarizes the key findings from the preceding chapters and highlights the novel contributions of this research. Additionally, the recommendations outlined in Chapter 7 focused on areas of interest and literature gaps identified but not addressed in this thesis.

Chapter 2

Literature Review

2.1 Asphalt Binder Aging – Chemistry and Mechanisms

2.1.1 Chemistry of Asphalt Binder

Asphalt binder is a complex organic material primarily composed of hydrocarbons, with a chemical composition of 80-88% carbon, 8-12% hydrogen, 0-9% sulfur, 0-2% oxygen, 0-2% nitrogen, and trace amounts of metals such as vanadium, nickel and iron at quantities of lower than 1% (Y. Li et al., 2022a). It is hydrophobic with high adhesion to other materials and has a wide variety of applications (Polo-Mendoza et al., 2022a). Asphalt binder contains thousands of different molecules which exhibit various chemical bonds, functional groups, activities, and polarities, all contributing to its overall behaviour (Y. Li et al., 2022a; Polo-Mendoza et al., 2022a; Remisova & Briliak, 2023a). Each asphalt binder has a distinct chemical composition due to the differences in the origins of the base crude oils and, thus, different engineering properties and resulting performance. Nevertheless, studies have shown a significant correlation between the component ratios, elemental contents, and surface energy of asphalt (Hadole et al., 2021; B. Li et al., 2021; Tanzadeh & Shafabakhsh, 2020; Zakirova et al., 2007). Other studies investigated the relationship between the chemical composition and physical properties of asphalt and showed that the colloidal dispersion state, molecular polarity, hydrogen bonding, and pi-pi intermolecular interactions significantly affect the physical and rheological properties of asphalt during long- and short-term aging periods (C. A. Hunter & Sanders, 1990; Yut & Zofka, 2014). Aging deteriorates the colloidal structure in which asphaltenes act as micelles surrounded by resins, affecting rheological properties and rate of oxidation (X. Liu et al., 2015). Molecular weight of asphalt and polarity of components were also found to have significant effects on rheological properties (Michalica et al., 2008). The major mechanism through which aging occurs can typically be explained by oxidation and changes in chemical composition of the binder over time. For instance, after thermo-oxidative aging of SBS-modified binders, a reduction in butadiene functional groups and an increase in asphaltene micelles were observed. These chemical changes are associated with the oxidation of the binder and degradation of the SBS modifier, leading to altered macroscopic properties like increased softening point and complex modulus (S. peng Wu et al., 2009).

Asphalt binder is mainly hydrocarbon in nature and sometimes referred to as a natural polymeric material in some studies, consisting of two major components, asphaltenes which are heavier and maltenes, the light components. Maltenes are further broken down into saturates, aromatics and resins which, together with asphaltenes, make up the SARA fractions in bitumen (Baghaee Moghaddam & Baaj, 2016). Table 2.1 below shows the main characteristics of the SARA fractions in asphalt binder. Asphalt binders are usually considered a colloidal system in which micelles of asphaltenes (solid particles with high polarity and

molecular weight) are stabilized by maltenes (oily environment with lower polarity and molecular weight composed of saturates, aromatics and resins). Resins surround asphaltene micelles and stabilize them in the maltenes (Remisova & Briliak, 2023a; Rossi et al., 2018a; Tan et al., 2008a). An opposing, but equally valid theory that has been proposed in literature, to explain the structure of asphalt binders is the solubility model (Porto et al., 2022). In this model, asphalt binders are considered as a solution of disaggregated asphaltenes dissolved in maltenes, which act as a solvent (Aftgelt & Harle, 1975). The resins and maltenes are considered fundamental in keeping the asphaltenes in solution (Koots & Speight, 1975). Therefore, the asphaltenes are not considered to exist as micelles but rather asphaltene-resin complexes. Numerous other theories have been put forward to explain the structure and composition of asphalt binder, however, the two models above are more widely supported by experimental evidence. Nevertheless, the colloidal model is more broadly accepted within the research community (Porto et al., 2022). Virgin binder usually possesses a large fraction of maltenes and a small fraction of asphaltenes. As the binder ages, this ratio shifts with the volatilization and agglomeration of lighter components, leading to aged asphalt with larger asphaltene fractions causing reduced viscoelastic properties (X. Yu et al., 2014). Oxidation influences the polar components in bitumen, causing asphaltenes to increase, leading to stiffening of the binder. Aromatics which are mainly non-polar, tend to control the flexibility of binder. (Vijayan et al., 2023a).

Table 2.1: Characteristics of SARA fractions in asphalt binders. (Polo-Mendoza et al., 2022a)

Characteristics	**Saturates**	**Aromatics**	**Resins**	**Asphaltenes**
Description	Hydrocarbons with straight or branched chains and saturated rings	Naphthenic aromatic compounds	Condensed aromatic compounds	Polycyclic aromatic compounds with a chain length larger than 40 carbons
Principal compounds	Mix of paraffins and napthenes.	Mix of paraffin, napthenes, and aromatics with sulfur components	Multi-ring aromatic structures and heteroatoms	Paraffins, napthenes, and polycyclic aromatic structures
Polarity	Non-polar	Slightly polar	Highly polar	Highly polar
Molecular weight (g/mol)	500 – 800	800 – 1000	800 – 1000	1000 – 10,000
Proportion in the bitumen (%)	5 – 20	40 – 65	20 – 40	5 – 25
Consistency	Viscous oil	Viscous liquid	Solid to semi-solid	Solid
Color	White	Dark brown	Dark brown	Black or brown
Penetration point	Great	Great	Zero	Zero
Softening point	Low	Low	High	High
Solubility	*n*-heptane wash through alumina	Toluene wash through alumina	Pyridine wash through alumina	Toluene

Paraffins, mainly composed of alkanes, are hydrocarbons with single bonds between carbon atoms, which allows them to form straight or branched chains that can be very long (J. Hu et al., 2017a; Sirin et al., 2018; Vijayan et al., 2023a). Naphthenes, on the other hand, are cyclic hydrocarbons with saturated carbon rings, and they can also form long chains when their rings link together in a chain-like structure. The length of these chains can vary widely, from just a few carbon atoms to thousands in some cases (J. Hu et al., 2017a; Sirin et al., 2018; Vijayan et al., 2023a). The physical properties of these compounds, such as their melting point and viscosity, can change depending on the length and structure of their carbon chains. Figure 2.1 below shows the typical structures of SARA fractions.

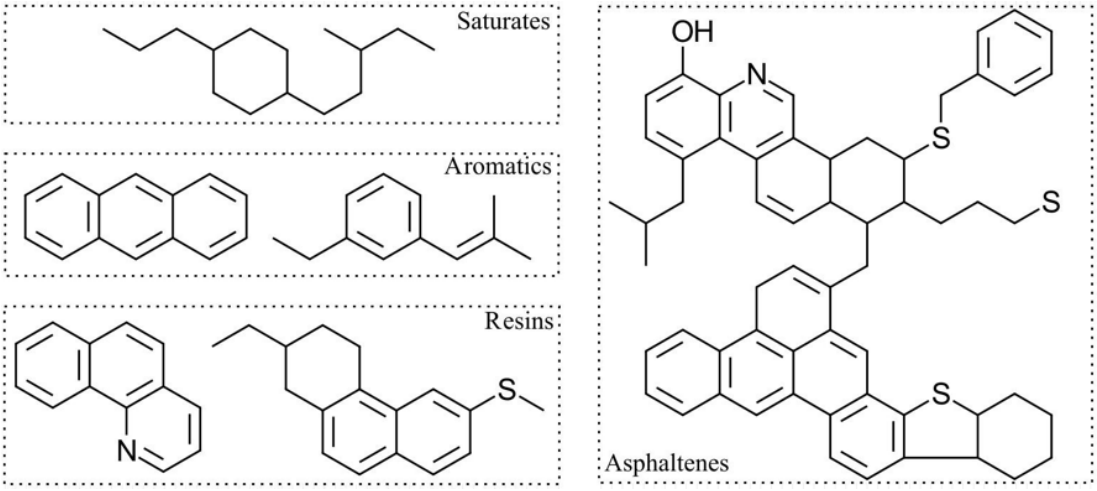


Figure 2.1: Typical structure of SARA fractions. (Polo-Mendoza et al., 2022a)

Based on research, the following were concluded (Apostolidis et al., 2017; Cháves-Pabón et al., 2019a; R. Hunter et al., 2015; Kaya Ozdemir et al., 2021a; Y. Li et al., 2022a; Polo-Mendoza et al., 2022a; Qian & Fan, 2020; Tauste et al., 2018a):

(i) more saturates and aromatics lead to a more liquid-like state (sol-like) asphalt binder;

(ii) more resins and asphaltenes form an asphalt binder with a more solid-like and rigid state (gel-like binder);

(iii) more aromatics and asphaltenes develops high-temperature properties, whilst a low asphaltene content improves the temperature sensitivity behaviour;

(iv) the viscosity increases proportionally to the resins content (including polar aromatics); and

(v) saturates, aromatics and asphaltenes facilitate the flow of the asphalt binder

The proportion of SARA fractions plays a fundamental role in the performance of bituminous materials and their engineering properties. It is clear that the engineering performance of bitumen is governed by a delicate chemical equilibrium in the SARA fractions. Aging of the asphalt binder usually causes transition from a sol-like to gel like state, inducing a decrease in the colloidal stability (Eberhardsteiner et al., 2015; B. He et al., 2019; Peng et al., 2015).

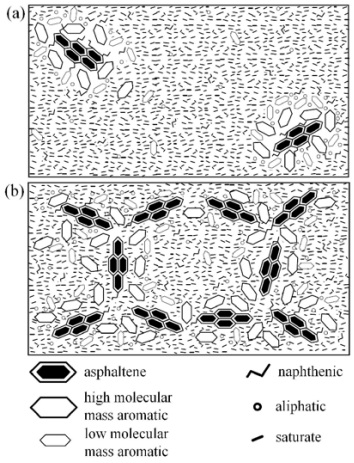


Figure 2.2: Schematic of the colloidal structures in (a) sol- and (b) gel-type asphalt binders.(R. Hunter et al., 2015)

2.1.2 Aging Mechanism

Asphalt binder is an organic material, which, during production, storage, and service period, are exposed to heat, oxygen, water and ultraviolet (UV)/solar radiation contributing to aging (Feng et al., 2013). After aging, as mentioned earlier, the binder becomes brittle and hard, in addition to reduced water stability and low temperature/fatigue cracking resistance. Pavement distresses are also accelerated due to aging coupled with repeated heavy loading; hence the pavement is gradually destroyed, reducing service life. During the use of asphalt pavement, it is subjected to multiple, complex, service environment factors and vehicle loads, leading to decay and deterioration of road performance. This leads to the need for significant road maintenance and repair/rehabilitation activities. These tasks require additional new raw materials leading to an increase in extraction of natural resources like stone, asphalt binder, etc. increasing environmental burden (Azimi Alamdary et al., 2022a; Y. Li et al., 2022a; Vijayan et al., 2023a). This highlights a major challenge facing the asphalt industry, causing significant negative economic and environmental impacts. In order to develop effective strategies to address these challenges it is important understand the mechanisms involved in the aging process (J. Hu et al., 2017a; Y. Li et al., 2022a).

Asphalt aging is a complex process of physical and chemical reactions which have significant impacts on the asphalt binder and degradation of technical properties. The generally accepted pathway of asphalt aging includes (Cháves-Pabón et al., 2019a; Y. Li et al., 2022a; Polo-Mendoza et al., 2022a):

1) Physical/Steric Hardening (reversible) - which changes macroscopic technical properties but not chemical composition. This process is associated with formation of ordered waxy structures in the soft asphaltene phase under the influence of straight chain alkanes in the asphaltenes. This develops slowly at room temperature but is rapidly accelerated as temperature decreases and usually is related to the internal reorganization of the molecules in the binder. Increasing temperature tends to reverse this and thus the effect of hardening is weak and can usually be disregarded.

2) Volatilization/Evaporation of low molecular weight components (mainly saturates and aromatics) – This depends mainly on the temperature of the binder and exposure conditions such as diffusion rate/length or thickness of diffusion path. As temperature increase, rate of volatilization increases, but the effect of this is limited when compared to oxidation. Only a limited number of compounds that can be volatilized actually exist in binder. Volatilization is also more significant during thermo-oxidative/short-term aging. During long-term and UV aging, in-service temperatures are usually lower than 70°C, therefore rate of volatilization is slower.
3) Oxidation – This is the most significant pathway during long-term and UV aging. Studies showed that components in asphalt binder (especially asphaltenes and resins) absorb oxygen and determined that aging is not only caused by physical hardening, but also oxidation (which is an irreversible, diffusion driven phenomenon and controlled mainly by thermal reactions between O_2 and asphalt components, altering chemical properties of asphalt binder) (Prosperi & Bocci, 2021; J. Wang et al., 2012). UV radiation also causes photo-oxidation aging reactions on the surface of the binder. Since asphalt binder is a good light absorber, photo-oxidation can contribute to aging even in low intensity UV radiation. In modified asphalt, especially with polymer, this effect can also age and degrade modifiers. Since the presence of oxygen is required for oxidation, the entire process is closely related to diffusion properties of oxygen in the matrix (Das et al., 2014; Fernández-Gómez et al., 2014).
4) Other minor mechanisms involve, polymerization, separation, syneresis, thixotropy and others. Polymerization is defined as the combination of molecules in order to form larger ones. Thixotropy is defined as the progressive hardening that asphalt binder undergoes due to the formation of an internal structure in the colloidal system, as a product of reorientation of molecules and crystallization of certain chemical components. This process may be reversed up to a certain degree with asphalt reheating and manipulation. Syneresis is defined as an exudation reaction of oils or lighter components, which are exuded to the surface of the asphalt layer. With the loss of these oils, asphalt binder begins to harden. Finally, separation is defined as the removal of oily components, resins or asphaltenes from the binder, caused by the selective absorption of pores in the aggregates.

The life cycle of asphalt binder typically involves (Remisova & Briliak, 2023a; Sirin et al., 2018; Tan et al., 2008a):

Production → Storage → Construction → Service life (multiple factors influencing aging) → End of Life

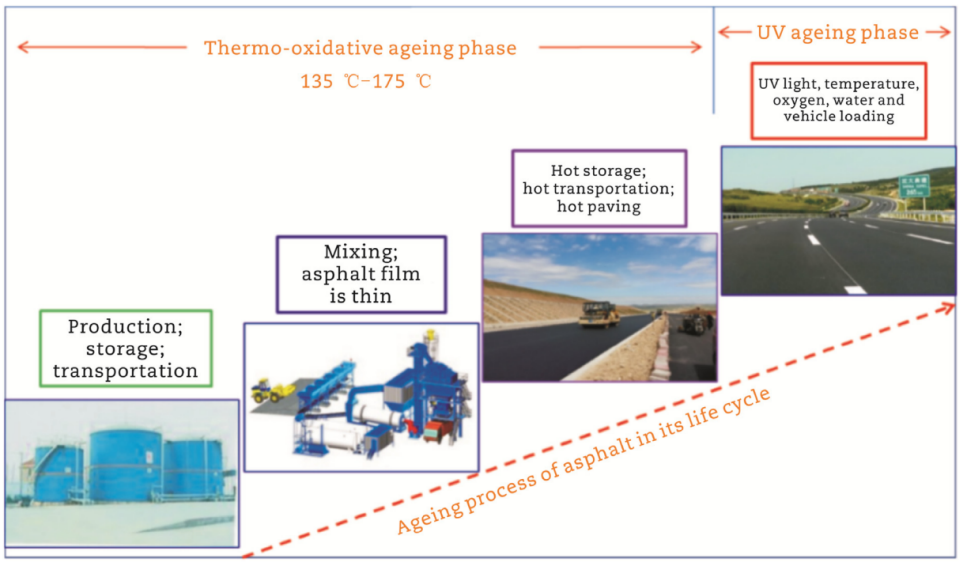


Figure 2.3: Different stages in the life cycle of asphalt binder.(Y. Li et al., 2022b)

The aging process is usually split into two phases, short-term aging (STA) and long-term aging (LTA).

1) Short Term Aging (STA) (Baqersad & Ali, 2019; Khavandi Khiavi et al., 2021a; Tauste et al., 2018a)

During production and storage binder experiences hot storage, hot transportation, storage tank preheating, and blending processes. During this stage various lighter components in the binder are lost through volatilization and asphalt at the surface of the storage tank reacts with oxygen causing aging. Aggregates are usually heated to 170-180°C even up to 190°C. Asphalt binder is spread on the surface of high temperature aggregates with a very thin film (approx. 14um or 6-10um for some mixtures) and large surface area. Therefore, lighter components in the asphalt film evaporate quickly and chemical reactions occur under the coupled effects of temperature and oxygen. During these stages, thermo-oxidative aging is more severe when compared to production and storage. After construction and paving the effects of thermo-oxidative aging are minimal. STA is the dominant type of aging that occurs during the stages described above and has been well studies in previous literature. Laboratory methods have been standardized for simulating and studying the effects of STA. Once of the most commonly used methods in North America is Rolling Thin Film Oven (RTFO) aging. Since STA mainly involves thermo-oxidative aging, high temperatures and air blowing onto a thin film of binder are conditions used for this aging method. The specific parameters used for RTFO aging are described in the AASHTO T-240 standard (AASHTO T 240, 2013).

2) Long Term Aging (LTA) (Carpenter & Wolosick, 1980; Margaritis et al., 2019; Menapace et al., 2017a)

During the in-service phase of the asphalt pavement life cycle, aging mainly occurs due to environmental factors such as moisture, climatic conditions, UV radiation, and traffic loading with minimal thermal oxidation. The presence of water can also accelerate aging and reducing cohesion and adhesion cause

stripping (Remisova & Briliak, 2023a). Since the in-service temperature is much lower than production and construction phases, volatilization of lighter (low molecular weight) components are no longer the main reason for aging, and photo-oxidation aging under UV light and oxygen/moisture, is the main contributor to LTA of asphalt pavements. Previous studies (Cháves-Pabón et al., 2019a; Karim et al., 2021; L. Ma et al., 2011a) have also confirmed that the asphalt binder on surface layers tend to experience more aging than the layers below. The most commonly used method for simulating LTA of asphalt binder, in the laboratory is called Pressure Aging Vessel (PAV) aging, as described in the AASHTO R-28 standard (AASHTO R 28, 2022). This method considers the effect of elevated temperatures, air exposure, and pressure.

Numerous research (A. Chen et al., 2018; Omairey et al., 2021; F. Wang et al., 2020a) and standardized tests exist for thermo-oxidative aging, (RTFO, PAV, etc.), however, these mainly evaluate oxidation resistance of asphalt binders, under experimental temperatures and oxygen/pressure conditions but do not account for the effects of the multiple factors actually experienced by pavement in service. This literature review will focus more on UV and multifactor aging since thermo-oxidative aging is well-studied. The polymer photochemical theory, states that the mechanism of asphalt aging due to UV radiation is completely different from that of thermo-oxidative aging, hence, RTFO and PAV aging methods cannot accurately simulate the effects of both.

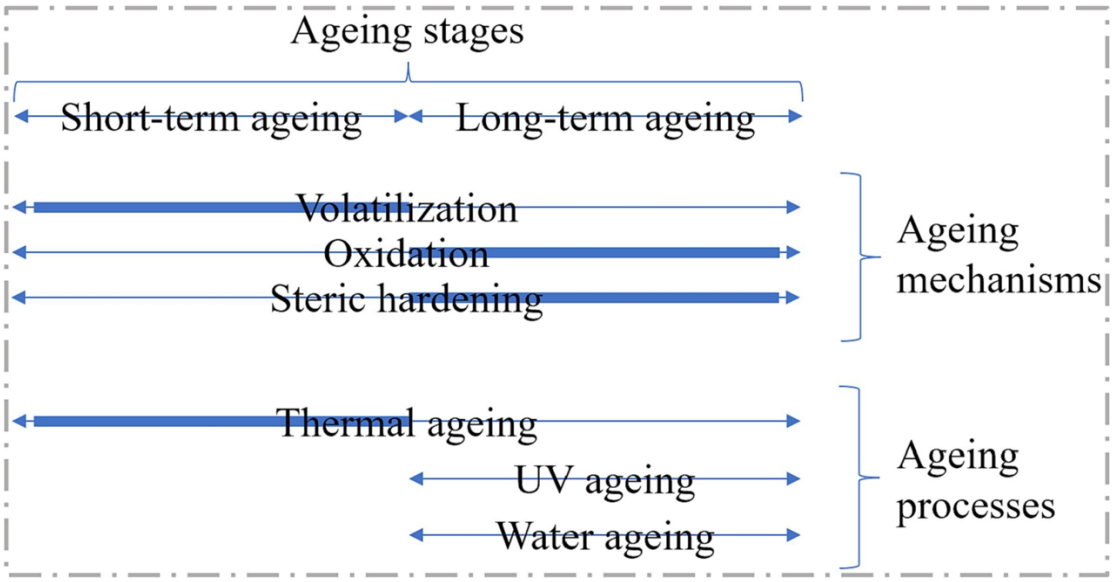


Figure 2.4: Pathways involved aging process at different stages in asphalt life cycle. (Polo-Mendoza et al., 2022a)

UV aging does not initiate volatilization or steric hardening, but it could accelerate these mechanisms (Gedik, 2021; S. Liu, 2013). Moisture and humidity can catalyze these physical-chemical changes significantly, so much so, that some researchers classify moisture damage as an aging mechanism on its own (Hosseinnezhad et al., 2019; M. Yu et al., 2012; Zeng et al., 2015a). Water provides a source of

hydrogen atoms that can increase the oxidation reactions or disrupt the colloidal structure of the asphalt binder. Physically it can cause loss of adhesion, loss of cohesion and stripping.

Similar to thermo-oxidative aging, during exposure to UV radiation, active carbon and sulfur in asphalt can absorb oxygen, oxidizing and resulting in an increase in the oxygen content (forming carbonyl and sulfoxide groups). H. Yu et al., (2019) showed that after UV aging**,** C=C bonds in unsaturated olefins in asphalt are broken down to form C-H bonds causing a gradual increase in methyl and methylene groups; C–O is oxidized to C=O (carbonyl); and C–S bonds are broken to form S=O (sulfoxide) bonds. In SBS modified binders, UV aging can also break cross-linked structures. The relative contents of polybutadiene (PB) C=C and polystyrene (PS) C–H in SBS is decreased by UV aging. In general sunlight initiates the degradation process with heat and moisture causing adverse effects. The oxidized bitumen can be water soluble and therefore removed, exposing fresh unaged bitumen (J. Hu et al., 2017a). UV effects are often ignored although they are well known. Most lab aging studies focus on the use of standards and look for relationships between chemical and rheological properties (Borghi et al., 2017; Khavandi Khiavi et al., 2021a; Lu & Isacsson, 2002; T. Zhou et al., 2020).

Under elevated temperatures or exposure to UV light, asphalt can experience various chemical reactions, including addition, polymerization, oxidative dehydrogenation, and other processes involving short-chain compounds. These reactions lead to the formation of complex cyclic compounds and polar functional groups, such as carbonyl and sulfoxide groups, which increase the molecular weight and size of the asphalt. Additionally, lighter components, like aromatic compounds, are converted into heavier ones, such as asphaltenes (Y. Li, Wu, et al., 2020a). Oxidative aging can be described by three different chemical changes, namely fragmentation, oxygen addition, and condensation as shown in Figure 2.5.

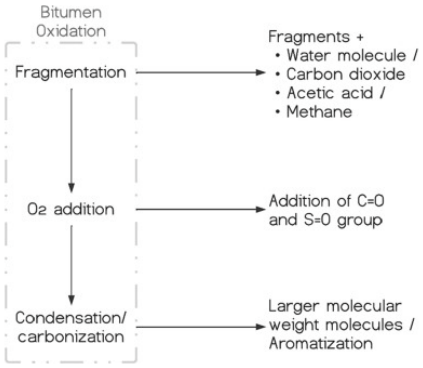


Figure 2.5: Different chemical change occurring during oxidation. (Polo-Mendoza et al., 2022a)

Typically, main functional groups associated with oxidized binders include ketones, sulfoxides, dicarboxylic anhydrides and dicarboxylic acids in much smaller concentrations (Rossi et al., 2018a). Figure 2.6 below illustrations the different functional groups naturally occurring in asphalt binder and those formed during aging. Aromatics decrease, asphaltenes and resins increase and saturates remain relatively

unchanged due to low reactivity (Rossi et al., 2018a; Tan et al., 2008a). Aromatics tend to transform to resins and resins transform to asphaltenes at the same time. Due to aging reactions, asphaltene content after UV exposure is much greater than after thermal aging, indicating some differences in the extent of reactions. It can potentially be feasible to estimate the extent of the aging reaction by observing the conversion to asphaltenes (Rossi et al., 2018a; Tan et al., 2008a).

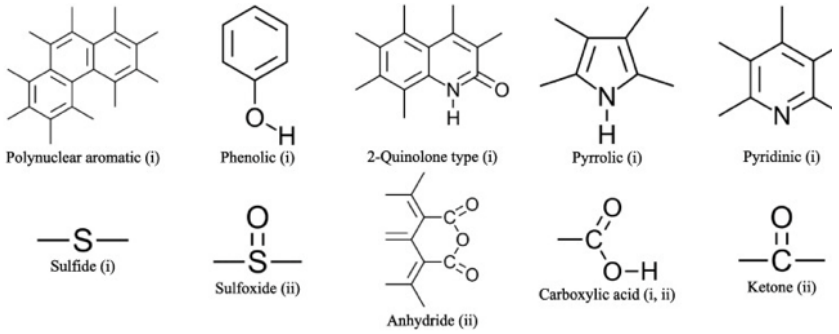


Figure 2.6: Functional groups in asphalt binders (i) naturally occurring and (ii) formed upon aging. (Polo-Mendoza et al., 2022a)

During oxidation, large molecules undergo fragmentation, resulting in the formation of smaller molecules and by-products such as water, carbon dioxide, acetic acid, and methane (Prabir Kumar Das, Baaj, et al., 2015; Y. Li, Li, et al., 2020). Consequently, the proportion of large molecules in the bitumen gradually diminishes, while the proportion of small molecules increases during this process (Z. Chen et al., 2020; Shi, 2014).

During the O_2 addition reactions, atmospheric oxygen reacts with bitumen molecules, resulting in the creation of new functional groups, mainly carbonyl (C=O) and sulfoxide (S=O) groups (Prabir Kumar Das, Baaj, et al., 2015; Lesueur, 2009; Prosperi & Bocci, 2021). However, it is important to recognize that other, less prominent groups, such as hydroxyl, acid, and ester groups, are also formed during these reactions (D. Hu et al., 2022; R. Hunter et al., 2015). These newly created oxygen-bearing molecules increase the oxygen content and the degree of unsaturation in the bitumen (Apostolidis et al., 2017; Villegas-Villegas et al., 2018; S. Zhang et al., 2021). Oxygen diffusion, which heavily impacts the rate of oxidation, occurs gradually and is influenced by both temperature and the duration of aging (Hung & Fini, 2019a; S. Wu et al., 2017). The final phase of oxidative aging is referred to as the condensation or carbonization stage, where larger/heavier bitumen molecules, including aromatic (benzylic) carbon groups, are generated (Prabir Kumar Das, Baaj, et al., 2015; Prabir Kumar Das, Balieu, et al., 2015). This formation is driven by polyaromatic oxidation reactions (Osmari et al., 2019a; Tauste et al., 2018a). The conversion of smaller molecules into larger macromolecules leads to the development of moiety networks and the homolytic cleavage of alkyl side chains (Apostolidis et al., 2017; Ding et al., 2019; D. Hu et al., 2022; H. Zhang et al., 2021; X. Zhou et al., 2020). As a result, this stage of oxidative aging is a key factor in increasing the

polarity, viscosity, and stiffness of the asphalt binder, along with reducing its flexibility (Apostolidis et al., 2017; C. Li et al., 2019; Omar et al., 2021; G. Xu & Wang, 2017).

Photo-oxidation, due to UV radiation, is similar to thermal oxidation, but induces more surface aging and then more degradation of properties in flexible pavements (P. K. Das et al., 2014; Hong et al., 2020). There is no consensus in the literature on UV aging phenomena in bitumen and bituminous mixtures. Nonetheless, when asphalt pavements are constructed, the surface is subjected to UV radiation under a particular frequency band in sunlight, which causes free-radical reactions and a progressive increase of specific functional groups. In addition, the high energy induced by the UV radiation on the asphalt binder generates atomic ionization and molecular free radicals that can alter the proportion of SARA fractions giving rise to several chemical compounds (mainly low-weight molecules) and induce molecular cracking. Exposure to the UV rays can excite the bitumen molecules and break the covalent bonds, leading to free radicals joining with available oxygen, thus developing a chain reaction of irreversible chemical changes as seen in the table below (Durrieu et al., 2007; X. He et al., 2018a; X. Sun et al., 2021).

Table 2.2: Chemical reactions involved in photo-oxidative aging. (Polo-Mendoza et al., 2022a)

Stage	**Sequence of reactions**	**Description**
1	$RH + O_2 \rightarrow R\bullet + HO_2\bullet$ (initiation)	Thermodynamically unfavorable reaction initiated by UV irradiation.
2	$R\bullet + O_2 \rightarrow ROO\bullet$ (O_2 addition)	Chain reactions form free radicals.
3	$RH + ROO\bullet \rightarrow ROOH + R\bullet$ (H abstraction)	
4	$RH + HO_2\bullet \rightarrow H_2O_2 + R\bullet$ (H abstraction)	
5	$R\bullet \rightarrow$ Isomerization, O_2 addition, homolysis, H abstraction, etc.	Due to the produced $R\bullet$ being unstable, the molecular structure of the bitumen suffers several reactions (isomerization, decomposition, and another H-abstraction reaction) that progressively destroy it.

A unified and effective connection has not been established among various chemical indicators. Most of the research on the chemical composition of asphalt focus on the changes of functional groups, chemical bonds, and structures, and the research angle is relatively single, and systematic and in-depth research is still needed at the molecular level of asphalt.

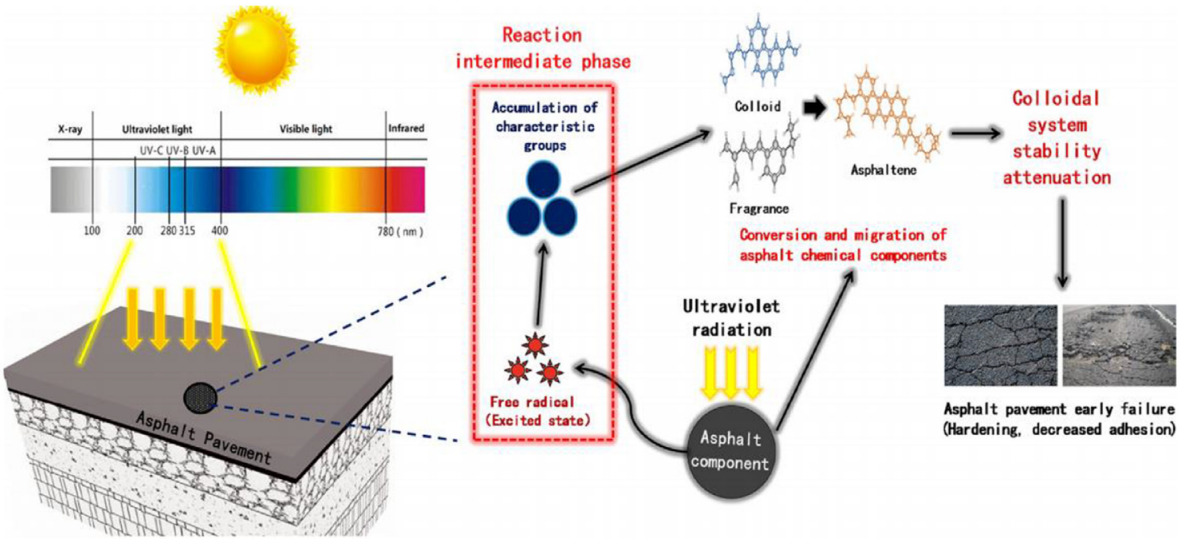


Figure 2.7: Major processes involved in UV aging. (X. Sun et al., 2020)

When comparing the number of studies done on thermo-oxidative aging of asphalt (mix/binder) to those done considering UV aging, there are relatively few on UV, many of which have several shortcomings. Research on the UV aging mechanism of binder has focussed on the changes of elemental content, chemical structure, microscopic morphology and components of asphalt binder during UV aging, in addition to UV light intensity, aging time, test temperature, etc (Y. Li et al., 2022a; Tan et al., 2008a; Vijayan et al., 2023a). Other factors such as effect of UV wavelength range on aging rate and the growth mechanism of asphalt aging depth is still unclear and the mechanism is still not fully understood.

Standardized thermo-oxidative aging methods do not consider the multitude of different factors that exist in the field. Several studies have investigated UV and multi-factor aging methods, however due to the lack of standardization, the equipment, factors and operation parameters considered in previous literature, are widely different (Han et al., 2011; B. He et al., 2019; Y. Li, Li, et al., 2020; H. Zhang et al., 2011). Many researchers create their own chambers or ovens with custom-designed UV lamps. Because this equipment is self-made, there are substantial differences in the simulation variables (such as temperature, duration, film thickness, intensity, and wavelength) across different studies. These variations make it difficult to synthesize or generalize the findings on UV radiation's effects on asphalt binder behaviour. Consequently, each study should be considered a unique case, and its conclusions should be interpreted accordingly. This makes it nearly impossible to compare results from different studies and draw reasonable conclusions. Consequently, it is crucial to thoroughly review the existing literature, methodologies, and results, comparing them with data from field-aged bitumen. This will allow for identification of the key factors, parameters, and exposure conditions that most accurately replicate long-term field aging in an accelerated manner, taking into account a wide range of variables. Based on this, it is crucial for an internationally

recognized body to establish standards for simulating the UV aging of bitumen. It should be noted that two ASTM standards, namely, ASTM- D4798(Accelerated weathering Test conditions and procedures for bituminous materials (Xenon-Arc method)) and ASTM- D4799M (Standard Practice for Accelerated Weathering Test Conditions and Procedures for Bituminous Materials (Fluorescent UV, Water Spray, and Condensation Method)) have been established for simulating multifactor aging of bituminous materials, however they have several short comings including the use of highly specialized, expensive equipment, and ambiguous recommendation for period of sample exposure, and water spraying rate/volume (ASTM, 2000, 2016). Another LTA method used in different studies, is the Viennese Aging Procedure (VAPro) developed in Austria (Steiner et al., 2016), which is an extension of the procedure outlined in SHRP-A-383 report (Bell et al., 1994). It utilises a unique configuration consisting of a triaxial cell with a forced flow of highly oxidative gaseous agents such as ozone and nitric oxide over the specimen, at a rate of 1 litre per minute. This reportedly simulates LTA closely resembling field conditions in 4 days, but approach requires intricate set up and costly configuration.

UV light which typically has wavelengths between 200-400nm, can be sub-categorized into UVa (320-400nm), UVb (280-320nm) and UVc (200-280nm). Solar radiation reaching the surface of the earth is significantly lower energy and intensity than that emitted directly from the sun. Only UVa and UVb radiation reaches earth's surface, and these initiate photochemical reactions in asphalt binders. UV light alone, only causes limited aging very slowly (Y. Li et al., 2022a). When UV radiation is coupled with oxygen, it is able to exert a catalytic effect that accelerates the photo-oxidative aging process leading to significant reduction in technical properties (Y. Li et al., 2022a; Polo-Mendoza et al., 2022a). Typically, shorter wavelength has more energy, and this can be calculated using the following equation:

$$E = h\frac{c}{\lambda}$$

Where h is planks constant, c is the speed of light (m/s) and λ is the wavelength of the UV light (m).

Molecules can undergo bond breaking when exposed to UV light leading to a series of oxidation processes. The occurrence of this depends on the wavelengths absorbed by molecular chains and the strength of the chemical bonds. The sensitivity of different structures to varying wavelengths are different. Main molecular bonds connected to benzene rings and other stable groups in asphalt binder are C-H, C-C, C=C and O-H. C=C and carbonyl groups in ketones are very prone to photodegradation or photo-oxidation, where breaking energy of C=C is only 270 kJ/mol. In order for a photochemical reaction to happen, a molecule has to have a characteristic absorption spectrum for particular wavelengths of UV light. If the exposure wavelength is not the sensitive wavelength of a certain structure, its photodegradation will be slow. The energy contained in different wavelengths of UV light and bond energies of common chemical bonds in asphalt binder are summarized in the tables below.

Table 2.3:Different UV light wavelengths and associated energy. (Y. Li et al., 2022a)

Wavelength of UV Light (nm)	**280**	**290**	**300**	**310**	**320**	**330**	**340**	**350**	**360**	**370**	**380**	**390**	**400**
Energy of Photon (kJ/mol)	427.4	412.6	398.9	386	374	362.6	352	341.9	332.4	323.4	314.9	306.8	299.2
Energy of Photon (kcal/mol)	102.1	98.6	95.3	92.2	89.3	86.6	84.1	81.7	79.4	77.3	75.2	73.3	71

Table 2.4: Bond energies of common bonds found in asphalt binder molecules. (Y. Li et al., 2022a)

Chemical Bond	**C–N**	**C–C**	**C–O**	**N–H**	**C–H**	**O–H**	**C=C**
Bonding Energy (kJ/mol)	290.9	347.9	351.6	389.3	413.6	463	615.3

When a molecule absorbs light within a sensitive wavelength range, if the energy of the absorbed photon exceeds the internal bond energy, the molecular bonds may break, leading to the formation of free radicals. These free radicals initiate photo-oxidative chemical reactions, a process explained by free radical theory, which describes UV aging in binders through three stages: chain initiation, chain growth, and chain termination as shown in Table 2.2. Conversely, if the energy absorbed is lower than the bond energy of the molecule, free radicals do not form, and the bond remains in an excited state. In the presence of a small number of heteroatoms or exposure to oxygen, the photo-oxidative degradation of organic materials can accelerate due to the influence of these elements.

In theory, many molecules are stable under sunlight because they lack chromophores that absorb wavelengths longer than 280 nm under ideal conditions, such as absolute purity. For instance, C–H bonds do not absorb light at wavelengths above 290 nm, and C–C bonds only absorb UV light at 195 nm and 230–250 nm. However, in reality, asphalt molecules degrade rapidly under sunlight because the industrial production process introduces impurities capable of absorbing UV light, such as residual catalysts, oxidation products, processing aids, and colorants. Asphalt, an organic binder composed of hydrocarbons with varying molecular weights and their non-metallic derivatives, typically contains around 10^5 to 10^6 different molecules, each susceptible to different UV-induced aging effects.

During asphalt binder production, certain catalytic components, such as metal ions and catalysts, inevitably enter the binder. Additionally, trace amounts of metals like nickel, vanadium, manganese, and iron are present, and their unfilled d-orbitals cause chemical instability and formation of complexes that can initiate photo-oxidative aging reactions. Moreover, the production, storage, and transportation of asphalt binder leads to thermo-oxidative aging, resulting in impurities like hydroperoxides, C=O compounds, or charge-transfer complexes that absorb UV radiation and trigger UV aging reactions (Yousif & Haddad, 2013).

In the polymer industry, when looking at aging, wavelength range of UV light used during aging is known to play a significant role. Lins et al., (2008) confirmed that carboxylic acids and esters have little or no sensitivity to UV light wavelengths over 290 nm. Another study used wavelengths 250-500nm on polymers for 1-8 hours of aging times. Results indicated that the yellow index of samples differed under UV radiation at different wavelengths, confirming the impact of wavelength on aging behaviour (Fernández-Gómez et al., 2014). Zeng et al., (2015) investigated polymethylmethacrylate (PMMA) and wavelengths 250-1000nm and found that range 260-320nm were the main cause of chain breakage and above 340nm, photodegradation was extremely weak. These studies confirm that different wavelengths have different aging effects on organic polymers.

One early study mentioned that UV with higher energy is more destructive (Airey, 2003), but other studies since then has proposed opposing theories. J. Hu et al., (2018) employed three different ranges with different central wavelengths. Results found that different wavelengths of UV light produced significantly different aging effects on the asphalt binder and the range of 300–350 nm had the strongest aging effect on asphalt, followed by that in the wavelength ranges of 260–300 nm and 350–400 nm. Shortcomings of this study however is that the central wavelength and wavelength range of the three UV lights were different, and the wavelength range of the UVs (40–50 nm) was relatively large, making the results of the study rather ambiguous. Y. Li et al., (2019) experimented with three different wavelength ranges 350–370 nm, 340–380 nm, and 200–400 nm, all of which had central wavelength of 360nm, radiation intensity of 7.0 W/m^2 and a maximum aging time of 288 hours. Although all had the same central wavelength, the shortest range had most significant aging impact and largest, the least. These studies confirm that the sensitive wavelength theory exists in asphalt. Therefore, it is not necessarily that higher energy wavelengths cause more aging. Based on numerous studies examined, the relative sensitive wavelength range for the UV aging of asphalt molecules is typically between 360-365 nm (Polo-Mendoza et al., 2022a). The variety of ranges and central wavelengths used in previous research, however, makes results difficult to compare to each other and with natural light.

Apart from wavelength, thickness of asphalt film on aggregates also affects the extent of UV aging that the asphalt binder experiences. Omairey et al., (2021) looked at UV aging of asphalt by coupling heat conduction, oxygen diffusion and oxidation reactions. Results found that an aging gradient exists similar to that shown in Figure 2.8. One early study mentioned that asphalt samples only had significant UV aging when the thickness was 3μm (Traxler, 1961). Kemp & Predoehl, (1981) showed that aging and hardening occur significantly only 5-10μm into the asphalt sample, and when thickness of binder was greater than 200μm, aging effects were significantly reduced. UV aging experiments on asphalt binder thicknesses 50, 100, 200, 500 and 1000μm showed that thinner asphalt samples yielded higher elastic modulus, and more carbonyl groups generated after UV aging, therefore, more significant aging as expected (Yamaguchi et al.,

2005). Meanwhile, Durrieu et al., (2007) demonstrated that after UV aging of a 10μm thick asphalt binder film, for only a few hours it reached PAV level. Hung et al., (2019)considered a 600 nm thick asphalt film prepared by a rotary coating machine and UV-aged in an accelerated UV-aging tester. The results showed that, as the UV radiation continued from 0 to 400 h, using FTIR, the hydrocarbon content of the films gradually decreased and the relative content of sulfoxide groups and carbonyl groups increased, reducing the solubility of asphalt in organic solvents. After 20 hrs of UV, nanoindentation showed increase in hardness and viscoelasticity of film and this continued to increase up to 50 hours.

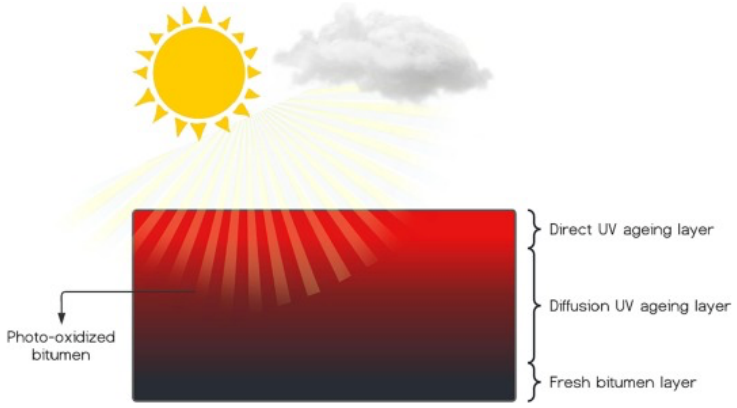


Figure 2.8: Aging gradient asphalt binder experiences when exposed to UV radiation. (Cháves-Pabón et al., 2019a)

Based on the results of the studies described earlier, it can be concluded that, when considering the chemical composition and technical properties of asphalt samples after UV aging, what is studied is actually a mixture of aged asphalt on the surface and unaged asphalt inside, such that the aging state of asphalt binder may not be accurately characterized. Thickness of sample is extremely important in UV aging but is inconsistent between different studies. Many studies confirm that the asphalt aging starts on the surface and gradually extends to the interior. Y. Li et al., (2021) looked at a layer-by-layer stripping method to remove asphalt in different aging states and revealed the aging depth growth mechanism. Under the same aging time conditions, the aging depth of asphalt was greater when using UV light with high UV irradiation intensity than that with low UV irradiation intensity. Therefore, increased intensity and irradiation time both independently and together increase aging depth (J. Hu et al., 2017a; Y. Li et al., 2021; Remisova & Briliak, 2023a). UV effects however cannot be ignored as some studies show that UV aging of RTFO aged binder can result in similar levels of aging as PAV only within a few hours (J. Hu et al., 2017a). Polo-Mendoza et al., (2022) presented a table that summarized the exposure parameters, conditions and settings used in a variety of different literature for simulating UV and multi-factor aging. Based on this table, most studies adopted an aging protocol which included RTFO followed by UV aging. The parameter setting for temperature, exposure duration, film thickness, UV intensity and wavelengths widely differed between different studies, but ranged between (Polo-Mendoza et al., 2022a):

- Temperature → 25°C – 80°C,
- Duration of exposure → 0.1 days to 60 days
- Film thickness → 32 – 3200μm with 3200μm being the most commonly used
- UV intensity → 0.45 – 1000 W/m^2 (it was noted that a shorter exposure duration was used when intensity was higher)
- Wavelength → 280 – 400nm, a few studies used broad spectrum UV lights with a range of wavelengths, but the majority of studies used UV lights with a single wavelength of 365 nm

2.3 Techniques for Evaluating Rheological and Chemical Properties of Asphalt Binder Aging

2.3.1 Chemical Testing Methods

This section delves into the common analytical techniques used for characterizing and monitoring changes in the chemistry of asphalt binder. These methods include separation techniques and a wide range of spectroscopic tools that provide details about the chemical nature of bitumen.

1) SARA Fractionation

Asphalt binder is a complex material composed of millions of molecules. For over 50 years, efforts have been made to simplify its study by characterizing and identifying its chemical composition. In a very early study(Stewart, 1957), chromatographic separation techniques and infrared spectroscopy were employed to analyze the chemical composition of both unaged and field-aged roofing bitumen achieving separation of asphaltenes and maltenes using n-pentane as a solvent. A decade later, Corbett, (1969) introduced elution-adsorption chromatography, further refining the separation into four fractions: saturates, naphthene aromatics, polar aromatics, and asphaltenes. This method has been adapted over time, leading to the development of the SARA (Saturates, Aromatics, Resins, Asphaltenes) fractionation technique, which remains the standard today as per ASTM D4124-01(ASTM, 1997).

Modern adaptations, such as the SARA-AD method developed by the Western Research Institute, have further refined these separations into subfractions (Adams et al., 2015). Although these variations exist, the overall concept of separating the material into fractions based on polarity has remained the same. It is important to recognise however that this separation is not a strict separation into a precise set of molecules but rather separation along a polarity gradient. The methods described above are very tedious and lengthy and has led to the modifications that are less time consuming. Techniques like solid-phase extraction, as developed by Sakib & Bhasin (2019), have streamlined the process, allowing for rapid separation of SARA fractions with excellent repeatability. This method has been widely adopted internationally, as evidenced by studies that use it to investigate the spectroscopic changes in SARA fractions during aging (Mirwald et al., 2020a, 2020b), the effects of rejuvenators (Guo et al., 2022), and the comparison with column chromatography (Schwettmann et al., 2022). The results from these studies have also been used for

molecular (MD) simulations (Guo et al., 2021). However, it is important to note that the exact chemical constituents of SARA fractions, including elements like carbon, oxygen, sulfur, and nitrogen, can only be determined through elemental analysis, which provides an overview of elemental composition without revealing the molecular structure.

2) Gel Permeation Chromatography (GPC)

Gel Permeation Chromatography (GPC) is another significant chromatographic technique used to characterize bitumen, offering insights into its molecular weight distribution. The system mainly consists of an autosampler, a photodiode array detector (PDA), a column-box and a pump. The detector is connected to the system to provide information regarding the concentration and molecular weight distribution of the sample. In this method, larger molecules travel faster through the column than smaller ones leading to a shorter retention time, and the resulting chromatogram correlates molecular weight with elution time. One of the earliest studies in which GPC was used along with high pressure-liquid chromatography (HPLC) was carried out by Such et al., (1979). The SHRP (Strategic Highway Research Program) report from 1993 also conducted experiments and reported results from GPC on SHRP binders and indicated that the methods can account for interactions between molecules (Buisine et al., 1993). GPC has been used to study bitumen aging (J.-S. Chen et al., 2018; M. Hu et al., 2022; Kim & Burati, 1993; K. Zhao & Wang, 2020), the impact of additives such as polymers (Lin et al., 2019; Singh et al., 2018; X. Zhao et al., 2016) and crumb rubber (Lee et al., 2011; Shen et al., 2007), alternative materials such as bio-binders (Mousavi et al., 2016) and the effects of recycling and rejuvenation agents (J.-S. Chen et al., 2018). Despite its utility, GPC requires specific equipment and complex sample preparation, which limits its widespread use in bitumen research. Other chromatographic techniques such as Thin-Layer Chromatography coupled with Flame Ionization Detection (TLC-FID) have been explored in literature for evaluating the development of SARA fractions as an alternative to solvent separation and HPLC (Tauste et al., 2018b).

3) Fourier Transform Infrared (FTIR) Spectroscopy

Fourier Transform Infrared (FTIR) spectroscopy is the most widely used analytical method in asphalt binder research (Hou, Lv, et al., 2018). This technique can characterize materials containing IR-active functional groups that absorb infrared light. When IR light is absorbed, it alters the dipole moment of the molecules, causing them to rotate or vibrate, resulting in a distinct band for each functional group. Figure 2.6, presented earlier illustrated the main functional groups in bitumen. Among these, ketones and sulfoxides are especially important in bitumen analysis, as they form during the aging process and can be semi-quantitatively traced using FTIR spectroscopy.

A typical FTIR spectrum for asphalt binders is presented in Figure 2.9. Different functional groups are found at specific vibrational bands. The most common functional groups of interest with respect to asphalt binders, and associated wavenumbers around which bands appear are presented in Table 2.5 below. To

evaluate the significance of these functional groups, it is necessary to consider the changes in their intensities due to chemical processes such as aging. For instance, the alkyl bands listed in Table 2.5 generally remain stable during aging, often serving as reference bands. Meanwhile, the aromatic bands at 1600, 850, 810, and 750 cm^{-1} show a slight increase, which can be linked to the dehydrogenation of perhydro-aromatics like 9,10-dihydroantracenes — these molecules are believed to initiate oxidation mechanisms by reacting with oxygen (Petersen, 2009). In terms of quantifying bitumen aging, the ketone and sulfoxide functional groups at 1700 and 1030 cm^{-1} are of particular interest due to their significant changes during aging. Other groups such as 2-quinolones, carboxylic acids (Mirwald et al., 2020b; Petersen, 2009), or esters, which are primarily found in the resin fraction or formed during aging, are also relevant (Mirwald, Werkovits, et al., 2022; Petersen et al., 1971, 1975).

Table 2.5: Common functional groups in asphalt binders and corresponding wavenumber (adapted from Mirwald et al., 2020b)

Functional Group	**Assigned Vibration**	**Wavenumber [cm^{-1}]**
Alkyls	ν_{as} CH_2/CH_3	2920
Alkyls	ν_s CH_2/CH_3	2850
Alkyls	δ_{as} CH_2/CH_3	1455
Alkyls	δ_s CH_2/CH_3	1380
Alkyls	ρ $(CH_2)_n$	720
Aromatic	ν C=C	1600
Aromatic	γ CH_{aro}	860
Aromatic	γ CH_{aro}	810
Aromatic	γ CH_{aro}	750
Alkene	δ (CH)	960
Ketones	ν C=O	1700
2-Quinolone	ν C=O	1655
Carboxylic Acids	ν C=O	1730
Sulphoxides	ν S=O	1030
Sulphones	ν SO_2 (out-of-phase)	1310
Sulphones	ν SO_2 (in-phase)	1160
Sulphate Ester	ν_{as} SO_3	1260
Sulphate Ester	ν_s SO_3	1080
Sulphate Ester	ν S-O-C	810

Stewart, (1957) was among the first to document the infrared spectra of roofing binders. Initial FTIR experiments with bitumen required the binders to be prepared and measured in transmission mode (Lamontagne, Dumas, et al., 2001; Petersen, 1975; Petersen et al., 1971). Due to the lack of transparency, asphalt binder, in its solid state, had to be dissolved and applied onto a suitable substrate, such as a KBr, CsI, or NaCl crystal window (Weigel & Stephan, 2018a), a process that was time-consuming and reduced practicality. The introduction of attenuated total reflection (ATR) geometry, which allows for the direct

placement of solid bitumen samples onto the ATR crystal, significantly improved the usability and convenience of FTIR. ATR crystals are typically made from diamond, germanium, or zinc selenide.

The increased popularity of ATR-FTIR led to questions about routine measurement and universal applicability, as there is currently no standard for measuring bitumen with FTIR spectroscopy. Consequently, various measurement routines and approaches for spectral evaluation have been developed. Typical spectral evaluation includes the normalization and integration of regions of interest, such as the carbonyl region around 1700 cm^{-1} or sulfoxides at 1030 cm^{-1}. Lamontagne, Dumas, et al., (2001),the Belgian Road Research Centre (BRRC), Laboratoire Central des Ponts et Chaussées (LCPC), and participants from the French national project MURE (Multi-recycling and Warm Mix Asphalts) used the valley-to-valley or tangential integration method to evaluate FTIR spectra (Anne et al., 2017; Lamontagne, Durrieu, et al., 2001; Weigel et al., 2021). To address questions surrounding repeatability and sensitivity, a study was conducted regarding the effects of oxidation by comparing raw data with normalized spectra and using full-baseline and tangential (valley-to-valley) integration methods (Hofko et al., 2017). Subsequent research explored the impact of sample preparation, thermal history (heating time and temperature), as well as storage time and conditioning on unmodified and modified bitumen using ATR-FTIR spectroscopy (Mirwald, Nura, et al., 2022a; Mirwald, Werkovits, et al., 2022). More sophisticated approaches have been developed for spectral data evaluation by applying standard normal variant (SNV) transformation combined with multivariance analysis to detect differences in binder origins and predict its properties (Weigel & Stephan, 2017, 2018a). L. Ma et al., (2023) employed principal component analysis (PCA) and linear discriminant analysis (LDA) models to study the effects of aging via FTIR spectroscopy, correlating specific bands or wavenumber regions to the source, type, and aging state of asphalt binders. Other studies have also used multivariance analysis to identify differences in the FTIR spectra of various laboratory and field-aged bitumen, highlighting the influence of different aging-inducing factors (Primerano et al., 2023). Literature on the application of multivariate analysis for evaluating repeatability and reliability of FTIR are however still needed. Another area that requires focus in future studies is the use of these methods and analysis techniques on modified binders.

FTIR spectroscopy is also applicable for characterizing common bitumen modifiers like SBS. Both styrene and butadiene, being IR-active functional groups, can be monitored using infrared spectroscopy (Luo et al., 2020; Margaritis et al., 2021; D. Sun et al., 2011). In FTIR spectra, the polybutadiene band appears at 966 cm^{-1} and the polystyrene band at 699 cm^{-1}. These bands can help identify whether bitumen contains SBS or whether the polymer is undergoing changes, such as degradation, due to factors like aging. For instance, a previous study used FTIR spectroscopy to quantify the SBS polymer content in different bitumen samples, ranging from 2 to 6% (D. Sun et al., 2011). Conversely, Mouillet et al., (2008) quantified the degradation of SBS polymer due to UV aging by observing changes in the butadiene double bond band at 966 cm^{-1}.

This principle also applies to other additives, such as rejuvenators or extenders, where FTIR can be used for characterization if the materials contain IR-active functional groups.

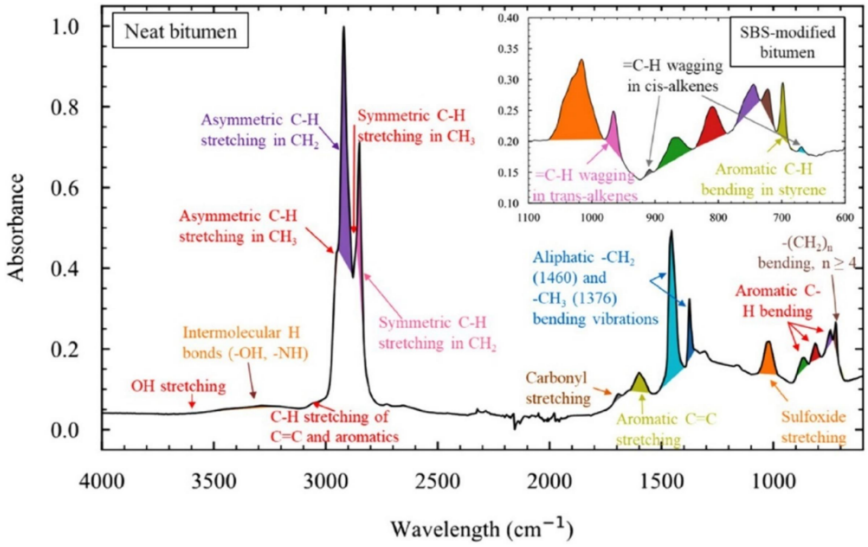


Figure 2.9: Typical FTIR spectrum for asphalt binder with SBS (adapted from (L. Ma et al., 2023))

4) UV-Vis (ultraviolet-visible) and Fluorescence Spectroscopy

Light in the visible and ultraviolet ranges can be utilized to gather distinctive information about the chemical composition of bitumen. A previous study investigated bitumen that had undergone laboratory aging and was dissolved in tetrahydrofuran (THF) using UV–vis absorption spectrophotometry. Their results indicated changes in absorption at longer wavelengths near 600 nm, which increased with aging (Soenen et al., 2016). Similar outcomes were reported by Hou et al., (2018) and Hung & Fini, (2019b) where aging was associated with an increase in the wavelength range of 700–900 nm, attributed to the rise in asphaltene content.

Various bitumen samples were examined using synchronous excitation emission (SEE) fluorescence spectroscopy, detecting a significant fluorescence signal in the 250–600 nm range. These signals are linked to aromatic rings of varying sizes, with longer wavelengths corresponding to larger aromatic rings (Buisine et al., 1993). Similar studies were conducted using fluorescence spectroscopy on unmodified solid bitumen and its SARA fractions. Their excitation scans, emission scans, and fluorescence excitation-emission mapping (FEEM) revealed a general decline in fluorescence intensity, which was be attributed to the reduction in aromatic content during aging (Grossegger et al., 2018; Handle et al., 2016). Analysis of the SARA fractions showed that the majority of the intensity originated from the aromatic fraction, which exhibited fluorescence intensity two orders of magnitude greater than the other fractions. The overall decrease in intensity with aging is due to the significant decay of the aromatic fraction.

Fluorescence spectroscopy was combined with optical fluorescence and darkfield microscopy to explore the differences among various long-term aging procedures. FEEM results indicated not only an overall decrease in fluorescence intensity but also a shift towards higher emission wavelengths and potential quenching effects (Mirwald et al., 2021).

Recent research integrated fluorescence spectroscopy with FTIR spectroscopy and Nuclear Magnetic Resonance (NMR) spectroscopy to examine the effects of aging on bitumen and its SARA fractions. Emission scans and FEEM maps confirmed a shift towards longer wavelengths with prolonged aging. These patterns were further emphasized in differential FEEMs, where the loss of small aromatics in the saturates and aromatics fractions was noted, which reappeared in the more polar fractions (Werkovits et al., 2022, 2024).

Like FTIR spectroscopy, fluorescence spectroscopy can also be used to detect SBS polymers in polymer-modified asphalt binder. This is because SBS exhibits significantly higher autofluorescence than bitumen itself. A study (Polacco et al., 2006) identified the contribution of SBS in fluorescence spectroscopy, showing a strong signal around 350 nm in excitation mode. Surfaces with varying amounts of SBS displayed different intensities of this signal around 350 nm (Maschauer et al., 2022).

5) Nuclear Magnetic Resonance (NMR) Spectroscopy

NMR (Nuclear Magnetic Resonance) spectroscopy is a powerful technique primarily used for analyzing materials that contain elements with an odd number of protons, like hydrogen, carbon, or phosphorus. Given that organic substances such as bitumen are largely composed of these elements, they are well-suited for NMR analysis. However, the complex molecular composition of bitumen, containing millions of different molecules, often results in overlapping signals that can obscure the analysis. Despite this, researchers have successfully employed ^{1}H and ^{13}C NMR spectroscopy to study bitumen, particularly focusing on changes brought about by laboratory aging (Filippelli et al., 2012; Herrington et al., 1994; Lu et al., 2021; Michon et al., 1997; Oliviero Rossi et al., 2018; Pipintakos, Soenen, et al., 2021a; Siddiqui, 2010). However, these studies frequently encounter some challenges due to overlapping spectral bands, necessitating additional post-separation analysis to clarify the results.

At the bitumen level, several studies used ^{1}H and ^{13}C NMR spectroscopy to examine the SARA fractions, revealing trends such as an increase in aromatic carbon content and a decrease in cycloalkane carbon with increasing polarity (Guo et al., 2021; Huang, 2010; Woods et al., 2008). Poly-condensed aromatic rings were also detected in the aromatic, resin, and asphaltene fractions. However, the requirement for separation makes this method cumbersome and less practical. As an alternative, combining different NMR techniques has been explored to address the issue of overlapping signals. This approach was applied by Werkovits et al., (2022) using various NMR techniques like HSQC and ^{31}P NMR on different bitumen samples and their SARA fractions. This provided valuable insights into the H/C ratio, aromatic systems, and the average

molecular size of both the binder and its fractions. For instance, HSQC NMR spectra of bitumen revealed variations in the chain lengths of aliphatic substituents, while ^{31}P NMR identified small quantities of alcohols and carboxylic acids, particularly in the resins, as indicated by characteristic chemical shifts. NMR relaxometry is another technique that has been implemented for studying and developing aging parameters for asphalt binder and mixes (Menapace et al., 2017b; Oliviero Rossi et al., 2018; Szerb et al., 2018; W. Wu et al., 2022). Overall, the application of NMR spectroscopy in bitumen research has increased, but there is still a need for deeper understanding at the chemical level and the integration of NMR with other analytical techniques to achieve more definitive results.

6) Other Techniques

Apart from the analytical methods presented above, other more expensive, time consuming, and frequently inaccessible techniques have also been used. Similar to how NMR spectroscopy uses an electromagnetic field to study the nuclei of molecules, electron paramagnetic resonance (EPR) spectroscopy also employs an electromagnetic field but focuses on unpaired electrons or their spins. Research (Pipintakos et al., 2020; Pipintakos, Soenen, et al., 2021a)explored the oxidation process of bitumen using EPR spectroscopy, integrating it with FTIR spectroscopy, ^{1}H NMR, and Time-of-Flight Secondary Ion Mass Spectrometry (TOF-SIMS). The EPR analysis indicated that carbon-centered radicals are produced during oxidation, while vanadyl-porphyrins remain largely unaffected. Additionally, studies (Rossi et al., 2018b)examined the impact of antioxidants on the aging process by analyzing asphaltenes and maltenes with EPR, combined with rheological studies. The EPR results demonstrated the antioxidants' effectiveness, showing a lower concentration of radicals in the antioxidant-containing fractions. While each technique mentioned in section 2.3.1 have their own strengths and weakness, the power of chemical analysis emerges when complementary methods, such as FTIR and NMR, are combined to reveal a deeper understanding of the asphalt binder material and how its composition changes after undergoing processes such as aging and rejuvenation. Future research is still required in this area, in order to determine different ways in which the data from different testing methods can be combined in a meaningful way.

2.3.2 Rheological Testing Methods

From an engineering standpoint, the performance of asphalt binder is primarily evaluated based on its rheological and physical characteristics. As discussed earlier, the viscoelastic and waterproofing properties of asphalt binder makes it a good choice for road-related applications. In Europe, bitumen is typically classified based on physical properties like penetration depth and softening point. However, these traditional measures, along with viscosity, fall short in differentiating newly developed complex binders. Consequently, efforts in North America, with the development of the SuperPave Grading system, are

moving towards a more comprehensive classification system that includes mechanical and physical characterization, as well as the use of CAS numbers to ensure bitumen quality (Zaumanis et al., 2014).

The adequacy of physical properties alone to fully understand the behaviour of asphalt binder has been questioned for some time. SHRP incorporated time and age-dependent mechanical properties, known as rheology, into its classification system (ASTM D 7175-08, 2008). Bitumen, and by extension, asphalt pavements, can crack at low temperatures if too stiff, and can become prone to rutting at high temperatures when too soft. Two key metrics used to evaluate resistance of asphalt binders to these issues are the fatigue and rutting factors, both derived from the complex shear modulus and phase angle.

These parameters are determined using a Dynamic Shear Rheometer (DSR) in a strain or stress-controlled test. The device applies a consistent rotational or oscillatory strain to a bitumen sample sandwiched between two plates, where the lower plate is fixed. The resulting stress measurement provides the complex shear modulus (G*) and the phase angle (δ), representing stiffness and the lag between stress and strain, respectively. Additional important parameters include the storage modulus G' and the loss modulus G". Selecting the appropriate stress or strain is critical to maintain the linear viscoelastic domain for most rheological evaluations. The typical fatigue and rutting factors mentioned earlier, can be derived from these measurements using $G^*.\sin(\delta)$ and $G^*/\sin(\delta)$ respectively.

Various DSR tests have been developed to assess rheological properties of asphalt binders, with the frequency-temperature sweep being a common method. This test involves subjecting the material to different temperatures across a range of frequencies, which affects the phase angle and complex modulus. A lower phase angle indicates more elastic behaviour, while a higher phase angle suggests a more fluid-like response. Data from these tests can be used to create a master curve, which represents the complex modulus and phase angle over a wide range of frequencies and temperatures.

Master curves are valuable for examining aging, modifications, and susceptibility to specific distress types under varying climatic conditions. The relationship between the phase angle and complex modulus, often displayed in a black space diagram, illustrates the complexity of rheology. These graphs can also highlight polymer activity and the presence of additives in polymer-modified bitumen. A characteristic "feathering" effect is often observed in the master curve when the polymer is active (Margaritis et al., 2021). Additionally, new parameters related to distress resistance, such as the Glover-Rowe parameter and ΔT_c, have been introduced in recent years, providing further insights into the performance and aging of asphalt binders.

The Glover-Rowe (G-R) parameter, for instance, is used as a surrogate for measuring ductility and cracking propensity, with specific thresholds indicating the onset of cracking or severe distress (Anderson et al., 2011; Margaritis et al., 2020). The ΔT_c parameter, initially developed to detect re-refined engine oil in bitumen, has been adapted to evaluate low-temperature performance using a Bending Beam Rheometer

(BBR) (Anderson et al., 2011). Recent developments have also led to the characterization of low temperature properties use a 4 mm DSR plate, which requires less material and offers satisfactory conversion. The advantage of using the DSR for determining low temperature properties of asphalt binder are particularly evident when testing aged binders recovered from pavements, where material availability is limited (Pipintakos, Blom, et al., 2021).

Other rheological tests performed with DSR include the Linear Amplitude Sweep (LAS) test, based on the AASHTO TP101-14 standard, and the Multiple Stress Creep Recovery (MSCR) test, which adheres to both American and European standards. The LAS test assesses damage susceptibility using viscoelastic continuum damage theory and evaluates cracking resistance at various strain levels, simulating weak or strong pavement structures. The MSCR test, which uses a 25 mm plate, evaluates the relaxation and resistance of asphalt binders to permanent deformation by measuring the non-recoverable creep compliance J_{nr} and recovery percentage, R%, after repeated stress cycles (Hintz et al., 2011).

Changes in rheological properties are often indicative of aging, modification, or rejuvenation. Aging typically results in an increase in the complex shear modulus and a decrease in phase angle, whereas rejuvenators tend to have the opposite effect. Aging is also associated with a decrease in ΔT_c, and crossover modulus, and an increase in crossover temperature, frequency, R-value, and G-R parameter. Fatigue life, as assessed through LAS, generally increases with aging for strong pavement structures, while the ability of the material to relax, as measured by MSCR, decreases (Jacobs et al., 2021; Jing et al., 2020).

While similar trends can be observed in polymer-modified asphalt binder, it is important to note that many of the newly developed rheological parameters from frequency sweeps were designed for conventional bituminous binders. Therefore, the application of parameters like the G-R parameter should be approached with caution. The MSCR test is considered the most suitable for evaluating elastomeric polymer-modified bitumen, which shows enhanced J_{nr} and R% values. For more complex binders, such as those containing wax, re-refined engine oil, bio-derived materials, or nanomaterials, the applicability of the time-temperature superposition principle (TTSP) and internal phenomena within the binder should be carefully evaluated (Soenen et al., 2006). The various rheological parameters mentioned and associated implications of them are presented in the table below.

Table 2.6: Summary of Rheological Parameters (adapted from Pipintakos et al., 2024)

Rheological value	Definition	DSR Plate geometry	Evolution with aging	Indication
Crossover modulus (Gc)	The modulus, frequency and temperature at the point where the loss modulus G" coincides with the storage modulus G'	8 and 25 mm	↓	Elastic/viscous transition, brittleness, hardness
Crossover frequency (ωc)		8 mm	↑	Rutting and cracking
Crossover temperature (Tc)				
Shape parameter (R)	Difference between the moduli of glassy behaviour and crossover point	4, 8 and 25 mm	↑	Width of relaxation spectrum, fatigue cracking
Glover-Rowe (G-R)	A parameter based on the complex modulus and phase angle under a specific frequency in correspondence with ductility at the same temperature and specific elongation rate	8 mm	↑	Durability, non-load related cracking
ΔT_c	Difference of two lower continuous grading temperatures related to creep stiffness and relaxation	BBR or 4 mm DSR	↓	Aging-induced cracking

Overall, both rheological and chemical testing are fundamental in understanding the behaviour of both modified and unmodified binders, and this has been the subject of many previous studies. However, a major gap that exists in literature surrounds combining and linking chemical properties to rheological parameters.

2.3.3. Micro-characterization of asphalt binder structure

Over the past 50 years, various techniques have been used to examine the structure of bitumen, which tends to develop unique surface microstructural patterns. Theories such as the 'wax theory' and the 'asphaltene theory' attempt to explain these patterns. The wax theory attributes them to paraffinic waxes, while the asphaltene theory links them to polar asphaltene micelles within the SARA fractions. Scattering techniques like Small-Angle Neutron Scattering (SANS), Small-Angle X-ray Scattering (SAXS), and Wide-Angle X-ray Diffraction (WAXD)(Bunn & Holmes, 1958; Dwiggins, 1965; Eyssautier et al., 2011) have been used in previous studies to understand the microstructure of asphalt binder and provide evidence for these theories. Atomic Force Microscopy (AFM) (Ahmed & Hossain, 2021a) and fluorescent microscopy (Handle et al., 2016) have also been employed to analyze surface microstructures, revealing patterns like 'bee structures' and assessing polymer-modified bitumen. Despite these advancements, questions still remain around the value and impact of information obtained from these techniques due to the challenges associated with linking surface to bulk properties, complicating the correlation between microstructure and rheological properties.

2.4 Common Approaches to Improve Sustainability and Combat Effects of Aging

2.4.1 RAP + Rejuvenators

Reclaimed Asphalt Pavement (RAP) is defined as removed and/or reprocessed asphalt pavement material (National Asphalt Pavement Association, 2010). Being 100% recyclable, RAP is amongst one of the most recycled materials in North America (Ontario Asphalt Pavement Council, 2017) and provides numerous economic and environmental benefits. Production of asphalt pavements from virgin materials requires a constant source of precious non-renewable aggregates and petroleum resources (e.g., bitumen). Incorporation of RAP into asphalt mixes, reduces this demand for, and cost of, enormous amounts of virgin materials, while making the pavement production process more sustainable and cost effective, promoting a circular economy (Ontario Asphalt Pavement Council, 2017; X. Zhang et al., 2020).

Nevertheless, the use of RAP may come with some drawbacks since the binder found in RAP is significantly oxidized. The presence of the oxidized RAP binder typically leads to an increased stiffness and therefore improved rutting resistance. However, when large amounts of RAP are used in asphalt mixes, some performance issues such as fatigue and low temperature cracking can become more likely (Baqersad & Ali, 2019). Agencies, therefore, restrict the amount of RAP that can be recycled in mixtures (Behnood, 2019a). In Ontario, RAP is restricted to 20% and 30% when used in the surface and binder courses respectively. These restrictions, limit the significant benefits that RAP can offer (Baqersad & Ali, 2019; Behnood, 2019a). Consequently, research and investigation into the production of higher content RAP mixtures with performance comparable to virgin mixtures is on the rise. Asphalt mixtures that qualify as high content RAP varies widely depending on location. In Canada, asphalt mixtures that possess a RAP Binder Ratio (RBR) of greater than 25% are considered high content RAP mixtures (Ontario Asphalt Pavement Council, 2017). Literature has found the use of rejuvenators or rejuvenating agents in RAP mixtures could be a promising solution to the issues associated with high RAP content (Ahmed & Hossain, 2021b; Behnood, 2019a).

While it is impossible to reverse the aging of the asphalt binder in RAP, rejuvenating agents aid in the restoration of the physical, chemical, and rheological properties of the asphalt binder, to a level which closely resembles that of virgin binder (S. Yu et al., 2017). During the rejuvenation process, the rejuvenator begins to diffuse and soften the outer layer of aged binder. As the diffusion continues, the viscosity of the aged binder begins to decrease, which allows for mixing and blending of virgin and mobilized aged binder (Carpenter & Wolosick, 1980). The typically mechanism through which asphalt aging occurs was presented earlier. Similarly, with the addition of a rejuvenator, several processes occur simultaneously, which together, are referred to as the rejuvenating mechanism.

2.4.1.1 Rejuvenating Mechanism

The issues associated with aged bitumen in RAP can be combatted with the use of rejuvenators. Aged bitumen is oxidized, and it is impossible to reverse this process, however, rejuvenating agents can help restore the rheological and physical properties to a level that closely resembles that of virgin bitumen (S. Yu et al., 2017). Some rejuvenators can also aid in rebalancing the SARA fractions but are unable to restore the original chemical composition (X. Yu et al., 2014).

There are typically two categories of rejuvenators that are used in the asphalt industry, bio-based and petroleum-based rejuvenators (Behnood, 2019a). Bio-based rejuvenators are made from renewable resources such as vegetable oils and industrial/agricultural waste products. The chemical composition of most commercially available bio-based rejuvenators is proprietary; however, it generally contains a mixture of fatty acids and alcohol (cyclic, branched, or straight chain), esters, and in some cases resin acids and phenolic compounds (Y. Ma et al., 2020). Petroleum-based rejuvenators are made from by-products of the petroleum refining process and contains a mixture of aromatic hydrocarbons, saturates (straight/branched chain hydrocarbons), and highly reactive polar resins (Y. Ma et al., 2020). While the chemical compositions of bio-based and petroleum rejuvenators are quite different, both attempts to restore the physical, chemical, and viscoelastic properties of the asphalt binder by breaking down agglomerated molecules, redispersing SARA fractions and rebalancing the chemical composition.

The rejuvenation process involves the diffusion of rejuvenators into the RAP binder. Typically, there are three factors that affect the rejuvenation mechanism (Behnood & Modiri Gharehveran, 2019; Y. Ma et al., 2020):

1) Dispersion of the virgin binder, aged binder, and rejuvenator in the mixture
2) Diffusion of the rejuvenator into the aged binder
3) Compatibility between the rejuvenator and the binder blends

An important distinction to be made is that dispersion involves physical mixing, but diffusion is the process where aged binder tries to absorb the hydrocarbon-type liquid in the rejuvenators (Kaseer et al., 2019). Literature has suggested four steps that occur in the diffusion process (Carpenter & Wolosick, 1980):

1) The rejuvenator surrounds the highly aged binder layer coating the recycled aggregates
2) The rejuvenator begins to diffuse and soften outer layer of the aged binder
3) As the diffusion process continues, the rejuvenating agent causes the viscosity of the aged binder to decrease allowing for blending and gradual mixing of aged and virgin binder
4) The diffusion process is completed when an equilibrium is reached after a certain time.

The diffusion mechanism of the rejuvenator has been studied in different research, including finite element modeling of the process (Zaumanis & Mallick, 2013) and MD simulations (G. Xu et al., 2018), however, the actual diffusion and rejuvenation mechanism in three component systems (rejuvenator, virgin binder

and RAP binder) is still not fully understood, and this continues to limit the capacity to select suitable rejuvenators (Rajib et al., 2020).

Typically, the diffusion mechanism is modeled using the Stoke-Einstein's equation (2.1) and Fick's Law (2.2).

$$D = \frac{K_B T}{6\pi\mu(R)} \tag{2.1}$$

$$\frac{\partial C}{\partial t} = \nabla.(D\nabla C) \tag{2.2}$$

Where D, is rate of diffusion (m^2/s), R is the mean molecular radius (m), μ is dynamic viscosity (Pa·s), K_BT is the internal heat energy, K_B is Boltzmann's constant ($1.3807 \cdot 10^{-23}$ J/K), T is absolute temperature (K) and C is concentration (mol/m^3).

Zaumanis & Mallick, (2013) simulated the two-component diffusion process between RAP binder and rejuvenator, under ideal conditions using Equations (2.1) and (2.2) and concluded that the diffusion simulation results only partially correlated to bitumen and mix testing results indicating that diffusion may not be the only process taking place in the binder film or the model was insufficient for fully describing the entire process. The binder undergoes chemical and molecular changes and redistribution as diffusion occurs during rejuvenation. Three component diffusion in mixtures with virgin binder, RAP binder and rejuvenator is not well investigated in literature.

One theory proposed for describing how molecules interact in bitumen is a colloidal system, as described earlier, where asphaltenes are dispersed throughout the maltenes phase. Referring to Figure 2.10, in colloidal systems, asphalt binders with low asphaltene content (5-10%) are typically defined as "sol-type" asphalts while binders with high asphaltene content (20-35%) are defined as "gel-type" asphalts (Behnood & Modiri Gharehveran, 2019). Sol-type asphalts typically possess high ductility, high temperature susceptibility and low rate of age hardening, while the opposite is true for gel-type asphalts. Asphalt binders used in practical applications are usually "sol-gel" types that exhibit viscoelastic behaviour. As previously mentioned, aging causes an increase in the asphaltene fraction leading to RAP with aged binder which resembles gel-type asphalts. With the addition of the right amount of rejuvenator to the aged binder, the asphaltene and maltene ratio can be rebalanced to closely resemble that of virgin binder and therefore, an asphalt binder with properties of a sol-gel type asphalt is formed. However, addition of too much rejuvenator to aged binder, can lead to the formation of a sol-type asphalt which has low viscosity and resistance to deformation at high temperatures.

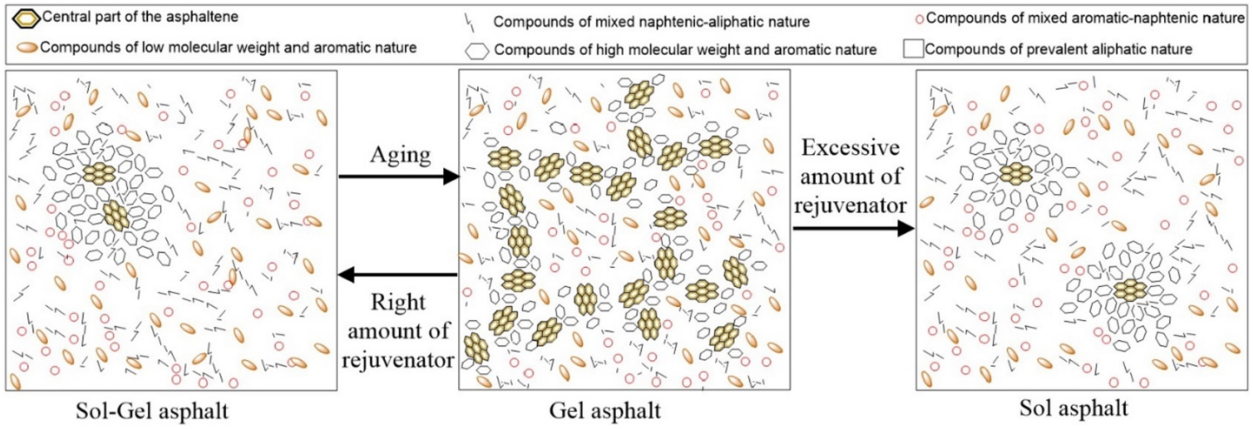


Figure 2.10: Effect of aging and rejuvenation on asphalt binders (Behnood, 2019)

It is necessary to characterize the rejuvenation and diffusion mechanism, in order to properly select rejuvenators that are compatible with asphalt, providing an area of focus for future research. Previous studies which investigated and simulated the diffusion process, have mainly focused on diffusion in an ideal scenario, and have agreed that, in practice, the entire diffusion process does not occur during mixing, and therefore needs time (i.e. storage time) for the rejuvenator to diffuse fully and activate the RAP binder. This therefore means that storage time is crucial to the integrity and performance of the resulting asphalt mix with RAP. Kadhim, (2019), concluded that optimal silo storage time for activation of RAP binder in mixes with up to 30% RAP and no rejuvenator, was between 8 and 12 hours at about 135°C, noting a significant decrease in stiffness after storage for the suggested period of time. Once the RAP binder is activated due to the presence of the rejuvenator, this allows for blending of virgin and RAP binder. The degree/extent of blending is another crucial parameter that influences the resulting performance of RAP mixes. Simulating the diffusion process, as mentioned above, can help with determining and predicting degree of blending (DOB), as well as optimal conditions for maximizing degree/extent of blending.

One significant gap in the current literature on RAP and bio-based rejuvenators is the lack of research on re-aging of RAP mixtures treated with bio-based rejuvenators. Ziari et al., (2019) investigated the effect of three different rejuvenating agents, Cyclogen (aromatic extract), Rapiol, and Waste Cooking Oil (WCO), on RAP mixtures. The study utilized 50% RAP mixtures and evaluated performance by conducting resilient modulus, dynamic creep, indirect tensile fatigue and intermediate-temperature fracture test. It concluded that all rejuvenating agents were effective in restoring the performance to similar levels as that of virgin HMA. However, the aging resistance of RAP mixtures containing bio-based rejuvenators was low when compared to virgin HMA and those containing petroleum-based rejuvenators. A possible reason for this could be the higher amount of oxygen in bio-based rejuvenators (Behnood, 2019a). This is contrary to previous studies done by Borghi et al., (2017) and Kaseer et al., (2018), which both agreed that bio-rejuvenators incorporated into aged binders displayed excellent resistance to re-aging. Additionally,

Ingrassia et al., (2020) concluded that bio-based oils such as those derived from wood demonstrated aging resistance that was better than virgin base asphalt. Future studies in this area, with a variety of different rejuvenators are required to investigate the validity of these study and verify or disprove findings. Furthermore, comprehensive studies, that closely replicate asphalt aging in the field, considering all or a combination of factors such as UV exposure, moisture, oxygen exposure and volatilization is needed to effectively evaluate the aging characteristics of rejuvenated binders and mixtures.

2.4.2 SBS

Asphalt pavements inevitably experience a process called aging, over their service life, intensifying distresses such as rutting and cracking. Styrene Butadiene Styrene (SBS) triblock co-polymer, a thermoplastic elastomer, has been widely used as a modifier in asphalt binders to improve and prolong pavement service life (T. Ma et al., 2012a). Styrene in the polymer is referred to as the hard block, and gives SBS its strength, while butadiene, the soft block, yields the elastic nature of the polymer due to the presence of the carbon-carbon double bond (C = C) (T. Ma et al., 2012a; F. Wang et al., 2020b). Due to these unique properties of SBS, when added to asphalt binders it has been shown to reduce low-temperature stress cracking and improve rutting resistance (T. Ma et al., 2012a; F. Wang et al., 2020b). Moreover, several studies have also confirmed the ability of SBS to improve the aging resistance of asphalt binders and, therefore, resulting pavement structures (Penetration, 2013; F. Wang et al., 2020b), using conventional rheological tests (Cong et al., 2021), viscosity tests (Davidson et al., 2014) and chemical tests (M. F. Ali & Siddiqui, 2001).

Studies conducted on both aged and unaged SBS-modified asphalt binder (M. F. Ali & Siddiqui, 2001; Shan et al., 2019), confirmed through Fourier Transform Infrared (FTIR) spectroscopy, that less oxygen containing groups (carbonyls, hydroxyls and sulfoxides) are formed in SBS modified binders when compared to neat bitumen at the same aging levels. SBS was also found to degrade during aging (Hossain & Wasiuddin, 2019). It is important to note however, that most studies described in the latter (Cong et al., 2021; Davidson et al., 2014; Słowik, 2017), only considered conventional laboratory aging methods for asphalt binders, such as short term, Rolling Thin Film Oven (RTFO), and long-term Pressure Aging Vessel (PAV) thermo-oxidative aging. Research considering Ultraviolet (UV) aging in addition to thermo-oxidative aging indicated that UV plays a critical role in the aging process of SBS-modified binders, with some studies claiming that after UV aging, most or all of the SBS present in the binder was degraded. In contrast, thermo-oxidative aging, for the same time duration, yielded less SBS degradation (Hossain & Wasiuddin, 2019). SBS co-polymer is sometimes considered as a sacrificial component, oxidizing in preference to the asphalt binder, resulting in slower aging of the asphalt binder (Shan et al., 2019; Słowik, 2017).

The interaction between SBS and asphalt binder is widely considered as more of a physical interaction where cross-linking, entanglement and different intermolecular forces exist due to the long chain structure of SBS, resulting in enhanced performance (Yilmaz & Çeloğlu, 2013). However, as the modified binder ages, when exposed to UV radiation, heat, moisture and oxygen, chemical reactions can occur, one of which is oxidation reactions, causing the breakdown and degradation of components in both the SBS polymer and the asphalt binder itself (Słowik, 2017). This can lead to changes in behaviour and performance. One specific property that has been shown to improve with the addition of SBS to asphalt binders, but also changes with aging levels is temperature sensitivity. The temperature sensitivity of an asphalt binder refers to how much the material property changes within a given temperature range (Penetration, 2013; Shan et al., 2019; F. Wang et al., 2020b). Low-temperature sensitivity is usually desirable for asphalt binders since it allows the material to maintain its suitable properties over a larger temperature range. SBS-modified asphalt binder has been shown to have a lower temperature sensitivity when compared to neat asphalt binders. As asphalt binder ages (whether modified or unmodified) the temperature sensitivity increases which can lead to pavement distresses (Osmari et al., 2019b).

A major challenge related to polymer-modified binders, especially with SBS, is the lack of appropriate tests and methods for characterizing performance and grading. The current Superpave Performance Grading (PG) system is more suitable for unmodified binders (Takahashi et al., 2019a). With the development of the PG Plus and MSCR test, some performance aspects of SBS-modified asphalt binders can be better quantified. However, it is still inadequate. Another important consideration when modifying asphalt binder is its compatibility with SBS (K. Wang et al., 2019). Compatibility primarily depends on the asphalt chemical composition, the equilibrium of the asphalt colloidal structure and the nature and characteristics of the SBS (L. Ma et al., 2011b; Pipintakos, Soenen, et al., 2021a). Chemical composition is important in determining the physical properties and performance of asphalt (Werkovits et al., 2023). The composition information is useful for improving asphalt performance through modification additives, blending, etc. Altering molecular interactions in asphalt by the addition of SBS modifiers can improve the durability and properties of the asphalt binder (Khavandi Khiavi et al., 2021b). A better understanding of the chemistry of asphalt and intermolecular interactions of components, both those initially present and those formed during the aging process or by treatment with SBS and other additives, can result in significant improvements to asphalt products with better performance and durability (Qiu et al., 2022; Werkovits et al., 2023). The use of advanced chemical testing methods like FTIR and NMR spectroscopy in combination with conventional tests can allow for a more comprehensive understanding of the behaviour and performance of SBS-modified asphalt binder (Betancourt Cardozo et al., 2016; W. Wu et al., 2022). Although, NMR can capture more revealing information about structures and composition when compared to FTIR, literature on the use of NMR with asphalt binders, modified and unmodified, is still limited.

2.4.3 Anti-aging additives

In recent years, the incorporation of UV-blocking materials as modifiers has gained attention for their potential to prevent asphalt aging. Various anti-UV aging methods have been developed, addressing the primary pathways of UV-induced aging mentioned earlier. These methods primarily involve the use of anti-aging agents, which can be broadly categorized into four groups (Camargo et al., 2021; Y. Li et al., 2022b):

1. UV Absorbers: These compounds absorb harmful UV radiation and convert it into less damaging forms of energy, such as vibrational energy or secondary radiation (e.g., fluorescence). Notable examples include octabenzone and bumetrizole, which absorb UV light within the 240-340nm and 270-380nm ranges, respectively. By selectively absorbing these harmful wavelengths, UV absorbers improve the resistance of asphalt binder to UV aging.
2. Antioxidants: These compounds function as either primary antioxidants (free-radical scavengers) or secondary antioxidants (peroxide inhibitors) and play a crucial role in slowing down the oxidative degradation process, thereby extending the service life of asphalt binders and pavements as a whole.
3. UV Stabilizers: These agents shield or absorb UV light, disrupt the formation of reactive oxygen species, and decompose hydroperoxides into inactive substances. For instance, Tinuvin 770, a hindered amine stabilizer, enhances heat resistance when used in combination with antioxidants, further improving the anti-aging performance of asphalt.
4. Inorganic Fillers and Nanomaterials: Materials such as titanium dioxide, silica, graphene oxide, and montmorillonite (MMT) are used as fillers to enhance UV resistance. These materials either convert light to heat or act as barrier materials, increasing the diffusion path length for oxygen and reducing its penetration rate. Additionally, they scatter or reflect UV light, weakening its impact on the asphalt binder.

Several studies have evaluated the effectiveness of various UV aging modifiers, including layered double hydroxides (LDHs), organomontmorillonite (OMMT), and carbon black (CB). These studies have found that modified asphalts generally exhibit better resistance to UV-induced aging compared to unmodified asphalts. For example, LDHs, with their sheet-like structure, not only physically block UV radiation but also absorb it, significantly enhancing the rheological and fatigue properties of asphalt. In contrast, carbon black, an organic protective material, effectively absorbs UV radiation and improves low-temperature properties (J. Hu et al., 2017b).

Inorganic UV-blocking materials like titanium dioxide and silica convert UV light into heat, while nanocomposites such as MMT have layered structures that enhance the diffusion properties of oxygen, further improving UV resistance. These materials provide chemical stability and good thermal performance, making them more durable in engineering applications compared to organic additives.

Recent studies have also explored natural antioxidants such as phospholipids, ascorbic acid (Vit. C), and lignin from rice husks for their potential to reduce age hardening in asphalt binders. When tested using the Rolling Thin Film Oven (RTFO) method, phospholipids-treated binders exhibited the highest resistance to oxidation, with the smallest increase in stiffness after aging(Rossi et al., 2018b). This highlights the potential of these abundant, natural, and environmentally friendly materials as effective anti-aging agents.

Other common factors that can be manipulated to reduce or slow aging include air void content of asphalt mixes and the use of conventional fillers, such as mineral powder with particle sizes below 0.075 or 0.063 mm, have been shown to improve the resistance of asphalt to photo-oxidative aging. These fillers contain open micro voids on their surfaces that can absorb polar molecules like ketones, anhydrides, and carboxylic acids—compounds prone to oxidation (Lesueur, 2009b; Y. Li, Wu, et al., 2020b). By absorbing these molecules, fillers provide a protective effect against oxidation. Residual air voids in pavements are a critical factor influencing UV aging. Asphalt mixes with low air void content (<5%) exhibit lower aging rates, while those with higher air void content (>7%) show intensified aging, particularly due to increased moisture penetration. Fine-graded asphalt mixes, which have smaller air voids, are generally better at preventing sunlight infiltration and reducing the contact area between oxygen and the asphalt mixture, thereby minimizing aging(Charrié-Duhaut et al., 2000).

In summary, a traditional filler is a crucial component in the asphalt mixture design process, as it provides a means to slow down oxidation by absorbing some of the smaller molecules in the asphalt binder, thereby shielding and protecting them from oxidation. While this can positively impact the anti-aging properties of the asphalt binder, the improvement might be somewhat limited. Antioxidants and light stabilizers primarily work by reducing the rate of UV aging in asphalt, thereby enhancing the resistance to UV aging; this is achieved by slowing the oxidation process. However, when organic antioxidants, UV absorbers (UVAs), and light stabilizers are used alone, their effectiveness diminishes over time, which presents limitations in engineering applications. Compared to organic aging-resistant materials, inorganic UV-barrier materials offer advantages such as chemical stability and good thermal stability. These inorganic materials can scatter or reflect UV light at the interface, thereby reducing the amount of UV radiation that penetrates the asphalt and consequently slowing the oxidation process, reducing volatilization. Apart from the few mentioned above, there are a significant number of studies on the performance of a variety of different anti-aging additives in asphalt binders and mixes. The table presented below, while not exhaustive, presents a summary of the most widely tested anti-aging additives and the references in which they can be found.

Table 2.7:Summary of anti-aging additive used in literature (modified from Camargo et al., 2021)

Additive and Additive Content Range (wt%)	**Reference**
(3-Aminopropyl) triethoxysilane (APTES) surface-modified silica nanoparticles (SNPs) (4%)	Karnati et al., 2019
Bumetrizole (0.5–0.6%)	Cong et al., 2013b; Feng et al., 2016; Kuang et al., 2014; Tan et al., 2008b
Calprene 6120 (3%)	Dessouky et al., 2015; Kassem et al., 2019
Carbon black (0.5–5%)	Cong et al., 2013b; Kassem et al., 2019; Nare & Hlangothi, 2019; Tan et al., 2008b
Crumb rubber modifier (CRM) (8–16%)	Ali et al., 2013; Ghavibazoo et al., 2015; Yin et al., 2013
Crumb rubber (CR) treated with gamma radiation or irradiated by microwave (5–15%)	Ibrahim et al., 2015; Yin et al., 2013
Diatomite (2–16%)	Baldi-Sevilla et al., 2016; Cong et al., 2016; P. Zhang et al., 2019
Dilaurylthiodipropionate (DLTDP) (1–1.5%)	Apeagyei, 2011
Furfural (1–5%)	Apeagyei, 2011; Fini et al., 2016
Hydrated lime (1–20%)	Apeagyei, 2011; Kassem et al., 2019; Lesueur et al., 2016; Nare & Hlangothi, 2019
Hydrophobic diatomite (4%; 8%; 12%; 16%)	Cong et al., 2016
Irganox E201 (3%)	Dessouky et al., 2015
Irganox 1010 (0.2–10%)	Apeagyei, 2011; Kassem et al., 2019; Kuang et al., 2014; Nare & Hlangothi, 2019; Zhao et al., 2015
Irganox 1076 (3%)	Dessouky et al., 2015
Layered double hydroxides (LDHs) (2–5%)	Wu et al., 2012; S. Xu et al., 2015; C. Zhang et al., 2016
Lignin (2–10%)	Arafat et al., 2019; G. Xu et al., 2017
Limestone fillers (20%)	Lesueur et al., 2016
Micronized Polyethylene Terephthalate (Pet) Waste (4–6%)	Arimateia Almeida E Silva et al., 2015
Nanosila (2–6%)	Baldi-Sevilla et al., 2016; Fini, Hajikarimi, et al., 2016; Karnati et al., 2019; Yao et al., 2013
Nano calcium carbonate (CaCO3) (4%)	Nazari et al., 2018
Nano silicon dioxide (SiO2) (4%)	Nazari et al., 2018
Nano titanium dioxide (TiO2) (4%)	Nazari et al., 2018
Naphthenoil oil (1%)	Ouyang et al., 2006; Yuan et al., 2019
Octabenzone (0.5–0.6%)	Cong et al., 2013b; Feng et al., 2016; Kuang et al., 2014; Tan et al., 2008b
Organic intercalated layered double hydroxides (OLDHs) (3%)	S. Xu et al., 2015
Organo-montmorillonite (OMMT) (3%)	Yu et al., 2009
Phenol-formaldehyde resin (2%)	Zaidullin et al., 2013
Phenyl-β-naphthylamine (2%)	
Phospholipids (Commercial mix) (2%)	Rossi et al., 2018b
Redicote AP (1%)	Dessouky et al., 2015
Rice husk (2%)	Rossi et al., 2018b
Sulphore 1205 (2–3%); Solprene 4318 (3%)	Dessouky et al., 2015
Tinuvin 770 (0.6%)	Feng et al., 2016
Triethoxyvinylsilane surface organic modified layered double hydroxides (TEVS-LDHs) (2%; 4%)	C. Zhang et al., 2016
Vitamin C (2%)	Rossi et al., 2018b
Vitamin E (1–6%)	Apeagyei, 2011; Dessouky et al., 2013; Kassem et al., 2019; Zhao et al., 2015
Zinc dialkyldithiophosphate (ZDDP) (1%)	Cong et al., 2013b; Ouyang et al., 2006a, 2006b; Tan et al., 2008b
Zinc diethyldithiocarbamate (1–4%)	Adwani et al., 2023; Haghshenas et al., 2019
Carbon black (5%) + Dilaurylthiodipropionate (DLTDP) (1.5%)	Apeagyei, 2011
Carbon black (3%) + Irganox 1010 (3%)	Kassem et al., 2019
Carbon black (3%) + Vitamin E (3%)	Cong et al., 2012; Cong et al., 2013
Carbon black (1%) + Octabenzone (0.5%)	Apeagyei, 2011
Carbon black (1%) + Bumetrizole (0.5%)	
Furfural (2%) + Vitamin E (2%)	
Furfural (1.5%) + DLTDP (2%)	Kassem et al., 2019
Irganox 1010 (1%) + Dilaurylthiodipropionate (DLTDP) (1%)	Kassem et al., 2019

The integration of UV absorbers, antioxidants, and inorganic fillers into asphalt binders has proven effective in enhancing resistance to UV-induced aging. While organic additives like antioxidants and UV stabilizers initially show promising results, their performance may diminish over time. This limits their long-term effectiveness in real-world applications. In contrast, inorganic UV-blocking materials offer greater chemical and thermal stability, making them more suitable for long-term use. Further research is required to explore the synergistic effects of combining these additives to develop more robust solutions for extending the lifespan of asphalt pavements.

2.5 Summary of Literature Review

Asphalt pavements are a fundamental part of facilitating transportation. They are made up of aggregates and asphalt binder (obtained from crude sources), both of which are non-renewable resources, causing negative environmental impacts. Pavement performance and service life are directly related to the asphalt binder, which acts as the adhesive that holds the aggregates together resulting in useable pavement structure. This binder is prone to aging, which can lead to an exacerbate pavement distresses such as permanent deformation and different types of cracking. This literature review presents an in-depth overview of asphalt binder chemistry and the mechanisms directly affecting the aging process. As aging occurs, this ultimately reduces the service life of asphalt pavements. Therefore, one of the main tasks of research within the asphalt pavement industry is developing ways for increasing sustainability of asphalt pavements, without compromising performance and prolonging service life.

Three of the main ways that have been proposed in this literature review include:

1) Use of RAP and rejuvenators to reduce the constant need for precious and non-renewable resources.
2) Use of polymers, mainly SBS, to improve performance and slow aging.
3) Use of anti-aging additives to reduce aging and prolong service life.

Although these three areas have been investigated in different ways, as presented throughout literature review above, several gaps still remain and were identified as follows:

- Although NMR has been employed to analyze the molecular composition and structural characteristics of asphalt, there is limited research on how these properties evolve specifically during the aging process. The existing studies often focus on short-term aging, leaving a significant knowledge gap regarding long-term aging (thermo-oxidative and UV) effects and the associated chemical transformations. Information regarding sample preparation methods, experimental protocol, and normalization/data analysis methods are also missing. Regarding 2-D NMR, not only are there few studies available, but the methods for analyzing data to extract valuable information are also quite limited.

- Despite the advancements in understanding asphalt binder aging, there remains a significant gap in the literature regarding the combined use of NMR and FTIR, which are easily available and relatively simple testing methods, for analyzing the aging of both modified and unmodified asphalt binders. While individual studies have explored these techniques separately, the integration of NMR and FTIR data using multivariate analysis techniques is underexplored. Moreover, there is limited research assessing the repeatability and reliability of these techniques, which is crucial for establishing robust and reproducible methodologies in asphalt binder analysis.
- While thermo-oxidative aging has been extensively studied, particularly in relation to its impact on the long-term durability and performance of asphalt, UV and multi-factor aging remains less explored with limited standardization. UV and moisture exposure can significantly alter the chemical and rheological properties of asphalt binders. Moreover, there is a need for more comprehensive research comparing UV to thermo-oxidative aging in addition to linking changes in chemical properties induced by these aging processes to the corresponding changes in rheological properties. Understanding these connections is crucial for predicting the long-term performance of asphalt pavements under various environmental conditions.

Chapter 3

Research Methodology

3.1 Scope

This chapter provides a brief overview of the materials and methods employed throughout the research. Chapters 4 through 6 focus on the chemical and/or rheological characterization of various modified and unmodified asphalt binder blends, examined at multiple ageing stages. This thesis was written using a paper-based format, therefore, each subsequent chapter presents a detailed description of the materials and methods specific to its scope, the purpose of this chapter is to offer a holistic view of the research and illustrate how the chapters are interconnected.

3.2 Materials and Methods

Chapter 4 provides a detailed examination of the repeatability, reliability, and application of Attenuated Total Reflection–Fourier Transform Infrared (ATR-FTIR) spectroscopy in distinguishing unmodified asphalt binders based on their crude sources and ageing states. Three unmodified base binders, labeled A, B, and C, sourced from different crude oils, were selected for this study. Short-term and long-term ageing simulations were performed on each binder using the Rolling Thin Film Oven (RTFO) and Pressure Aging Vessel (PAV) methods, following AASHTO standards. In this chapter, PAV ageing was conducted for 20 hours. Samples for ATR-FTIR analysis were prepared using two different methods—one prepared using a small sample quantity (<1g) and the other prepared using a larger quantity of asphalt binder (>5g) directly from the metal storage cans. Figures below show the prepared samples and ATR-FTIR equipment used. A comparison between these two preparation methods was conducted to determine which preparation method is more suitable for obtaining repeatable results.



Figure 3.1: Prepared ATR-FTIR samples before testing.

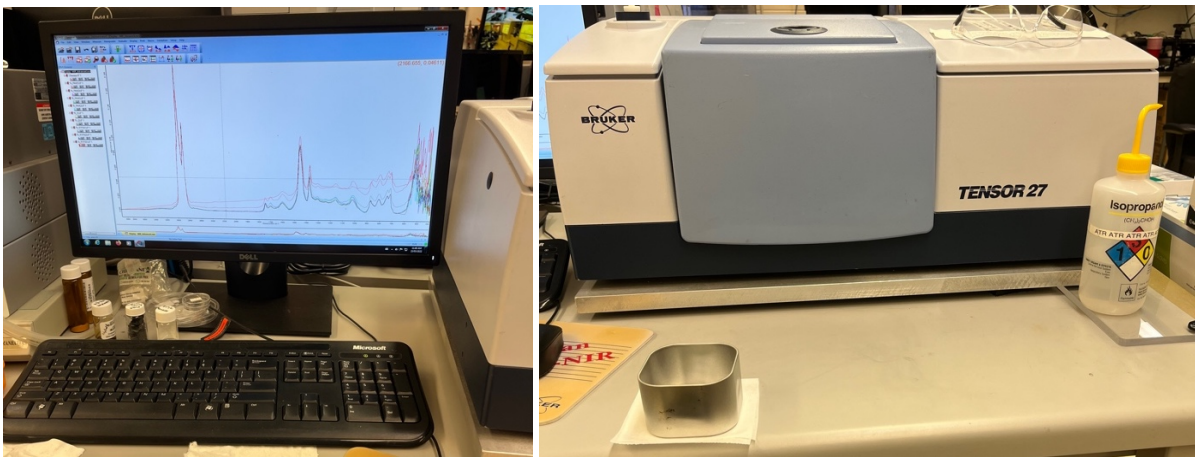


Figure 3.2:ATR-FTIR equipment and set up for data collection.

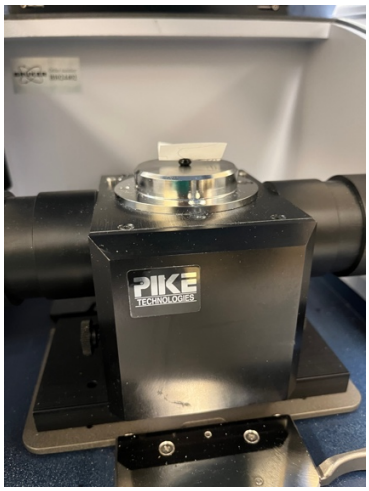


Figure 3.3:Asphalt binder sample placed on ATR-FTIR diamond crystal.

Chapter 5 investigates the effects of Styrene-Butadiene-Styrene (SBS) modification on binder performance and ageing behaviour. Two different base binders from those used in Chapter 4, graded PG 58-28 and labeled A and B, were modified with 2% and 4% SBS. The details of the modification process, including how the SBS was incorporated into the binders, are thoroughly outlined in this chapter. Both unmodified binders, along with their SBS-modified counterparts, were aged using the RTFO method, followed by 20, 40, and 60 hours of PAV ageing to monitor the evolution of binder and polymer properties under different stages of thermo-oxidative ageing. Samples from each ageing state (unaged, 20-, 40-, and 60-hours PAV-aged) were tested using the Dynamic Shear Rheometer (DSR) for temperature-frequency sweeps, as shown in Figure 3.4, the Bending Beam Rheometer (BBR) for low-temperature stiffness and relaxation properties (samples shown in Figure 3.5), and ATR-FTIR and Nuclear Magnetic Resonance (NMR) spectroscopy (shown in Figure 3.6) for chemical analysis. Master curves were constructed using DSR data, while low-performance grade (PG) temperature and the ΔTc parameter were derived from BBR data. Spectroscopic

data were analyzed to quantify functional groups and chemical environments, using FTIR and NMR data respectively. Thereafter, multivariate analysis techniques were employed to explore these relationships between spectroscopic data and rheological properties.

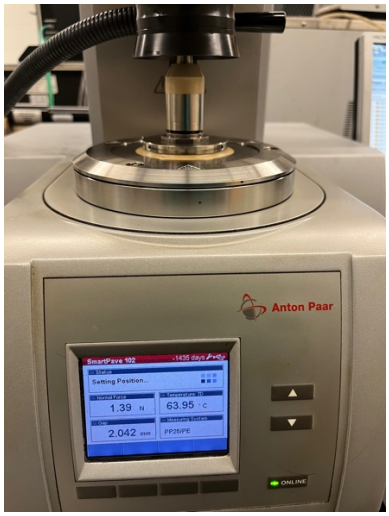


Figure 3.4: Asphalt binder sample being tested in DSR.

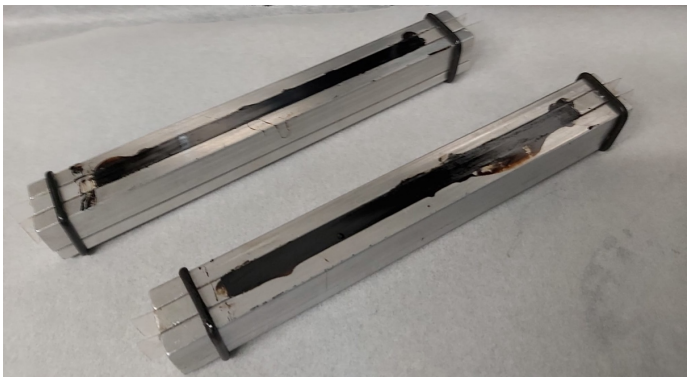


Figure 3.5: Asphalt binder beams prepared for testing in the BBR.



Figure 3.6: NMR spectroscopy equipment.

Chapter 6 presents a comparative study of the performance of both modified and unmodified asphalt binder blends under two ageing conditions: UV exposure (primarily UVa) with water spray cycles and thermo-oxidative ageing via PAV (Figure 3.9). A novel UV ageing chamber, as shown in Figure 3.8, was designed specifically for this research. A third base binder, labeled IO and graded PG 58-28, different from the base binders used in Chapters 4 and 5, was used exclusively throughout chapter. In addition to the unmodified binder, the study included IO blends modified with anti-ageing additives and two RAP-Virgin-Rejuvenator blends, with RAP binder that was extracted and recovered from a single source RAP obtained from a local asphalt plant. The bio-based rejuvenators A and B were incorporated into these blends at optimal dosage of 4.01% and 4.03% respectively. The anti-ageing additives used were Zinc Diethyldithiocarbamate (ZDC) at concentrations of 3%, 4%, and 5%, and ascorbic acid (Vit. C) at concentrations of 1%, 2%, and 3% (shown in Figure 3.7). The blending methods for incorporating these additives into the IO binder are detailed in chapter 6. A total of nine unaged blends were evaluated, including three ZDC-modified blends, three Vit. C-modified blends, the unmodified IO binder, and two RAP-Virgin-rejuvenator blends. All blends underwent short-term ageing via RTFO before UV or PAV ageing. UV ageing was performed on all blends for six days, after which the best-performing anti-ageing blend, the best-performing RAP-Virgin-rejuvenator blend, and the IO base binder (as a control) were subjected to extended UV ageing for up to 21 days. For PAV ageing, all blends were aged for 40 hours, except the unmodified IO binder, which was aged for both 20 and 40 hours. The same set of rheological (DSR, BBR) and spectroscopic (NMR, ATR-FTIR) tests conducted in Chapter 5 were applied to the unaged and aged samples.

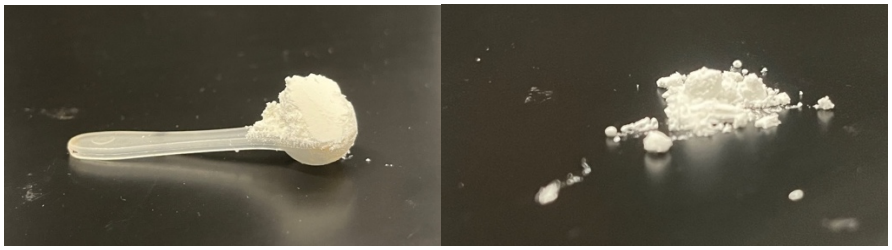


Figure 3.7:Anti-aging additives, Ascorbic Acid (Vit.C), (left) and Zinc Diethyldithiocarbamate (ZDC) (right).



Figure 3.8:Constructed UV aging Chamber.



Figure 3.9: (a) Metal pan with RTFO aged binder, (b) Sample rack, (c) Pressure vessel

3.3 Overview of Material and Methodology

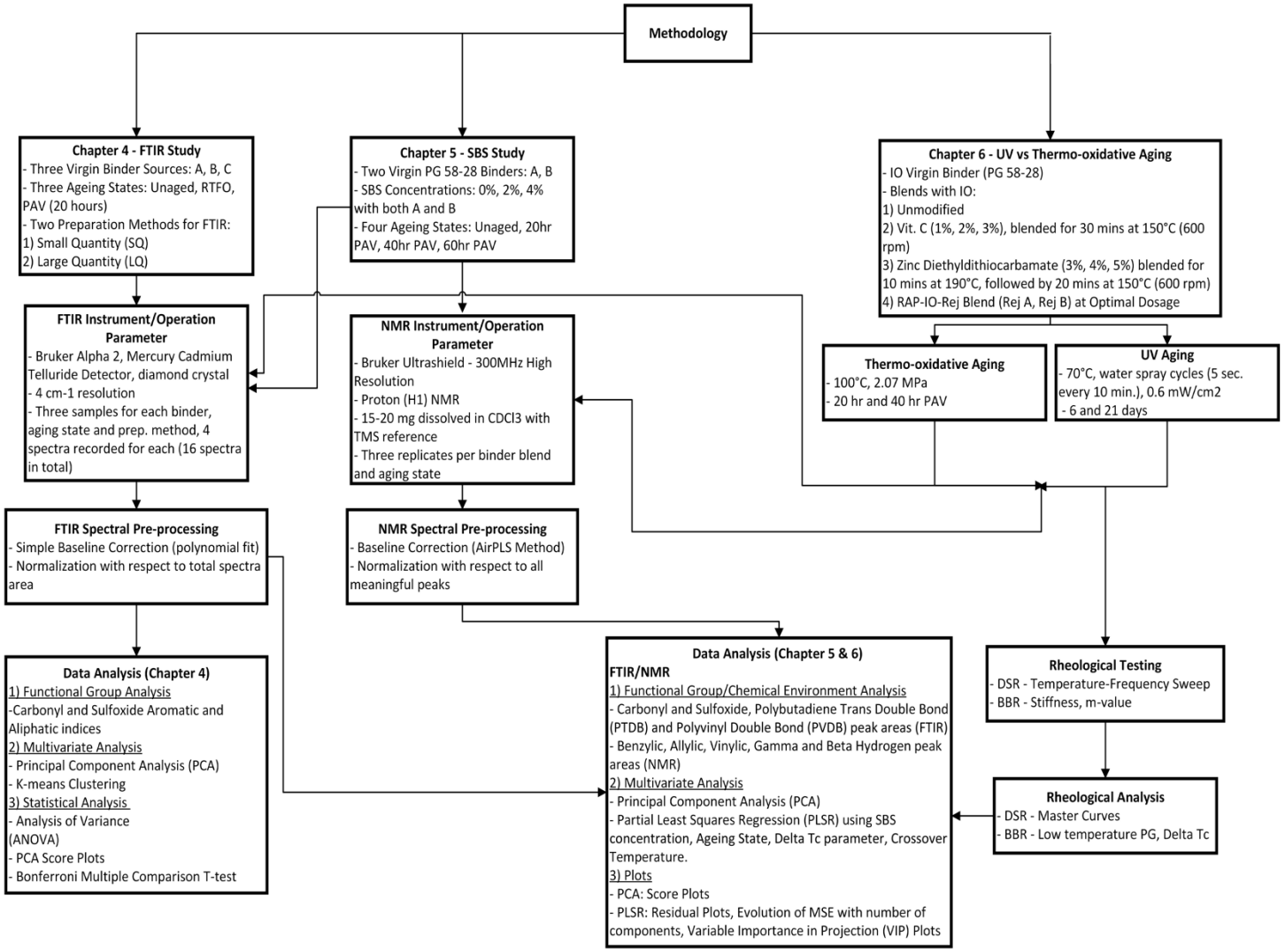


Figure 3.10:Summary of the materials and methods used in each chapter throughout research

Chapter 4

Repeatability of FTIR in Characterizing Unmodified Binder Sources and Aging States

4.1 Introduction

Over the past two or three decades, Fourier Transform Infrared (FTIR) spectroscopy has played a crucial role in the asphalt industry (Baqersad & Ali, 2019; L. Ma et al., 2011a; Rathore & Zaumanis, 2020; Z. Wang et al., 2020). Recently, Attenuated Total Reflection (ATR) – FTIR has garnered increased interest due to its straightforward and rapid analytical capabilities (Baqersad & Ali, 2019; Margaritis et al., 2019; Mikhailenko et al., 2016; Yan et al., 2022a). Major applications of ATR-FTIR include 1) Quality Control for both modified and unmodified binders (Khavandi Khiavi et al., 2021a; T. Ma et al., 2012b; F. Wang et al., 2020a), 2) Surface property evaluation for identifying binder sources and modifiers (Margaritis et al., 2019; Pipintakos, Soenen, et al., 2021b), and 3) Investigating Chemical Changes due to processes such as thermo-oxidative ageing, Ultraviolet (UV) ageing, and water exposure (Baqersad & Ali, 2019; L. Ma et al., 2011a; Rathore & Zaumanis, 2020; T. Zhou et al., 2020). Although ATR-FTIR is an extremely powerful tool that offers a lot of insight into the chemical and molecular compositions/structures, as well as ageing state of the binder, and numerous studies, mentioned earlier, have been performed using ATR-FTIR, there are still no standardized methods for sample preparation and conducting the test. Based on the type of instrument used, and sample preparation method, variability and repeatability of results can differ significantly, if careful consideration is not taken when preparing samples and running the test (Margaritis et al., 2019; Mirwald, Nura, et al., 2022b). This highlights the need for standardization.

In this chapter, ATR-FTIR was performed on asphalt binders from three difference sources at three different ageing levels, using two of the most widely used sample preparation techniques found in literature with replicates. Using this data, after pre-processing (baseline correction, normalization), different multivariate analysis techniques were used to firstly, evaluate the repeatability and variability of ATR-FTIR, secondly, determine whether there are statistically significant differences between the different sample preparation methods, and lastly, establish if ATR-FTIR can be used for distinguishing between different binder sources and ageing states. The main multivariate analysis techniques used in this chapter include Principal Component Analysis (PCA) and k-means cluster analysis. Since the results of ATR-FTIR include spectral data, which includes a large number of variables, these techniques help to analytically reduce dimensionally and reduce/remove noise, while maintain important variables and information contained in the spectra.

4.2 Material Preparation and Methodology

Three binders from different sources, hereafter referred to as A, B, and C, were sourced and used for the testing performed in this chapter. For each binder source, Rolling Thin Film Oven (RTFO) followed by Pressure Ageing Vessel (PAV) ageing protocols according to AASHTO T 240-22 (AASHTO T 240, 2013) and ASTM D6521 (ASTM, 2022) respectively were performed, and binders were stored in metal cans. For each source and ageing state, ATR-FTIR was conducted following protocols described by RILEM TC 295 – FBB TG1 Fingerprinting bituminous binders using physico-chemical analysis (Mirwald et al., 2022). Two different sample preparation methods were followed. The first method (Small Quantity - SQ) involved using a spatula to remove a small quantity (< 1g) of binder from the metal can which was then heated using a hot plate at 180°C. A thermometer probe was used to continuously stir the binder and monitor the temperature. Once the binder was flowable, the probe was used to place a small drop of the binder onto a piece of paper. The second method (Large Quantity - LQ) followed a similar procedure as that described above, but a larger quantity of the binder (> 5g) in the storage metal can was heated in the oven. Thereafter, binder drops were made for testing. For each sample and method, four replicates were prepared. All sample underwent ATR-FTIR testing within two hours of sample preparation using a BRUKER Alpha 2 spectrometer with a Mercury Cadmium Telluride detector and a diamond crystal. A spectral resolution of 4 cm^{-1} , 24 scans, and a range of 4000 – 600 cm^{-1}, in the OPUS software was used for acquiring the spectrum for each droplet. The crystal was cleaned before and after each droplet measurement using kerosene followed by isopropyl alcohol. For each droplet, a background measurement was taken, after which the sample was placed on the crystal and slight pressure was applied to the drop to ensure good contact with the crystal. Four spectra were recorded for each droplet, resulting in a total of 16 spectra for each binder type at a single ageing state and preparation method. The following table summarize the different binder types and ageing states used in this chapter. All spectral data collected were preprocessed using baseline correction and normalized using the height of the largest peak. Conventional analysis using carbonyl and sulfoxide peaks was performed in addition to PCA and k-means multivariate analysis.

Table 4.1: Different Asphalt Binder Types and Ageing States tested using ATR-FTIR

Binder Source	Ageing States	Method 1 - SQ	Method 2 - LQ
A	Unaged	16 spectra for each binder type at a specific ageing state (36 seconds to acquire each spectrum)	16 spectra for each binder type at a specific ageing state (36 seconds to acquire each spectrum)
	Rolling Thin Film Oven (RTFO) Aged		
	Pressure Ageing Vessel (PAV) Aged		
B	Unaged		
	Rolling Thin Film Oven (RTFO) Aged		
	Pressure Ageing Vessel (PAV) Aged		

C	Unaged		
	Rolling Thin Film Oven (RTFO) Aged		
	Pressure Ageing Vessel (PAV) Aged		

4.2.1 FTIR Spectra Functional Group Analysis

Carbonyl indices (CI) and sulfoxide indices (SI) were calculated to examine differences in ageing levels, and compared for different binder sources, using spectral data after pre-processing. Both the CI and SI have been widely used in previously literature (Baqersad & Ali, 2019; Hettiarachchi et al., 2020; Mikhailenko et al., 2016; T. Zhou et al., 2020) to indicate and evaluate ageing levels and potential. The noted trends indicate that both CI and SI increase upon ageing, with CI showing more pronounced increases. Other indices presented in previous studies (Gui et al., 2023; Pipintakos, Soenen, et al., 2021b; Redelius & Soenen, 2015) include the aromaticity index (ArI), and aliphatic index (AlI), which are known to have different trends with increasing ageing level based on the source of the binder. The equations presented below were used for calculating these four indices.

$$\text{Sulfoxide Index (SI)} = \frac{A_{1030}}{\sum A} \quad (4.1)$$

$$\text{Carbonyl Index (CI)} = \frac{A_{1700}}{\sum A} \quad (4.2)$$

$$\text{Aromaticity Index (ArI)} = \frac{A_{1600}}{\sum A} \quad (4.3)$$

$$\text{Aliphatic Index (AlI)} = \frac{A_{1460}+A_{1376}}{\sum A} \quad (4.4)$$

where ∑A is defined as the sum of the peak areas at wavenumbers 2952, 2862, 1700, 1600, 1460, 1375, 1030, 864, 814, 743 and 724 cm^{-1}(Gui et al., 2023). A_{1700}, A_{1600}, A_{1460}, A_{1376} and A_{1030} are defined as the area under peaks located at 1700 cm^{-1}, 1600 cm^{-1}, 1460 cm^{-1}, 1376 cm^{-1} and 1030 cm^{-1} respectively. After calculating these indices, the variance, repeatability and reliability of using these indices for determining different ageing levels were evaluated using Analysis of Variance (ANOVA).

4.2.2 FTIR Multivariate Analysis

Multivariate methods are typically comprised of a large number of advanced statistical techniques. There are a variety of different techniques all of which are somewhat complementary. In these section, one popular method, widely used for spectral analysis and exploratory purposes, namely Principal Component Analysis

(PCA), was discussed. k-means clustering, a specific type of clustering technique for quantifying groupings determined from multivariate techniques like PCA was also mentioned.

4.2.2.1 Principal Component Analysis (PCA)

PCA is a multivariate technique that aims to take high-dimensional data and present it in a more tractable, lower-dimensional form without losing too much information (Beattie & Esmonde-White, 2021). This is done by relying on the dependencies between different variables (Bartholomew, 2009). PCA is known to be one of the oldest, most robust and simplest ways of performing dimensionality reduction, with applications in a variety of different fields. It is mainly used for determining the inter-relationship among variables in a large data set. In summary, PCA is a method of analyzing data sets to determine whether the total variation can be accounted for by a number of principal components or factors smaller than the number of initial variables. In many cases, PCA can yield a 2-D or 3-D window through which the data can be visualized, although the data set contains significantly more variables (Bartholomew, 2009; Wheelwright et al., 2020). This section provides a very high-level overview of PCA and how it works to reduce dimensionality as it pertains to FTIR spectral data, or any spectral data in general.

Consider a situation where FTIR spectral data from a single binder source at three different ageing levels (Unaged, RTFO aged and PAV aged) are collected. If 16 replicates are collected for a binder at each ageing level, a data matrix, X can be constructed with all n = 48 spectra. If each spectrum is collected using a resolution of 4 cm^{-1} between wavenumbers 4000 – 600 cm^{-1}, each spectrum will have approximately p = 850 absorbance values at respective the wavenumber values.

Asphalt Binder Source 1 →Unaged (16 spectra collected)

→RTFO aged (16 spectra collected)

→PAV aged (16 spectra collected)

In this scenario, the data matrix, X, will have dimensions [n x p], where p is the number of independent variables (or wavenumbers in this case), at which data is collected.

PCA is an unsupervised algorithm which attempts to decompose this X data matrix into:

1) A component or factor SCORE matrix of dimensions [m x n], and
2) A component or factor LOADING matrix of dimensions [p x m]

The following figure represents this visually.

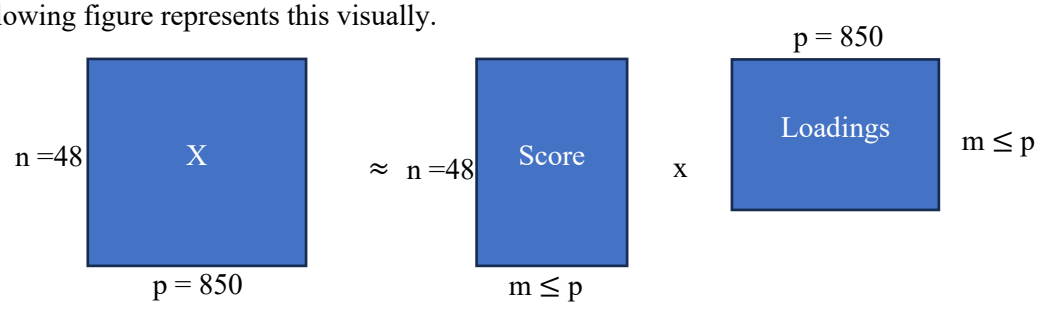


Figure 4.1: Showing a quick mathematical overview of what PCA does.

The score and loading matrices, show the inter-relationships among the variables as well as the observations. The use of PCA is extremely powerful when analyzing large data sets with n-observations (in this case n-spectra) and p-variables. The method summarizes the total variance/variation/variability, in the data by replacing p-variables with "m", much less, principal components. The PCs can be expressed as linear combinations of the original variables, as below:

$$PC_i = a_{i1}x_1 + a_{i2}x_2 + \cdots + a_{ip}x_p \quad (4.5)$$

Where the weights (or coefficients) of the j-th variable x in the k-th PC is denoted by a_{kj}.

These PCs can be thought of as constructed variables and are referred to as loadings. In theory, as seen in Figure 4.1, the X data matrix can be decomposed into 'p' PCs, however, the objective is to explain most of the variability in the data, by using or keeping only the first few PCs. Typically, the first principal component (PC_1) has the largest variance of all possible variables, whether constructed or not, PC_2 has the second largest variance and so on, with PC_p having the smallest variance (Kherif & Latypova, 2019).

If all the weights or 'scores' a_{kj}, for a particular PC, are placed in a vector, it happens to be an eigenvector of the correlation or Fisher Information Matrix (FIM) (X'X) where X is the original [n x p] data matrix presented in Figure 4.1. The scores corresponding to the first PC is associated with the largest eigenvalue of the FIM, scores corresponding to the second PC is associated with the second largest eigenvalue and so on. Therefore, by determining the eigenvectors of the FIM, the scores can be determined iteratively one vector at a time. After extracting 'm' PCs where 'm' is significantly less than 'p', there are 'm' PCs in the loading matrix and 'm' weighting (or score) vectors. The 'm' weighting vectors can then be concatenated to form the score matrix seen in Figure 4.1 above. In this way, the dimensionality of the X data matrix is reduced, and the weights (scores) can be used for determining which variables (PCs) in the loading matrix are useful for detecting patterns in the data and identifying outliers (Syms, 2019). After determining which PCs describe most of the variability in the data, regression can be performed using the chosen PCs. This is known as Principal Component Regression (PCR) (Vidal et al., 2016). PCR was not used in this chapter but can provide additional valuable information when predicted variables are quantitative (Vidal et al., 2016), unlike the data presented in this chapter.

After performing PCA, groupings or clusters can be identified visually when PCs are plotted in a 2-D or 3-D space. Applying alternative clustering methods to the PCs can provide further verification of clusters. One of these clustering methods that is widely used in chemometrics is k-means clustering (Pérez-Ortega et al., 2020).

4.2.2.2 K-means Clustering

K-means clustering is another unsupervised learning algorithm, similar to PCA, meaning that it uses an unlabelled data set to identify and group similar data points within a large dataset. Clustering typically uses given inputs such as, $x_1, x_2, \ldots x_n$, and attempts to learn the structure from the unlabelled data X assigning

them to groups. For the FTIR spectral data, the inputs can be thought of as the scores for the principal components determined during PCA. In this case, the user must specify or "guess" the number of clusters 'g', that may be present in the data and the output would be $z_1, z_2, \ldots z_n$, where z_i is one of those 'g' classes for example 1, 2, 3, … g. A cluster is usually assigned based on closet centroid which is the average of some group of data. For the FTIR dataset presented earlier, the number of potential clusters is already known to be 18 based on the different binder sources, ageing states, and sample preparation methods. Typically, the Euclidean distance of points within a cluster, from the cluster centroid is used as a measure to determine outliers and points with low or high error (Pérez-Ortega et al., 2020; J. Wu, 2012).

The main objective of k-means is to assign points to a cluster based off the points' distance from a centroid. This therefore means that a shorter distance will create better clustering when using this algorithm. The basic steps involved in the algorithm are as follows (Salkind, 2013):

Given a dataset of 'n' data points and a particular choice of 'k' clusters,

1. Guess the number of 'k' centroids in the data based on knowledge of the samples, testing parameters and how the data was collected.
2. Initialize the centroids $\mu_1, \mu_2, \ldots, \mu_k$ randomly to points in the dataset.
3. Assign each point to its closest centroid such that

$$z_i = arg\min_j \|\mu_i - x_i\|_2^2 \tag{4.6}$$

4. Update the centroids to the mean of all the point assignments from the previous step (i.e. the centre of mass for the clusters)

$$\mu_j = \frac{\sum_{i=1}^{n} 1(z_i=j)x_i}{\sum_{i=1}^{n} 1(z_i=j)} \tag{4.7}$$

5. These steps are repeated until the one of the following conditions of convergence are met:

- When the cluster assignments have not changed
- Centroids have not changed locations
- Some numbers of max iterations have passed

When performing this algorithm, it is important to remember that k-means is heavily dependent on its starting assignments to ensure global convergence as opposed to local. To avoid this issue, the initialization step (step 2) can be done more methodically, using k-means ++ initialization method. Using this method can lead to faster and more accurate/reliable convergence of centroids(Pérez-Ortega et al., 2020). The main steps involved in the k-means ++ initialization include:

1. Choose first centroid $\mu_1$uniformly at random from the dataset.
2. For j = 1 to 'k', compute the distance between each datapoint and its closest centroid for the current set of centroids (note that when j = 1, the first centroid will be the only centroid)

3. Choose a new centroid μ_j from remaining datapoints with probability of x_i being chosen proportionally to the squared distance between x_i and its closest centroid (it's current assigned center)
4. In this algorithm, the centroids are chosen iteratively creating one additional centroid with each iteration until 'k' centroids have been chosen
5. Run k-means algorithm using these determined centroids

Using this method is, however, more computationally expensive at the beginning when compared to random initialization as the distance of each point to its nearest centroid needs to be stored and updated each time a new one is selected.

For the FTIR data in this chapter, in terms of multivariate analysis, PCA was performed to reduce the dimensionality of the data, obtain a 3-D window through which the data can be viewed, and visually identify clusters or groupings. Thereafter, the results from PCA were used to perform k-means clustering to quantitatively verify the groupings identified qualitative. Statistical analysis was also performed on results from PCA, and k-means clustering and are presented in the next section.

4.3 Results and Discussion

As mentioned in the methodology section 16 ATR-FTIR spectra were collected for each sample at each ageing state, for three different sources of asphalt binder and two different sample preparation methods. This resulted in 288 spectra in total. Figure 4.2 shows all 288 spectra superimposed on one graph and identifies key regions of interest in the spectra. All spectra were collected at a resolution of 4 cm^{-1} between 6000 – 600 cm^{-1} yielding 1736 absorbance values for each spectrum. The X data matrix therefore consisted of ~ 500000 elements. The C-H region was used as the reference region for normalizing absorbances of all other peaks. As can be seen from Figure 4.2, the C-H reference absorbance remained relatively consistent for all samples while the five other peaks of interest showed changes with respect to binder source, ageing state and in this case, sample preparation method as well. It is difficult to discern the difference between different sample when looking at the spectra as a whole, therefore, several regions of interest, or peaks, as shown in the red ovals were isolated for analysis.

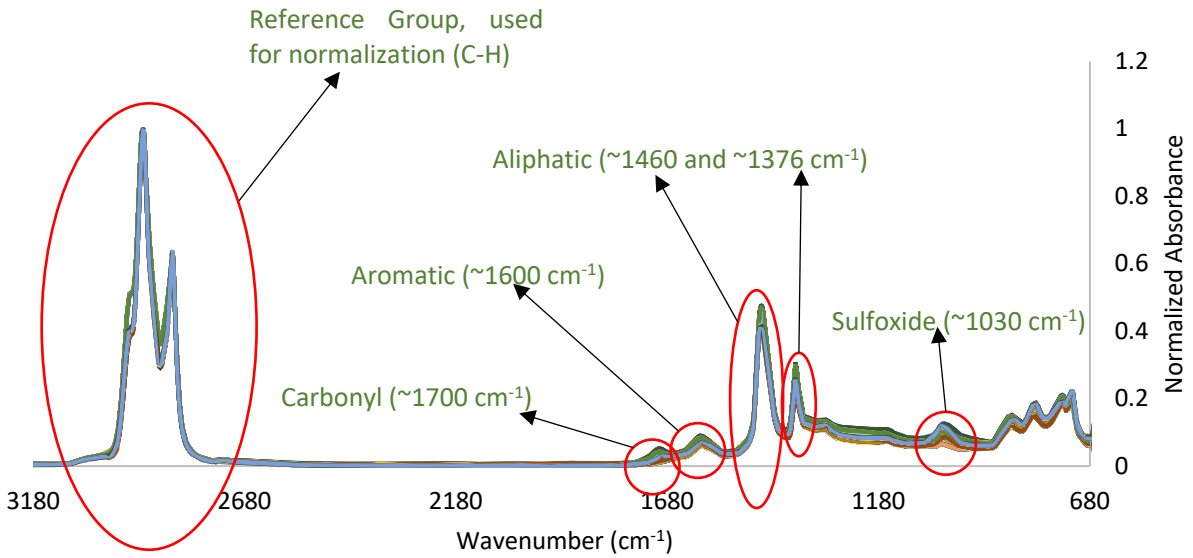


Figure 4.2: ATR-FTIR Spectra for all binder samples presented in Table 4.1 including replicates. (n=16)

4.3.1 FTIR Functional Group Analysis – Chemical Indices

Firstly, ageing indices (CI, SI, ArI, AlI) were estimated using equations (4.1) - (4.4) for each sample including the replicates to determine standard deviations (error bars). Trends of the indices, with increasing ageing state were examined and are presented in Figures 4.3-4.5.

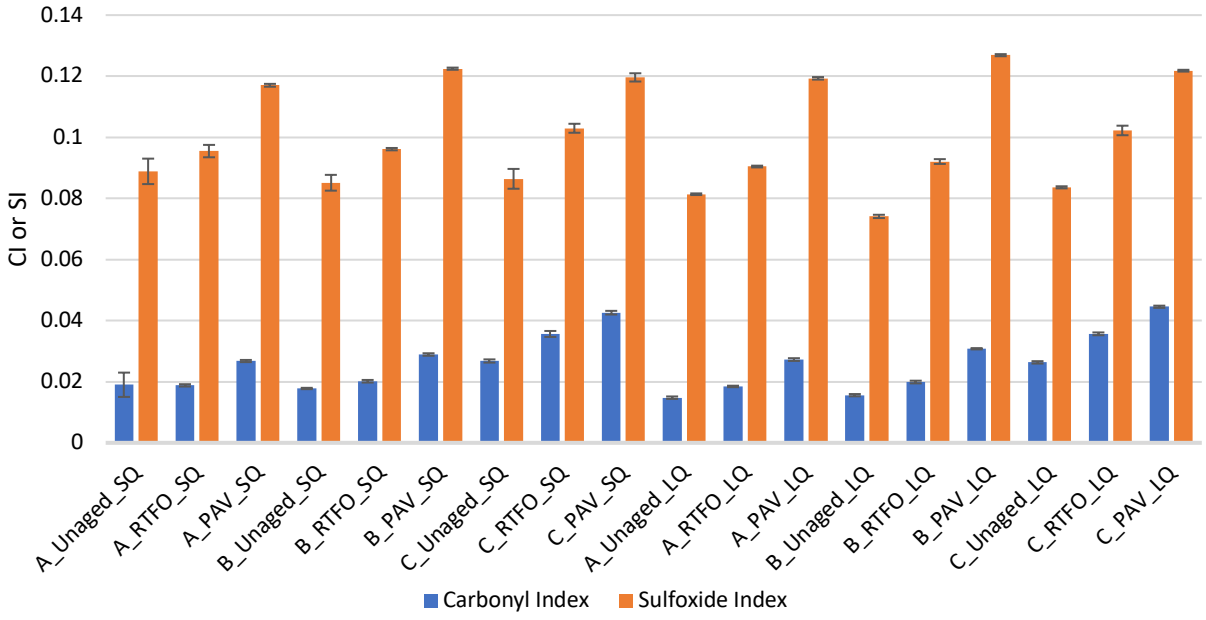


Figure 4.3: Carbonyl and Sulfoxide Indices for all 9 binder samples using both preparation methods SQ and LQ. (Error bars represent standard deviation, n = 16).

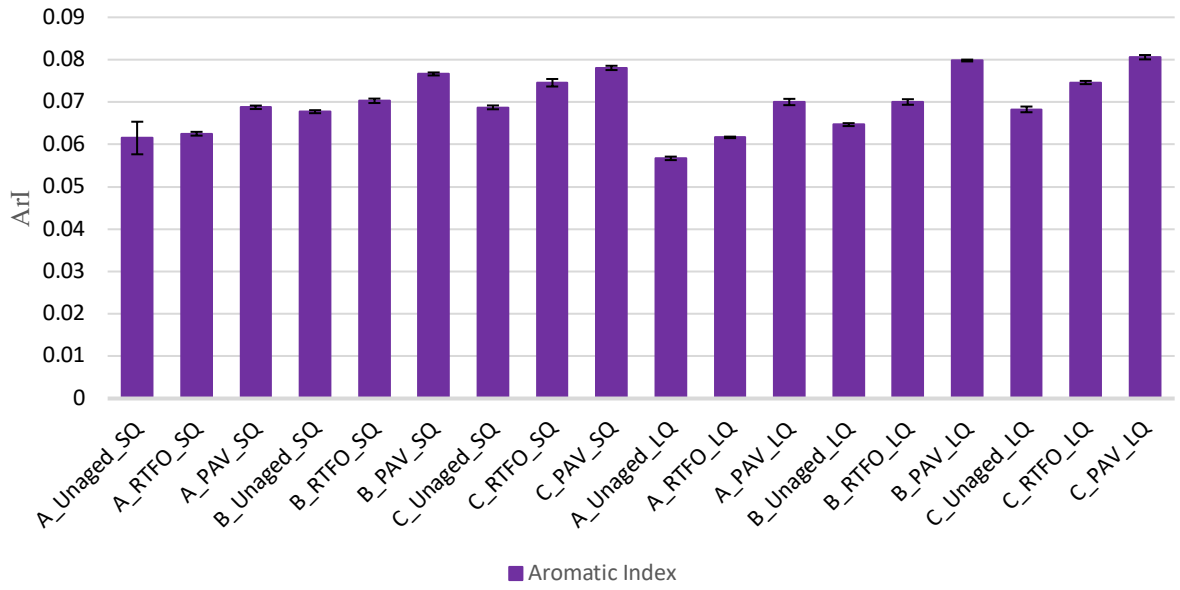


Figure 4.4: Aromatic Indices for all 9 binder samples using both preparation methods SQ and LQ. (Error bars represent standard deviation, n = 16).

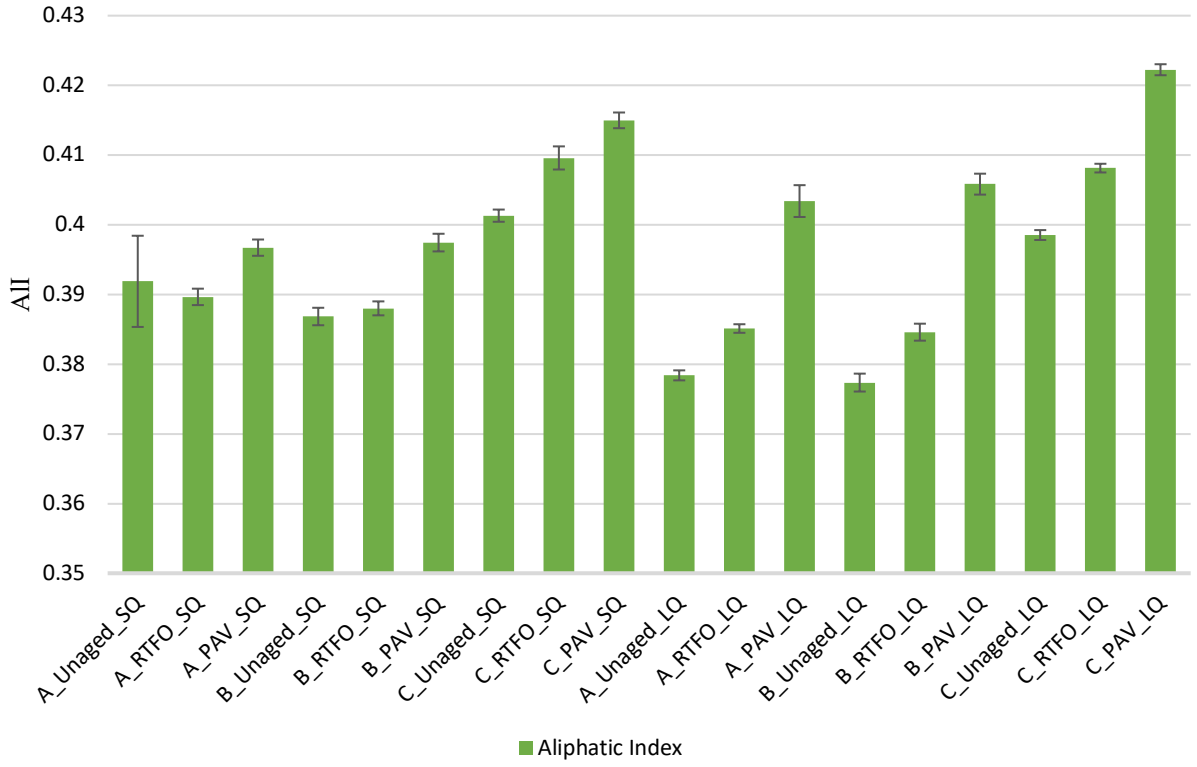


Figure 4.5: Aliphatic Indices for all 9 binder samples using both preparation methods SQ and LQ. (Error bars represent standard deviation, n = 16)

Several important observations can be made from Figures 4.3-4.6 and are summarized in the points below: All indices CI, SI, ArI and AlI were found to increase with increasing ageing level for all binder sources. Based on previous literature (Azimi Alamdary et al., 2019a; Baqersad & Ali, 2019; L. Ma et al., 2011a; Mikhailenko et al., 2016), CI and SI have been shown to increase with ageing. This is because when an asphalt binder, at elevated temperatures, is exposed to oxygen in the atmosphere, several components such as the aromatic and aliphatic hydrocarbons, as well as sulfur containing compounds oxidize to C=O and S=O groups respectively, therefore increasing the overall carbonyl and sulfoxide content in the aged asphalt binder. This oxidation process is accelerated and facilitated by heat and oxygen in the atmosphere. The general trend for ArI and AlI was also found to be increasing with ageing level, which also agrees with some previous studies (Gui et al., 2023; Redelius & Soenen, 2015). With respect to aromatic compounds, during the ageing process, long chain aliphatic hydrocarbons and other complex molecules can breakdown upon oxidation forming smaller chain aliphatic as well as aromatic compounds. Additionally, oxidative ageing can lead to condensation reactions where smaller hydrocarbons recombine to from more stable aromatic structures (Gui et al., 2023; Redelius & Soenen, 2015; Rossi et al., 2019). The combination of these two effects along with the volatilization of lighter components can lead to an increase in the ArI and therefore proportion of aromatic compounds present in the aged binder. Aliphatic compounds also undergo oxidation which can lead to the formation of new oxygenated aliphatic compounds that are more stable, like ketones and alcohols. Some studies (Y. Hu et al., 2022; Ren et al., 2022a) have noted a decrease in the aliphatic index with increasing ageing state which contradicts with the observations in this chapter, while others (Gui et al., 2023) agree with the increasing trend observed. When examining the SARA fractions in asphalt binder, saturates are the main fraction that contain primarily aliphatic compounds (although asphaltenes and resins do tend to have aliphatic side chains of various lengths). Literature (Takahashi et al., 2019b; Weigel & Stephan, 2018b; T. Zhou et al., 2020) that investigated how SARA fractions in asphalt binder change as the binder ages noted that the asphaltene and resins fractions tend to increase, aromatic fraction decreases due to volatilization of lighter molecular weight aromatics and the saturates fractions remained mostly unchanged. Therefore, one potential explanation for increase in AlI as the binder ages can be attributed to the fact that there is a concentration effect, where lighter aromatic fractions are lost, whereas the saturates fraction remains the same, resulting in a higher proportion of saturates (aliphatic compounds) in the overall binder, causing higher signal intensities in FTIR. Furthermore, during the ageing process, at high temperatures in the presence of oxygen, larger molecules can breakdown, leading to an increase in aliphatic compounds (L. Ma et al., 2011; F. Wang et al., 2020). While certain explanations are provided for the trends observed with respect to the aliphatic and aromatic indices presented in this chapter, it is important to note that ageing of asphalt binder is a complex phenomenon which involves many processes occurring simultaneously, resulting in a variety of different physical and chemical changes in the binder.

Trends observed with increasing CI and SI upon ageing are established to be consistent regardless of binder source, because of the inevitable oxidation process that occurs. However, trends observed with respect aliphatic and aromatic compounds can vary significantly, depending on the source of the asphalt binder and therefore, its initial chemical composition.

The second and third major observations are related to the error bars and repeatability of the different sample preparation methods. Overall, the error bars (or standard deviations) associated with the small quantity sample preparation method are at least 2 times larger when compared to the large quantity method for all indices, although it is more pronounced with CI and SI. Moreover, the increasing and decreasing trends observed for all indices with increasing ageing level are more distinct and consistent for LQ method when compared to SQ method. For example, when looking at Figure 4.3, for Binder A, comparing SQ and LQ preparation methods for all ageing states, the increasing trend of the SI is more pronounced and consistent for LQ when compared to SQ. Both of these qualitative measures (error bars and trends) indicate, firstly that there is a noticeable difference between the sample preparation methods, and LQ method seemed to provide more repeatable results when comparing the standard deviations for each sample and replicates. Comparing the sample preparation methods, since LQ uses a larger quantity of the asphalt binder, it allows for more homogeneity in the sample which could potentially explain the reason for higher repeatability and reliability. In order to confirm the differences observed qualitatively from Figures 4.3-4.5, ANOVA was performed on both CI and SI to determine if there were statistically significant differences between the preparation methods binder sources and ageing states.

Table 4.2: ANOVA on CI with respect to Binder Source, Ageing State and Sample Preparation Method.

Source	SSE	D.F.	MSE	F	P-value
Binder Source (1)	0.01218	2	0.00609	5274.61	0
Ageing State (2)	0.00891	2	0.00446	3860.37	0
Preparation Method (3)	0.00001	1	0.00001	7.64	0.0061
1:2	0.00059	4	0.00015	128.63	0
1:3	0.00004	2	0.00002	18.65	0
2:3	0.00017	2	0.00008	72.36	0
Error	0.00032	274	0		
Total	0.02222	287			

*Note: SSE. – Sum of Squared Error, D.F. = degrees of freedom, MSE – Mean Squared Error, F – F-statistic Value

Table 4.3: ANOVA on SI with respect to Binder Source, Ageing State and Sample Preparation Method

Source	SSE	D.F.	MSE	F	P-value
Binder Source (1)	0.00089	2	0.00044	129.45	2.63e-40
Ageing State (2)	0.07111	2	0.03556	10378.68	5.48e-259
Preparation Method (3)	0.00044	1	0.00044	128.07	1.28e-24
1:2	0.00221	4	0.00055	161.31	9.34e-71
1:3	0.00015	2	0.00007	21.72	1.75e-09
2:3	0.00124	2	0.00062	180.56	9.57e-51
Error	0.00094	274	0		
Total	0.07697	287			

*Note: SSE. – Sum of Squared Error, D.F. = degrees of freedom, MSE – Mean Squared Error, F – F-statistic Value

Tables 4.2 and 4.3 show the ANOVA results for CI and SI respectively. The first thing to note is, in some cases, the P-values in the last column are shown to be zero. This does not represent an actual P-value of zero but simply indicates that the P-values are very small. For both CI and SI, the F-values are very high and P-values are very low (<0.05) for all three factors, binder source, ageing state, and preparation method indicating that all factors are significant. As expected, binder source and ageing states, as previously established in literature have significant impact on the CI and SI. However, the value of this ANOVA mainly lies in establishing that, while sample preparation method has a smaller F-value (larger P-value) when compared to binder source and ageing state, the influence of sample preparation method is very significant when considering a significance level of alpha = 5%. In terms of practical significance, this indicates that the same sample, if tested using different sample preparation methods, are highly likely to yield different SI and CI. This has not been well investigated in previous literature and highlights an important aspect of performing and analyzing ATR-FTIR data. The question of which sample preparation method is best, therefore, depends on which method yields more repeatable results. As seen earlier in Figures 4.3-4.5, the LQ method showed smaller standard deviations giving a potential indication of higher repeatability and reliability. This was investigated further in the following section where multivariate analysis is discussed.

The ANOVA table also verifies, as expected, that there are significant interactions between all pairs of factors. This implies that the effect of one factor depends on the level of other factors. These interactions are important to consider when attempting to understand the overall behaviour of the binders and subsequently the indices. The SSE presented in the tables are also very small when compared to the total sum of squares (SST) which is another potential indication that there is high repeatability of ATR-FTIR in general. Overall, the ANOVA table indicates that all the factors and their interactions are statistically significant in determining the carbonyl and sulfoxide indices of asphalt binder samples. The source of binder and ageing state are the most influential factors, while the sample preparation method also plays a

significant role, although to a lesser extent. While the CI and SI are widely used indicators for investigating the ageing states of asphalt binders, it gives limited information about binder sources. Additionally, since CI and SI only focus on one or two specific peaks, the valuable information contained in the remain peaks and portions of the spectrum as well as the correlations between them are lost when focusing only on a few indices. In order to maximize the amount of valuable information that can be extracted from spectral data, PCA and k-means cluster analysis was performed on the raw ATR-FTIR data presented in Figure 4.2.

4.3.2 Multivariate Analysis – PCA and k-means Cluster Analysis

4.3.2.1 PCA analysis

The algorithm presented in section 4.2.2.1 was applied to a data matrix X, of dimensions 288 x 1736, containing all 288 spectral data for the different binder samples including replicates. After performing PCA, score and loading matrices were obtained, and 287 PCs were determined. The following table shows the amount of variability explained by PC_1-PC_4. As mentioned earlier, the first PC accounts for the most variability in the data while the last PC accounts for the least, therefore only PCs that explain more than 1% of variability in the data are presented.

Table 4.4: Percentage of Variability in the data explained by first four principal components

PC	Variability Explained by PC (%)
1	74.69
2	16.69
3	4.54
4	2.91

Based on the table above, a 2D plot of the scores for PC_1 and PC_2 was created since more than 91% of the variability in the data was explained by the combination of both. Figure 4.6 below shows that several clusters can be visually identified from plotting PC_1 vs PC_2.

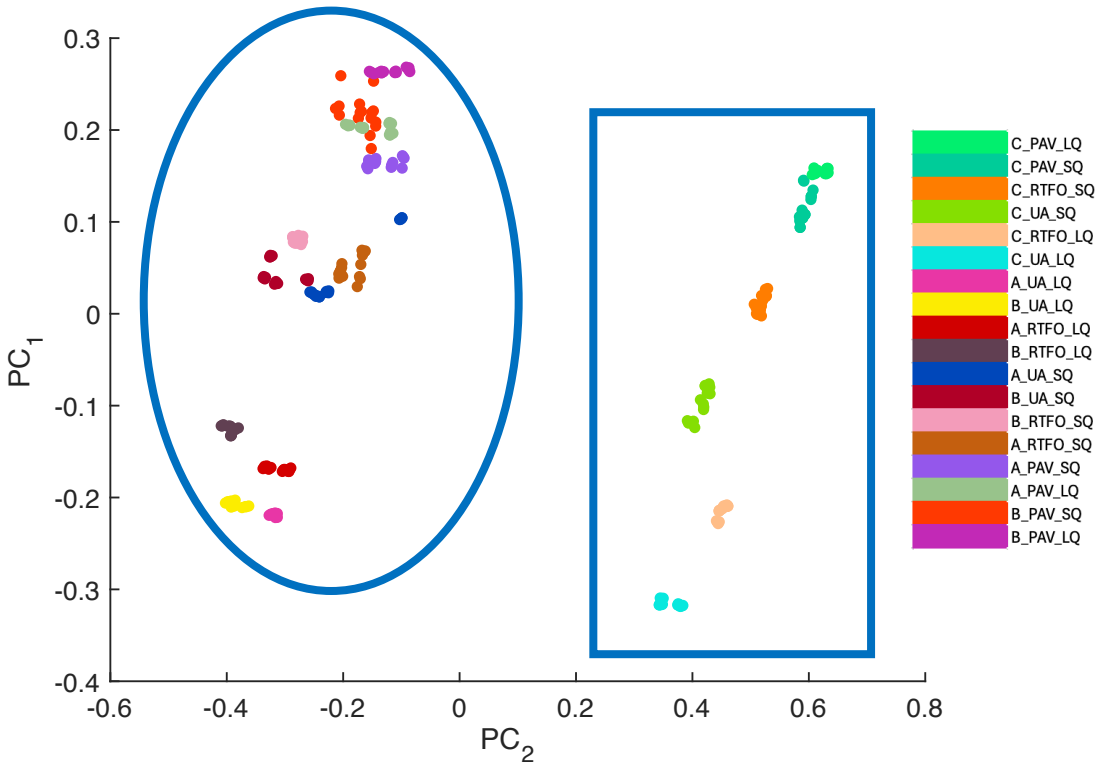


Figure 4.6: Plot of PC_1 vs PC_2 after performing PCA analysis on ATR-FTIR Raw Data. Legend on the graph is of the following form Source_Ageing State_Preparation Method.

The blue rectangle shown in Figure 4.6 illustrates that clusters or groupings can be clearly identified. However, for the points presented in the blue oval, clusters were not as distinct. In an attempt to decouple clusters further, a third dimension with PC_3 was added and is presented in Figure 4.7. Clusters associated with the SQ preparation method are presented in red rectangles and LQ in circles. Several observations were made based on the 3-D plot such as:

- Clusters were more distinct and easier to identify in the 3-D plot (Figure 4.7) when compared to the 2-D plot (Figure 4.6), with 18 different groups being identified, agreeing with what was expected.
- At all ageing states, clear differences between clusters were seen for different binder sources, highlighting the fact that PCA was able to identify differences between sources of binder.
- Another general trend identified was that PAV aged binders tend to cluster more on the left of side of the figure (larger PC_1) whereas unaged and RTFO aged binders were found more in the middle or to the right of the graph (lower PC_1). RTFO and unaged asphalt binder clusters were noticed to have smaller separation between the clusters when compared to PAV, implying that RTFO aged binder was not as different as PAV aged binder, in terms of functional groups when compared to the unaged binder.
- In general, a wider spread of points within clusters were observed for the SQ sample preparation method when compared to LQ, indicating higher variability when SQ method was used. This was consistent

with the observations from conventional analysis that noted higher standard deviation of indices calculated for samples prepared using the SQ method. Although less difference was noted between preparation method for PAV aged binders, there was still higher variability when using the SQ method.

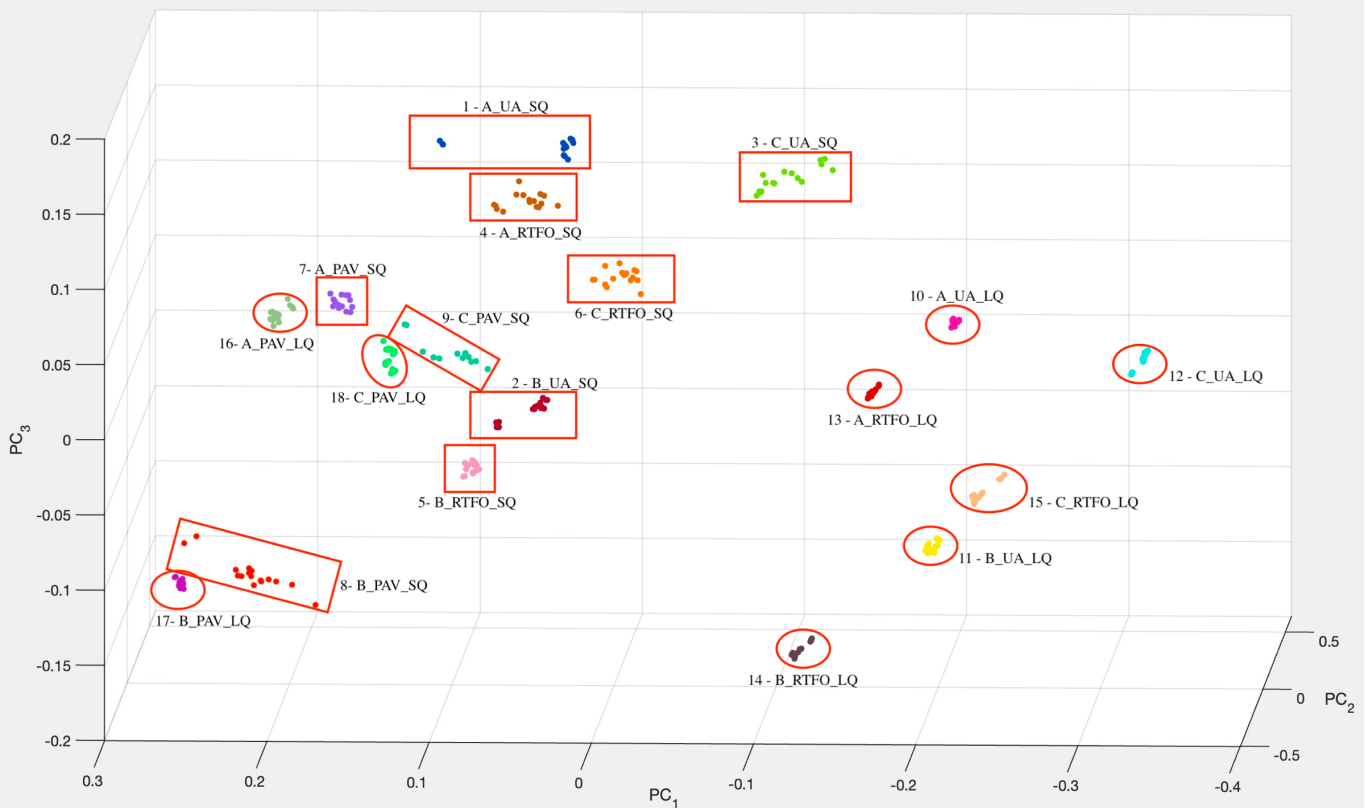


Figure 4.7: 3-D Plot of PC_1, PC_2 and PC_3 scores obtained from performing PCA analysis on ATR-FTIR Raw Data.

Note the A, B and C represents the different binder sources, UA (Unaged), RTFO and PAV represent ageing states and SQ/LQ represent the sample preparation methods small quantity and large quantity respectively. The labels on the graph are of the following form Source_Ageing State_Preparation Method

In order to quantify the effect of different factors and determine repeatability of ATR-FTIR as a whole, ANOVA was also performed using the scores of the first three principal components in order to compare with the ANOVA table obtained from conventional analysis. Performing ANOVA on the PCs yield similar results to MANOVA (Multivariate Analysis of Variance). Although less information is obtained from ANOVA, key observations and conclusions can still be made. Table 4.5 summarizes the ANOVA table acquired from performing ANOVA using PC_1 scores. ANOVA was also done using PC_2 and PC_3, yielding similar results, therefore only the table for PC_1 was shown here. Overall, the conclusions drawn from the ANOVA table using PCs were the same as those obtained from conventional analysis. One important thing to note however, was that higher SSE and MSE values were found since the entire spectrum data and therefore variability within the spectrum as a whole was considered for PCA, unlike the indices where only one specific peak was used. With respect to the significance of factors, the same conclusions can be drawn

from this ANOVA, however the p-value associated with sample preparation method (3), was much smaller when considering PCs, instead of single index (peak), emphasising another advantage of multivariate analysis techniques like PCA which captures more information from raw data.

Table 4.5: ANOVA on PC_1 with respect to Binder Source, Ageing State and Sample Preparation Method

Source	SSE	D.F.	MSE	F	P-value
Binder Source (1)	35.2713	2	17.6357	31308.54	4.94e-324
Ageing State (2)	1.7424	2	0.8712	1546.65	5.42e-150
Preparation Method (3)	0.2210	1	0.2210	392.42	8.22e-55
1:2	0.1433	4	0.0358	63.6	5.62e-38
1:3	0.0388	2	0.0194	34.46	4.47e-14
2:3	0.2041	2	0.1021	181.18	7.30e-51
Error	0.1543	274	0.0006		
Total	37.7754	287			

4.3.2.2 K-means Cluster Analysis

Although different groups/clusters can be identified visually after performing PCA and creating plots, as seen in Figure 4.7, to confirm the locations of the clusters observed in score plots, and verify quantitatively, another method for specifically examining clusters was applied. One of the methods that can be used to easily do this is k-means clustering as described in section 4.2.2.2. K-means clustering with k-means ++ initialization was performed using the algorithms described earlier with the first three principal components from PCA. Figure 4.8 below shows the results of k-means clustering, i.e. the centroids of groups identified, overlapped onto the 3-D PCA plot.

In the figure below, the black outlined points represent the locations of 18 centroids determined using k-means cluster analysis. As can be seen, in general, the determined centroids agreed with the groupings visually identified in Figure 4.7 statistically verifying the locations and difference between clusters. If clusters identified visually, in Figure 4.7 were not true groupings, centroids determined through k-means clustering would not have coincided as well with the predetermined clusters from PCA.

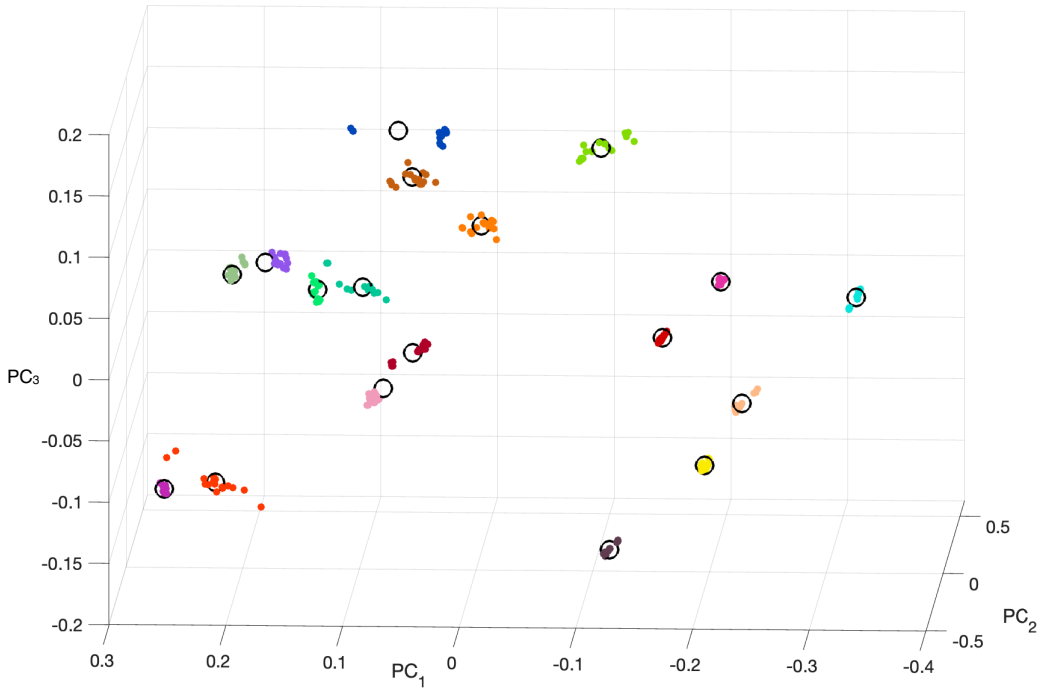


Figure 4.8:Showing centroid locations determined from k-means clustering superimposed onto 3-D PCA plot

To further verify the that clusters determined were statistically significantly different from each other, ANOVA was carried out on the results. The k-means clustering algorithm, in addition to generating centroids, assigns numbers 1-18 to each of the 288 points plotted in Figure 4.7, based on their distance from the different centroids identified. This assignment along with the PCs were used for performing ANOVA. To further explain, ANOVA was done on each of the PCs separately using the assigned numbers (or clusters), to determine if the differences observed in clusters were statistically significant.

Table 4.6: ANOVA on significance of different clusters using PC 1

Source	SSE	D.F.	MSE	F	P-value
Groups	37.7003	17	2.21767	7980.46	0
Error	0.075	270	0.00028		
Total	37.7754	287			

Table 4.7: ANOVA on significance of different clusters using PC 2

Source	SSE	D.F.	MSE	F	P-value
Groups	8.38504	17	0.49324	2214.22	1.02e-278
Error	0.06015	270	0.00022		
Total	8.44519	287			

Table 4.8: ANOVA on significance of different clusters using PC 3

Source	SSE	D.F.	MSE	F	P-value
Groups	2.27903	17	0.13406	2054.48	2.31e-274
Error	0.01762	270	0.00007		
Total	2.29664	287			

Based on Tables 4.6-4.8, and the very small P-values calculated, it can be concluded that there are significant differences between clusters. The degrees of freedom used for groups/clusters was 17 (i.e. n – 1) since 18 groups were identified. It should also be noted that when comparing the ANOVA using PC_1, PC_2 and PC_3, the P-value, and therefore the differences between groups for the respective PCs decreases on moving from PC_1 to PC_3. This agrees with the fact that most of the variability in the data can explained by the first PC with each successive PC explain less data variability than the one before, as seen in Table 4.4. Note that the total error associated with PC_1 matches that presented in Table 4.5 earlier, as expected, since ANOVA it was done on the same data using the additional column of the assigned clusters, to, in this case, determine if the difference between groupings was statistically significant. The result from ANOVA is limited to some extent in the information it provides. It only indicates that differences between groups are likely to be significant, but no information about how different each group is from the other can be obtained from the ANOVA.

Therefore, from a visual perspective, another way to verify if groups are significantly different is by performing multiple comparison tests such as the Bonferroni test. This is where the means of each group can be compared to all others. The results from this test for using PC_1 are presented in Figure 4.9 below. In this figure, the circles represent the mean of PC_1 (scores) for each cluster identified, and the lines through the circles represent comparison intervals. For example, if looking at the blue point on the figure, dotted lines can be seen on either side of the point, encompassing the entire comparison interval of that point. Dotted lines similar to these can be drawn for each point. The value of this plot lies in its ability to identify which groups are significantly different from each other and which are not. If points or comparison intervals overlap with the dotted lines of another point, then clusters associated with these points are not statistically significantly different from each other (i.e P-value would be greater than 0.05 if pairwise tests were performed). If there is no overlap, difference between clusters is statistically significant. Overall, the information from all pairwise comparison tests are therefore represented in Figure 4.9. The ANOVA is only able to indicate that clusters can be identified and overall, the impact of clusters found are significant, but no information about how each cluster related to others can be obtained. The main conclusion that can be drawn from ANOVA in this case was there exists variability between groupings. However, the multiple comparison test yields more information about each cluster in comparison to each other. From the figure, certain groups can be identified as clearly different from all other 17 clusters, while some can be seen to

only be statistically significantly different from 15 or 16 groups. This still indicates that the presence of clusters and centroids themselves, in general are significant and can be identified. Similar comparison tests were performed using PC_2 and PC_3. The results are presented in Figures 4.10 and 4.11.

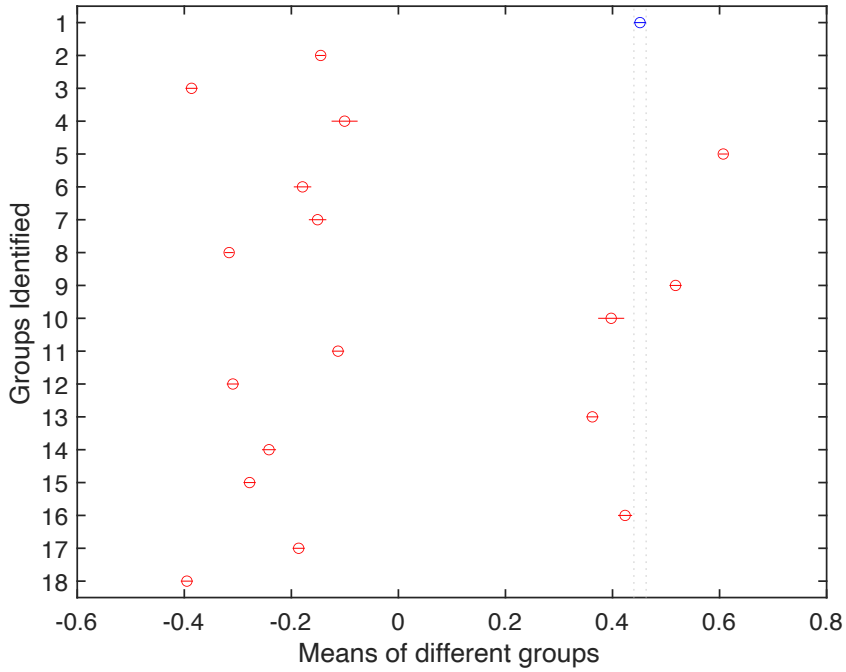


Figure 4.9: Multiple Comparison of PC_1 means for different groupings identified using k-means cluster analysis

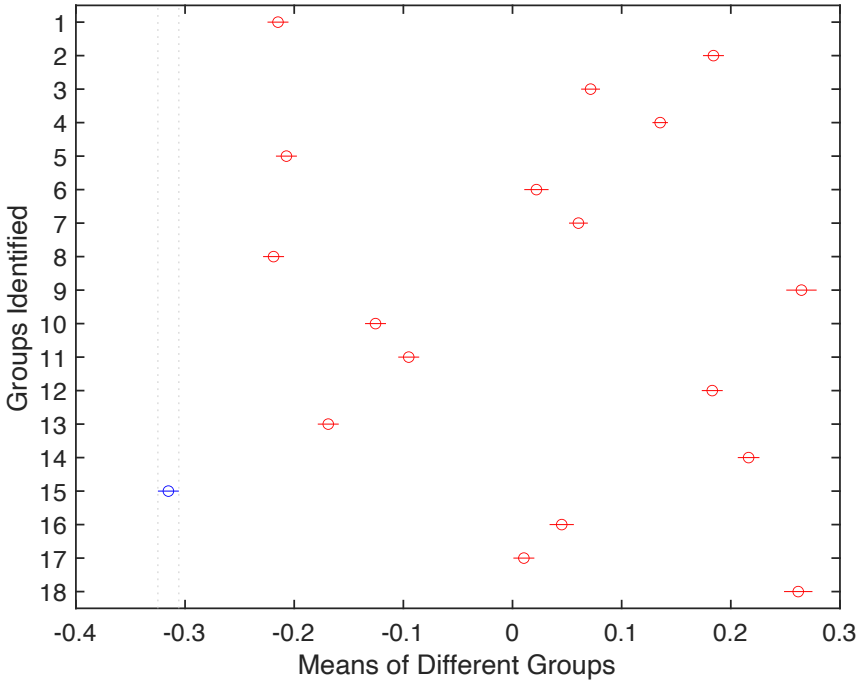


Figure 4.10: Multiple Comparison of PC_2 means for different groupings identified using k-means cluster analysis.

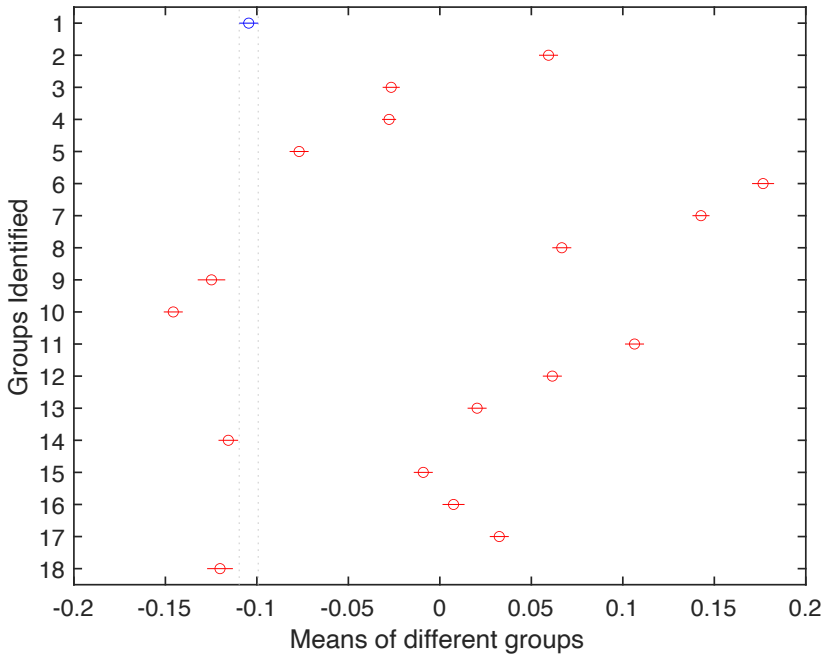


Figure 4.11: Multiple Comparison of PC_3 means for different groupings identified using k-means cluster analysis.

4.4 Conclusions

Based on the comprehensive analysis conducted in this chapter, several key conclusions can be drawn regarding the application of ATR-FTIR spectroscopy in studying asphalt binders and impactful analysis techniques:

- ATR-FTIR spectroscopy, particularly when coupled with multivariate analysis techniques like PCA and k-means clustering, proves to be a robust tool for characterizing asphalt binders. It enables detailed insights into chemical compositions, binder source and ageing states, which are crucial for quality control and research purposes.
- A comparative analysis between Small Quantity (SQ) and Large Quantity (LQ) sample preparation methods revealed that LQ method tends to offer more consistent and reliable results, particularly evident in reduced variability in indices like CI and SI across ageing states.
- Statistical analyses, including ANOVA, emphasized the significant impact of binder source, ageing state, and sample preparation method on the spectral indices (CI, SI). This highlights the need for careful consideration of these factors in experimental design and data interpretation.
- PCA facilitated dimensionality reduction while preserving critical spectral information, aiding in visualization and identification of patterns across different binder sources and ageing states. ANOVA using PCA scores confirmed the significance effect of sample preparation methods and other factors, showcasing the ability of PCA to capture variability across the entire spectrum data. Subsequent k-

means clustering validated observations, providing an additional quantitative support as shown by centroids overlapping with PCA distinct groupings based on spectral data.

- Multiple comparison tests such as the Bonferroni test further detailed pairwise differences between clusters, providing additional insights into the statistically significant differences.
- Further research should focus on refining standardization protocols for ATR-FTIR analysis in asphalt binders, exploring additional spectral indices beyond CI and SI, and integrating advanced data processing techniques to enhance predictive capabilities.
- The use of PCA and k-means techniques in this chapter highlights the importance of multivariate approaches in asphalt binder characterization, offering comprehensive views beyond conventional single-peak analysis.

In summary, while ATR-FTIR spectroscopy holds immense promise in asphalt research, addressing methodological standardization and advancing analytical approaches are pivotal in maximizing its utility for future applications in the field.

Chapter 5

Chemical and Rheological Effects of Oxidative Aging on SBS-modified Asphalt Binders

5.1 Introduction

Asphalt pavements inevitably undergo aging over their service life, which exacerbates distresses such as rutting and cracking. To enhance durability and extend pavement life, Styrene Butadiene Styrene (SBS), a thermoplastic elastomer, is widely used as a modifier in asphalt binders. SBS is composed of styrene, the hard block providing strength, and butadiene, the soft block that contributes to the elasticity of the polymer due to its carbon-carbon double bonds (C=C) (T. Ma et al., 2012a; F. Wang et al., 2020b). These unique properties enable SBS to reduce low-temperature cracking and improve rutting resistance when added to asphalt binders (T. Ma et al., 2012a; F. Wang et al., 2020b). Additionally, multiple studies have demonstrated ability of SBS to enhance the aging resistance of asphalt binders, leading to improved pavement performance. This has been confirmed through rheological (Cong et al., 2021; Penetration, 2013), viscosity (Cong et al., 2021; Davidson et al., 2014), and chemical tests (M. F. Ali & Siddiqui, 2001; Davidson et al., 2014; Shan et al., 2019).

Research on both aged and unaged SBS-modified asphalt binders has shown, via Fourier Transform Infrared (FTIR) spectroscopy, that fewer oxygen-containing groups (such as carbonyls, hydroxyls, and sulfoxides) form in SBS-modified binders compared to unmodified bitumen under similar aging conditions. However, SBS itself degrades during aging (Hossain & Wasiuddin, 2019; Słowik, 2017). Notably, most studies have focused primarily on conventional laboratory aging methods, including short-term Rolling Thin Film Oven (RTFO) and long-term Pressure Aging Vessel (PAV) thermo-oxidative aging (Cong et al., 2021; Davidson et al., 2014; Hossain & Wasiuddin, 2019; Słowik, 2017). Recent research incorporating Ultraviolet (UV) aging in addition to thermo-oxidative aging has revealed that UV radiation plays a significant role in the degradation of SBS-modified binders. Some studies have suggested that after UV aging, most or all of the SBS in the binder is degraded, whereas thermo-oxidative aging results in less SBS degradation (Hossain & Wasiuddin, 2019). In some cases, SBS is viewed as a sacrificial component, oxidizing in preference to the asphalt binder, thereby slowing the aging process of the binder itself (Shan et al., 2019; Słowik, 2017).

The interaction between SBS and asphalt binder is primarily considered physical, with cross-linking, entanglement, and intermolecular forces playing key roles due to long-chain structures in SBS. These interactions result in enhanced binder performance (Hossain & Wasiuddin, 2019; Yilmaz & Çeloğlu, 2013). However, during aging—particularly when exposed to UV radiation, heat, moisture, and oxygen—chemical reactions such as photo-oxidation can occur, degrading both the SBS polymer and the asphalt

binder (Hossain & Wasiuddin, 2019; Słowik, 2017). This degradation leads to changes in binder behaviour and performance, particularly in terms of temperature sensitivity. SBS-modified binders generally exhibit lower temperature sensitivity than unmodified binders, a desirable trait as it allows the binder to maintain its desirable properties over a wider temperature range (Penetration, 2013; Shan et al., 2019; F. Wang et al., 2020b). Nonetheless, as the binder ages, its temperature sensitivity increases, potentially leading to pavement distresses (Osmari et al., 2019b; Penetration, 2013; F. Wang et al., 2020b).

One major challenge with SBS-modified binders is the lack of appropriate testing methods and grading systems to fully characterize their performance and aging. The current Superpave Performance Grading (PG) system is better suited for unmodified binders (Davidson et al., 2014; Hossain & Wasiuddin, 2019; Takahashi et al., 2019a). Although the PG Plus and Multiple Stress Creep Recovery (MSCR) tests have been developed to better quantify the performance of SBS-modified binders, they remain inadequate (Hossain & Wasiuddin, 2019; Takahashi et al., 2019a). Another critical factor in modifying asphalt binders is their compatibility with SBS, which depends on the chemical composition of the binder, the equilibrium of its colloidal structure, and the characteristics of SBS itself (Shan et al., 2019; Takahashi et al., 2019a; K. Wang et al., 2019). The chemical composition of the binder is essential for determining its physical properties and performance (L. Ma et al., 2011b; Pipintakos, Soenen, et al., 2021a; Werkovits et al., 2023), and altering molecular interactions through SBS modification can significantly improve binder durability and properties (Khavandi Khiavi et al., 2021b; Qiu et al., 2022).

A deeper understanding of the chemistry of asphalt, along with the interactions between its components—including those formed during aging or through treatment with SBS and other additives—can lead to significant improvements in binder performance and durability (Qiu et al., 2022; Werkovits et al., 2023). Advanced chemical testing techniques, such as Attenuated Total Reflection–Fourier Transform Infrared (ATR-FTIR) and Nuclear Magnetic Resonance (NMR) spectroscopy, when used alongside conventional rheological tests, provide a more comprehensive understanding of the behaviour and performance of SBS-modified asphalt binders (Betancourt Cardozo et al., 2016; W. Wu et al., 2022). FTIR and NMR are commonly used in the polymer industry to study the chemical composition and molecular structure of complex materials (Betancourt Cardozo et al., 2016; Oliviero Rossi et al., 2018; W. Wu et al., 2022). While FTIR is valuable, NMR can sometimes provide more detailed and quantitative information about molecular structures and compositions. Therefore, both techniques were employed and compared in this study. FTIR has been well studied in the field of asphalt however, the limited use of NMR in asphalt binder research highlights one of the significant contributions of this study.

NMR is a very powerful spectroscopic technique that takes advantage of the magnetic properties of specific nuclei. The basic principle behind NMR is that some nuclei exist in specific nuclear spins when exposed to an external magnetic field. NMR observes transitions between spin states that are specific to the particular

nuclei of interest. There are several types of NMR; however, in the case of asphalt binders, which is mainly composed of hydrocarbons, both hydrogen (^{1}H) and carbon (^{13}C) nuclei exhibit specific spin states and can be identified using Proton (^{1}H) - or Carbon (^{13}C)- NMR spectroscopy respectively. This chapter focussed on ^{1}H NMR since it is abundant and quicker than ^{13}C. Additionally, limited literature is available on how to prepare, run and analyze NMR testing results for bitumen. NMR complements FTIR by not only identifying certain types of functional groups within the asphalt binder through chemical environment peaks, but also revealing their arrangements and interrelations.

5.2 Motivation and Objectives

Understanding the aging behaviour of asphalt materials is critical to creating a comprehensive pavement management plan and ensuring the longevity of flexible pavements. However, evaluating the aging of polymer-modified asphalts (PMA) can be more difficult as conventional tests focus mainly on changes in the rheological properties, which makes it difficult to accurately characterize PMA performance. As such, more advanced chemical testing techniques are required to create reliable aging indicators for PMAs. Two spectroscopic techniques, NMR and FTIR can provide useful information with respect to monitoring and understanding the ageing process in SBS modified asphalts specifically. The use of FTIR for this purpose has been well documented in literate, while NMR is not as widely use. NMR spectroscopy is a high-resolution analytical technique often used in the polymer industry to evaluate molecular structure and quantify the concentration of chemical species. This powerful technique provides detailed information about the chemical composition and interactions within a material by investigating the magnetic response of atomic nuclei after applying strong radiofrequency pulses. However, due to the complex chemical composition of asphalt binders, this technique has seen limited use in the asphalt industry. Therefore, the major objectives of this study include:

1. To investigate the impact of increasing SBS concentration on the aging behaviour of asphalt binders through comprehensive rheological and chemical analysis using both NMR and FTIR spectroscopy in addition to conventional rheological tests.
2. To establish correlations between parameters obtained from rheological and spectroscopic testing of SBS-modified asphalt binders thereby enhancing the understanding of oxidative aging behaviour.

5.3 Methodology

5.3.1 Materials

The materials utilized for sample preparation and testing were (1) Deuterated Chloroform (CDCl3) – Sigma Aldrich, Product Number:151823, 99.8 atom % D, (2) Tetramethylsilane (TMS) – Sigma Aldrich, Product

Number: T24007, NMR Grade .99.9 %, (3) Styrene-Butadiene-Styrene (SBS), (4) Kerosene - Reagent Grade (> 99% purity), (5) Isopropyl Alcohol – Reagent Grade (> 99% purity).

5.3.1 SBS Modified Asphalt Binder Preparation

Two neat asphalt binders from different sources, both graded PG 58-28, hereafter referred to as A and B, were used to produce SBS-modified asphalt binders. The SBS polymer used possessed a linear structure with a 31.6% styrene content. Both asphalt binders, A and B, were preheated to 170°C, SBS was added, and a Silverson high shear mixer with a heating mantle were used to blend the SBS into the binder. Blending was carried out for one hour at 3500 RPM. After, a crosslinking agent was added at 10% by weight of the polymer, based on the guidance of previous literature (Penetration, 2013; Shan et al., 2019; F. Wang et al., 2020b), and blending was continued for an additional 30 minutes. The speed of the high shear mixer was reduced to 3000 RPM and further blended for another hour, where temperature was maintained at 180°C. For both binders A and B, SBS was blended at a concentration of 2% and 4% by weight of the binder. Binders A and B, with different concentrations of SBS (0%, 2% and 4%), were then exposed to short-term RTFO aging followed by 20, 40, and 60 hours of long-term PAV aging. Rheological and chemical testing was then carried out on the different combinations of aging levels, as well as SBS concentrations for binders A and B. Table 5.1 summarizes the different binder types tested.

Table 5.1: Summary of different asphalt binder samples tested for binders A and B

SBS Content	PAV Ageing (hours)
0% (w/w)	0 (Virgin)*
	20
	40
	60
2% (w/w)	0 (Virgin)*
	20
	40
	60
4% (w/w)	0 (Virgin)*
	20
	40
	60

*Only NMR testing performed on these samples (No DSR or BBR testing)

5.3.3 Rheological Testing

Temperature-frequency sweeps were performed using the Dynamic Shear Rheometer (DSR) on all binders A and B samples (Unmodified and modified with SBS, Unaged and Aged). This was done using the 25-mm and 8-mm DSR plates. Three replicates were performed for each binder sample. Low-temperature testing was also performed using the Bending Beam Rheometer (BBR), after which creep stiffness and m-values were determined. Three replicates were performed for each sample at two different temperature (-

18 and -24°C). Testing temperatures were determined based on the Superpave PG binder grading and recommendations in AASHTO standards. Master curves were constructed, and parameters such as the crossover temperature were determined for modified and unmodified binders at different aging levels. All rheological tests were performed according to the respective AASHTO standards (AASHTO T 313-22, AASHTO T 315-22).

5.3.4 Chemical Testing

5.3.4.1 ATR-FTIR Spectroscopy

ATR-FTIR was conducted following protocols described by RILEM TC 295 – FBB TG1 (Fingerprinting bituminous binders using physico-chemical analysis) (Shan et al., 2019) . The samples were heated in metal cans (~50 g) until flowable using a heating plate at 180°C and stirred continuously. Once the samples were homogenized, the thermometer was used to drop a specimen of the binder onto a slip of paper. Three droplets were prepared for each binder sample and underwent ATR-FTIR testing within two hours of preparation using a BRUKER Alpha 2 with a Mercury Cadmium Telluride detector and a diamond crystal. A spectra resolution of 4 cm^{-1} and a range of 4000 – 600 cm^{-1}, in the OPUS software was used for acquiring the spectra for each droplet. The crystal was cleaned before and after each droplet measurement using kerosene followed by isopropyl alcohol. For each droplet, a background measurement was taken, after which the sample was placed on the crystal and slight pressure was applied to the drop to ensure good contact with the crystal. Four spectra were recorded for each droplet. The raw data was analyzed using Spectragryph. Baseline was taken using 2400 – 2000 cm^{-1} and each spectrum was normalized to the total area under it.

Several indexes were used to evaluate the aging of the bitumen with the FTIR spectra. The first two indexes are typically used to look at the polymer degradation and are expressed as ratios of the polybutadiene bonds to the polystyrene which is considered stable based on the findings of previous literature. Equations 5.1 uses the polybutadiene trans double bond and Equation 5.2 uses the vinyl double bond for calculating indices (D. Sun et al., 2011; K. Wang et al., 2019):

$$I_{PTDB} = \frac{A_{PTDB}}{A_P} \tag{5.1}$$

$$I_{PVDB} = \frac{A_{PVDB}}{A_P} \tag{5.2}$$

where A_{PTDB} is defined as 925 – 981 cm^{-1}, A_{PVDB} is defined as 896 – 925 cm^{-1} and A_P is defined as 680 – 711 cm^{-1}. A lower rate of change would be indicative of a lower rate of degradation, and this has been observed with highly polymer modified bitumen (D. Sun et al., 2011; K. Wang et al., 2019).

Sulfoxide and Carbonyl indexes were used to monitor general aging trends within the bitumen and are shown in Equations 5.3 and 5.4:

$$\text{Sulfoxide Index (SI)} = \frac{A_{1030}}{\sum A} \tag{5.3}$$

$$\text{Carbonyl Index (CI)} = \frac{A_{1700}}{\sum A} \tag{5.4}$$

where ∑A is defined as the sum of the peak areas at wavenumbers 2952, 2862, 1700, 1600, 1460, 1375, 1030, 864, 814, 743 and 724 cm^{-1} (Feng et al., 2016; Karlsson & Isacsson, 2003; Mirwald, Nura, et al., 2022a). A_{1030} is defined as 979 – 1079 cm^{-1} and A_{1700} is defined as 1650 – 1820 cm^{-1}. These indexes are commonly used to assess the aging potential of different asphalt binders.

5.3.4.2 Proton (^{1}H) NMR Spectroscopy

^{1}H NMR was conducted using a Bruker UltraShield, 300MHz, high resolution spectrometer (manufactured in Germany). Asphalt binder samples need to be dissolved in a solvent in order to perform liquid state ^{1}H NMR. For this study, 10-15 mg of asphalt binder was dissolved in 1 ml of $CDCl_3$ with a small amount of TMS, a common reference and internal standard used in NMR. Once fully dissolved, the solution was added to an NMR tube, up to a height of 3.5 cm, and then placed in the spectrometer for testing. The following schematic, Figure 5.1, shows an overview of the procedure.



15-20mg asphalt binder

1 ml Deuterated Chloroform with Tetramethylsilane (TMS) internal standard

Ensure complete dissolution

NMR tube with solution to height of ~3.5 cm

Place sample into NMR equipment (Bruker UltraShield - 300MHz high resolution)

Figure 5.1: Overview of the steps involved in running 1H NMR spectroscopy.

The output from the NMR spectrometer is usually recorded in the time domain. When the signal is converted to the frequency domain using Fourier Transform (FT), a spectrum similar to that seen in FTIR is obtained. In this case, the y-axis represents intensity, and the x-axis represents the chemical shift usually expressed in ppm. Chemical shift is basically a measure of the resonance frequency of the nuclei being

studied, in this case, hydrogen. Spectra were collected for all samples listed in Table 5.1 (binders A and B). Preprocessing, such as phasing, baseline correction, shifting based on the TMS reference (known to appear at 0 ppm) and normalization, was carried out on all spectral data collected. Phasing was done using the Bruker – TopSpin 4.4.1 software, and all other preprocessing was done in MATLAB R2024b after importing the phased spectral data with a user-written script. All spectra were normalized to the area under all meaningful peaks (all peaks excluding solvent, $CDCl_3$ and reference peak, TMS). For baseline correction a non-traditional method called Adaptive Iteratively Reweighted Penalised Least Squares (AirPLS) baseline correction was used (Yan et al., 2022b). The airPLS is proposed as a baseline correction method to avoid the user intervention. It comprises a least-squares smoothing together with a penalty on non-smooth behaviour of an estimated baseline. The optimisation objective of the airPLS algorithm is presented in Equation (5.5). The first part of Equation (5.5) expresses the fit of the baseline while the second part expresses the smoothness of the baseline.

$$\arg\min_{z}\left[\sum_i \boldsymbol{w}_i^t|\boldsymbol{x}_i-\boldsymbol{z}_i^t|^2+\lambda\sum_i|\boldsymbol{z}_i^t-\boldsymbol{z}_{i-1}^t|^2\right] \tag{5.5}$$

Where: $\boldsymbol{z}$ is the corrected baseline vector;

$\boldsymbol{x}$ is the measured spectrum vector;

$\boldsymbol{w}$ is the weight vector which discriminates between the baseline region and peak region;

t is wavenumber;

λ is the penalty parameter to balance the smoothness with fit.

In a traditional penalized least-square baseline correction without an adaptive iteratively reweighted procedure, the peak regions need to be defined by the user beforehand. **w** is set to zero in peak regions and set to one in baseline regions. However, the existence of noise makes it difficult to find peak regions, and it can be problematic to define peak regions for an unknown sample. To overcome this limitation, airPLS is proposed, and uses a different way to assign **w**. In airPLS, the weight vector **w** is obtained adaptively using an iterative method. **w** for each iteration is calculated as shown in Equation (5.6).

$$w_i^t=\begin{cases}0 & x_i\geq z_i^{t-1}\\ e^{\frac{t(x_i-z_i^{t-1})}{|d^t|}}, & x<z_i^{t-1}\end{cases} \tag{5.6}$$

Where: $\boldsymbol{d}^t$ is the sum of negative elements of the subtraction between $\boldsymbol{x}$ and $\boldsymbol{z}$

Figure 5.2 and 5.3 below shows the comparison of raw data to the baseline corrected data, using the airPLS method. This figure shows that the airPLS method significantly improves the spectra baselines, resulting in more accurate analysis.

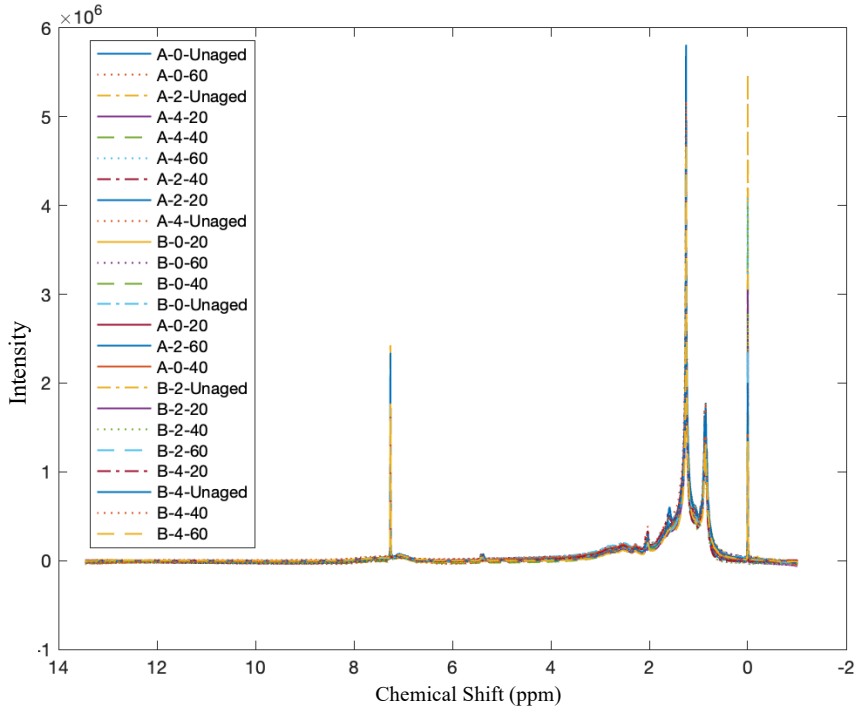


Figure 5.2: Comparison of NMR spectral data before and baseline correction.

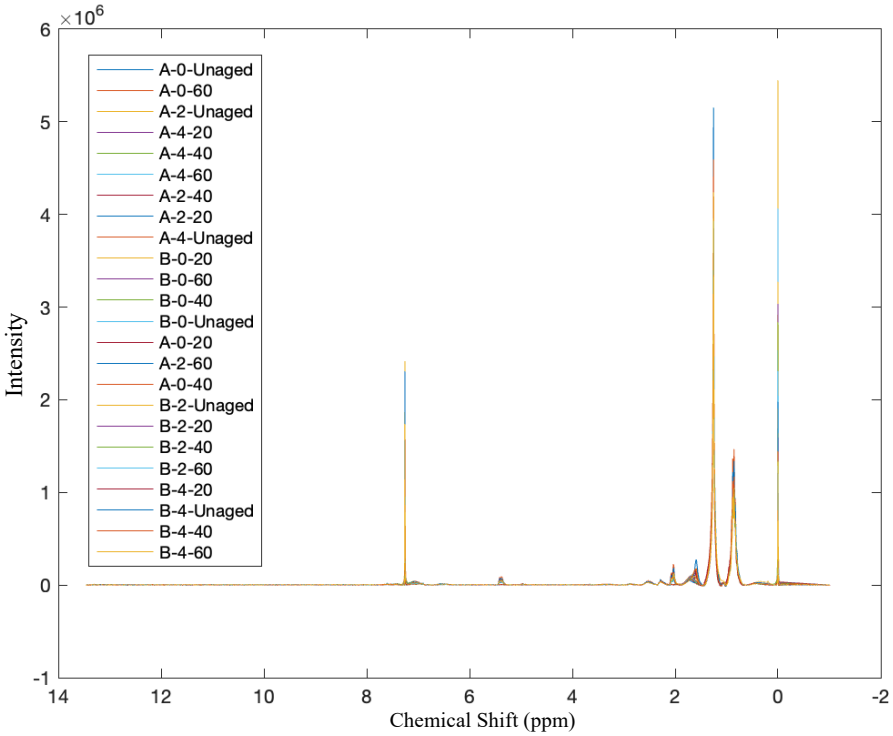


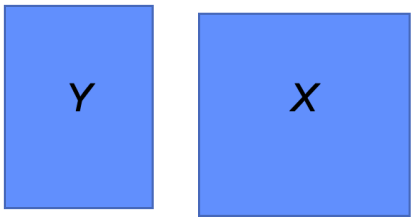
Figure 5.3: Comparison of NMR spectral data after baseline correction.

5.3.5 Multivariate Analysis Techniques

For analysis of FTIR and NMR data collected, in addition to functional group/chemical environment analysis as performed in **Chapter 4**, multivariate analysis was carried out. Principal Component Analysis (PCA), thoroughly described in **Chapter 4**, as well as Partial Least Squares Regression (PLSR) were the two multivariate techniques chosen for use throughout this chapter. The following section describes the theoretical background behind PLSR.

5.3.5.1 Partial Least Squares Regression (PLSR)

PLSR is another multivariate technique, similar to PCA, which can be used for obtaining complementary, but slightly different information from multidimensional datasets. Unlike PCA, PLSR uses a supervised algorithm to perform dimensionality reduction, make predictions and understand correlations between different predictor variables. The major difference between PCA and PLSR lies in the fact that PCA only considers the X data matrix, however, PLSR attempts to reduce dimensions methodically by relating two blocks of variables (both independent and dependent) (K. Wang et al., 2019).



In relation to spectral data, the X matrix can be considered as the same data matrix presented in the PCA section discussed in **Chapter 4**, whereas the Y matrix includes column vectors for example $\mathbf{y_1}$ – concentration of additive, $\mathbf{y_2}$ – ageing time, etc. Unlike conventional forms of regression, where there is only one set of Y variable, in this case, there can be multiple at each observation or test. PLSR has been widely used for a variety of different applications, but in the field of analytical chemistry, it has been used for predicting compositions, physical properties, etc. from spectral data such as NMR, FTIR and Near Infrared (NIR). This was one of the first major practical applications of PLSR. This section presents a very high-level overview of how PLSR is performed and the mathematical theory behind it (Abdi, n.d.; Yan et al., 2022b).

One of the major drawbacks of PCA in its original form is that it results in standard linear combinations (SLCs) of variables which represent different PCs. These, however, only capture the characteristics of the X-vector or predictive variables. No importance is usually assigned to how each predictive variable may be related to the dependent or target (Y) variables. For this reason, PCA is referred to as an unsupervised dimensional reduction technique. If attempting to perform multivariate regression, significant improvements can be made if the SLCs of predictive variables are built to include as much information

from the raw data matrix, X, as well as the relation between predictor and the target variables (Y). PLSR allows this to be achieved while also providing an alternate yet complementary approach to PCA.

In the context of spectral data, consider a similar scenario to that presented in the PCA section, where 48 spectra were recorded for a single binder at different ageing states. If another binder source was introduced with the same three ageing states and number of replicates, the data matrix, X, would have dimensions [n x p] and consist of (48 spectra x 2 binder sources), n = 96 spectra. In this case, 'p' remains the same as in the PCA section since all spectral data were collected using the same resolution, i.e. the number of wavenumbers at while intensity values were collected. The target variables matrix, Y, would consist of 'n' rows and q columns (where q is the number of different target or Y variables e.g. ageing state/concentration of SBS) resulting in the dimensions [n x q].

PLSR works by successively extracting factors (similar to PCs in PCA), from both the X and Y matrices such that the covariance between the factors from X and Y is maximized. Covariance is a measure of the relationship between two (random) variables and to what extent each change with the other. If covariance is high, this indicates good (high) correlation or between variables (Ergon, 2013; Ruby-Figueroa, 2015).

PLSR therefore, attempts to find a linear decomposition (similar to PCA) of both X and Y such that:

$$X = TP^T + E \tag{5.7}$$

$$Y = UQ^T + F \tag{5.8}$$

Where X is the data matrix of dimensions [n x p], Y is the target variables matrix with dimensions [n x q], T and U are the score matrices of X and Y respectively, with dimensions [n x r], and P and Q are the loading matrices of X and Y with dimensions [p x r] and [q x r] respectively. E and F are the residual matrices of X and Y with dimensions [n x p] and [n x q] respectively. The decomposition is therefore done by finding T and U matrices of X and Y which maximizes the covariance between them (T and U). There are multiple algorithms that can be used to solve the PLSR problem, however they all involve an iterative process to extract the X- and Y-scores. The scores/factors for X and Y are extracted successively and the number of factors or scores extracted (r) depends on the rank of the matrix X and Y. One of the most widely used algorithms for solving the PLSR problem is eigenvalue decomposition where each extracted X-score are linear combinations of X, again here, similar to PCA (Ergon, 2013; Ruby-Figueroa, 2015). At each iteration, one column of the X-score matrix, T is extracted and is of the form:

$$\boldsymbol{t} = X\boldsymbol{w} \tag{5.9}$$

Where $\boldsymbol{t}$ is one column in the score matrix T and $\boldsymbol{w}$ is an eigenvector corresponding to the first eigenvalue of the variance matrix $C_{xy}C_{yx}$, where C_{xy} is the covariance matrix of X and Y and C_{yx} is the covariance matrix of Y and X. Therefore, $\boldsymbol{t}$ can be found by determining the eigenvectors of the $C_{xy}C_{yx}$ matrix (Ruby-Figueroa, 2015). Referring to equation (5.7), the corresponding column in the loading matrix, T, can be found using the following equation:

$$\boldsymbol{p} = X^T \boldsymbol{t} \tag{5.10}$$

In a similar manner, one column of the Y-score matrix, Q, can be extracted, and is of the form:

$$\boldsymbol{u} = Y\boldsymbol{c} \tag{5.11}$$

Where $\boldsymbol{u}$ is one column in the score matrix U and $\boldsymbol{c}$ is an eigenvector corresponding to the first eigenvalue of the variance matrix $C_{yx}C_{xy}$. The corresponding column in the Y-loading matrix can be extracted using the following equation:

$$\boldsymbol{q} = Y^T \boldsymbol{u} \tag{5.12}$$

After extracting the first columns in the score and loading matrices for X and Y, the original matrix values of X and Y can be deflated according to the following equations:

$$X_1 = X - \boldsymbol{t}\boldsymbol{p}^T \tag{5.13}$$

$$Y_1 = Y - \boldsymbol{u}\boldsymbol{q}^T \tag{5.14}$$

This process can then be repeated from Equation (5.9) extracting one addition column of the score and loading matrices for X and Y, until X_i and Y_i are reduced to a null matrix. The number of latent variables (factors/scores) that is kept is determined by the user since, in theory, the same number of factors as predictor variables in the X data matrix can be extracted. The multivariate analysis in this chapter was performed using both PCA and PLSR. The methods were compared and contrasted, in order to extract as much valuable information from the spectral data as possible.

5.4. Results and Discussion

5.4.1 Rheological Testing Results

The master curves in Figures 5.4 and 5.5 below show that as the polymer content increases, there is an increase in the complex modulus at low frequencies and a slight decrease in the complex modulus at low and intermediate temperatures. These trends are observed at all aging levels. Figure 5.4 shows the master curves for binder A with 0%, 2% and 4% SBS at 20, 40 and 60 hours of PAV aging. At 20- and 40-hour PAV aging, there is a slight difference in complex modulus at low and intermediate temperatures. However, the difference is much larger at 60-hour PAV aging. Similarly, Figure 5.5, which depicts binder B, shows small differences in complex modulus at low and intermediate temperatures for the 20-hour PAV. However, a much larger difference is noted at 40-hour PAV aging and a more subtle difference at 60-hour PAV aging. The overall trend remains the same for both binders A and B, showing the advantages of SBS modification at all aging levels on high and intermediate temperature properties. This confirms that the presence of SBS continues to improve rheological properties even after long-term oxidative aging. Although degradation of the SBS chains in the bitumen occurs upon oxidation, the rheological behaviour in the temperature-frequency sweep master curves indicate that the improved rheological characteristics are maintained despite

aging. This may result from good compatibility between the bitumen and SBS due to the presence of a cross-linking agent.

The crossover temperature for each binder sample with different SBS contents and aging levels were calculated. The crossover temperature (T_{cross}) of an asphalt binder is the point where the storage modulus and loss modulus are equal, or "crossover". It was determined when the phase angle of the asphalt binder equals 45° at the intermediate temperature range. This parameter offers more insightful information to characterize the viscoelastic behaviour of the binder blends at the intermediate service temperatures and represents the point at which the dominant behaviour of the binder transitions from elastic to viscous.

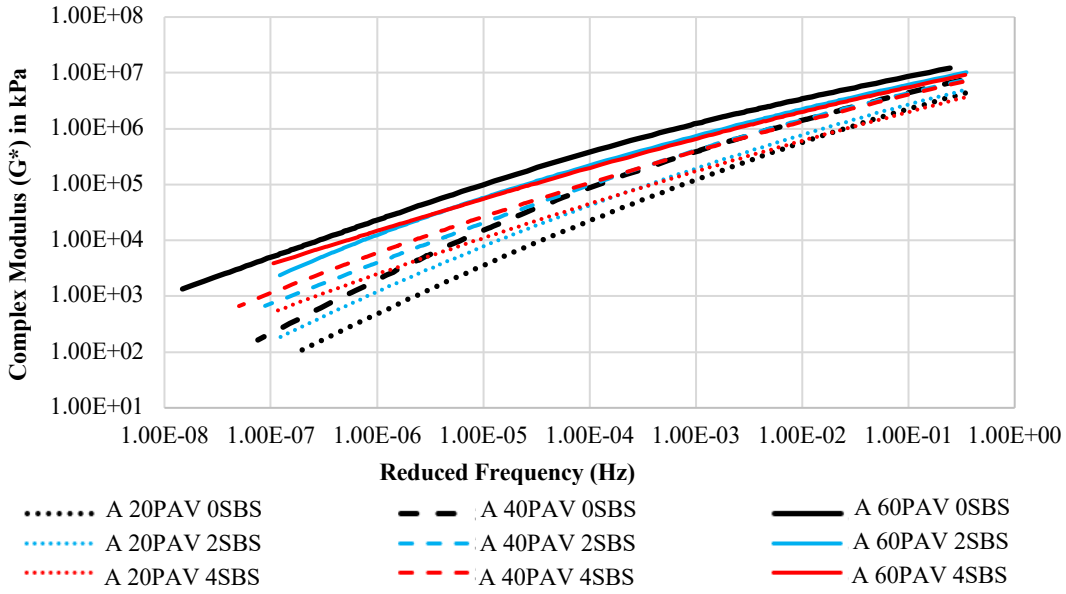


Figure 5.4: Representative Master Curves for Binder 58-28A with 0, 2 and 4% SBS at different aging levels.

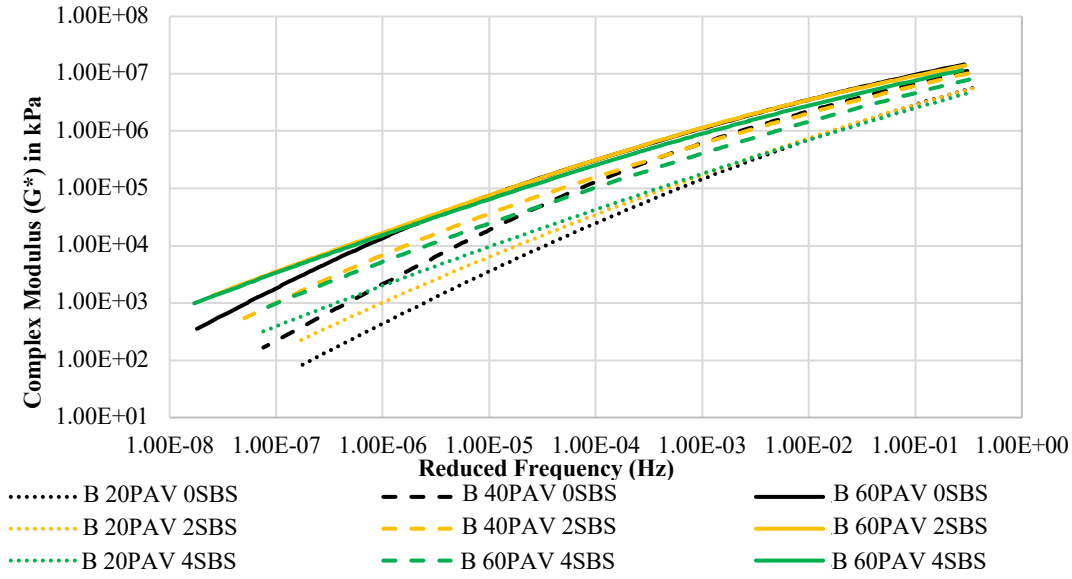


Figure 5.5: Representative Master Curves for Binder 58-28B with 0, 2 and 4% SBS at different aging levels.

BBR test results were also used to determine the m-value and creep stiffness, followed by the ΔT_c parameter for all binder samples. The ΔT_c parameter is the difference between the low PG temperature based on creep stiffness and the low PG temperature based on the m-value. Some literature (Aurilio et al., 2020b, 2023; Kaya Ozdemir et al., 2021b; T. Ma et al., 2012a) mentioned that these parameters are not well suited for polymer-modified asphalt binders. Nevertheless, studies have used them as indicators of the aging level, where a more positive ΔT_c value indicates a less aged binder. The addition of SBS appears to mimic the aging process when evaluating rheological properties. This results in a "flatter" shape master curve and difficulty in properly accounting for the improvements in field performance observed when using SBS-modified asphalt. The relationship between the crossover temperature and SBS content has also been shown to be dependent on temperature (Yan et al., 2018). The following table summarizes and presents these parameters.

Table 5.2: Crossover temperature and ΔTc parameter for asphalt binder samples. (T_{cross}± 0.83, n = 3; ΔT_c± 1.01, n = 3).

Sample Name	T_{cross} (°C)		ΔT_c	
	Binder A	Binder B	Binder A	Binder B
20PAV 0SBS	13.4	17.4	1.73	0.56
40PAV 0SBS	23.8	26.1	-0.99	-1.33
60PAV 0SBS	34.2	28.6	-2.04	-3.65
20PAV 2SBS	16.4	16.8	1.04	0.59
40PAV 2SBS	26.1	27.7	-2.15	-2.67
60PAV 2SBS	36.6	34.0	-5.08	-4.09
20PAV 4SBS	12.7	15.8	1.32	1.05
40PAV 4SBS	26.4	25.0	-2.18	-1.57
60PAV 4SBS	35.0	30.8	-4.16	-5.05

5.4.2 ATR-FTIR Analysis

Figures 5.6 and 5.7 below show the FTIR spectra for 58-28A and 58-28B, respectively, with insets to depict the region between 650 cm^{-1} and approximately 1900 cm^{-1}. The spectra from both binders were similar despite being produced by different refineries from a similar crude source. The increase in SBS concentration can be observed with the increase peak height for the polystyrene peak (A_P). Small differences in peak height can be observed at all aging levels indicating the SBS concentration is detectable and is further discussed later. The presence of this peak and the differences between the samples with increasing SBS concentration make it suitable for evaluating the degradation of SBS. Similar trends can be observed with the peaks for polybutadiene trans double bond (A_{PTDB}) and polybutadiene vinyl double bond (A_{PVDB}).

Sulfoxide (A_{1030}) and carbonyl peaks (A_{1700}) also show increase in peak height with aging. The sulfoxide peak can also be seen to experience a shift towards ~1020 cm^{-1} with increasing ageing level, which may indicate the formation of other functional groups. The peaks around 868, 817 and 744 cm^{-1} represents out-of-plane deformation vibrations of aromatic CH groups, and actual location of peaks are dependent on the number of adjacent aromatic H atoms in the aromatic system (Tammer, 2004; Werkovits et al., 2023). In combination with regions mentioned in last point and increasing total aromatic C content shows that the average aromatic structures possibly experience changes during the aging process such as an increase in the size of aromatic systems. An overall decrease of the band at 1167 cm^{-1} and a slight increase of the band at 1125 cm^{-1} was also observed with increasing ageing levels. Signals in fingerprint region were difficult to interpret, since many different bands of various functional groups contribute and superimpose.

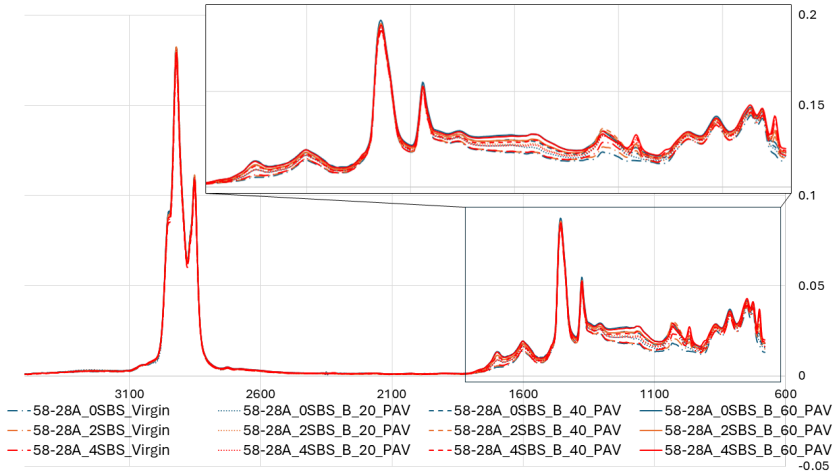


Figure 5.6: FTIR spectra for 58-28A with 0, 2 and 4% SBS at 20-, 40- and 60-Hour PAV Aging.

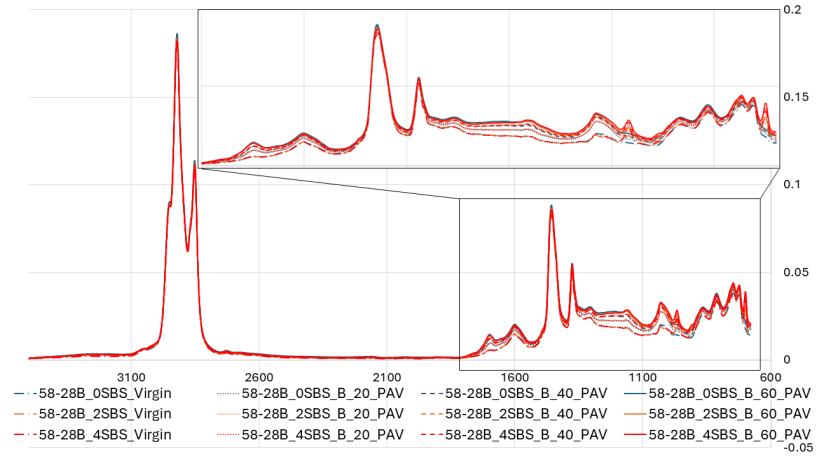


Figure 5.7: FTIR spectra for 58-28B with 0, 2 and 4% SBS at 20-, 40- and 60-Hour PAV Aging.

Degradation of the SBS chains within the bitumen is possible as oxidative aging takes place. I_{PTDB} and I_{PVDB} have been used to evaluate the degradation potential of SBS modified bitumen by other researchers (Ren et

al., 2022b; Yan et al., 2018). The ratio of the polybutadiene vinyl and trans double bonds to the ratio of polystyrene tends to increase indicating the relative amount of vinyl and trans double bonds is increasing compared to polystyrene. This trend can be observed in Figure 5.8 and occurs for both bitumen sources as the aging time increases. The increasing ratio indicates that the presence of the vinyl and trans double bonds is increasing faster than the increase in the polystyrene peak. Degradation would be indicated by a decrease in this ratio as the polybutadiene bonds break down more readily. This corresponds with the observations of the rheological behaviour in the temperature-frequency sweep master curves presented earlier indicating that the improved rheological characteristics are maintained despite aging and that degradation may not pose a serious issue with this combination of SBS and bitumen. This may be a result of good compatibility between the bitumen and SBS but may also be attributed to the presence of a cross-linking agent which improved the level of bonding in the polymer network.

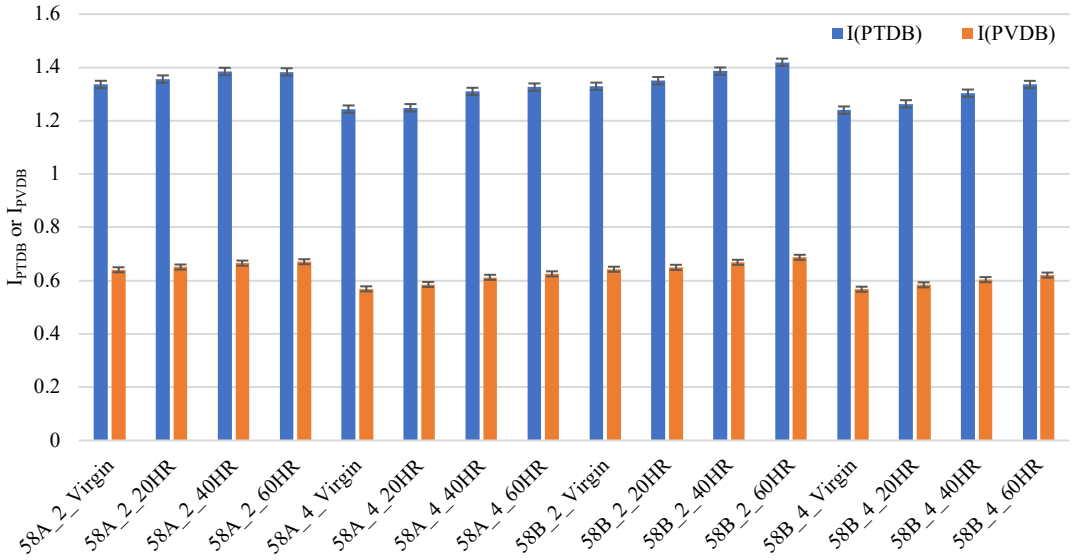


Figure 5.8: Changes in polybutadiene vinyl double bond and trans double bond-based indexes with aging and SBS modification. (Error bars represent standard deviation, n = 12).

The more commonly used carbonyl and sulfoxide indices indicate that the aging characteristics of the two bitumen sources are similar. As observed in Figures 5.9 and 5.10, the trend is similar between both binders, with 58-28A showing a slight increase in carbonyl index from 20 to 60 hours of PAV aging, but also showing a plateauing in sulfoxide index. Sulfoxide index tends to plateau with increased aging as the reactive sites are used up (Ren et al., 2022b).

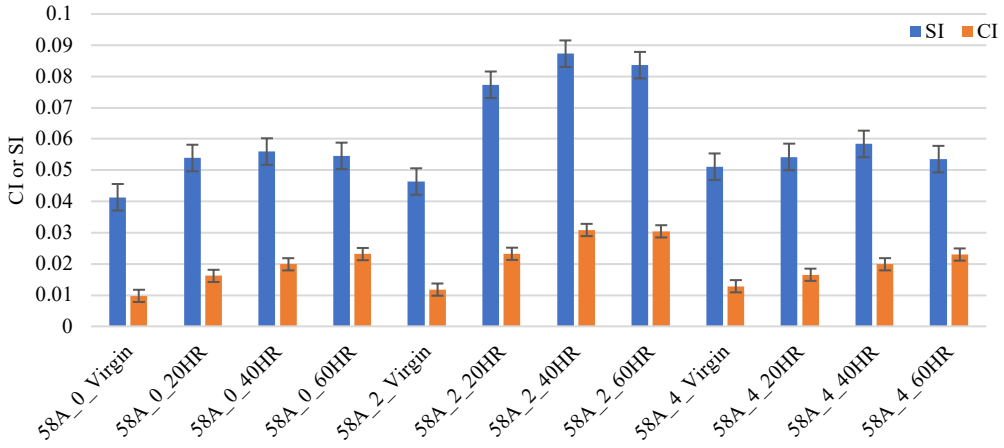


Figure 5.9: Sulfoxide Index (SI) and Carbonyl Index (CI) at different aging conditions and SBS contents for PG 58-28A. (Error bars represent standard deviation, n = 12).

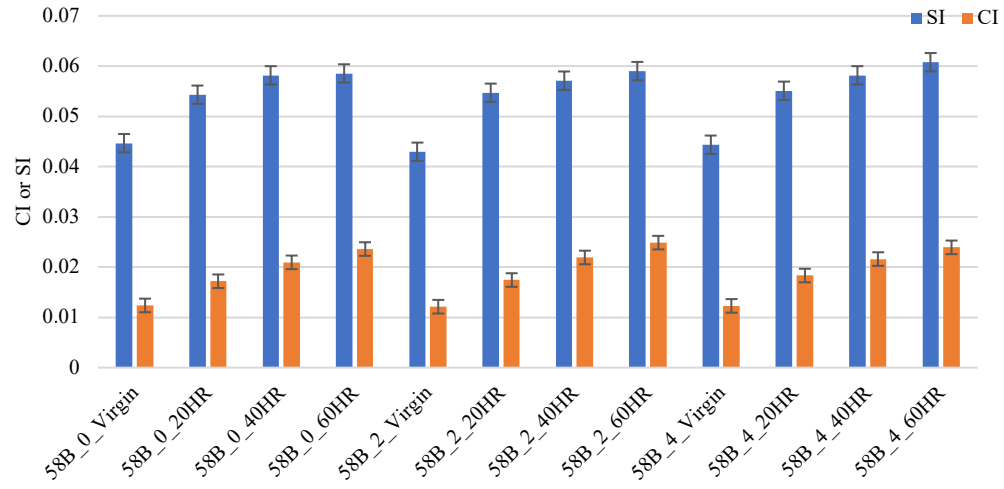


Figure 5.10: Sulfoxide Index (SI) and Carbonyl Index (CI) at different aging conditions and SBS contents for PG 58-28B. (Error bars represent standard deviation, n = 12).

The aging trends of the polymer modified bitumen is similar to the trends seen with the unmodified bitumen. Figure 5.9 shows a large increase in sulfoxide and carbonyl index for the 58-28A with 2% SBS at 20-, 40- and 60-Hours PAV aging, but this result was unexpected. The trend for 58-28A at all SBS contents was a small decrease or plateauing of the sulfoxide index at 60 hours PAV. 58-28A tends to have a lower modulus at low and intermediate temperatures compared to the 58-28B for 2 and 4% SBS at each aging level as seen in Figure 5.4. 58-28A with 0% SBS may appear to age more quickly than 58-28B with 0% SBS, but the SBS modified 58-28A samples appear to have improved rheological properties. The carbonyl index of the 58-28A with 4% SBS also increases at the slowest rate of all the bitumen combinations in this chapter. The sulfoxide and carbonyl indices of 58-28B change at a consistent rate even as the SBS content increases for all aging levels. The addition of SBS may be improving the aging characteristics of 58-28A, but only has

minimal impact on the aging characteristics of 58-28B. However, the compatibility between the bitumen and SBS may play a more important role. Techniques such as Gel Permeation Chromatography can be applied in future research to further understand the impact of aging on the SBS microstructure.

5.4.3 ^{1}H NMR Analysis

The following figures show a sample spectrum using raw data for neat and SBS-modified asphalt binders. Major peaks of interest are also identified and described in the figures. After pre-processing the spectral data, peak heights and the area under peaks of interest were obtained and normalized to the mass of bitumen in the sample. The height and area under peaks in an NMR spectrum are proportional to the number of nuclei that give rise to the signal at a specific chemical shift value (Qiu et al., 2022). Typically, in ^{1}H-NMR, different protons appear at different chemical shift values. The typical region of interest (ROI) ranges for H_γ, H_β and H_α protons are found between 0.5-1.0, 1.0-2.0 and 2.0-4.0, respectively (Betancourt Cardozo et al., 2016; W. Wu et al., 2022). H_γ protons are hydrogens linked to γ-carbon of the aromatic nucleus and γ beyond CH_3 and CH groups, while H_β is linked to β-carbon of the aromatic nucleus and β beyond CH_2 and CH groups. Similarly, H_α protons are hydrogens linked to α-carbon. Figures 5.11 and 5.12 below highlight the bitumen proton regions of interest as well as the TMS and $CDCl_3$ peaks.

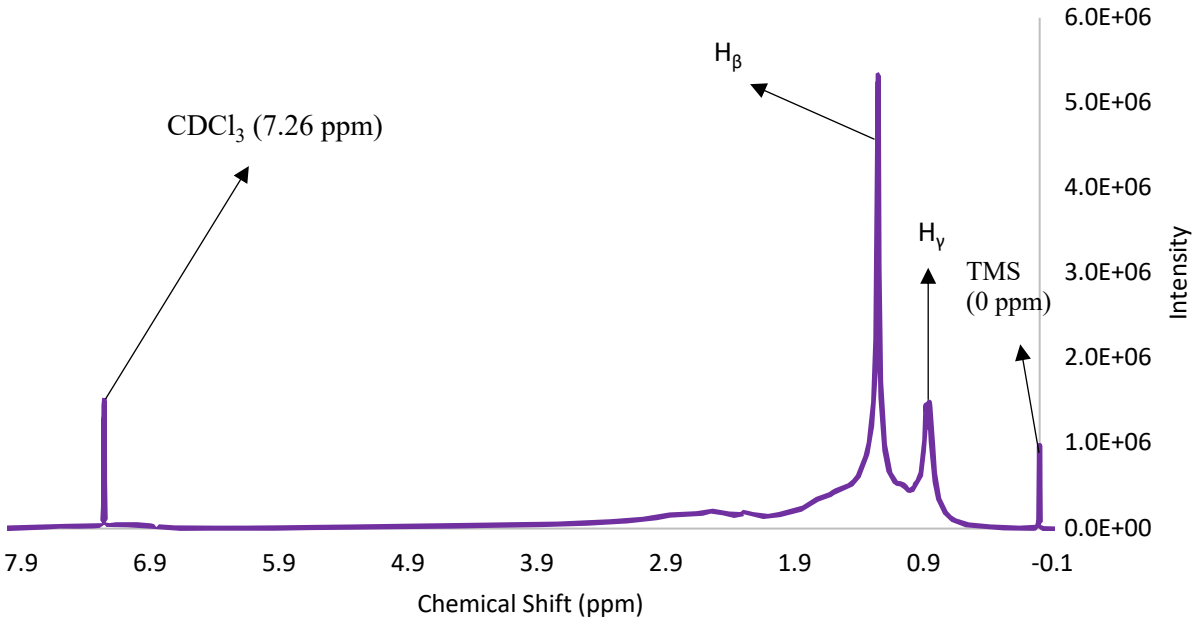


Figure 5.11: Typical ^{1}H NMR spectrum obtained for neat asphalt binder.

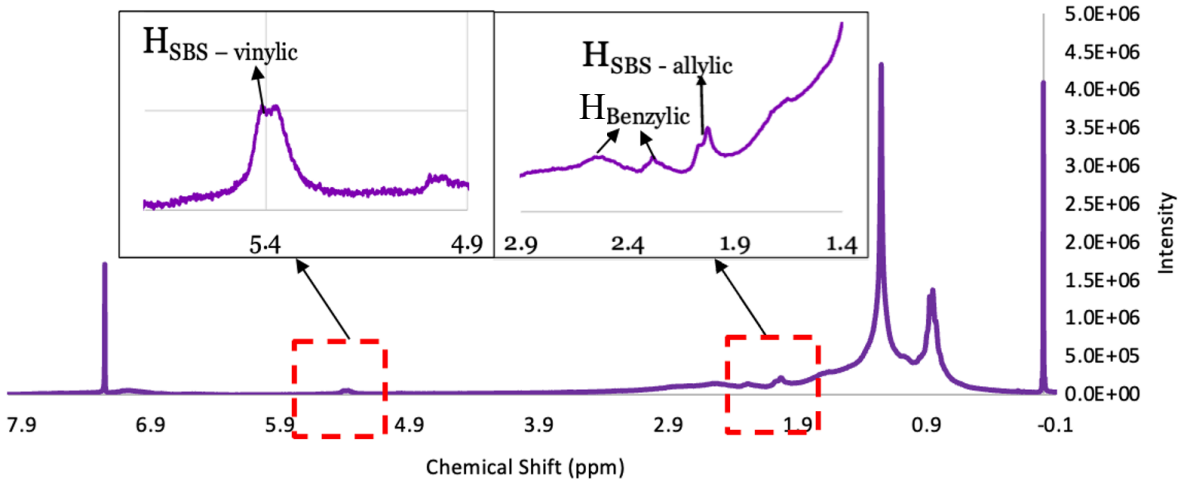


Figure 5.12: Showing the ^{1}H NMR spectrum for asphalt binder with 2% SBS.

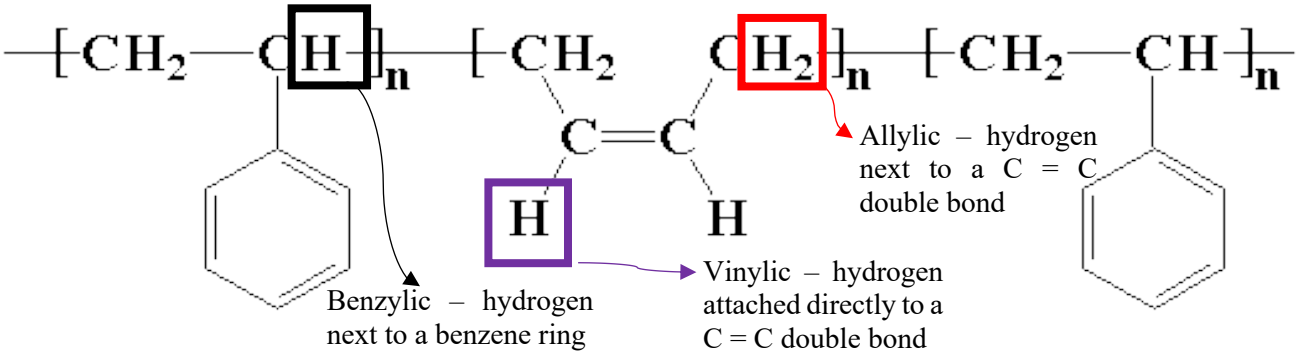


Figure 5.13: The structure of SBS with identification of the spatial locations of characteristic SBS peaks.

The peaks which are characteristic of SBS, identified in Figure 5.12, indicate the location of hydrogens found in the triblock SBS co-polymer. For further clarification of the nuclei locations, shown in Figure 5.13 indicates the typical molecular structure of SBS and the spatial arrangement of hydrogens corresponding to the SBS peaks shown in the spectra.

Based on the NMR spectral data collected, the area under several peaks of interest, mentioned earlier, was calculated and related to sample type and SBS content. Figure 5.14 shows the relationship between the area under peaks that are known to be related to aging (H_{γ}, H_{β}) based on the findings of previous studies (Betancourt Cardozo et al., 2016; Huang, 2010; Siddiqui, 2010) and the sample type (aging level and SBS content). The figure shows a noticeable decrease in peak area for both aging peaks with increasing aging level at all concentrations of SBS, with an approximately linear relationship. Since peak area in NMR is directly proportional to the amount of a specific species present in specific chemical environments, all binders were found to have a smaller amount of H_{γ} when compared to H_{β}. This was expected since is H_{β}, typically relates to the hydrogens found in CH_2 groups while H_{γ} is associated with the presence of $-CH_3$ groups. Most of the molecules in both SBS and asphalt binders are relatively long-chain molecules; therefore, $-CH_2$ is more likely to be abundant in these chains than $-CH_3$ since methyl can only exist as a

terminal group. Finally, when comparing the unaged binders with 0%, 2%, and 4% SBS, the area under the aging peaks decreases with increasing SBS content. This can potentially be explained by the fact that increasing SBS content leads to higher levels of interactions, crosslinking, structural modifications and entanglement, resulting in less free H_γ and H_β present.

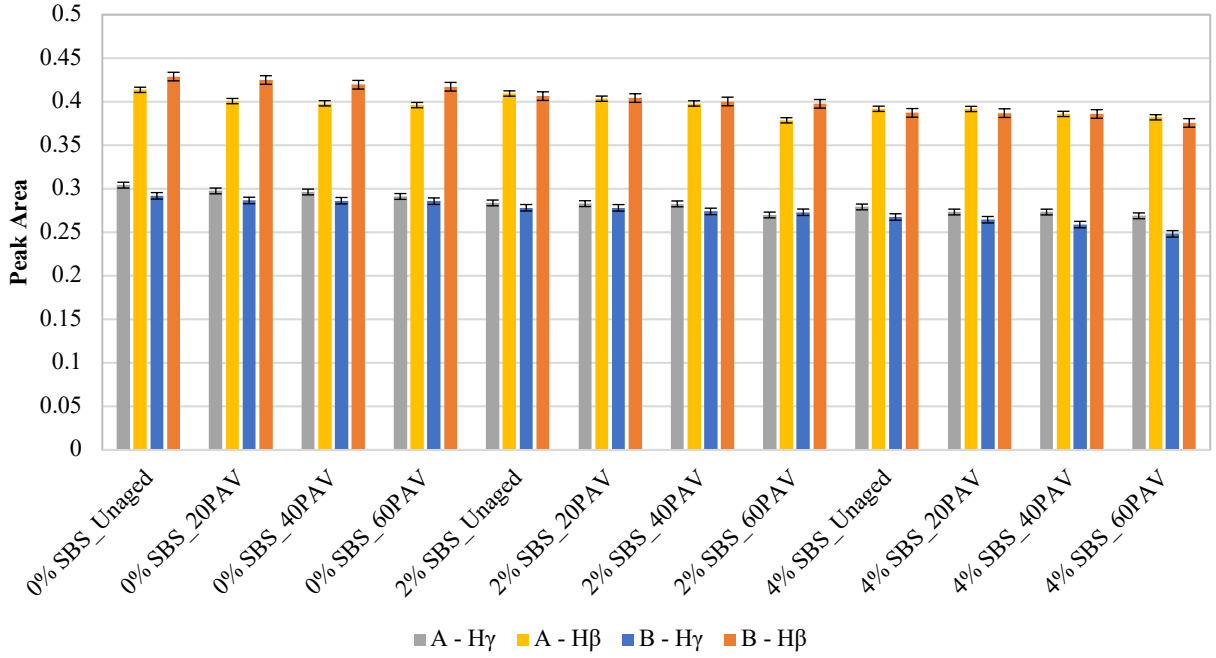


Figure 5.14: The area under H_β (1.25 ppm) and H_γ (0.9 ppm) Peaks for Binders A and B. (Error bars represent standard deviation, n = 3).

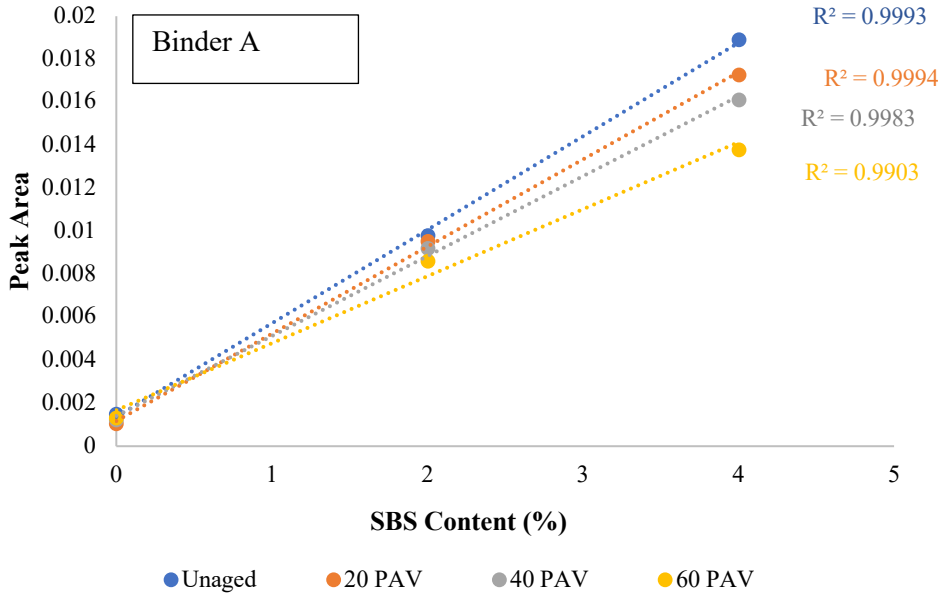


Figure 5.15: Area under Vinylic H (~5.4 ppm) peak vs SBS content for Binders A.

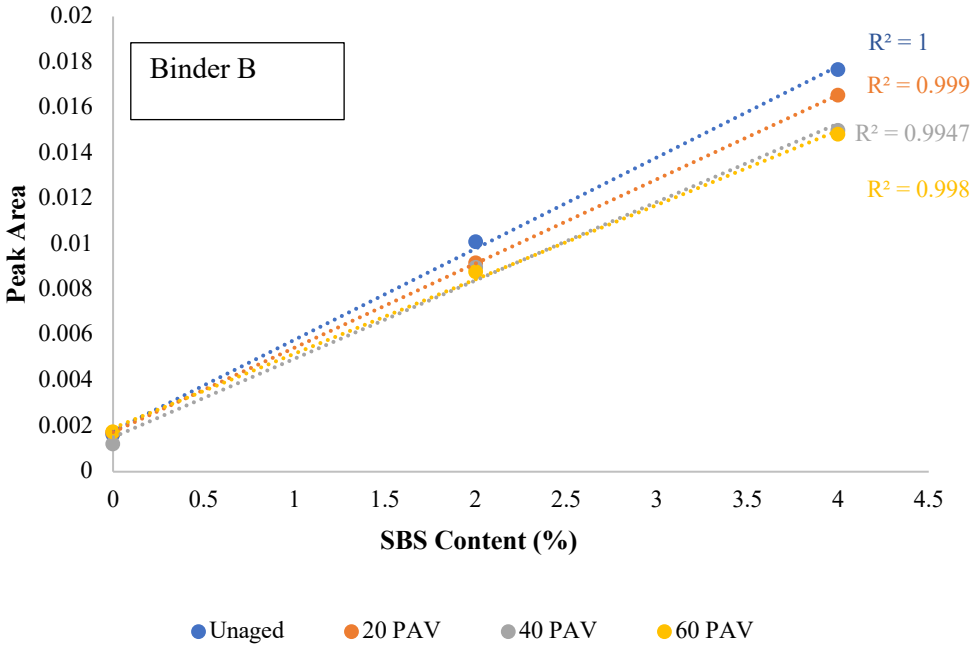


Figure 5.16: Area under Vinylic H (~5.4 ppm) peak vs SBS content for Binders B.

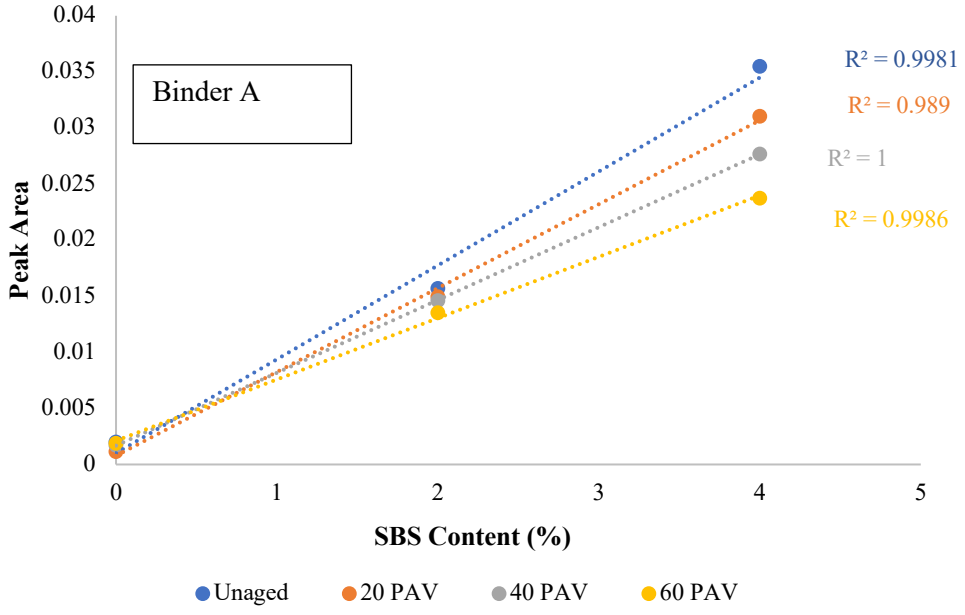


Figure 5.17: Area under Allylic H (~2ppm) peak vs SBS content for Binders A.

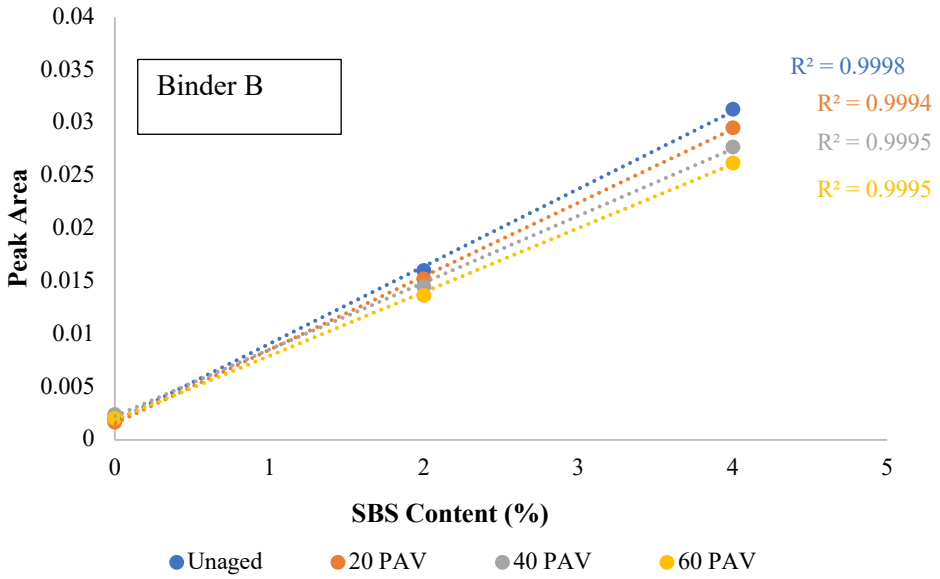


Figure 5.18: Area under Allylic H (~2ppm) peak vs SBS content for Binders B.

Figures 5.15 – 5.18 above present the relationship between the area under characteristic SBS peaks ($H_{SBS\text{-}Allylic}$ and $H_{SBS\text{-}Vinylic}$) and SBS content for both binders A and B at different aging levels. These peaks were established as being specifically associated with SBS, based on the fact that they only appear in binders with SBS, as well as from findings in previous literature (Qiu et al., 2022). In general, the peak area for both binders increased with higher SBS concentration. Furthermore, a strong linear correlation was found between these peak areas and SBS content, as indicated by the well-fitted trend lines and high R^2 values. Another crucial observation is the decrease in peak areas when comparing samples with the same SBS content and increasing aging state. This can be attributed to increased degradation or breakdown of the SBS at higher aging levels. The effect of this breakdown on the rheological performance of the binders is explored further in the following section, where the relationships (if any) between chemical and rheological results are presented.

5.4.4 Correlations Between Rheological and NMR Testing

This section attempts to determine whether any correlations exist between aging peaks obtained from NMR and rheological testing data. Figures 5.19 – 5.22 present plots of the area under aging peaks for both binders A and B vs crossover temperature, while Figures 5.23 – 5.26 shows the same y-axis (aging peak area) vs the ΔT_c parameter.

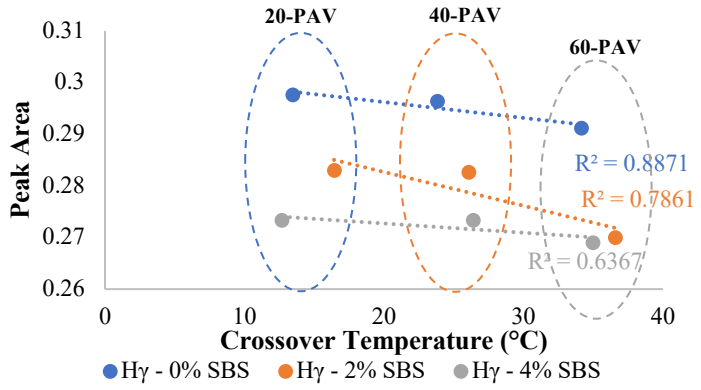


Figure 5.19: Relation between Crossover Temperature and H_γ at different SBS contents for A.

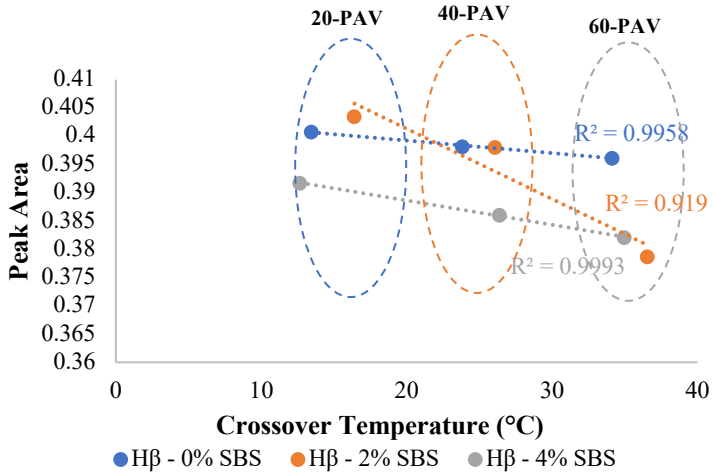


Figure 5.20: Relation between Crossover Temperature and H_β at different SBS contents for A.

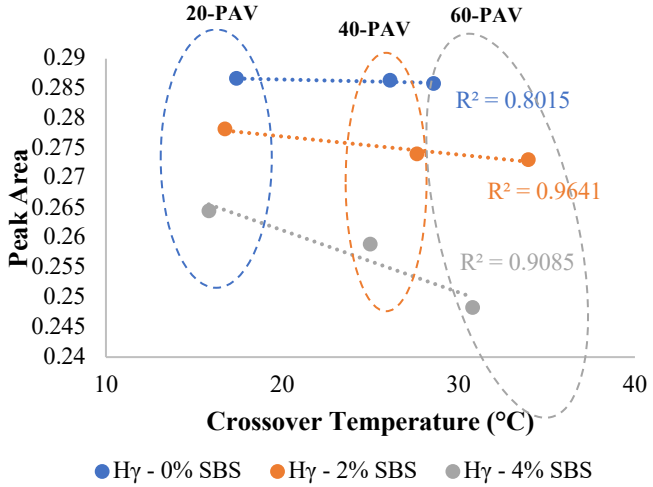


Figure 5.21: Relation between Crossover Temperature and H_γ at different SBS contents for B.

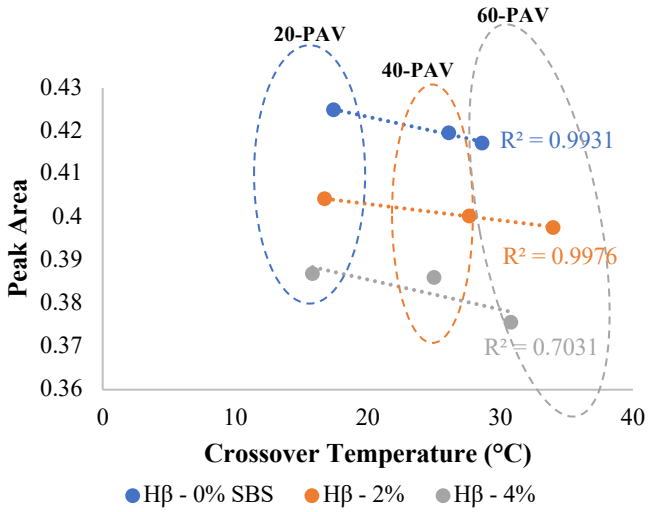


Figure 5.22: Relation between Crossover Temperature and H_β at different SBS contents for B.

Focusing on the crossover temperature, the results for both binders A and B demonstrated highly significant linear correlations between the aging peak areas and the crossover temperature. When comparing the two binders, stronger linear correlations were observed for binder B, suggesting higher correlation between rheological and chemical characteristics. Additionally, across different SBS contents, an increase in the aging level corresponded with an increase in crossover temperature, indicating that the binder became more rigid with aging, which is consistent with typical oxidative aging and loss of volatiles in asphalt binders. Comparing SBS contents of 0%, 2%, and 4%, it was observed that higher SBS content led to a slower rate of increase in crossover temperature with aging, supporting the theory that SBS enhances aging resistance in asphalt binders. Furthermore, as SBS content increased, the aging peak areas at equivalent aging levels decreased, suggesting increased interaction between SBS and the asphalt binder. This interaction likely results in more extensive cross-linking or alterations in the chemical environment of the hydrogens. Overall, these findings indicate that the addition of SBS improves the high-temperature performance and durability of asphalt binders over time. The significant reduction in peak area with higher SBS content suggests enhanced polymer interactions, which could improve elasticity and resistance to permanent deformation of the binders. This ultimately leads to improved resistance to rutting and thermal cracking. The network formed by the interactions can also hinder oxygen diffusion into the pavement structure, therefore, increasing aging resistance. Since there is also less available H_γ and H_β, for oxidation in unaged 2% and 4% SBS binders when compared to unaged 0% SBS, as seen by the decreasing peak areas observed in Figure 5.14, less oxidation can occur, limiting the rate of reaction, resulting in increased aging resistance.

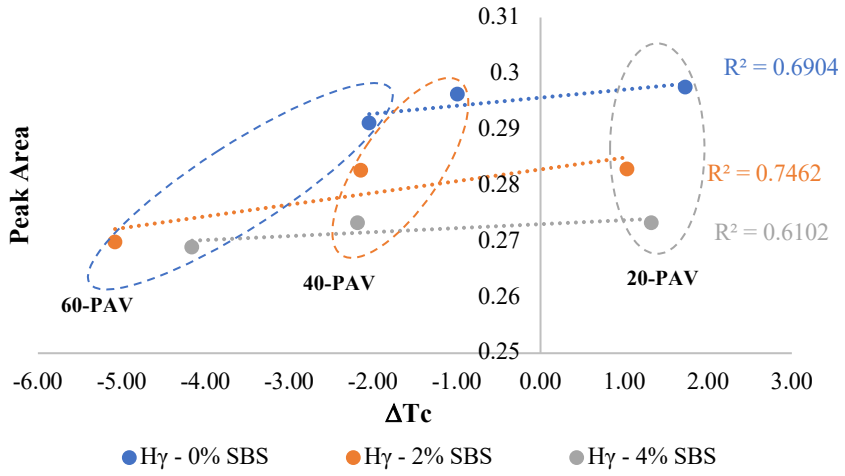


Figure 5.23: Relation between ΔT_c and H_γ at different SBS contents for A.

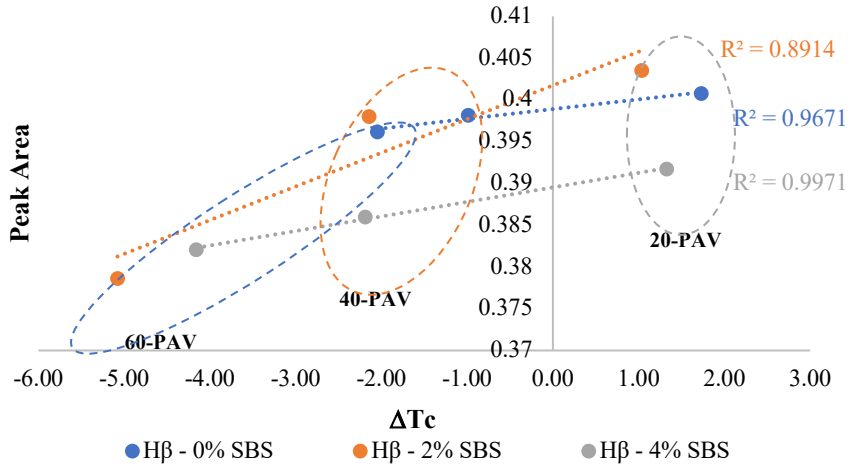


Figure 5.24: Relation between ΔT_c and H_β at different SBS contents for A.

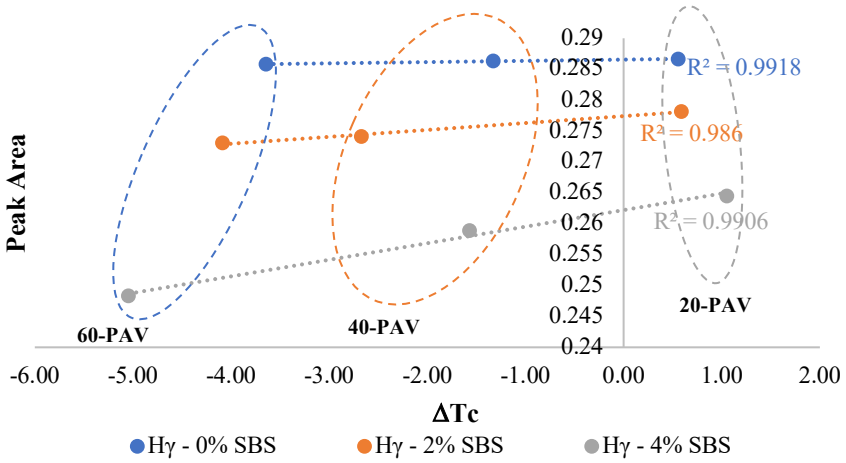


Figure 5.25: Relation between ΔT_c and H_γ at different SBS contents for B

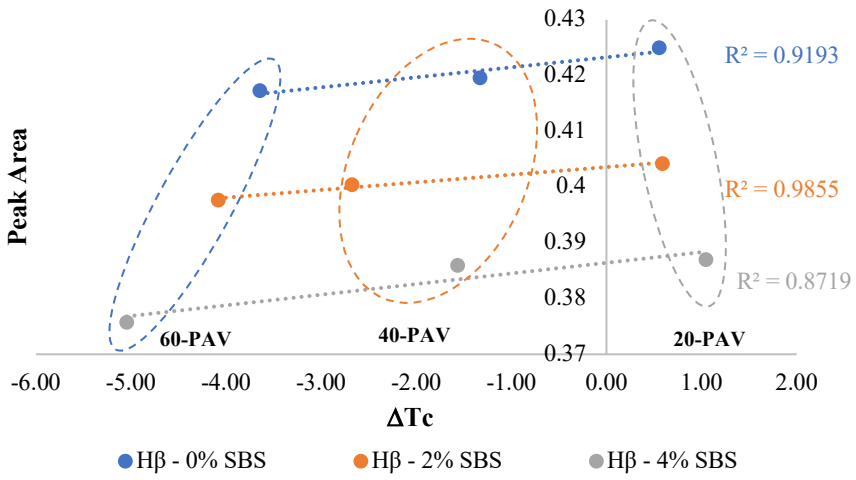


Figure 5.26: Relation between ΔT_c and H_β at different SBS contents for B

Figures 5.23 – 5.26 show the relationship between the area under the H_γ and H_β peaks and the ΔT_c parameter obtained from BBR measurements of asphalt binders A and B with different SBS contents and aging states. As the aging time increases from 20 hours to 60 hours, there is a general trend of decreasing ΔT_c values. Similar to crossover temperature, a linear correlation between ΔT_c and aging peak areas for each SBS content was observed at all concentrations of SBS, as indicated by the fitted lines with their R^2 values. However, higher linear correlations were observed between the crossover temperature and peak areas. In general, the ΔT_c parameter indicates the low-temperature performance of an asphalt binder, which typically decreases with aging due to increased stiffness and brittleness, as observed in these figures. The figures also support the statement that the type of SBS used in this study, may be more compatible with binder B when compared to binder A since higher linear correlations and more distinct trends are observed in the results of binder B. On comparing increasing SBS contents, the rate of decrease in ΔT_c increases. This can indicate that the SBS could be slightly worsening the low-temperature performance. Previous literature on SBS (Cui et al., 2023)found that while the addition of SBS did not cause a change in the overall low PG of the asphalt binder, there was an increase in continuous low PG, which was determined as the SBS percentage increased. This also does not account for the change in glass transition temperature that occurs with the addition of SBS. The cross-plots provided in this section gives insight into the relationship between chemical and rheological properties, however a deeper understanding can be obtained through multivariate analysis which is discussed in the following sections.

5.4.5 Multivariate Analysis of Spectroscopic Data for SBS-modified Asphalt Binders A and B

Multivariate analysis methods are typically comprised of a large number of advanced statistical techniques. There are a variety of different techniques most of which are somewhat complementary. Principal

Component Analysis (PCA) was discussed in **Chapter 4** and was used in this section of analysis as an exploratory technique. Partial Least Squares Regression (PLSR), another multivariate technique, introduced in this chapter, was used to further determine if FTIR and NMR can be used for estimating parameters such as SBS concentration, ageing state and binder sources, in addition to rheological properties. In this section, both PCA and PLSR, were performed separately on FTIR and NMR data following which they were compared.

5.4.5.1 PCA on FTIR and NMR Spectral Data

PCA is a very powerful tool when attempting to explore data structures and clusters, however, preprocessing of the data is crucial for obtaining meaningful insights and logically sound observations. The concept of garbage-in, garbage-out, applies heavily when utilizing any multivariate analysis technique. For FTIR data, simple baseline correction available in the Spectragryph software (which applies polynomial curve fitting for adjusting baseline shifts) was performed followed by normalization of the spectra with respect to the area under all meaningful peaks in the FTIR spectra. For NMR preprocessing, the data was first phased to obtain gaussian peaks, baseline corrected, using the airPLS algorithm mentioned in section 5.3.4.2, and finally normalized with respect to all meaningful peaks (excluding solvent/reference peaks). For both NMR and FTIR data, PCA was performed on the data set for binder A alone, binder B alone, and lastly on the concatenated data with both binders A and B to determine whether PCA could help with differentiating between different binder sources. To illustrate the importance of proper spectral pre-treatment, the figures presented below show results from PCA analysis of binder A before and after preprocessing. A clear observation can be made, where the data clusters/groupings are more well-defined and distinct when compared to no pre-processing.

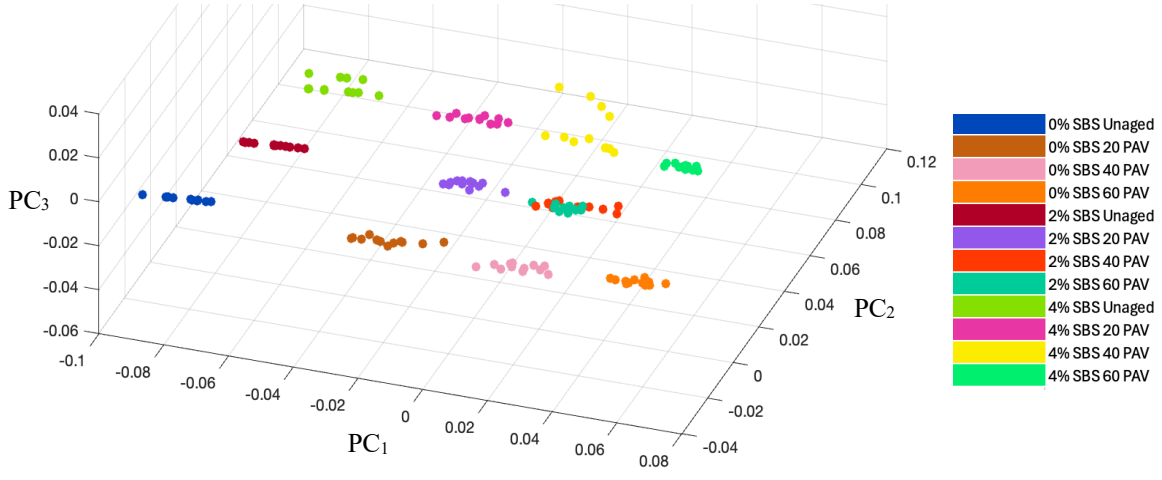


Figure 5.27: Score Plots obtained from PCA Analysis on FTIR Data (after pre-processing) for Binder A.

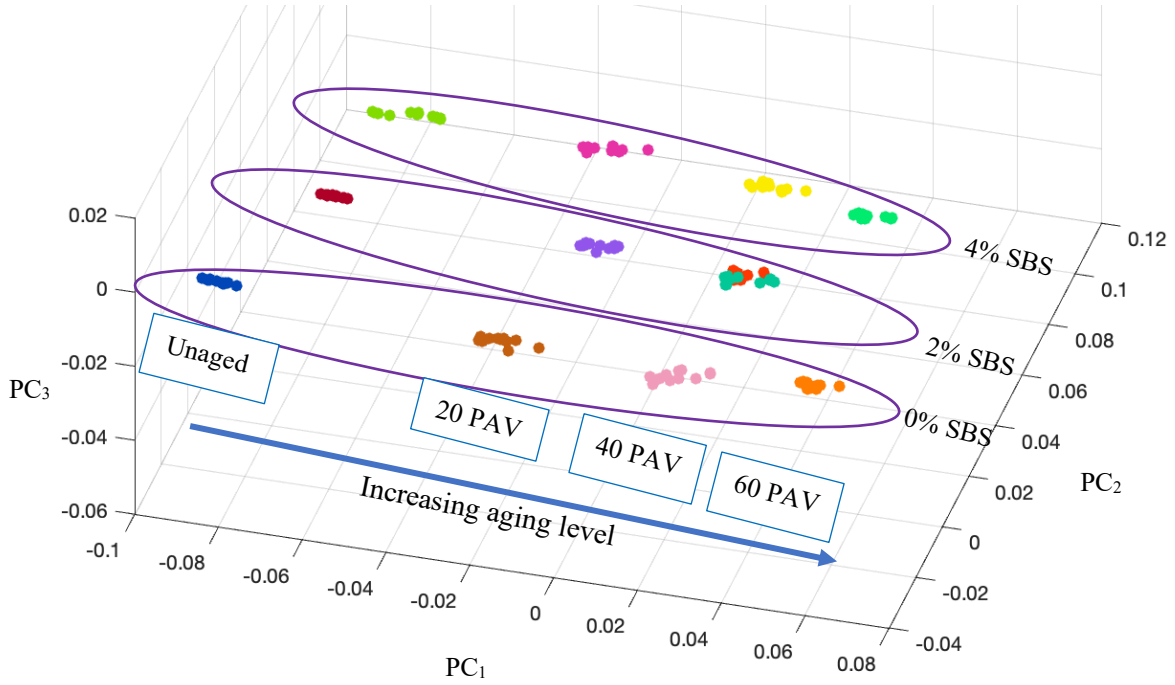


Figure 5.28: Score Plots obtained from PCA Analysis on FTIR Data (after pre-processing) for Binder A.

On comparing Figures 5.27 and 5.28, a notable difference was observed. Clusters were found to be more defined, and distances between clusters were much larger in Figure 5.28. This highlights the importance of pre-processing for obtaining reasonable results. It is important to note that the labels presented in Figure 5.28 also apply to Figure 5.27. PCA was capable of differentiating all ageing states and SBS concentrations for binder A with the exception of 2% SBS at 40 and 60 hr. PAV ageing level. Many reasons can potentially explain this, one of which can be possible errors during the aging protocol the 60 hr. PAV aged sample, leading to less significant ageing. Unaged binder A samples at all concentrations of SBS were also found to have a larger separation distance from clusters related to all other ageing states. Similar observations were made for binder B as shown in the score plot (after pre-processing FTIR data) presented below in Figure 5.29.

PCA was found to be capable of differentiating all SBS concentrations and ageing states for binder B, unlike binder A. This could support the statement that errors may have occurred during the ageing process/procedure of binder A at the 60 hr. PAV level. Overall, PCA was found to be well suited for an exploring the spectral data of both binders A and B, successfully distinguishing between aging states as well as SBS concentrations. One major concern with respect to using FTIR for asphalt binder characterization is whether or not it is able to differentiate between different sources when additives such as SBS are present. To investigate this further, the same PCA protocol was applied to the concatenated FTIR data from both binders A and B. The resulting score plot from this analysis is presented in Figure 5.30 below.

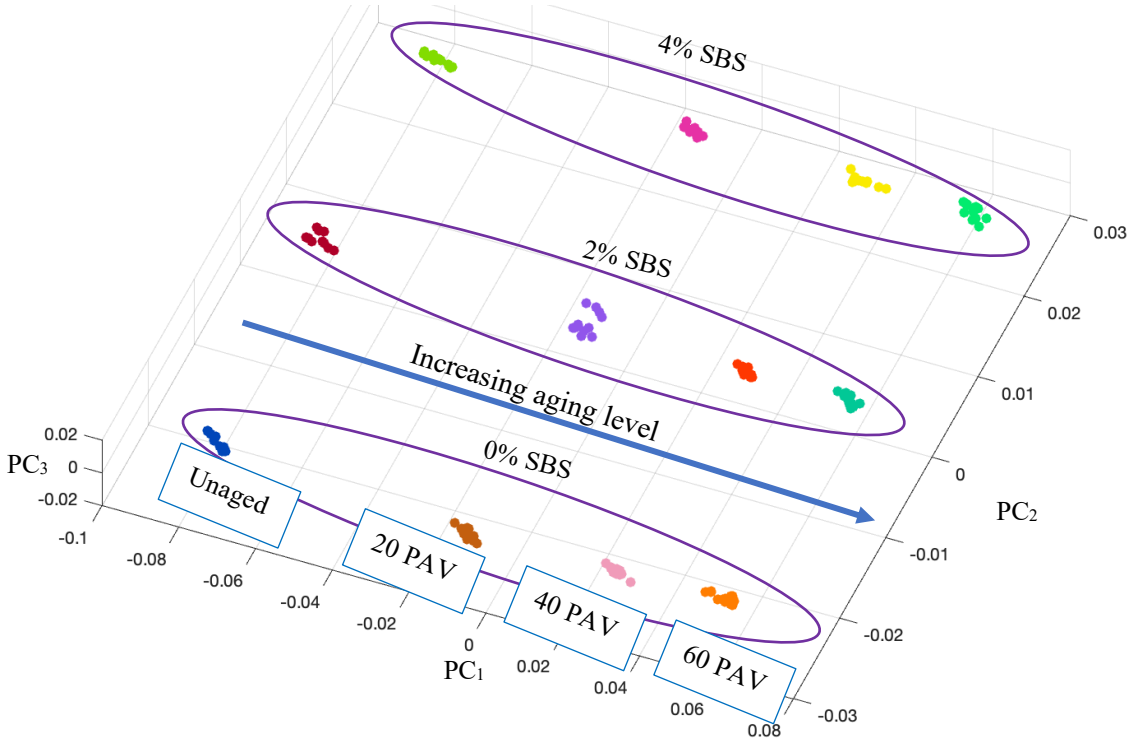


Figure 5.29: Score Plots obtained from PCA Analysis on FTIR Data (after pre-processing) for Binder B.

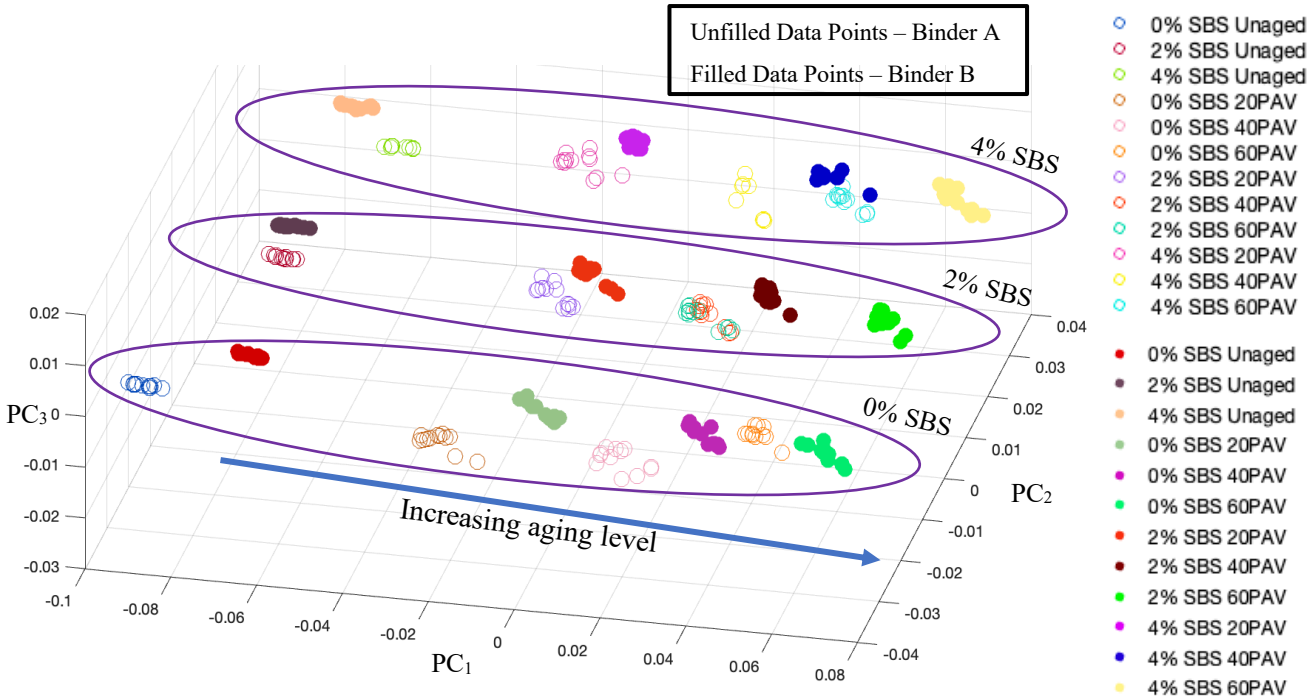


Figure 5.30: Score Plots obtained from PCA Analysis on FTIR Data (after pre-processing) for Binders A and B.

In general, binder A can be distinguished from binder B, however with increasing ageing state, the differences between binder sources in this case, become less prominent. Nevertheless, distinct groupings for different SBS concentrations and ageing states were identified in Figure 5.30. Based on these results, it

can be concluded that FTIR, when combined with PCA, is an extremely powerful tool for investigating factors such as different additive concentrations, ageing states and binder sources.

Since NMR can provide more insight into the structure of components found in asphalt binders and tends to have fewer overlapping peaks/signals, PCA was also applied to the NMR data collected for binders A and B, with less replicates, since NMR requires more time for sample preparation. The pre-processing stage with NMR spectral data was shown to be even more critical when compared to FTIR. In the case of FTIR, clusters were still somewhat identifiable when PCA was performed on data without pre-processing, which was not the case with NMR. Before pre-processing no distinct clusters could be identified. Pre-processing allowed for the identification of well-defined clusters with respect SBS concentration, but clustering with respect to ageing state was still ambiguous as shown in Figures 5.31 and 5.32. This could be attributed to the fact that significantly less NMR replicates were performed for each sample (3 replicates per sample) when compared to FTIR (12 replicates per sample). One significant advantage of NMR, however, lies in the smaller number of overlapping peaks present in the spectra. This allows for easier identification of additives with peak areas showing very high correlation with respect to additive concentration as presented earlier. Although PCA was not as revealing for the NMR data set in this scenario, when compared to FTIR, increasing the number of replicates can significantly improve the results of PCA.

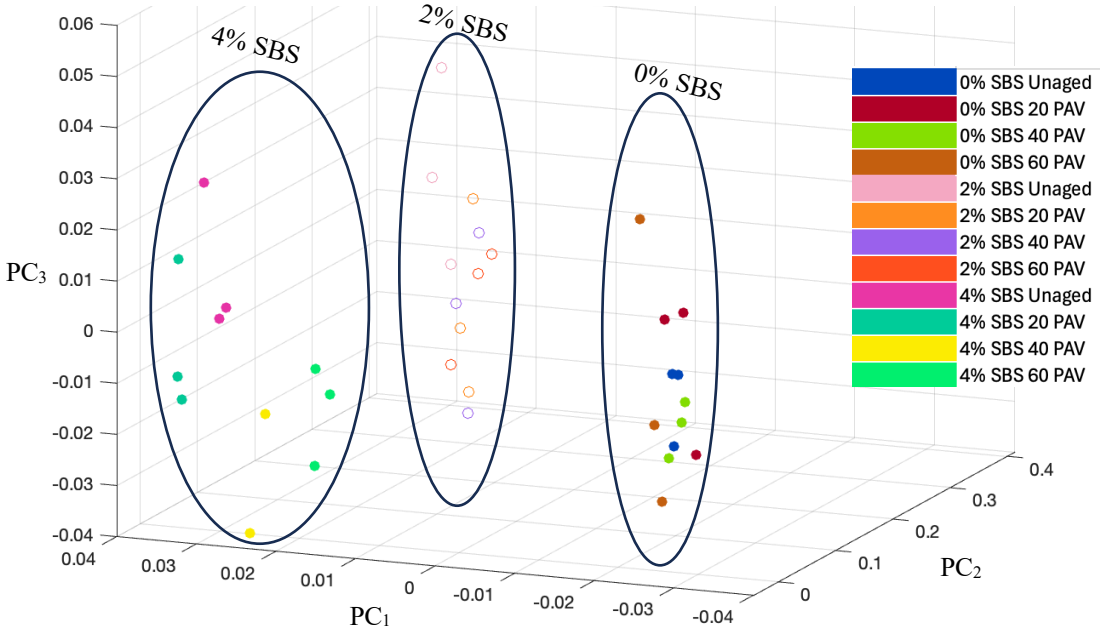


Figure 5.31: Score Plots obtained from PCA Analysis on NMR Data (after pre-processing) for Binders A.

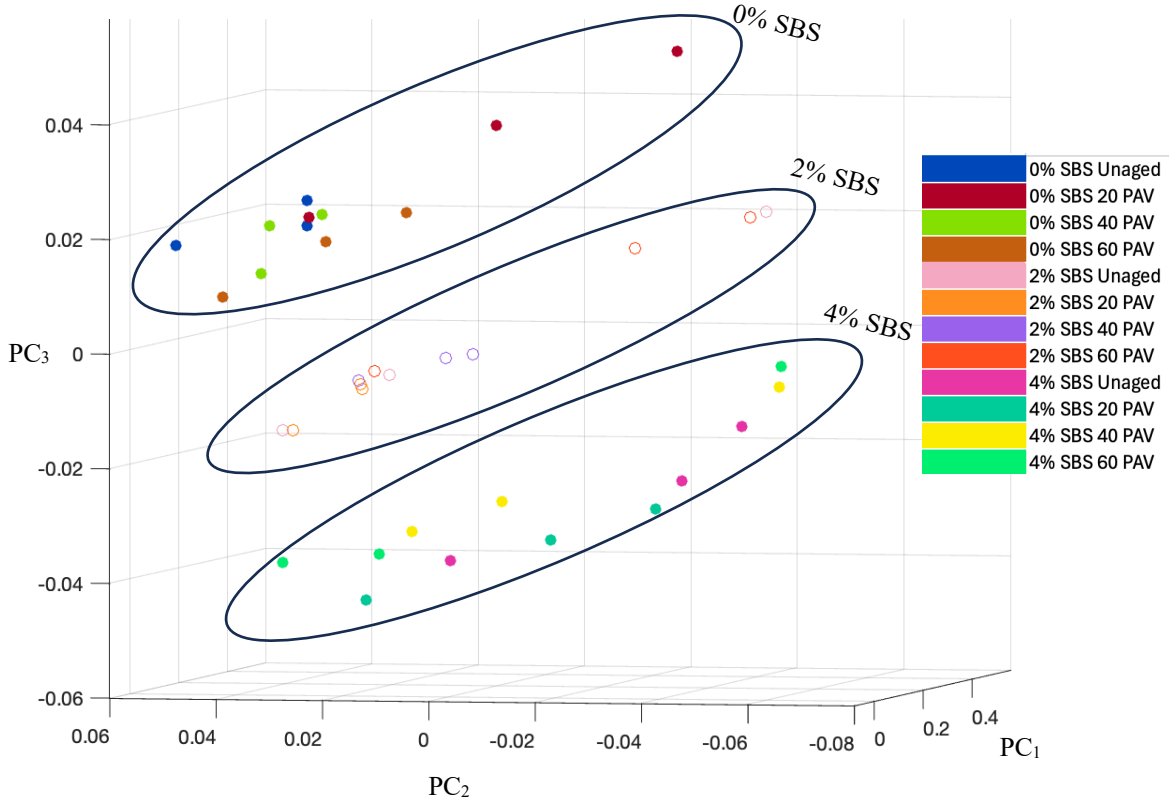


Figure 5.32: Score Plots obtained from PCA Analysis on NMR Data (after pre-processing) for Binders B.

Based on the information presented in this section, PCA was found to be a very useful tool for exploring both FTIR and NMR data sets, with FTIR yielding more informative details. The amount of variance in data explained by the first three principal components (PCs) for both FTIR and NMR are summarized in the table below. This comparison further highlights that PCA of FTIR data captures more variance in the data when compared to NMR, therefore indicating that the former may be better suited for this analysis technique Nevertheless, PCA is an unsupervised algorithm which is limited when attempting to use FTIR and NMR for determining quantitative relationships between the collected data and factors such as additive concentrations, ageing states, and in this case rheological properties. For this reason, other multivariate methods such as PLSR can prove to be very valuable in establishing these links and predicting factors/properties.

Table 5.3: Percentage of Variability in the data explained by first three principal components with FTIR and NMR data.

PC	Variability Explained by PC (%)	
	FTIR	NMR
1	76.26	75.26
2	14.05	12.10
3	6.12	4.47

5.4.5.2 PLSR on FTIR and NMR Spectral Data

PLSR was performed using FTIR and NMR data separately in order to determine which data provides a more accurate model fit for predicting the following:

- SBS concentration
- Ageing State
- ΔTc Parameter
- Crossover Temperature (T_{cross})

Several different scenarios were investigates including PLSR using:

1. NMR/FTIR data from Binder A only
2. NMR/FTIR data from Binder B only
3. NMR/FTIR data from both Binder A and B together

Only scenario 3 was discussed in this in detail throughout this section, however the results for scenarios 1 and 2 are presented in Appendix A. PLSR provides a variety of different valuable information including:

1) Residual plots - indicates how well certain data sets are able to predict dependent variables. These plots can also help in determining whether or not the regression model is sufficiently capturing the underlying pattern in the data without systematic biases.
2) Mean Squared Error (MSE) Plots/Tables – gives indication of how well the regression model performs in predicting dependent variables. MSE is preferred over residuals when comparing models since it gives a single, standard measure of how the model performs (at specific number of model components) as opposed to residuals.
3) Variable importance in projection (VIP) scores – gives insight into which X-variables (e.g. wavenumbers or PPM values in the case of FTIR and NMR respectively), are most influential in predicting dependent variables

Residual Plots

With respect to residual plots, there are two major pieces of information that can be extracted. Firstly, a random scatter of residuals about zero is desirable as it indicates the model is sufficiently specified and there is no evidence of non-linearity or systematic biases. Secondly, identification of extreme residuals become relatively easy, and could be an indication of outliers that affect the model disproportionately.

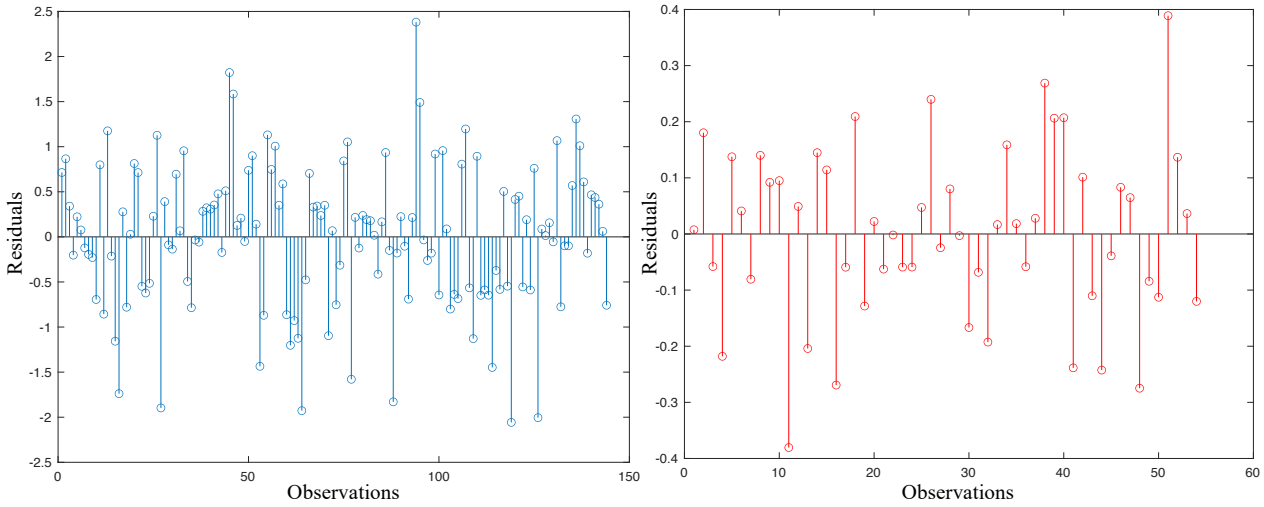


Figure 5.33: Residual Plot for aging state obtained from PLSR on FTIR (left) and NMR Data (right).

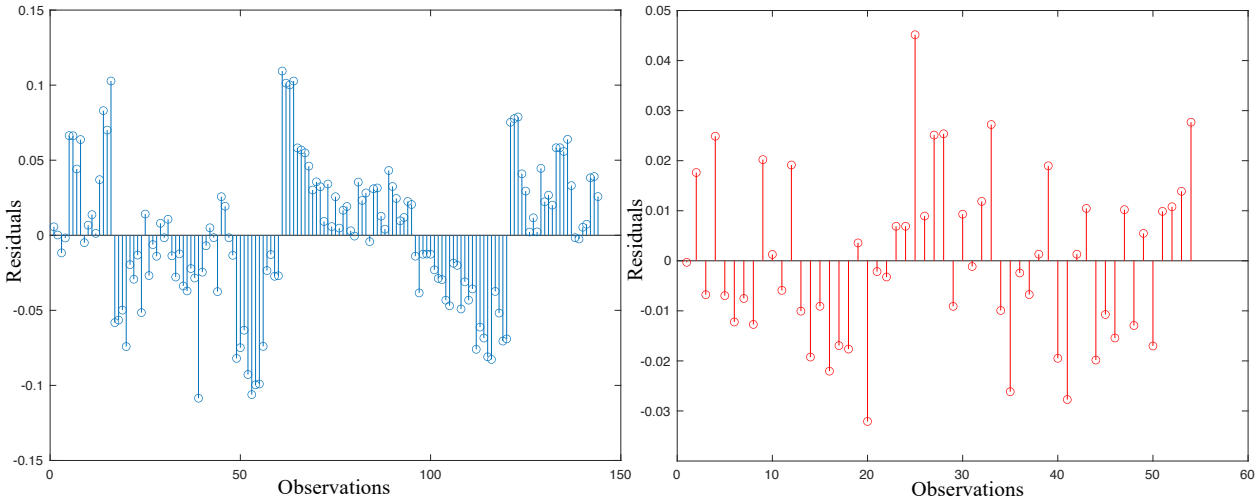


Figure 5.34: Residual Plot for SBS concentration obtained from PLSR on FTIR (left) and NMR Data (right).

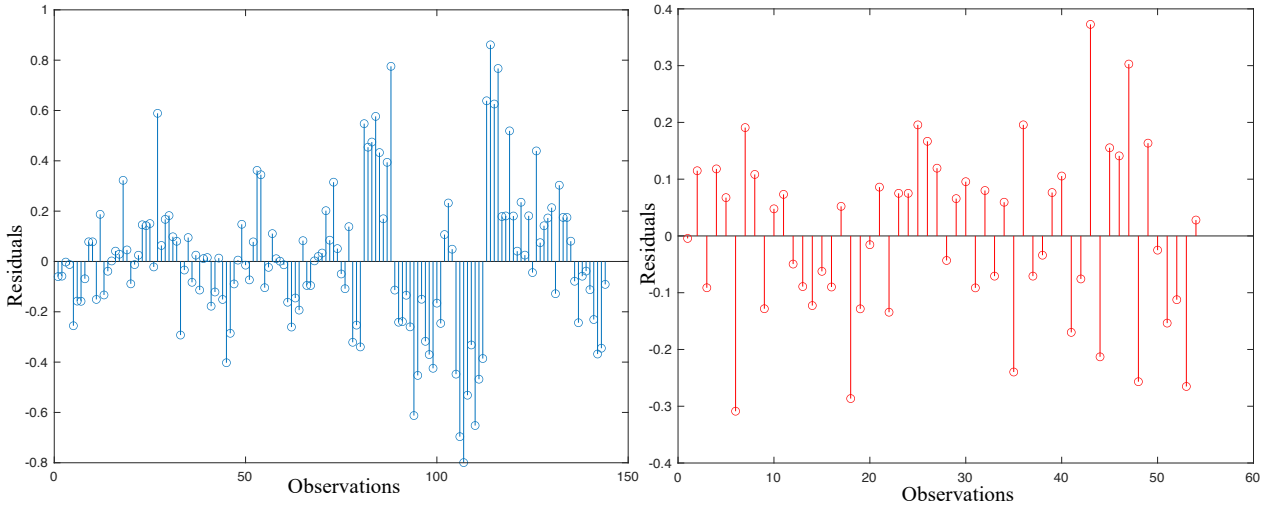


Figure 5.35: Residual Plot for ΔTc obtained from PLSR on FTIR (left) and NMR Data (right).

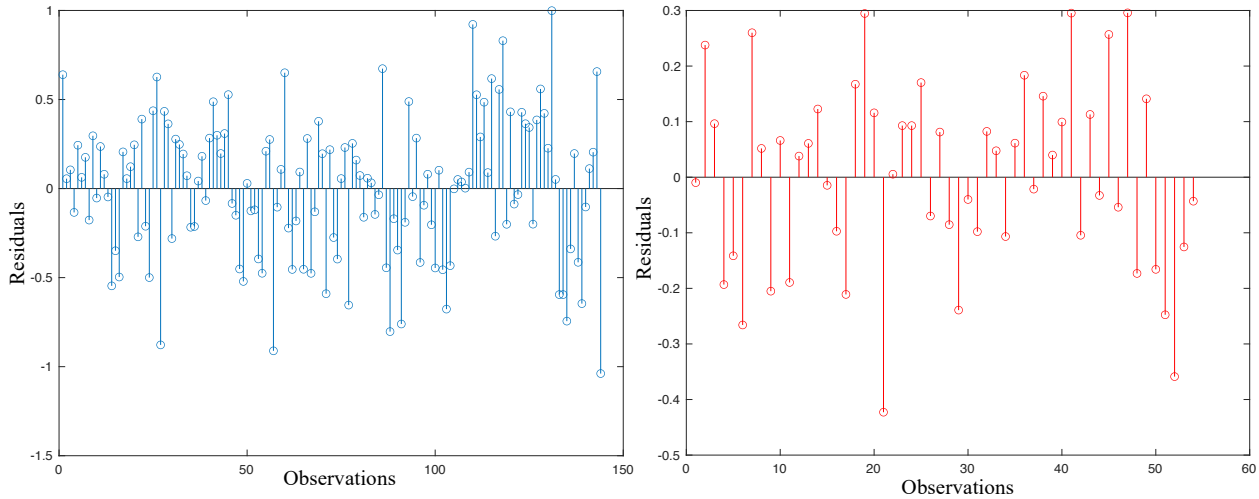


Figure 5.36: Residual Plot for T_{cross} obtained from PLSR on FTIR (left) and NMR Data (right).

Several general observations can be made from the residual plots as follows:

- The magnitude of residuals obtained using NMR data were in general significantly less than that obtained from FTIR data for all four y-variables (SBS concentration, Ageing State, ΔTc and T_{cross}). This indicates that the model obtained from NMR data predicted y-variables more accurately when compared to the model obtained from FTIR data. The largest and smallest residuals occurred when fitting ageing state and SBS concentrations respectively for both FTIR and NMR data, indicating that SBS concentrations were the most accurately predicted while ageing states were the least.
- The residual plots obtained from PLSR using NMR data were more randomly distributed for all y-variables when compared to FTIR. Randomly distributed residuals about zero indicate that the PLSR model performs well and sufficiently captures relationships between dependent and independent variables. It also indicates that the model adequately explains the variance in the data. The residual plots obtained from NMR data were all randomly distributed but the same was not true for FTIR. Based on Figures 5.34 and 5.35, clear patterns can be observed in the FTIR residual plots suggesting that the model is missing some information. The left plot in Figures 5.34 and to a lesser extent Figure 5.35 (corresponding to SBS concentration and ΔTc respectively) displays a clear oscillation, where residuals alternate systematically between positive and negative values in a wave-like manner. This is a strong indication of autocorrelation or cyclical trends in the data. In this case, adjacent data points or observations are likely correlated, which is a violation of the assumption of independence in most regression models. This type of pattern often arises in time series data or data with temporal dependencies, where residuals from one observation are not independent of the residuals from the next. The model may not be accounting for temporal or spatial trends adequately. The alternating pattern also points to possible model misspecification, where the form of the relationship between the predictors and the response variable is not correctly captured by the model. For instance, if the true

relationship is non-linear and a linear model was applied, this kind of periodic residual pattern can emerge. The randomness of residuals was determined visually in this case, however statistical tests can be performed in order verify that they are in fact randomly distributed. Overall, based on visual inspection of all residual plots, NMR data seems to predict all four y-variables better than FTIR data.

MSE Plots

Another metric that can be used for comparing models obtained from PLSR using FTIR and NMR data is the MSE value. The following plots show how the MSE value changes with respect number of components considered in the model. Both models considered 21 components as maximum. From Figure 5.37, as expected, as the number of components included in the model increased, the MSE decreased, however the MSE obtained using NMR data was found to be consistently lower than that obtained for FTIR data. This indicates that the PLSR model obtained from NMR data more adequately explains the variance in the data and accurately predicts all y values. It is important to recall that more replicates were performed for FTIR than NMR. Typically, when comparing data sets with different number of replicates, the dataset with more replicates (in this case, FTIR) usually achieves a lower MSE simply due to increased data reliability, rather than a true improvement in model performance. Due to an increase in sample size (i.e. more replicates), even tiny differences can be magnified to the point of becoming statistically significant therefore leading to a model which fits even the slightest noise in data, i.e. model overfitting.

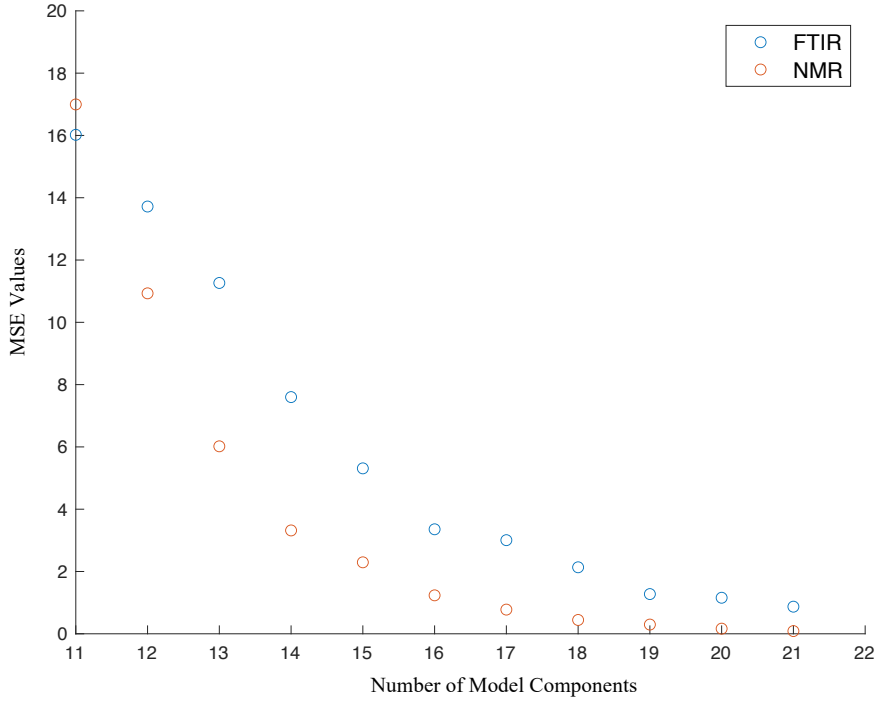


Figure 5.37: MSE vs Number of Components in PLSR model.

This is contrary to what is observed in this case, where the MSE was found to be consistently larger for FTIR data, indicating that even though less replicates were performed for NMR, it still demonstrates greater accuracy in predicting the y variables with consistency. The concept of model parsimony also plays an important role in this scenario. A parsimonious model is a model that accomplishes a sufficient level of explanation or prediction with as few predictor variables as possible. MSE is a measure of how well the regression model predicts or explains the observed values/variance in the data. Therefore, smaller MSE values typically indicate a good/accurate model fit. Figure 5.37 clearly shows that regression of the NMR data provides a more parsimonious model when compared to FTIR data, where few components can use in the NMR PLSR model, while still maintaining a lower MSE value.

VIP Plots

As mentioned earlier, in some cases, model overfitting or underfitting can become a major issue when performing regression. For this reason, it is important to identify which portions of the spectral data (wavenumbers or PPM values for FTIR and NMR data respectively), are most influential in predicting y-variables. This can be easily done by calculating the VIP scores as mentioned earlier. VIP scores are a crucial metric used in PLSR to determine the importance of predictor variables in explaining the response variable. The VIP score for each predictor variable reflects its contribution to the model, in terms of its role in explaining both the independent variables (predictors) and the dependent variables (responses). Typically, variables with VIP scores > 1 are considered important, while those with VIP scores < 1 contribute less to the model. Examining VIP scores can help reduce the dimensionality of the dataset by identifying and retaining the most important variables, while discarding less important ones, aiding in interpretation and improving model performance.

PLSR is a regression method used when the predictors are highly collinear or when the number of predictors is larger than the number of observations. It combines features from principal component analysis and multiple regression, projecting the predictors onto a lower-dimensional space where the covariance between predictors and responses is maximized. VIP scores are computed using the weights and loadings of the PLSR components. A mathematical overview of how they are derived is presented below:

1. **Compute Explained Variance**: For each PLS component, the amount of variance it explains in both the predictor matrix X and the response variables y is determine.
2. **Weighting by Explained Variance**: VIP scores are based on the amount of variance each predictor explains in relation to the variance explained by each component.

Mathematically, the equation used for calculating VIP scores for the j-th predictor variable is:

$$VIP_j = \sqrt{p \sum_{a=1}^{A} \left(\frac{Explained\ Variance\ in\ Y\ by\ component\ a}{Total\ Explained\ variance\ in\ Y} \right) \omega_{ja}^2} \quad (5.15)$$

Where:

p is the total number of predictors (wavenumbers or PPM values)

A is the total number of components

ω_{ja} is the weight of j-th predictor in the a-th component

In general, VIP scores reflect the importance of each predictor variable in the model, accounting for both the correlation with the response and its contribution across all components. A predictor with a high VIP score is considered highly important in predicting the response. The figures below show the VIP score plots for predictor variables in PLSR of FTIR and NMR data (red points represent VIP score greater than 1).

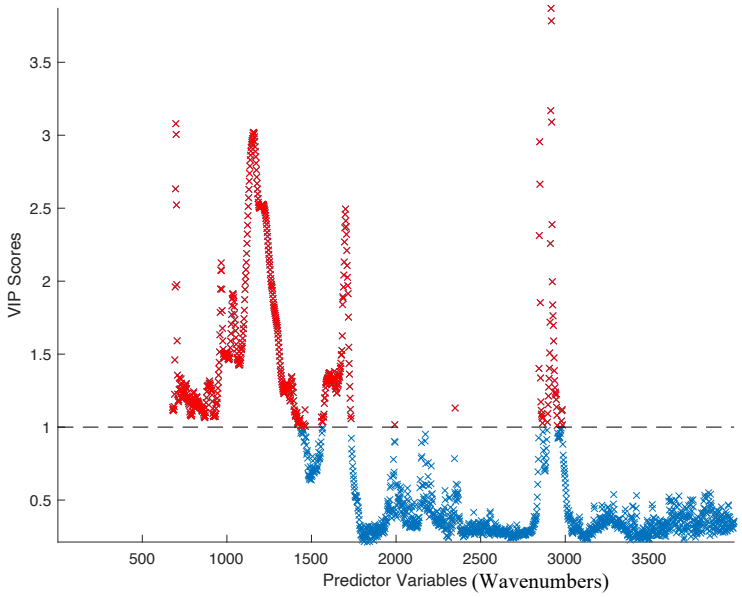


Figure 5.38: VIP Score Plot obtained from PLSR on FTIR Data. (Red points represent VIP > 1)

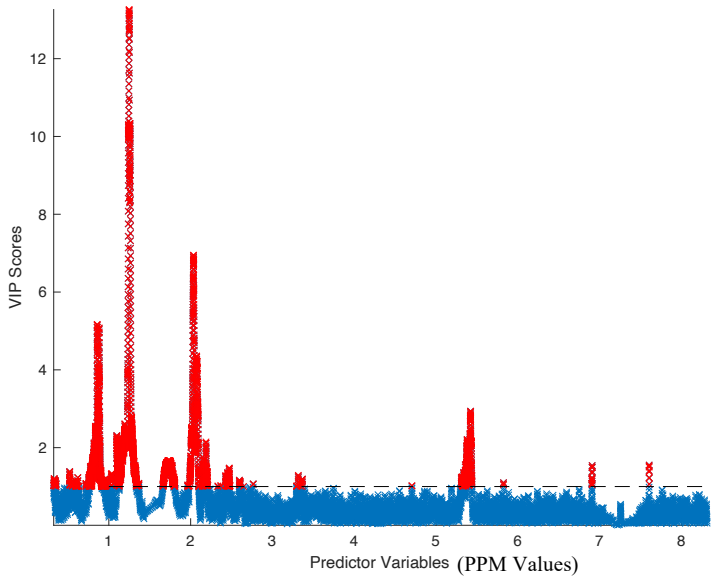


Figure 5.39: VIP Score Plot obtained from PLSR on NMR Data. (Red points represent VIP > 1)

With respect to Figure 5.38, the x-axis shows the wavenumbers within the range that FTIR data was collected, and the y-axis shows the VIP score of that respective predictor. The dotted line across the graph shows the threshold of VIP score equals one. Based on the plot, it can be concluded that the portion of FTIR spectra that are most important for predicting the y-variables mentioned earlier and explaining most of the variance in the data are peaks found between the ranges 1900-650 cm^{-1}. This agrees with expectations since most of the peaks associated with ageing (sulfoxide and carbonyl), and the presence of SBS are typically found within this region.

Similar observations can be made from Figure 5.39. However, in this case, the x-axis shows the PPM or chemical shift values within the range that NMR data was collected. Another major difference between Figures 5.38 and 5.39 include the number of points on the plots. It was relatively difficult to discern individual points in Figure 5.39. This is because the resolution of the NMR spectra collected was higher than that of FTIR spectra. Nevertheless, some major conclusions can still be drawn. Chemical shift values between the ranges 1 – 3 ppm, 3.2 – 3.5 ppm, and 5 – 6 ppm were found to have VIP scores greater than one and therefore were determined to be the most influential in predicting y-variables and explaining most of the variance in the data. These ranges were also expected since the major ageing peaks (H_γ, H_β and H_α) in addition to the benzylic, allylic and vinylic peaks corresponding to the presence of SBS are typically found within the mentioned ranges above.

VIP plots in general prove to be extremely useful tools when performing PLSR and provides a quantitative but visual way of identifying which portions of multi-dimensional data are most significant, therefore assisting in dimensionality reduction. With the identification of these highly influential regions multivariate analysis including PLSR and PCA can be repeated using only these specific regions of data. This could potentially lead to better fitting models, and a lower chance of overfitting by eliminating most of the noise in addition to less significant regions of the spectral data.

Based on all of the data presented in this section with respect to PLSR, NMR seems to perform better and yields a more accurate model for predicting all four y-variables, although less replicates were performed, when compared to FTIR data. This was somewhat expected since FTIR is known to be a semiquantitative technique while NMR is quantitative.

5.5 Conclusions

This chapter investigated the impact of varying concentrations of SBS on the aging behaviour of asphalt binders through a combination of conventional rheological and advanced chemical (spectroscopic) testing methods. Chemical testing methods included FTIR and NMR spectroscopy while the Bending Beam Rheometer (BBR) and Dynamic Shear Rheometer (DSR) was used for rheological testing. Three different SBS concentrations (0%, 2% and 4%) and ageing states (20, 40, and 60 hr PAV) were investigated. Master curves were constructed using DSR measurements and the crossover temperatures were calculated for all binders. Thereafter, BBR data was also used to calculated ΔT_c parameters. The results provide several key insights into the performance, behaviour and characterization of SBS-modified asphalt binders.

The addition of SBS significantly improved the high-temperature performance and durability of asphalt binders A and B. This was supported by the improved complex modulus and lower temperature sensitivity, which were observed consistently across all aging levels. The study provided some key results that supported previous literature findings which stated that SBS modification can potentially reduce the rate of oxidative aging. This improvement in aging resistance can be attributed to the unique molecular structure of SBS, which facilitates stronger intermolecular interactions and enhances elasticity and resistance to permanent deformation.

Chemical analysis using NMR and FTIR spectroscopy provided detailed insights into the molecular and chemical interactions as well as the aging processes within the asphalt binders. For both types of spectroscopic data, conventional functional group/chemical environment analysis (peaks areas) were conducted in addition to multivariate analysis. Principal Component Analysis (PCA) and Partial Least Squares Regression (PLSR) were the two multivariate analysis techniques used. Based on conventional analysis, the study found that increasing SBS content led to a decrease in the area under NMR peaks associated with aging (H_γ and H_β), suggesting that less free hydrogens were available for oxidation and SBS could be acting as a sacrificial component, undergoing oxidation preferentially, thereby protecting the asphalt binder. Based on FTIR data, general trends reported in previous literature, were verified where carbonyl (C=O) and sulfoxide (S=O) increased with ageing level while peak areas associated with SBS decrease indicating polymer degradation. PCA was used as an exploratory tool for both sets of spectroscopic data. Clusters were found on score plots for both data sets. More distinct clusters with respect to binder source, ageing state and SBS concentration were found on the plots obtained from FTIR data, while clusters with respect to SBS concentration only were observed in NMR score plots. PLSR attempted to relate NMR and FTIR data (X-parameters) to rheological parameters, ageing state and SBS concentrations (Y-parameters). NMR data was found to yield a more accurate model fit when compared to FTIR. Based on these results it can be concluded that FTIR may be more suitable for exploratory analysis,

while NMR may be more appropriate predicting factors such as additive concentration, ageing state, and physical/rheological parameters.

The study also attempted to investigate whether any correlations existed between parameters obtained from rheological and conventional NMR analysis. Strong linear correlations were found between NMR peak areas and rheological parameters such as crossover temperature and ΔTc presenting a new idea for further investigation. Additionally, the compatibility of SBS with different asphalt binders was highlighted. Binder B, in particular, showed stronger linear correlations between chemical and rheological parameters, as well as clustering patterns (using PCA), potentially indicating a higher degree of compatibility with the SBS used in this study. This suggests that the source of the asphalt binder as well as the type of SBS used for modification play crucial roles in optimizing the performance of SBS-modified binders.

Overall, the findings of this study highlight the significant benefits of SBS modification in enhancing the aging resistance and performance of asphalt binders. By improving the high-temperature performance, decreasing temperature sensitivity and reducing the rate of oxidative aging, SBS-modified binders can lead to more durable and resilient pavement structures. The use of advanced spectroscopic techniques like NMR/FTIR and multivariate analysis techniques, in conjunction with conventional rheological tests, provides a more comprehensive understanding of the aging mechanisms, interactions within modified asphalt binders and analysis methods for binder characterization.

Future research should focus on further optimizing SBS concentrations and exploring the effect of different asphalt binder sources or types of SBS on resulting binder performance. Developing and standardizing more accurate and reliable testing/analysis methods for (polymer-) modified asphalts is also paramount. Additional exploration into the potential reasonings for correlations observed in this study should also be conducted in future studies. Replication of the tests performed is also of utmost importance for ensuring the validity of the results presented. Lastly, combining the NMR spectroscopy results with complementary techniques like FTIR spectroscopy, can allow for a more in-depth understanding of the chemical, structural and molecular changes occurring in asphalt binders upon SBS (or any type of) modification and aging in addition to how these changes impact the resulting behaviour and performance of asphalt binders.

Chapter 6

Comparative Analysis of Thermo-Oxidative and UV Aging on Asphalt Binder Properties

6.1 Introduction

Asphalt binders are essential components of asphalt mixtures, providing the necessary flexibility, durability, and binding properties for pavement structures (Y. Li et al., 2022b; Remisova & Briliak, 2023b). However, over time, asphalt binders undergo significant aging, which leads to degradation of their mechanical properties, making pavements more susceptible to cracking, rutting, and other forms of distress (Rossi et al., 2018b; Tan et al., 2008b). Understanding the aging mechanisms of asphalt binders is crucial to prolonging pavement life, improving material design, and reducing maintenance costs. The aging of asphalt binders is a complex process that occurs due to exposure to environmental factors such as temperature, oxygen, and ultraviolet (UV) radiation (Y. Li et al., 2022b; Vijayan et al., 2023b). This chapter focuses on investigating two primary types of binder aging: thermo-oxidative and UV. These aging mechanisms, while related to different environmental conditions, contribute significantly to the long-term performance of asphalt mixtures.

Thermo-oxidative aging refers to the process by which asphalt binders undergo chemical changes due to exposure to oxygen at elevated temperatures (60-70°C). This process typically occurs during the production, storage, and service life of the pavement (Cháves-Pabón et al., 2019b; Omairey et al., 2019). Over time, the binder hardens, loses its elasticity, and becomes more brittle due to the formation of oxidation products such as ketones, sulfoxides, and carboxylic acids (Polo-Mendoza et al., 2022b). Thermo-oxidative aging is accelerated by higher temperatures and is often simulated in the laboratory using methods such as the Rolling Thin Film Oven (RTFO) and Pressure Aging Vessel (PAV), which exposes asphalt binders to elevated pressures and temperatures for extended periods to simulate short- and long-term aging respectively.

UV aging, on the other hand, occurs when asphalt binders are exposed to ultraviolet radiation from the sun. This process can cause photo-oxidation, leading to further hardening and embrittlement of the binder, particularly at the surface of the pavement (J. Hu et al., 2017b; Vijayan et al., 2023b). Unlike thermo-oxidative aging, UV aging involves additional factors such as radiation, moisture, and temperature fluctuations, which can intensify the degradation of asphalt binders (Azimi Alamdary et al., 2019b; M. Hu et al., 2021). To capture the effects of UV aging, it is necessary to simulate environmental conditions in the laboratory by replicating the combination of UV radiation, elevated temperature, and moisture exposure

that binders experience in real-world pavements. One of the significant gaps in the literature is the lack of investigation into how thermo-oxidative ageing and UV ageing differently affect asphalt binders.

In this chapter, a single (PG 58-28) base asphalt binder was used, and its performance under thermo-oxidative and UV aging was investigated. Two anti-aging additives, zinc diethyldithiocarbamate (ZDC) and ascorbic acid (Vit. C), were incorporated into the binder at three different concentration levels based on recommendations in previous literature (Adwani et al., 2023; Rossi et al., 2018b), to assess their effectiveness in mitigating aging effects. Additionally, the research included blends of recovered reclaimed asphalt pavement (RAP) binder, virgin binder, and two different rejuvenators (Rejuvenator A and Rejuvenator B) to study the behaviour of rejuvenated RAP binder under the same aging conditions.

The primary objectives of this chapter were twofold:

(1) To detail the construction of the novel UV aging chamber and the challenges encountered during its development.

(2) To investigate the effects of thermo-oxidative and UV aging on the chemical and rheological properties of asphalt binders, with a particular focus on identifying any differences between these two types of aging. Understanding these differences is crucial for developing more effective anti-aging strategies and improving the long-term performance of asphalt pavements under various environmental conditions. Through this comprehensive approach, the chapter contributes to a deeper understanding of the complex aging processes that asphalt binders undergo and provides valuable insights into the mitigation of their detrimental effects.

The binders were subjected to 40-hours PAV to simulate long-term thermo-oxidative aging. For UV aging, a novel aging chamber was developed to simulate environmental exposure to UV radiation, water spray cycles, and elevated temperatures. The chamber was designed to operate at a temperature of 70°C and allowed for binders to be aged for an initial period of six days. Based on preliminary results, two selected binders in addition to the PG 58-28 unmodified base binder, were further aged in the chamber for 21 days to assess the extended impact of UV exposure. The construction of this novel chamber required overcoming numerous challenges, such as optimizing UV light intensity, controlling water spray cycles, and ensuring uniform temperature distribution across binder samples. These challenges were described and addressed in detail in this chapter to highlight the innovative approach undertaken.

After undergoing thermo-oxidative or UV aging, the asphalt binders were evaluated using both rheological and chemical testing techniques. Rheological testing included bending beam rheometer (BBR) tests and dynamic shear rheometer (DSR) tests to assess the stiffness, relaxation properties and viscoelastic behaviour of the binders. Master curves were constructed from DSR data to compare the performance the binders before and after aging. Additionally, the crossover temperatures of each binder were calculated to evaluate the effects of aging on their thermal and mechanical properties. The BBR tests provided insight

into low-temperature performance, particularly in terms of stiffness and m-values, which are used to investigate pavement cracking resistance. Furthermore, the ΔT_c parameter, which measures the difference between the critical low PG temperature for stiffness and m-value, was also calculated to assess the performance of binders before and after aging.

To complement the rheological testing, chemical analyses were performed using Fourier transform infrared (FTIR) and nuclear magnetic resonance (NMR) spectroscopy. These techniques allowed for the identification and monitoring of oxidation products as well as other chemical changes in the binders due to aging. Multivariate analysis methods, including principal component analysis (PCA) and partial least squares regression (PLSR), were employed to analyze the FTIR and NMR data. This analysis aimed to determine whether chemical testing could detect differences between thermo-oxidative and UV aging that might not be evident through rheological testing alone. By combining rheological and chemical data, this chapter sought to establish relationships between the two sets of properties and determine the extent to which chemical changes can predict the mechanical behaviour of asphalt binders aged using different methods.

6.2 Methodology

6.2.1 Materials

One unmodified virgin binder, PG 58-28 (hereafter referred to as IO) was used for all of the binder blends in this chapter. RAP binder was extracted and recovered from a single source of RAP obtained from a local supplier (Steed & Evans). The methods mentioned in AASHTO 319-22 standard was followed using dichloromethane (DCM) as a solvent. Different binder blends with the base binder (IO) mentioned earlier were produced using:

- Two different rejuvenators (hereafter referred to as A and B) with RAP binder. For these binder blends, a RAP Binder Ratio (RBR) of 43% was used with optimal dosage of 4.01% and 4.03% by weight of total binder blend for A and B respectively. The two blends obtained were named Rej. A blend and Rej. B blend. Figure 6.1 below shows rejuvenators A and B.

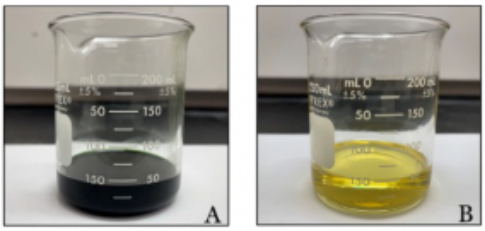


Figure 6.1: Rejuvenator A (mixture of bio-oils) and rejuvenator B (derived from Tall Oil).

- Zinc Diethyldithiocarbamate (ZDC) – an anti-aging additive (3%, 4% and 5% by weight of total binder blend based on recommendations in literature). For blending ZDC into the base binder, the following steps were followed. The base binder (~70 g) was pre-heated in an oven at 160°C until it was flowable. Thereafter, the binder was removed from the oven, placed on a heating plate, and maintained at a temperature of 190°C with a mounted stirrer at ~600 rpm as shown in Figure 6.2 below. The appropriate amount of ZDC (based on the dosages mentioned above), a white powder, was weighed out and added to the binder. Stirring was continued for 10 minutes at 190°C followed by 20-minutes of stirring at 150°C

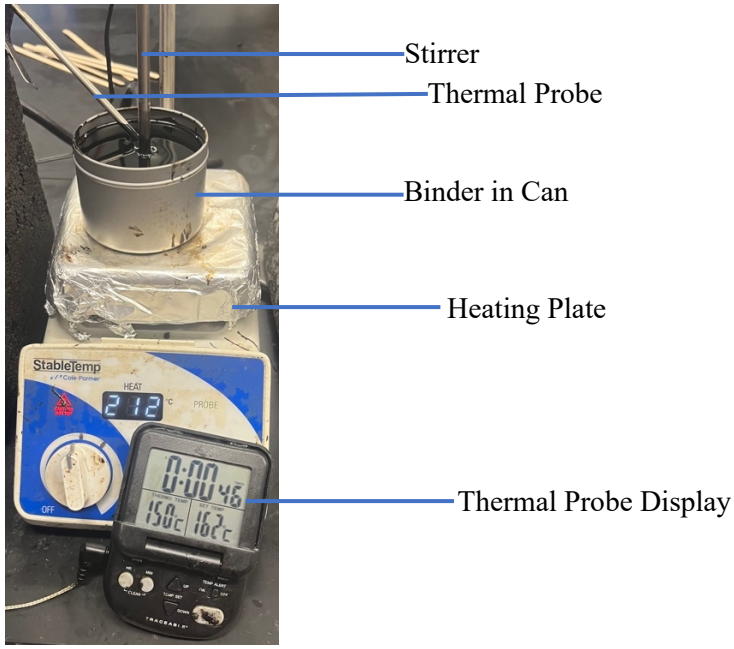


Figure 6.2: Binder Blending Set Up

- Ascorbic Acid (Vit. C) - an anti-aging additive (1%, 2% and 3% by weight of total binder blend based on recommendations in literature). A similar blending procedure as the one used for ZDC was followed, but a temperature of 150°C was used at the same rpm (600), for a period of 30 minutes.

This resulted in a total of 9 binders (base binder + 8 modified binders). All binders underwent RTFO aging according to AASHTO T-240 to simulate short-term aging. For each binder blend, the short-term aged binder was split into two portions of ~50 g each one of which was exposed to 20 or 40-hour PAV aging while the other portion was aged in a custom-built UV aging chamber for 6 and/or 21 days.

6.2.2 UV Aging Chamber Construction

Previous studies ((Azimi Alamdary et al., 2022b; J. Hu et al., 2017b; Y. Li et al., 2022b; Polo-Mendoza et al., 2022b) on UV aging of asphalt binders in addition to the specific settings, and parameters used. Upon thorough examination of the literature, a wavelength of ~365 nm and UV intensity of greater than or equal

to 100 Watts (W) were determined to result in the most severe UV aging. The containment chosen for enclosing the chamber was a temperature-controlled hybridization oven as seen in the Figure below. The temperature of the oven was set to 70°C for aging cycles in the chamber.



Figure 6.3: Hybridization Oven used for modification into UV aging chamber.

For simulating harsh UV conditions for asphalt binder based on the recommendations from previous literature (Y. Li et al., 2022b; Polo-Mendoza et al., 2022b), a single 365 nm wavelength (Uva) lamp, with a power of 100W and dimensions of 26.2 x 20.6 cm was used for the chamber construction (as shown in Figure 6.4 below).



Figure 6.4: UV lamp used in chamber construction.

The glass panel on the main oven enclosure door in addition to the carousel was removed to create an empty space of dimensions 34 cm x 34 cm. The UV lamp was mounted onto the door of the oven as shown in the Figure below. A metal frame with insulation material was used to bridge the gaps between the lamp and

the hollow perimeter where the glass pane had been removed. Additionally, a small hole was drilled in the lower right corner of the metal frame to accommodate tubing for the spraying mechanism, as well as sensors for temperature, humidity, and UV intensity.

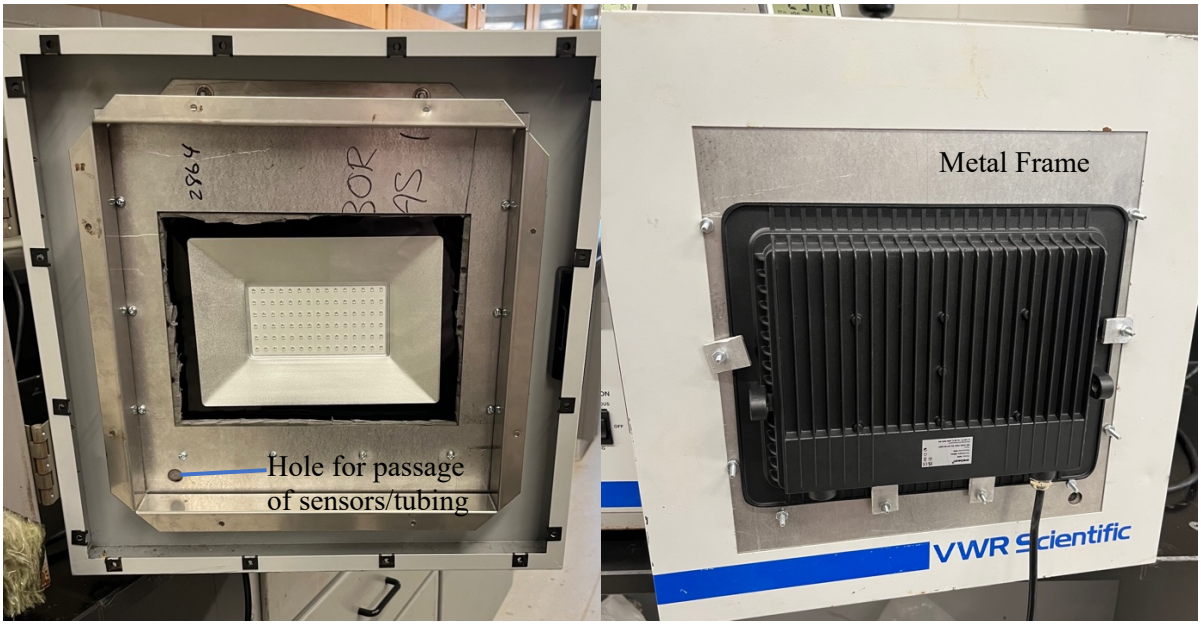


Figure 6.5: Showing the mounted UV lamp on hybridization oven.

UV lamps usually maintain a temperature of 60-70°C in the irradiated space. However, with respect to this lamp, although the inside of the oven was controlled to a temperature 70°C using the oven controls, the cooling fins on the back of the lamp heated up to a temperature of 80-90°C when in operation, which could pose a safety hazard. For this reason, a perforated casing was installed around the back of the lamp. Thereafter, an automatic timing mister was installed to allow for moisture introduction at a rate of 8 seconds of continuous misting every 10 minutes over the entire aging period. The initial set up included the misters located at the back of the oven, a temperature and humidity monitoring device and two PAV pans, with 50 g of asphalt binder as typically used in the PAV aging process. The figure below shows the first iteration of the aging chamber.



Figure 6.6: Iteration one of the UV aging chamber.

A trial test was conducted using binder samples in two PAV pans, aged for 5 days, using the set-up presented above. The resulting aged binders were evenly aged with pitting observed on the surface as presented in Figure 6.7. The relatively even distribution of pits was evidence of even aging. This set-up performed all the required functionalities required, however due to the absence of drains, leakage of water from the oven occurred continuously over the aging period. Another issue that arose was the presence of excess moisture in the sample after aging which led to complications during chemical and rheological testing. For this reason, the spraying periods were reduced to 5 seconds every 10 minutes for the second trial.



Figure 6.7: Aged binder obtained from the initial UV Chamber set up.

In order to resolve the issues with leakage, a silicone drip tray was installed for drainage and collection of run-off/residual water. Calking was also used to seal any gaps between the UV lamp and metal frame. Temperature and humidity sensors were installed to replace the in-chamber monitoring device, and the mounting mechanism for the misters were modified and attached to a metal rod as shown in the figure below.

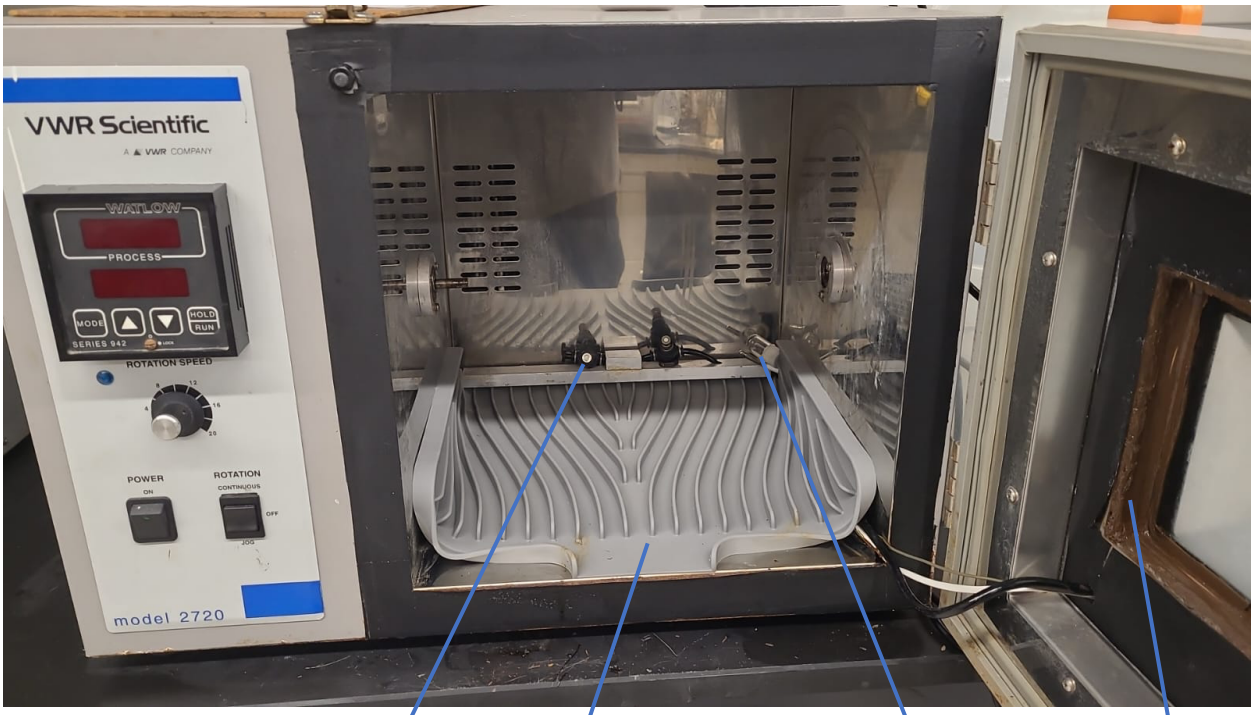


Figure 6.8: Iteration two of UV aging chamber.

A second trial was conducted using the set up presented in Figure 6.8. For this trial, an extra day of UV aging was added to the 5-day period, with spraying cycles (at a rate of 5 seconds every 10 minutes) for the first 5 days and no spraying cycles during the 6th day, to allow for residual moisture removal. The modifications resolved water leakage, UV light leakage and excess moisture issues mentioned. Due to the presence of the undulating drip tray, the bottom of the PAV pans seemed to receive unequal heating resulting in an observed pitting pattern on the surface of the binder sample which indicated severely uneven aging (refer to Figure 6.9).

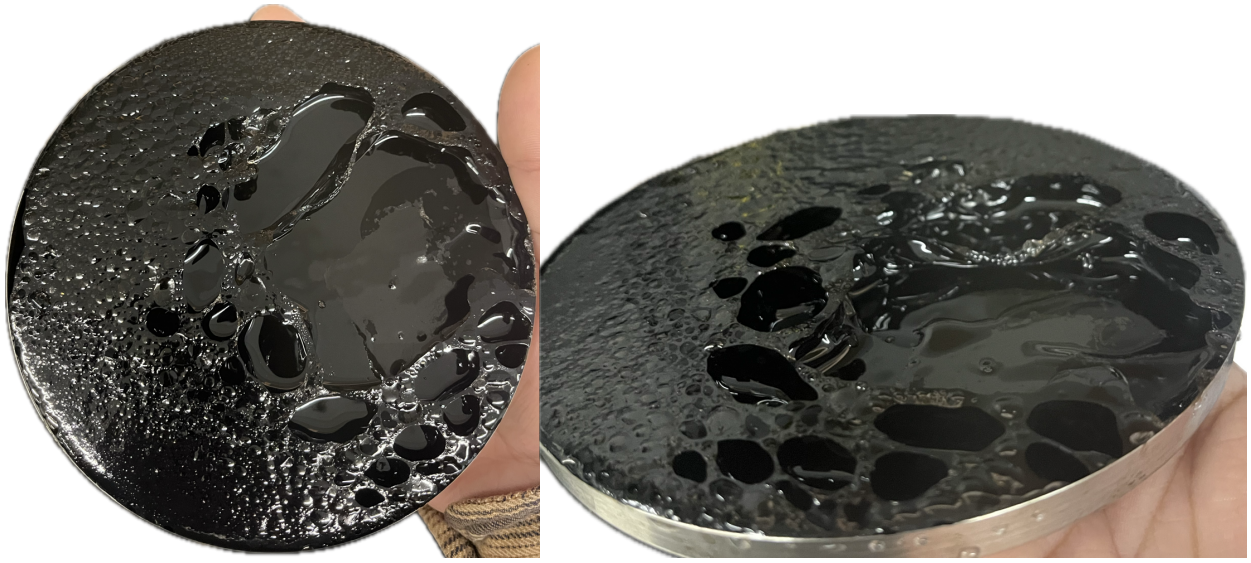


Figure 6.9: Pitting pattern observed on surface of asphalt binder after aging trial 2.

This issue was later resolved to produce the final iteration of the aging chamber where a thin aluminium plate was placed on top of the silicone drip mat in order to yield more equal heating of the PAV pans. A summary of the settings used for the final iteration of the UV aging chamber were as follows:

- Oven set temperature: 70°C
- UV, temperature and humidity sensor – average UV intensity reading of 0.6 mW/cm^2 over aging period, temperature maintained at approximately 70°C, and humidity cycled between 25-75% over each water spraying cycle.
- PAV pan positions were rotated through the aging period to ensure even exposure of each binder blend at each location
- Water spraying cycles of 5 s every 10 min throughout the aging period, plus one additional day of UV and elevated temperature exposure without spraying cycles to allow for evaporation of excess moisture.

Figures 6.10 and 6.11 below shows both the inside and outside (respectively) of the final set up used for the UV aging chamber.

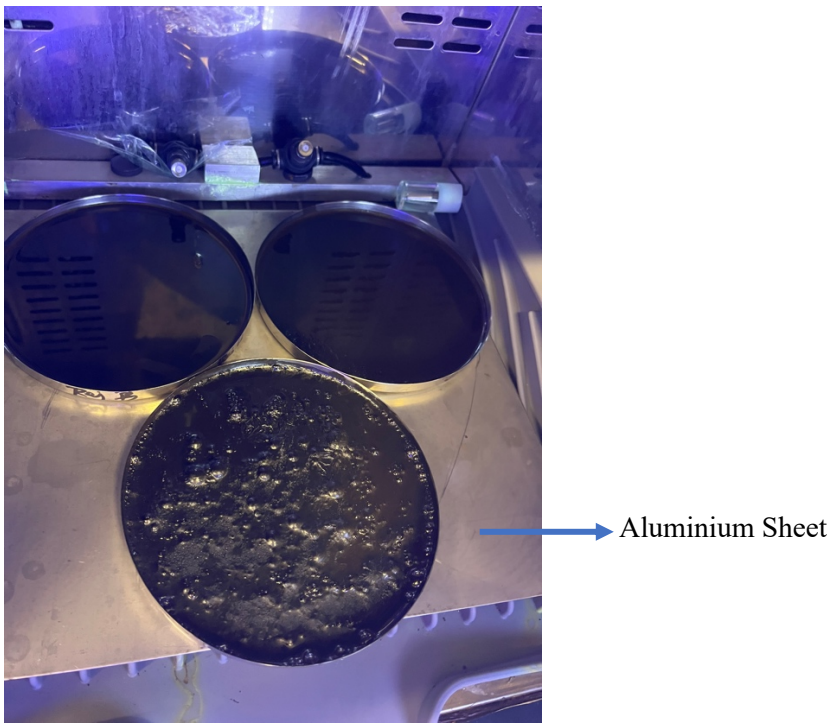


Figure 6.10: Asphalt binder samples in final iteration of aging chamber.

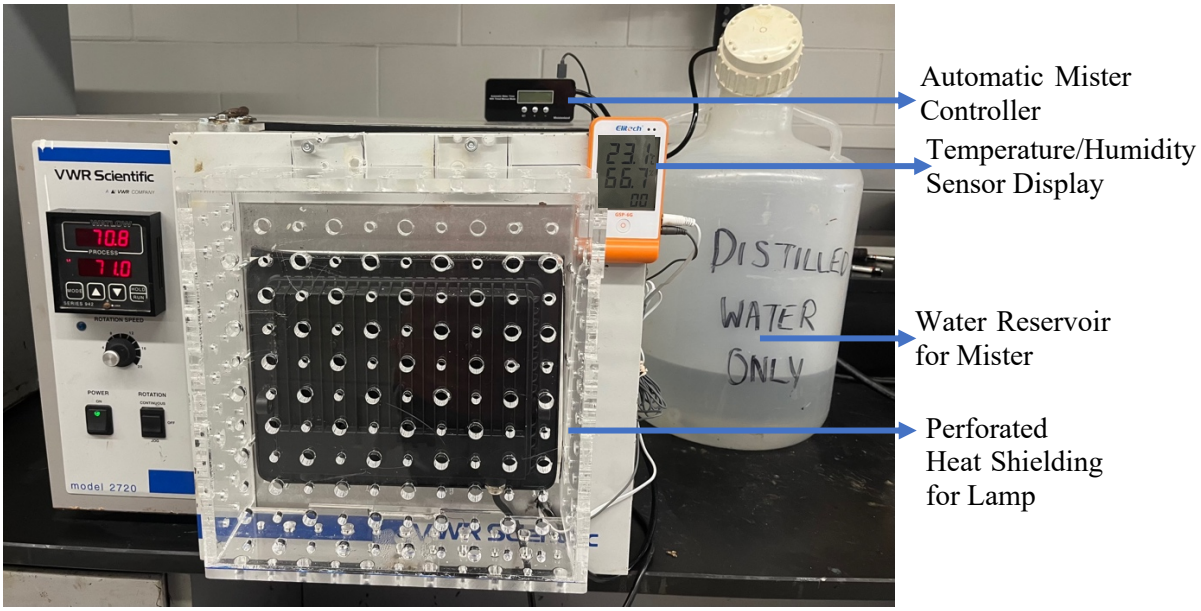


Figure 6.11: Overall set-up for final iteration of Aging chamber.

6.2.3 Testing Methods

After aging, the binders were tested using rheological and chemical analysis methods. Temperature-frequency sweeps were performed, following which master curves were constructed using the time-

temperature superposition principle (TTSP) and the 2S2P1D (2-Springs, 2-Parabolic elements, and one Dashpot) viscoelastic model. Two replicates were performed for each binder sample. Subsequently, crossover temperatures were calculated at 10 rad/s based on the master curve data. BBR testing was performed following AASHTO T-313 standard. The resulting data was used for determining stiffness and m-value parameters at two different temperatures (-24°C and -18°C or -18°C and -12°C) with two replicates at each temperature. Following the completion of the initial two replicates, the threshold for difference between the m-value (±2.9%) and stiffness (±7.2%) of replicates, as specified by the AASHTO standard, were evaluated. If the replicates fell outside the acceptable tolerance range, a third replicate was conducted. For FTIR and NMR spectroscopic testing, methods as described in previous chapters (**Chapter 4** and **Chapter 5)** were followed. The table below summarizes the different binder blend and aging states tested.

Table 6.1: Different binder blends and aging states investigated.

Binder Blends	PAV Aging Level		UV Aging Level	
	20-hours	40-hours	6-days	21-days
PG 58-28 unmodified	✓	✓	✓	✓
Rej. A Blend	✗	✓	✓	✗
Rej. B Blend	✗	✓	✓	✓
3% ZDC Blend	✗	✓	✓	✗
4% ZDC Blend	✗	✓	✓	✗
5% ZDC Blend	✗	✓	✓	✓
1% Vit. C Blend	✗	✓	✓	✗
2% Vit. C Blend	✗	✓	✓	✗
3% Vit. C Blend	✗	✓	✓	✗

6.3 Results and Discussion

6.3.1 Rheological Testing Results

6.3.1.1 DSR Testing

Figures 6.12, 6.13 and 6.14 shows the representative master curves for all RAP-Virgin-Rejuvenator, ZDC and Vit. C binder blends at different aging states (unaged, 40 hours PAV aged, 6 days UV aged, and 21 days UV aged) respectively. The base unaged binder (referred to as IO Unaged in the legends), was included in all master curve plots to serve as a reference point for evaluating the impact of additives and aging on all other binder blends. In general, as expected binder blends showed regular viscoelastic behaviour with higher stiffness at higher frequencies (or lower temperatures) and aging resulted increased stiffness.

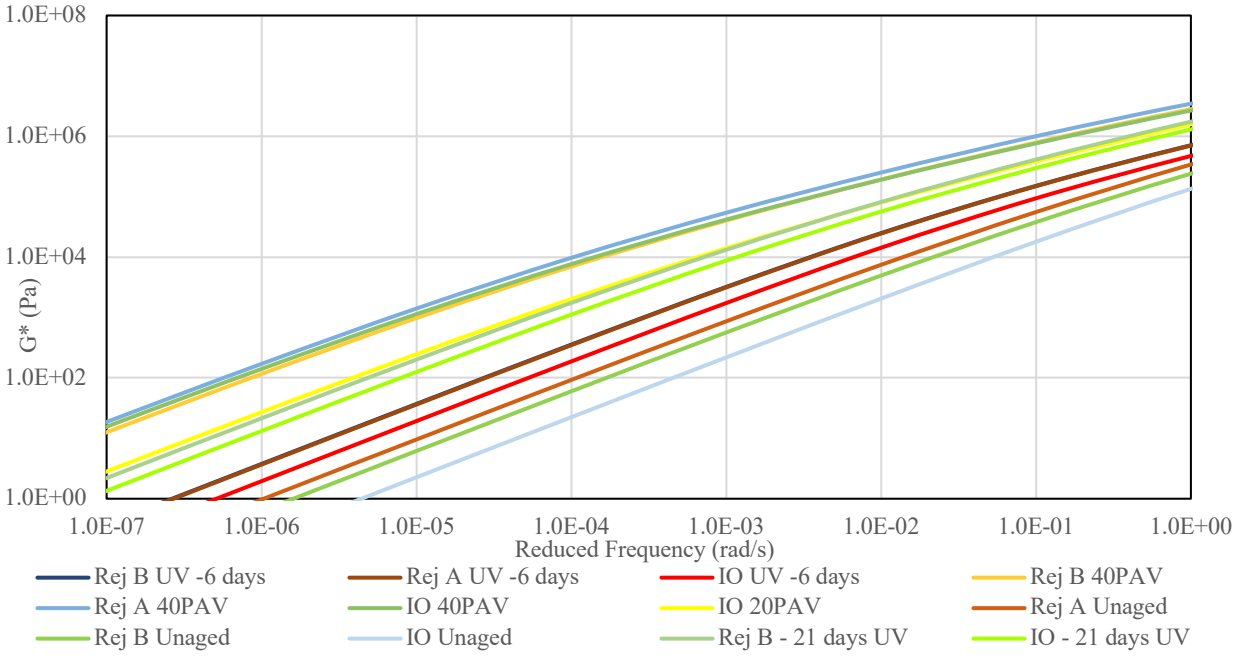


Figure 6.12: Representative Master Curves for IO and RAP-Virgin-Rejuvenator binder blends at different aging states.

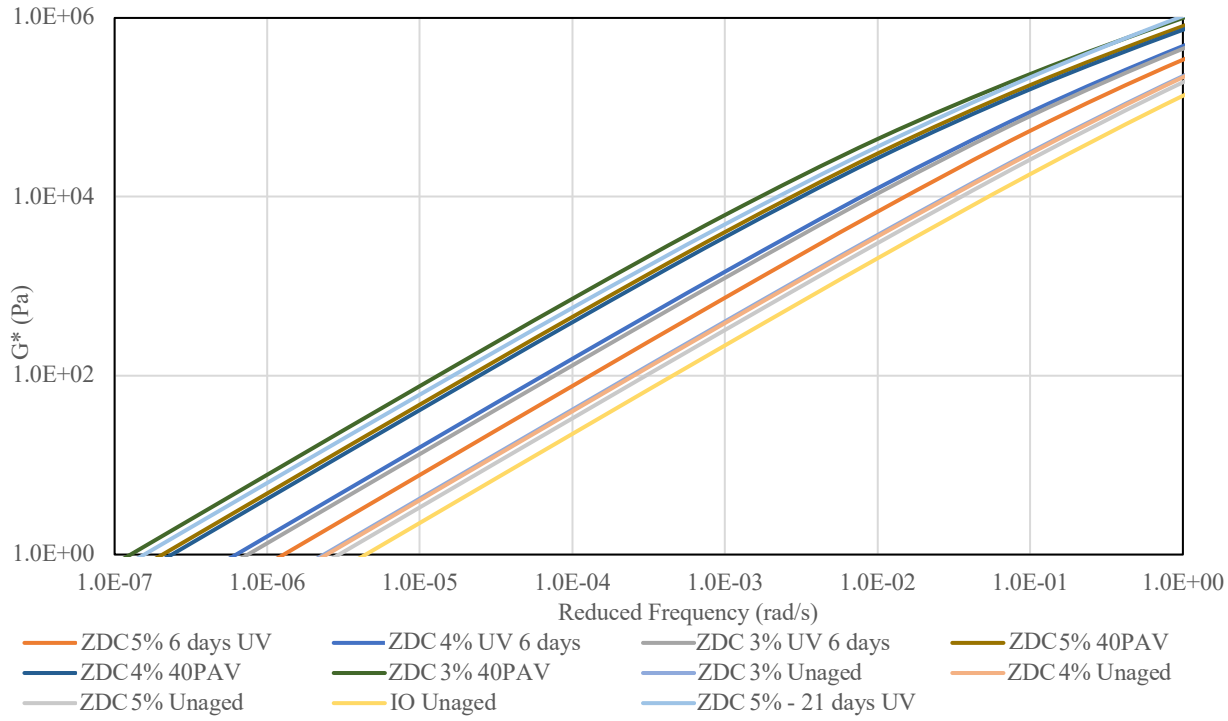


Figure 6.13: Representative Master Curves for ZDC binder blends at different aging states.

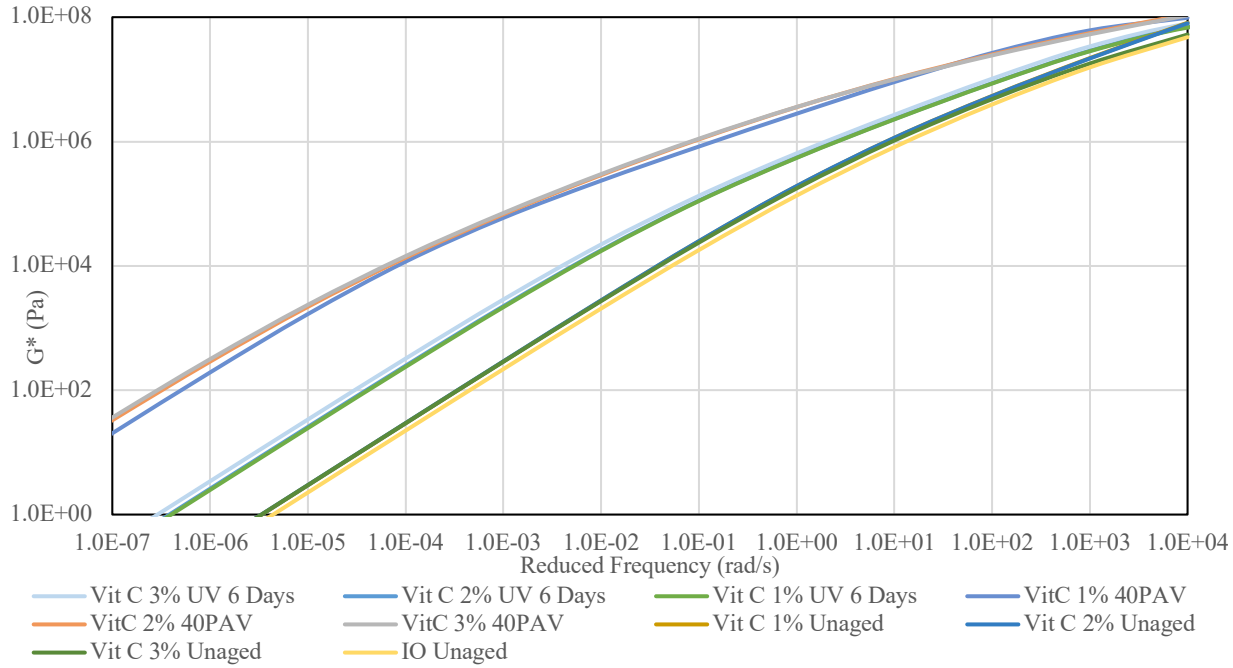


Figure 6.14: Representative Master Curves for Vit. C binder blends at different aging states.

Several specific observations can be made from the different Figures and are presented below:

- RAP-Virgin-Rejuvenator Blends (presented in figure 6.12)

IO unaged binder was found to have the lowest modulus (G*) at all frequences. The unaged (IO) binder blends containing RAP and rejuvenators A or B both exhibited higher modulus compared to the unaged IO base binder itself, suggesting that while both rejuvenators partially restored the viscoelastic properties of the RAP binder, they do not fully return it to the level of a virgin binder. Furthermore, the Rej. B blend showed slightly lower modulus than the Rej. A blend, indicating that Rej. B may have superior rejuvenation properties. Binder blends subjected to UV aging for both 6 and 21 days exhibited a smaller increase in modulus compared to blends aged for 20 and 40 h in the PAV. This is quite different from the trend shown in Figure 6.13 in which the ZDC-modified blends demonstrated more severe aging after 21 days of UV exposure when compared to 40 h of PAV aging. This suggests that while ZDC significantly mitigates thermo-oxidative aging, its effectiveness in reducing UV-induced aging is more limited. The general trend observed for the rejuvenator blends and IO aged for 6 days showed that both Rej. A and Rej. B exhibited similar viscoelastic properties, as demonstrated by their completely overlapping master curves. However, the IO base binder exhibited a smaller increase in modulus compared to the rejuvenated blends, indicating that the rejuvenator-modified binders with RAP underwent more significant aging under the same conditions.

The IO and Rej. B binder blends aged for 21 days in the UV chamber exhibited viscoelastic properties similar to the IO binder aged for 20 hours in the PAV, with only slight differences observed. This was

concluded based on the fact that the master curve of the IO and Rej. B blend aged for 21 days in the UV chamber was found to be very close to that of the IO binder aged for 20 hours in the PAV. Among these three binders, the IO binder aged for 21 days under UV conditions was the least aged, showing the lowest modulus, while the IO binder aged for 20 hours in the PAV was the most aged, displaying the highest modulus. Among the 12 binder blends shown in Figure 6.12, those subjected to 40 hours of PAV aging exhibited the most severe aging, with the highest modulus. The viscoelastic properties of the three binders aged for 40 hours in the PAV (Rej. B, Rej. A, and IO binder) were notably similar. Across all frequencies, the Rej. A blend aged for 40 hours in the PAV was the most aged and stiff. In comparison, the Rej B and IO binder blends, also aged for 40 hours, displayed similar performance but were less aged and less stiff when compared to the Rej. A blend. At lower frequencies, the IO binder aged for 40 hours had a higher modulus (indicating greater aging) than the Rej. B binder. However, at higher frequencies, the master curves for the IO and Rej B blends aged for 40 hours in the PAV completely overlapped, indicating nearly identical viscoelastic performance in this range, corresponding to lower temperatures.

- ZDC Blends (presented in figure 6.13)

Across all concentrations (3%, 4%, and 5%), the unaged binder blends with ZDC displayed similar trends where the addition of ZDC led to increases in modulus at all frequencies. ZDC at a concentration of 3% and 4% in unaged binder blends possessed very similar viscoelastic behaviour evidenced by the significant overlapping of both master curves. The binder blend containing 5% ZDC was found to exhibit the smallest increase in modulus when comparing unaged ZDC binder blends. ZDC binder blends UV aged for 6 days were found to cause a smaller increase in modulus when compared to 40 hours PAV aging, indicating that PAV caused more severe aging and hardening than 6 days of UV aging. ZDC-5% was found to exhibit the highest aging resistance and 4% the lowest, as shown by having the smallest and largest increase in modulus respectively, when compared to the IO unaged binder. Even after 6 days of UV aging, the ZDC-3% and ZDC-4% blends continued to exhibit similar performance.

With respect to 40-hours of PAV aging, ZDC binder blends displayed the most increase in modulus, and therefore most significant aging. A slightly different trend was also observed where ZDC-5% had the lowest modulus among all 40-hour PAV aged blends and ZDC-3% the highest at all frequencies, with ZDC-4% performing very similar to but slightly less aging resistant than ZDC-5%. Upon comparison of ZDC-5%, 40 hours PAV and 21-days UV aged, it was noted that 21 days of UV aging caused a slightly larger but similar increase in modulus when compared to 40-hours of PAV. This indicates that approximately 21-days of UV aging can result in a binder blend with similar level of performance (in terms of modulus) as that of a binder blend exposed for 40 hours of PAV aging in this scenario. Overall UV aging for longer durations (21 days), was found to have a more profound impact than PAV aging in the case of ZDC-modified binder blends.

- Vit. C Blends (presented in figure 6.14)

IO unaged binder was found to have the lowest modulus (G*) at all frequences. At lower frequencies, differences between the viscoelastic behaviour of binder blends with different concentrations and aging states were more drastic when compared to the performance at higher frequencies (equivalent low temperatures). Across all concentrations (1%, 2%, and 3%), the unaged binder blends with Vit. C displayed similar trends. Addition of Vit. C led to very slight increases in modulus at all frequencies (compared to IO unaged) with all concentrations exhibiting very similar performance at low frequencies, as evidenced by the overlapping master curves. However, at higher frequencies, the 3% Vit. C unaged binder blend showed a lower modulus than 1% and 2%. The binder blend containing 3% Vit. C was found to exhibit the smallest increase in modulus when comparing to the other Vit. C unaged binder blends.

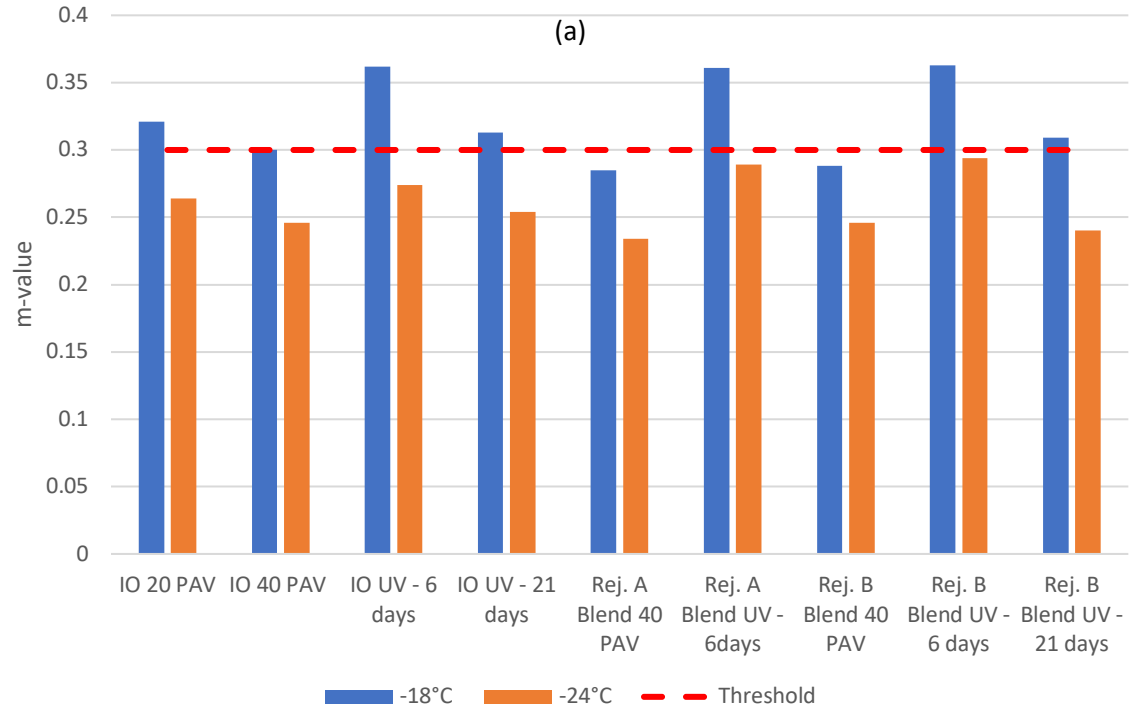
Vit. C binder blends that were UV aged for 6 days were found to cause a smaller increase in modulus when compared to 40 hours PAV aging, indicating again that the PAV caused more severe aging and hardening than 6 days of UV aging. Only very small differences were observed between the three different concentrations with 1% Vit C showing the least increase in modulus (highest aging resistance) while 2% and 3% Vit. C (UV aged for 6 days) were found to perform almost exactly the same at all frequencies. With respect to 40-hours of PAV aging, these aged binder blends displayed the most increase in modulus, similar to what was observed with the ZDC blends, and therefore most significant aging. Vit. C 2% and 3% binder blends at 40 hours PAV aging level were found to perform almost the exact same in terms of viscoelastic behaviour since both of the master curves overlap at all frequencies. At very low and very high frequencies, 1% Vit. C binder blend was found to be the least stiff while at intermediate frequencies all three concentrations performed very similarly.

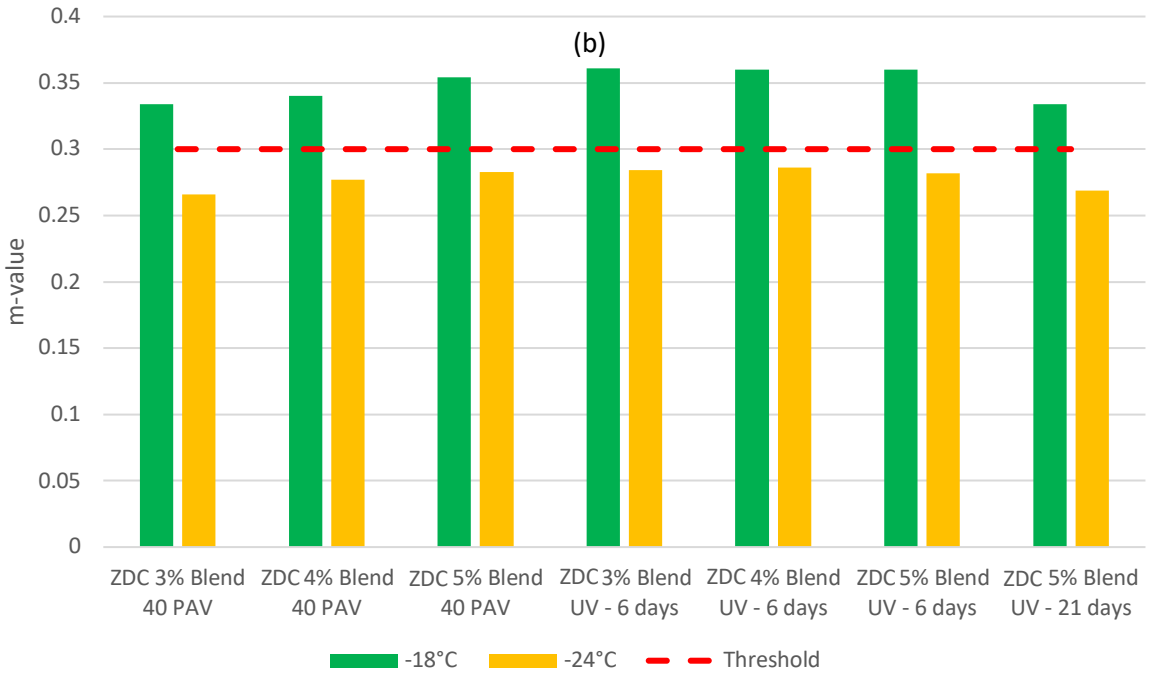
In general, 6 days of UV aging was found to cause significantly less severe aging when compared to 40 hours of PAV aging. On comparing Vit. C to ZDC binder blends, both UV and PAV aged, ZDC blends displayed significantly less aging (smaller increase in modulus), indicating that ZDC was a better performing antioxidant both with respect to UV and thermo-oxidative aging. When comparing Figures 6.12, 6.13, and 6.14, the Vit. C binder blends exhibited the lowest resistance to aging, followed by the RAP-Virgin-Rejuvenator blends. In contrast, the ZDC binder blends demonstrated the highest resistance to thermo-oxidative aging. Previous studies (Adwani et al., 2023) have confirmed the antioxidant properties of ZDC, which aligns with its significant reduction in thermo-oxidative aging shown in this study. However, its anti-aging effects were less significant with respect to UV aging. This supports the known mechanism by which Zinc Diethyldithiocarbamate works. The ZDC compound is known to behave mainly as a secondary antioxidant (peroxide inhibitor/decomposer) which works by decomposing hydroperoxides, chelating metal ions, or regenerating primary antioxidants, thereby slowing the initiation of oxidation. Although Vit. C has also been documented to possess antioxidant properties in the literature, mainly acting

as a primary antioxidant (radical scavenger), the findings in this chapter contradict this, as the Vit. C blends experienced the most pronounced aging, based on comparison of high and intermediate temperature viscoelastic properties.

6.3.1.2 BBR Testing

BBR testing was conducted exclusively on aged asphalt binder samples, which included binders subjected to 20 and 40 hours of PAV aging as well as 6 and 21 days of UV aging. As previously noted, based on preliminary DSR testing of binder blends aged for 6 days under UV exposure, the anti-aging additive with the best performance (ZDC, as opposed to Vit. C), the more effective rejuvenator (Rejuvenator B), and the IO base binder (for baseline comparison) were selected for extended UV aging for 21 days. The BBR data collected for all aged binder blends included stiffness and m-values (creep slope) at two temperatures: -18°C and -24°C. One binder blend—Vit. C 3% aged for 40 hours in the PAV—was tested at -18°C and -12°C due to falling outside the stiffness failure criteria at -18°C. In general, DSR testing is used for evaluating high and intermediate temperature performance of asphalt binders, while BBR evaluates mainly low temperature properties. Typically, higher stiffness values indicate better resistance to permanent deformation (which is more of a concern at higher temperatures), but more brittle and less flexible binders, with a reduced ability to relax stresses making them more susceptible to thermal cracking (main concern at lower temperatures). Conversely, a larger m-value implies that the binder is more capable of dissipating stresses over time and therefore possesses better relaxation properties. Overall, at low temperatures, lower stiffness measurements and higher m-values are desirable, since they indicate that a binder retains flexibility while effectively dissipating stresses, ultimately resulting in better low temperature cracking resistance. The figures below summarize the BBR results obtained for all aged binders.


(a)
0.4
0.35
0.3
0.25
0.2
0.15
0.1
0.05
0
m-value
IO 20 PAV
IO 40 PAV
IO UV - 6 days
IO UV - 21 days
Rej. A Blend 40 PAV
Rej. A Blend UV - 6days
Rej. B Blend 40 PAV
Rej. B Blend UV - 6 days
Rej. B Blend UV - 21 days
-18°C
-24°C
Threshold


(b)
0.4
0.35
0.3
0.25
0.2
0.15
0.1
0.05
0
m-value
ZDC 3% Blend 40 PAV
ZDC 4% Blend 40 PAV
ZDC 5% Blend 40 PAV
ZDC 3% Blend UV - 6 days
ZDC 4% Blend UV - 6 days
ZDC 5% Blend UV - 6 days
ZDC 5% Blend UV - 21 days
-18°C
-24°C
Threshold

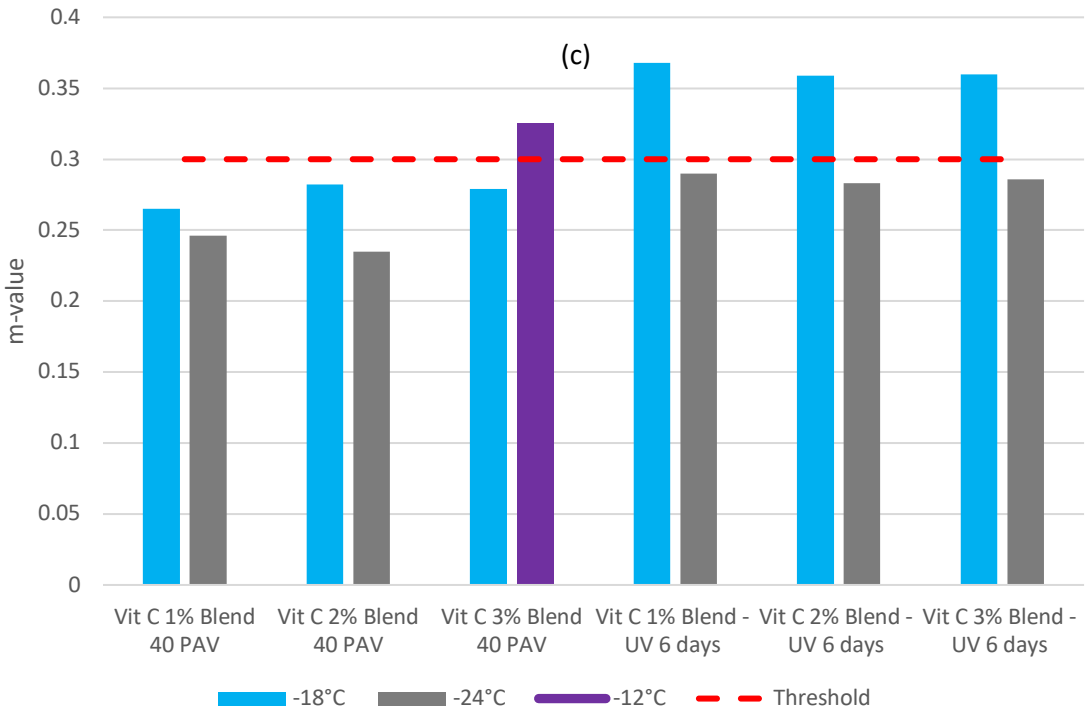
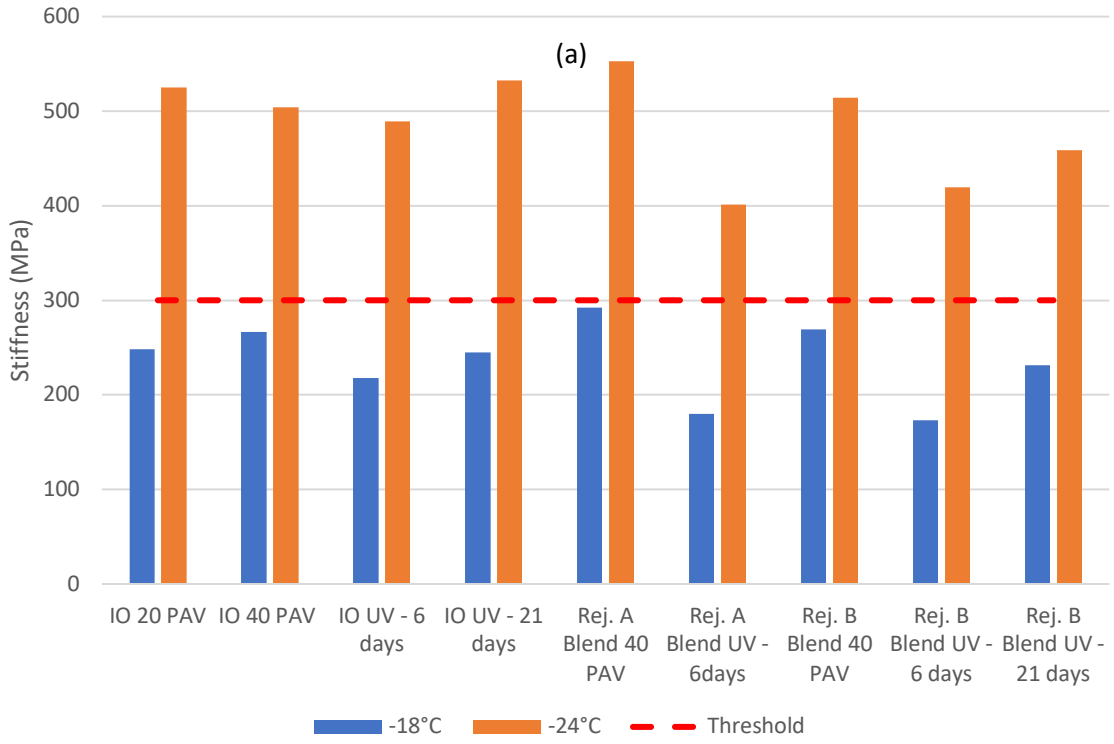


Figure 6.15: M-values obtained from BBR testing of (a) RAP-Virgin-Rejuvenator, (b) ZDC, and (c) Vit. C Blends.



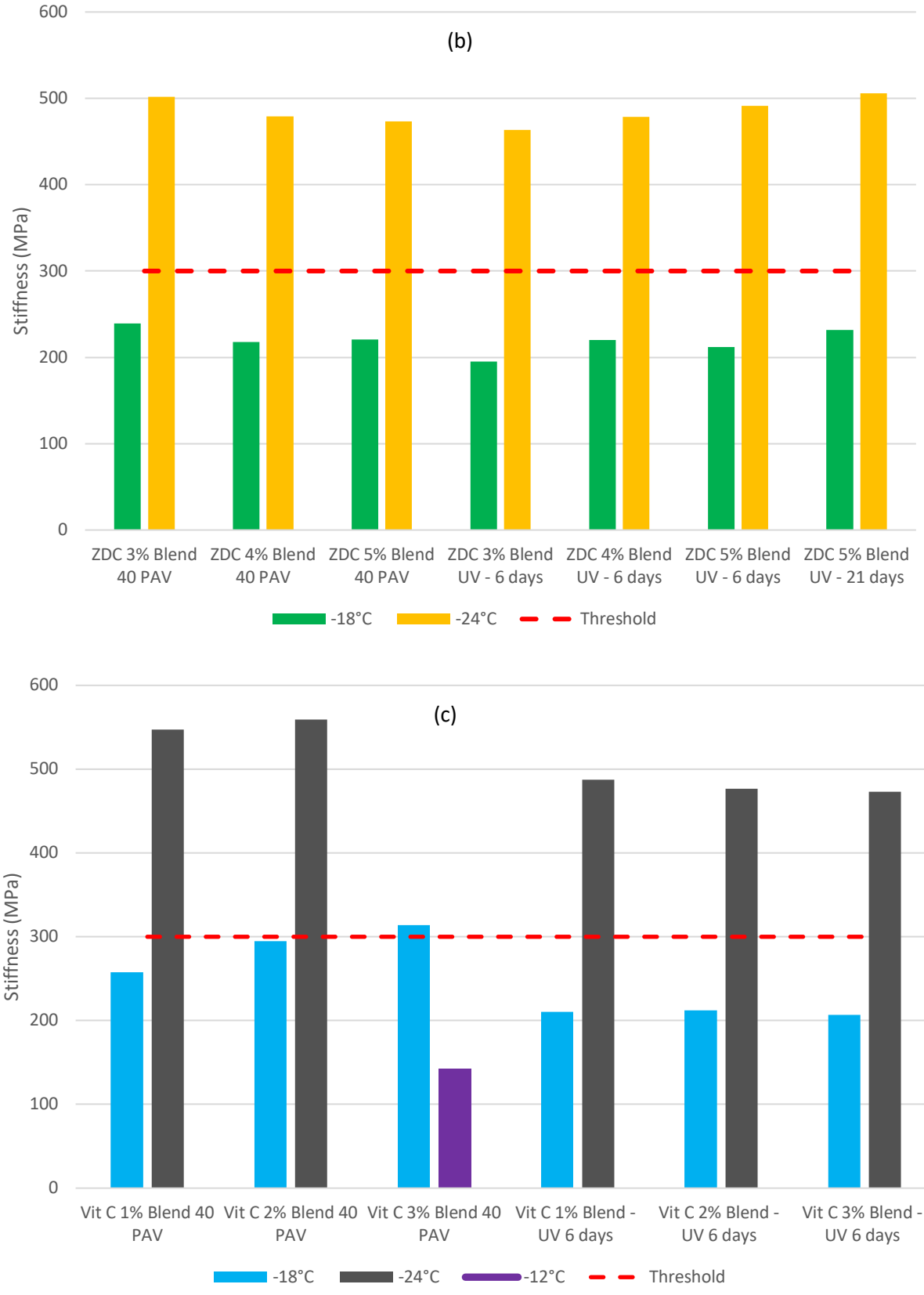


Figure 6.16: Stiffness values obtained from BBR testing of (a) RAP-Virgin-Rejuvenator, (b) ZDC, and (c) Vit. C Blends.

Figures 6.15 and 6.16 present the low temperature performance of aged asphalt binders based on m-value, which is a measure of stress relaxation rate, and stiffness, S from BBR testing. Several insights can be drawn from the figures presented above as follows:

- As expected, the 40-hour PAV-aged samples showed lower m-values and higher stiffness compared to the 20-hour PAV-aged samples, especially at -24°C. This trend suggests that increased oxidative aging in the PAV leads to a stiffer, more brittle binder at low temperatures, making it more prone to thermal cracking.
- Referring to Figures 6.15 (a) and 6.16 (a) the rejuvenated blends (A and B) exhibited slightly greater aging after 40 hours of PAV aging, as reflected by their higher stiffness values and lower m-values at both test temperatures (-18°C and -24°C) when compared to IO 40 PAV. This aligns with previous findings in literature (Behnood, 2019b), which suggest that while bio-based rejuvenators can restore certain properties of aged binders, rejuvenated blends tend to undergo re-aging more rapidly when compared to virgin binders. Notably, Rejuvenator B outperformed Rejuvenator A in terms of thermo-oxidative aging, displaying lower stiffness and higher m-values at both temperatures. Although Rejuvenator B showed marginally worse low-temperature performance compared to the IO binder after 40 hours of PAV aging, their performance was quite similar overall, further indicating that Rejuvenator B was more effective in slowing down the aging process when compared to Rejuvenator A.
- Both Vit. C and ZDC additives were selected for this study due to their reported antioxidant properties in previous literature (Adwani et al., 2023; Rossi et al., 2018b). Among the Vit. C blends, the 3% concentration exhibited the worst low-temperature performance, as reflected by both lower m-values and higher stiffness. In contrast, the 2% Vit. C blend showed superior low-temperature performance based on m-values, achieving the highest m-values at both test temperatures when comparing all three Vit. C concentrations. Meanwhile, the 1% Vit. C blend performed better in terms of stiffness, showing the lowest stiffness values at both temperatures. When comparing the Vit. C binder blends to the IO 40 PAV sample, IO 40 PAV demonstrated a higher m-value and lower stiffness when compared to all Vit. C blends, indicating better low-temperature performance. This suggests that, although Vit. C was added to the binder with the aim of slowing aging, the results indicate it may have actually accelerated thermo-oxidative aging.
- The ZDC-modified blends outperformed the Vit. C-modified blends, maintaining higher m-values and lower stiffness at both test temperatures. Overall, increasing the concentration of ZDC consistently enhanced the resistance of the binders to aging, as demonstrated by a general trend of higher m-values and reduced stiffness in blends with higher ZDC content. Notably, the blend with 5% ZDC exhibited the greatest resistance to thermo-oxidative aging. These findings align closely with the trends observed in the DSR analysis. Compared to the IO 40 PAV control, all ZDC-modified blends exhibited higher m-values and lower stiffness, confirming the effectiveness of ZDC in mitigating thermo-oxidative aging, which is further supported by the DSR results discussed in the previous section.
- The UV aging of binders for 6 days, as indicated by DSR data, did not result in as severe aging as 40 hours of PAV exposure. However, similar trends were observed in both cases, with the effects of 6 days of UV

aging being less pronounced. Interestingly, after 21 days of UV aging, the 5% ZDC blend showed more severe aging compared to its 40 hours of PAV aging counterpart, whereas the Rej. B blend and IO blend showed less aging after 21 days of UV exposure when compared to 40 hours of PAV aging. Both the DSR and BBR results confirm that while ZDC functions as an effective anti-aging additive for thermo-oxidative aging, it is less effective in resisting UV-induced aging.

- On comparing Vit. C binder blends and IO aged for 6 days in the UV chamber, all Vit. C blends showed lower stiffness values and higher m-values at both test temperatures than the IO binder exposed to UV aging for 6 days. Based on these results, it can be concluded that although Vit. C additive was found to accelerate thermo-oxidative aging it was marginally effective in slowing UV aging. This outcome aligns with previous literature, which identifies Vit. C as a primary antioxidant (radical scavenger) that mitigates oxidation by neutralizing free radicals and interrupting chain propagation reactions. Notably, free radicals are more commonly generated through UV exposure rather than elevated temperature and pressure.

6.3.1.3 Rheological Parameters: Crossover Temperature and ΔT_c

Based on the SuperPave PG tests and previous literature (Deef-Allah & Abdelrahman, 2022; Garcia Cucalon et al., 2019; Preciado et al., 2024; Yang et al., 2022), crossover temperature (from DSR data) and the ΔTc parameter (from BBR data) are two rheological parameters that have been found to provide additional insights into the performance and aging characteristics of asphalt binders that go beyond what can be inferred from master curves, m-values, or stiffness values alone. The crossover temperature is the temperature at which the storage modulus (G') equals the loss modulus (G"), indicating a transition from predominantly elastic behaviour to predominantly viscous behaviour in the binder. As binders age (either thermo-oxidatively or under UV exposure), the crossover temperature tends to increase, signaling increased stiffness and reduced relaxation potential. The crossover temperature is particularly sensitive to the effects of aging and comparing this parameter before and after aging can help in understanding the degree to which the binder has hardened. Master curves show overall viscoelastic behaviour, but the crossover temperature pinpoints the specific temperature where the balance shifts between elasticity and viscosity. This value can be used to predict the performance of asphalt binders at intermediate temperatures, providing insight into how a binder will behave under various climatic conditions or traffic loads. The ΔT_c parameter is the difference between the critical low PG temperature based on stiffness ($T_{c,stiffness}$) and the critical low PG temperature based on the relaxation rate/m-value ($T_{c,m\text{-}value}$). It is used to assess how well the binder relaxes thermal stresses at low temperatures, which is important for crack resistance. ΔT_c offers a more nuanced understanding of low-temperature cracking potential. While stiffness (S) and m-value from BBR are direct indicators of thermal cracking resistance, ΔT_c highlights the difference between these two, giving a sense of how much the ability the binder to relieve stresses (m-value) has deteriorated relative to its stiffness. A large negative ΔT_c suggests the binder is prone to cracking because it cannot relax stresses effectively, even if its stiffness is within acceptable limits.

The crossover temperatures and ΔT_c parameters calculated for all binder blends are summarized in Table 6.2 below. According to AASHTO standards, low-temperature BBR testing is typically conducted only on aged binders, which is why ΔT_c parameters for unaged binders are not reported in the table. The observed trends in crossover temperature and ΔT_c align closely with those previously discussed in the DSR and BBR results section respectively.

Table 6.2: Summary of Rheological Parameters Obtain from BBR (ΔT_c) and DSR (Crossover Temperature) testing.

Sample	ΔT_c Parameter (°C)				
	Unaged	20PAV	40PAV	UV 6 Days	UV 21 Days
IO (Control)	-	1.0	-0.9	2.3	0.1
Rej A	-	-	-2.9	1.8	-
Rej B	-	-	-1.4	2.3	-1.0
ZDC 5%	-	-	2.6	2.9	1.6
ZDC 4%	-	-	1.8	2.9	-
ZDC 3%	-	-	1.5	2.4	-
Vit C 1%	-	-	-2.3	3.2	-
Vit C 2%	-	-	-2.5	2.6	-
Vit C 3%	-	-	-2.6	2.7	-
Sample	**Crossover Temperature (°C)**				
	Unaged	**20PAV**	**40PAV**	**UV 6 Days**	**UV 21 Days**
IO (Control)	0.2	18.7	26.3	11.1	17.3
Rej A	5.2	-	27.5	13.6	-
Rej B	2.9	-	26.1	12.1	18.9
ZDC 5%	3.4	-	13.8	8.9	14.2
ZDC 4%	3.7	-	13.0	9.3	-
ZDC 3%	3.7	-	16.3	9.0	-
Vit C 1%	0.9	-	27.9	10.6	-
Vit C 2%	0.9	-	29.4	10.6	-
Vit C 3%	1.2	-	30.4	10.9	-

6.3.2 NMR and FTIR Spectroscopic Analysis

While rheological properties provide valuable insights into the physical and viscoelastic behaviour of asphalt binders, as well as how these properties evolve with aging or the addition of modifiers, they do not reveal the underlying chemical processes driving these changes. Previous studies have shown that thermo-oxidative aging and UV exposure induce distinctly different chemical reactions and pathways within asphalt binders (X. He et al., 2018b; Zeng et al., 2015b). However, despite these differences, the resulting binders may still exhibit similar viscoelastic properties. This highlights the need for complementary techniques, such as spectroscopy, to monitor aging processes, as chemical analysis could potentially detect changes that

rheological testing alone cannot capture. This section presents the FTIR and NMR spectroscopic testing results for all binders discussed in section 6.3.1 above, with the intentions of determining whether these techniques can identify changes in asphalt binders, after different aging processes, which are relatively undetected by rheological testing methods. For both FTIR and NMR data, conventional functional group and chemical environment analysis was performed. Figures showing the evolution of functional groups and protons in specific chemical environments are presented in Appendix B. Five sample FTIR and NMR spectra were presented in the figures below (all other raw spectra are presented in Appendix B) showing only the region where major differences were observed. Only the highest concentration of unaged ZDC, and Vit. C blends were presented below. For lower concentrations, similar spectra with decreasing intensity were observed for lower concentrations of the respective additives.

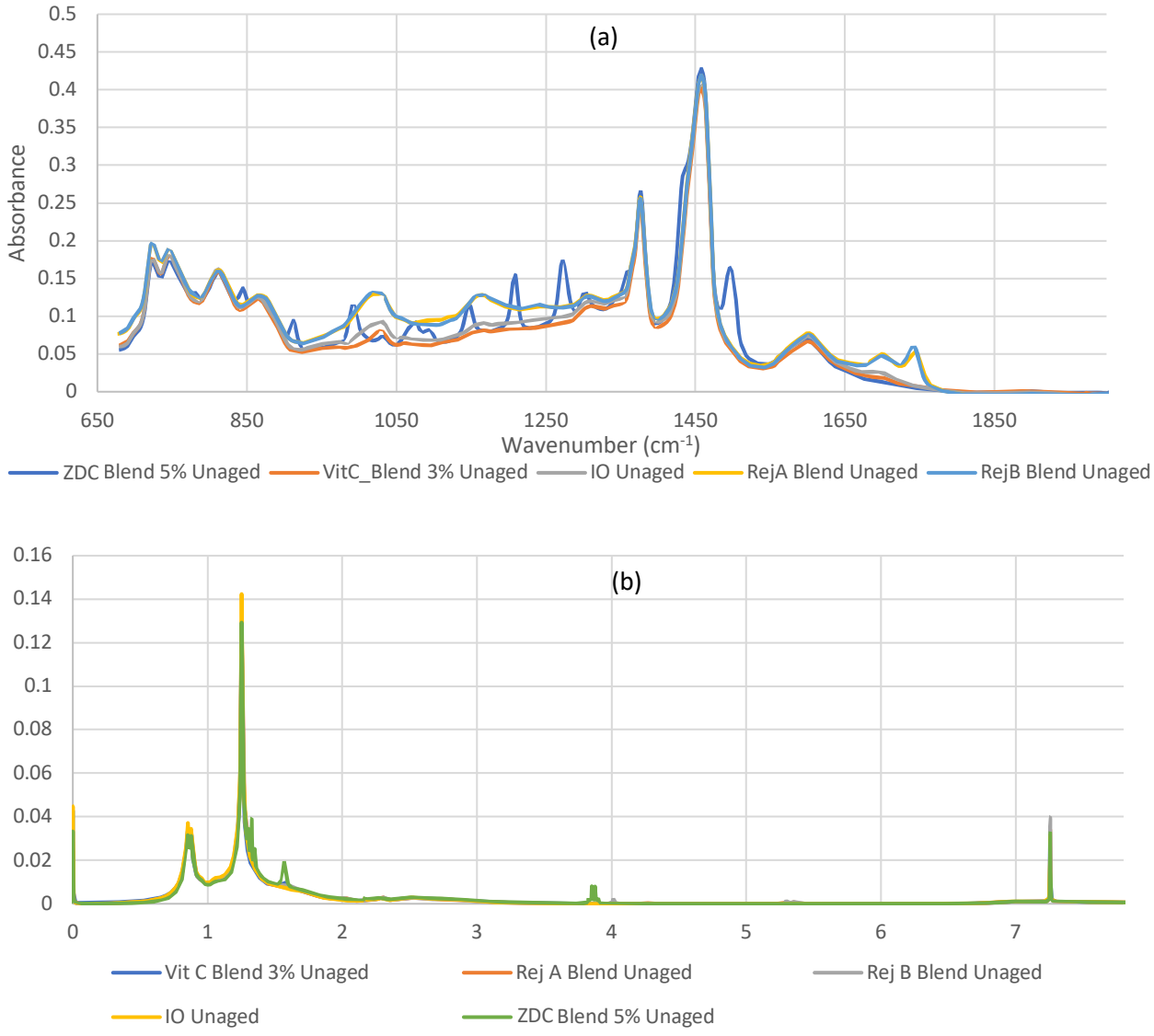


Figure 6.17: Sample (a) FTIR and (b) NMR spectra for unaged binder blends.

Examination of the raw FTIR and NMR spectra revealed that both UV and thermo-oxidative aging contribute to the increase in carbonyl and sulfoxide functional groups, with UV aging exhibiting a less pronounced effect on increasing sulfoxide index. Thermo-oxidative aging is generally associated with the formation of additional oxidation products such as ketones, phenols, and carboxylic acids, while UV aging predominantly results in the generation of photo-oxidation by-products like conjugated dienes, quinones and phenols. Furthermore, UV exposure leads to more significant increases in aliphatic and aromatic compounds (lighter hydrocarbons, including small alkenes and aromatic species resulting from chain scission), as well as the formation of aldehydes, peroxides, and alkyl radicals. Functional groups that such as carbonyl and sulfoxides were found to be more sensitive to thermo-oxidative aging, while aliphatic, aromatic and carbonyl groups are more sensitive to UV exposure.

In addition to spectral observations, multivariate analysis, which included Principal Component Analysis (PCA) and Partial Least Squares Regression (PLSR) techniques, described in **Chapter 4** and **Chapter 5** were conducted. The conventional functional group and chemical environment analysis was not presented in this chapter, but is included in the Appendix A, since the multivariate techniques are more suitable for highlighting overall and seemingly small differences between binder types, additives, and aging states. Therefore, this section highlights the multivariate analysis on spectroscopic data and focuses on key differences (if any) attributed to different aging processes. For performing multivariate analysis, the data was split into three groups in order to better study the impact of UV and thermo-oxidative aging. The three groups were as follows:

1) RAP-Virgin-Rejuvenator Blends – all aging states (including IO base binder)
2) ZDC Blends – all binders containing Zinc Diethyldithiocarbamate at all aging states
3) Vit. C Blends – all binders containing ascorbic acid at all aging states

6.3.1.1 PCA Analysis

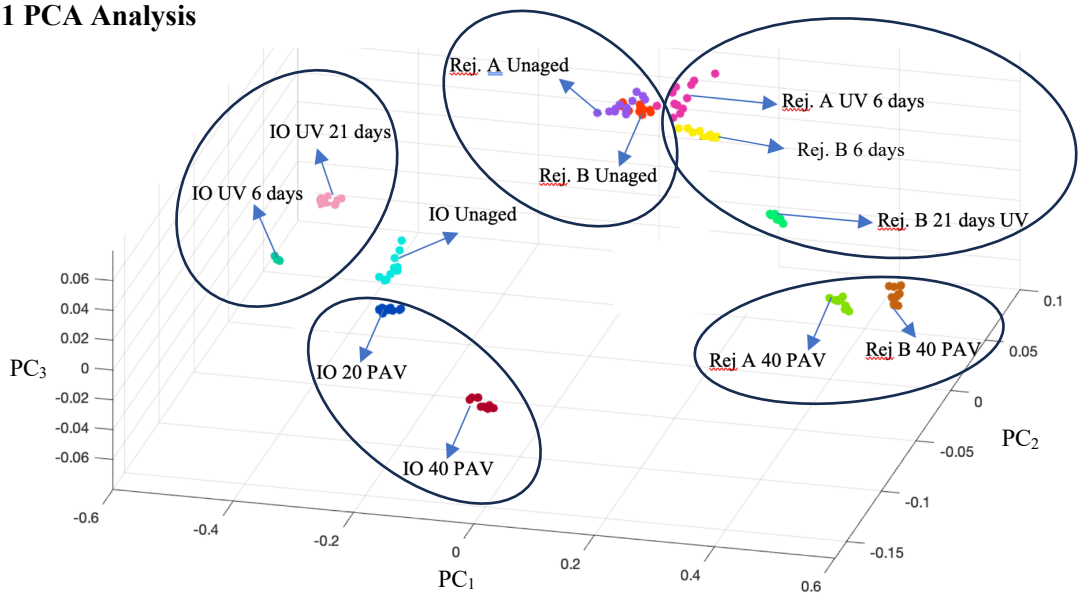


Figure 6.18: Score Plot for RAP-Virgin-Rejuvenator Binder Blends and IO at all aging states from FTIR data.

Figure 6.18 presented above shows the score plot obtained from PCA carried out on RAP-Virgin-Rejuvenator blends. There are key details that can be observed. The PAV-aged binders (20 PAV and 40 PAV) show a distinct clustering, with IO 20 PAV and IO 40 PAV forming groups separate from the unaged and UV-aged binders. This indicates that the chemical changes caused by PAV aging are different from those caused by UV aging. Although rheological parameters indicated that UV aging was less severe than PAV aging, the crossover temperatures for IO 20 PAV and IO UV (21 days) were found to be very similar (and ΔT_c value after 21 days of UV exposure was smaller than 20 PAV), suggesting comparable aging levels. However, the clustering patterns of these samples were notably different and not spatially close to one another. The IO 40 PAV samples are positioned further along the PC_1 axis compared to the 20 PAV, which suggests as expected, a higher level of aging with extended PAV exposure. The UV-aged binders (6 days) show some clustering by aging state, but the clusters were somewhat difficult to discern. Rej. A and B unaged blends were found to be very similar to each other, as evidenced by the overlapping clusters, agreeing well with the master curve data. UV aging of the rejuvenator blends over 6 days was found to be less severe than PAV aging. However, the differences between the Rej.A and Rej. B blends after 6 days of UV exposure were more pronounced compared to their unaged counterparts. As expected, prolonged UV aging (21 days) of the Rej. B blend resulted in more severe degradation than at 6 days. On comparing these two groups, extended UV aging led to a decrease in PC_3, an increase in PC_1, and relatively stable PC_2 values. Conversely, PAV (thermo-oxidative) aging produced similar but more pronounced shifts in PC_1 and PC_3, alongside a significant reduction in PC_2, a change not observed with UV aging.

Figure 6.19 presents the PCA score plots for the ZDC blends, revealing distinct clustering across all concentrations and aging states. Notably, the differences between UV and thermo-oxidative aging are clearly distinguishable. For instance, a comparison of the 5% ZDC blend aged for 6 days and 21 days under UV exposure demonstrates that prolonged UV aging induces more pronounced chemical changes compared to 40 hours of PAV (thermo-oxidative) aging. These differences, which were not detected by rheological testing can be effectively captured through FTIR combined with PCA.

Similarly, Figure 6.20 presents the PCA score plots for the Vit. C blends. Although distinct groupings are less apparent in this case, clear clustering based on aging state was evident. As highlighted in the plot, the binder blends undergo notably different processes and transformations depending on whether they were subjected to thermo-oxidative or UV (photo-oxidative) aging. These differences are detectable through chemical analysis methods such as, in this case, FTIR as confirmed by Figure 6.20.

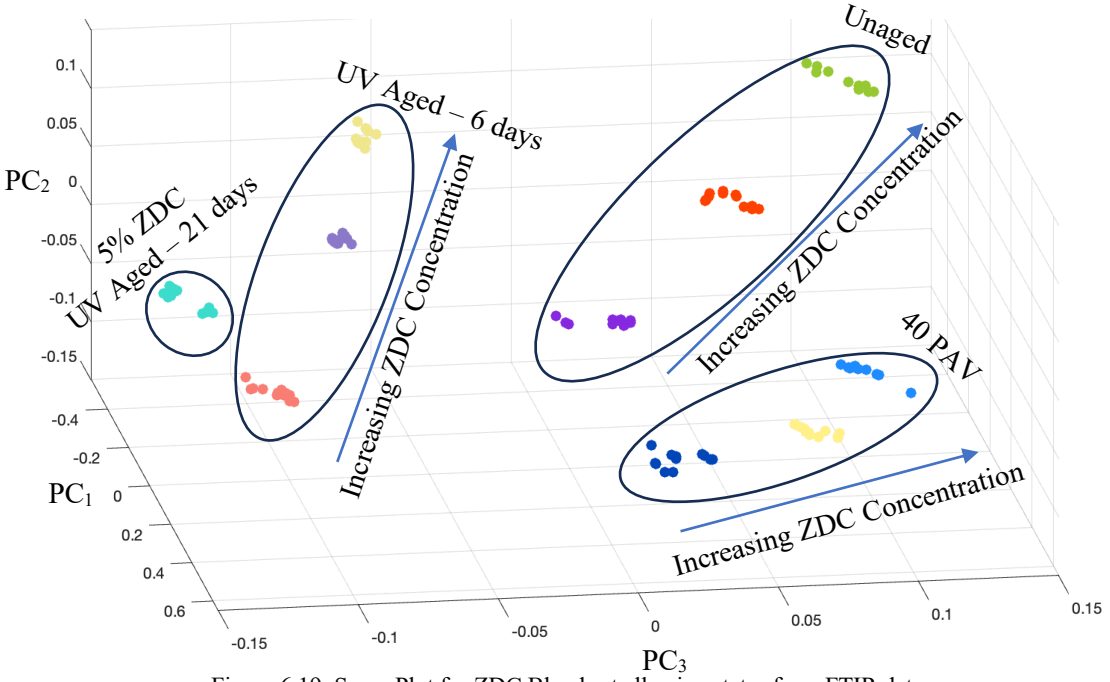


Figure 6.19: Score Plot for ZDC Blends at all aging states from FTIR data.

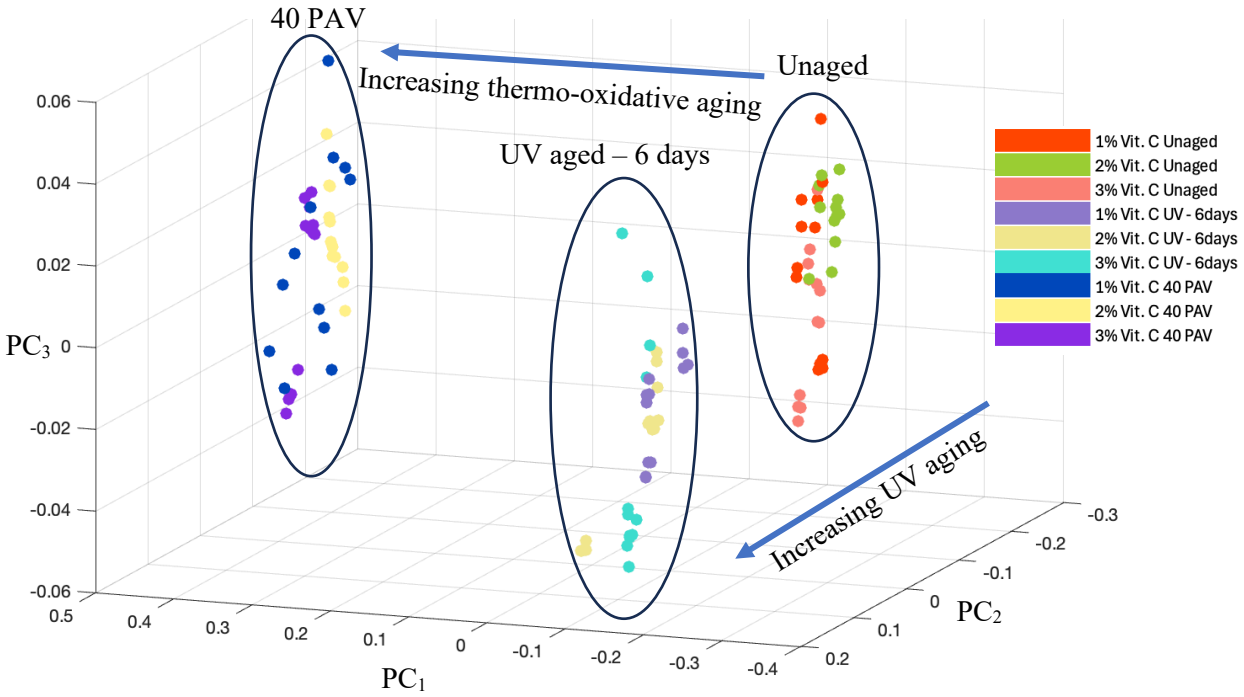
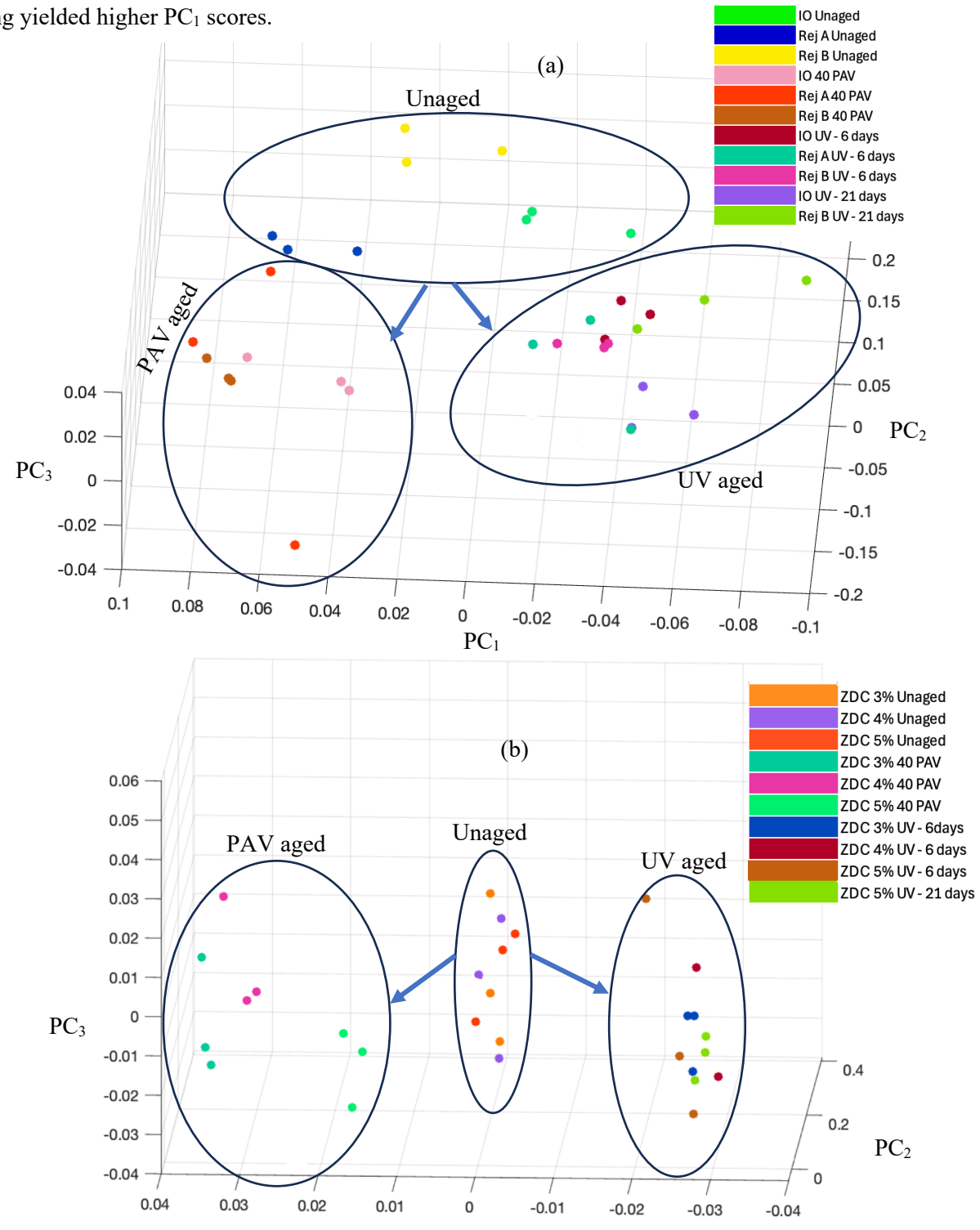


Figure 6.20: Score Plot for Vit. C Blends at all aging states from FTIR data.

In the case of NMR, the clustering patterns in the score plots are less distinct, primarily due to the smaller number of replicates conducted in comparison to FTIR. Consequently, the PCA score plots for the three groups of binder blends appeared quite similar with distinct clusters based on ageing state, but not with respect to additive type/concentration. Figure 6.21 presents all three score plots for all blend groups. While the clustering based on concentration (or additive type) was not discernible, the clusters according to aging

states were clearly defined, similar to what was observed in Figure 6.20. This further supports previous findings that chemical and spectroscopic testing techniques are more sensitive than rheological methods in detecting differences between different aging methods and processes. Interestingly, for both FTIR and NMR score plots, UV aged binders were found to mainly have lower PC_1 scores, while thermo-oxidative aging yielded higher PC_1 scores.



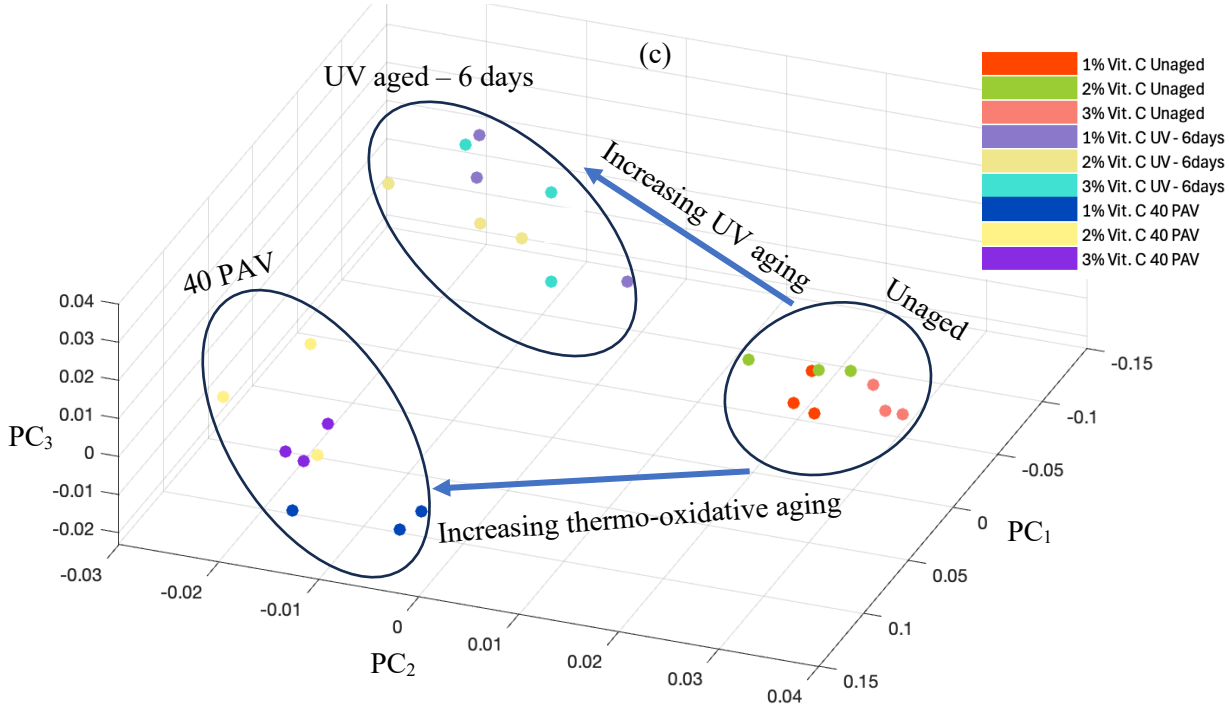


Figure 6.21: Score Plot for (a) RAP-Virgin-Rejuvenator, (b) ZDC, and (c) Vit. C Blends at all aging states from NMR data.

6.3.1.1 PLSR Analysis

PLSR was performed individually, with the same three groups of binder blends outlined earlier. Regression on both the FTIR and NMR data was used to determine whether these chemical testing methods could be used to detect and predict not only rheological parameters (crossover temperature and ΔT_c parameter), but differences in aging level and methods. MSE gives an indication of how well a regression model fits experimental data and predicts variables. A smaller MSE is preferred, and according to the principle of model parsimony, an ideal model fits experimental data with minimal error while using the fewest possible parameters. Figure 6.22 illustrates how the MSE values for PLSR models evolve as the number of components in the model increases using both NMR and FTIR data. Notably, NMR data consistently produced lower MSE values at a given number of components compared to FTIR data. This aligns with the findings in **Chapter 5**, which showed that NMR data generally leads to more accurate and parsimonious models for predicting rheological parameters and additive concentrations. It is important to note that since the number of replicates with respect to FTIR data used in this context was higher than that of NMR, it could have potentially led to overfitting of the model.

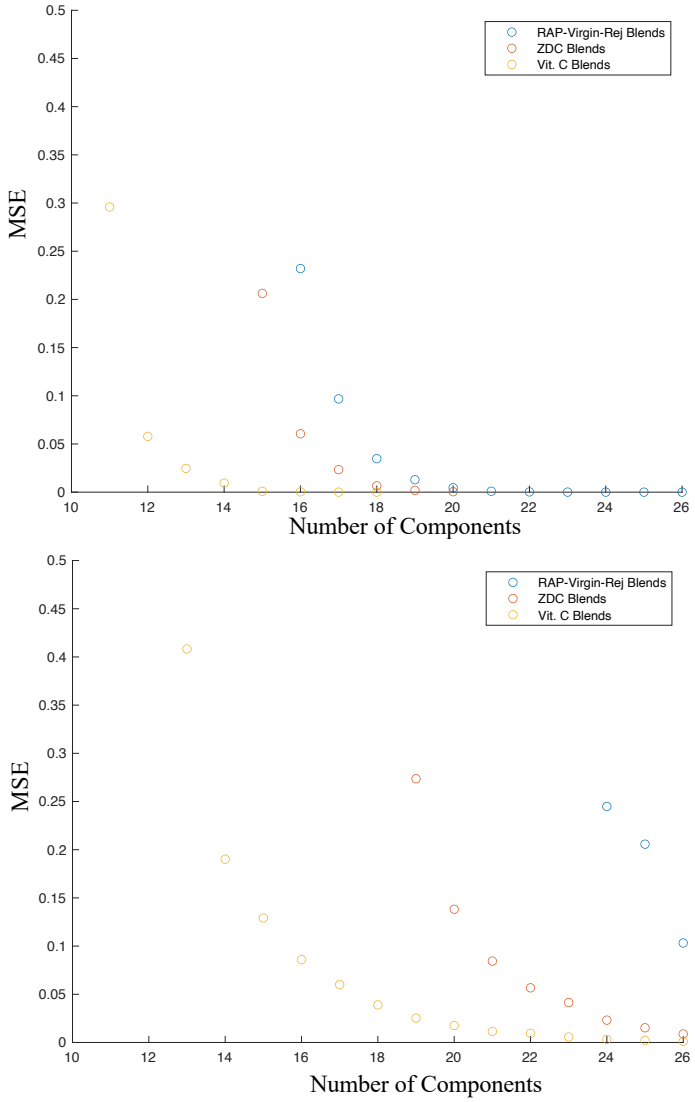


Figure 6.22: Evolution of MSE with Number of Components in PLSR models derived from NMR (top) and FTIR (bottom).

The final set of plots in this chapter, represented in Figures 6.23 and 6.24, are Variable Importance in Projection (VIP) plots. These plots highlight the influence of predictor variables on the fit of a model and predicted outcomes. For FTIR and NMR data, the predictor variables are the wavenumbers and chemical shift (PPM) values, respectively, over which the spectra were recorded. Typically, a VIP score greater than one is considered the threshold for identifying significant predictor variables in regression models. In the figures, VIP scores for each binder blend group and chemical testing method shown in red, indicate the predictor variables that are most important in distinguishing between/predicting rheological parameters, aging level and methods (UV vs. PAV). As expected, for FTIR, most of the predictor variables (wavenumbers) that heavily influence the PLSR model are within the fingerprint region (2000-600 cm^{-1}). On examining the NMR VIP plots, the most influential predictor variables were found to be between 0 – 3 ppm, where the majority of protons in hydrocarbons are detected. For binder blends with ZDC and Vit. C

additives, the characteristic chemical shift values corresponding to the presence of the respective additives were also found to significantly influence the PLSR model. The results demonstrate that different spectral regions are crucial for different binder blend groups when attempting to investigate aging processes, suggesting that identifying these key regions could guide future research on asphalt binder ageing and additive selection. This approach would enable the targeting of impactful spectral areas, reducing dimensionality and enhancing the performance of multivariate analysis techniques such as the ones used throughout this chapter.

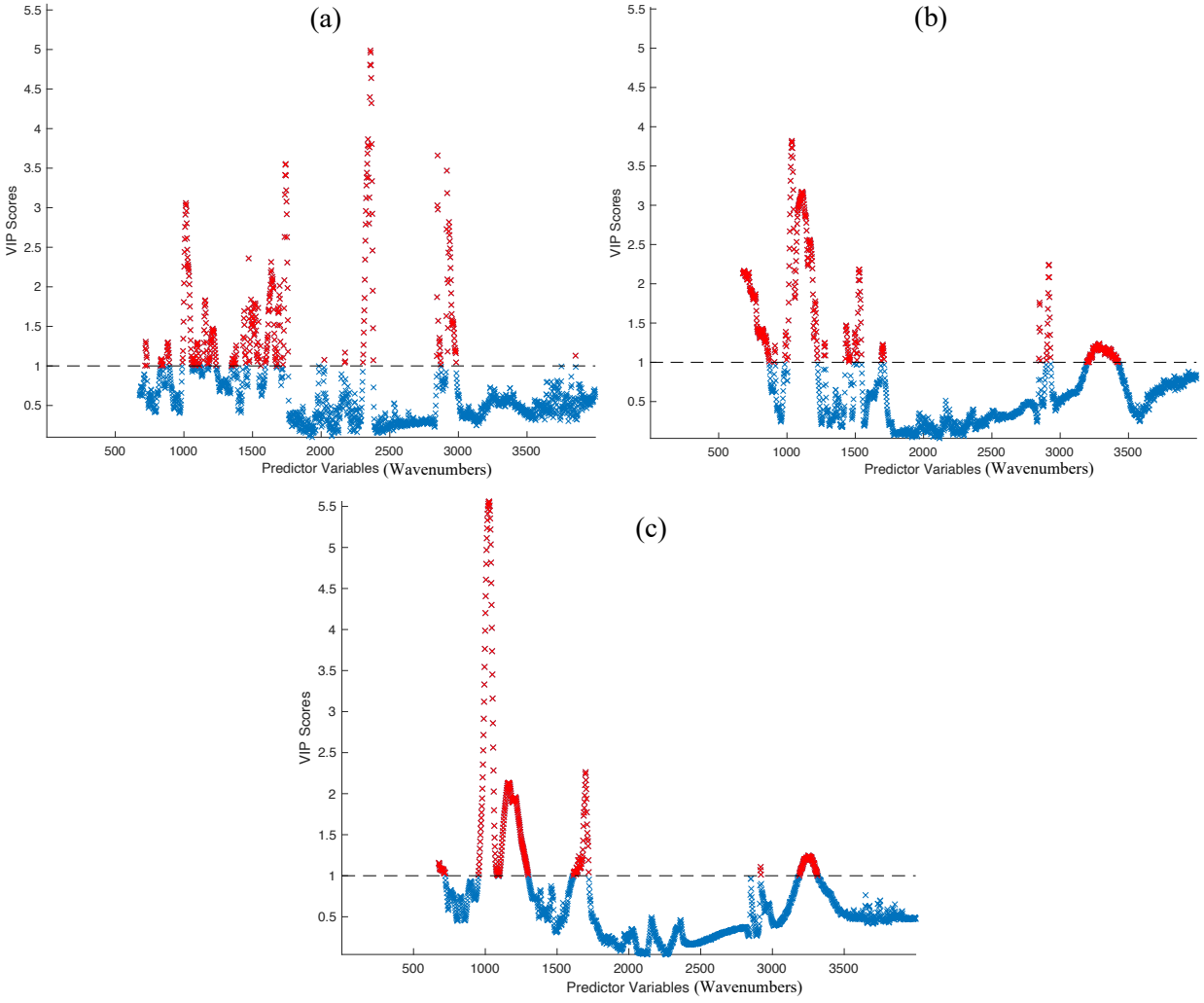


Figure 6.23: VIP Score Plots for (a)RAP-Virgin-Rejuvenator (b) ZDC and (c) Vit. C Blends obtained from FTIR.

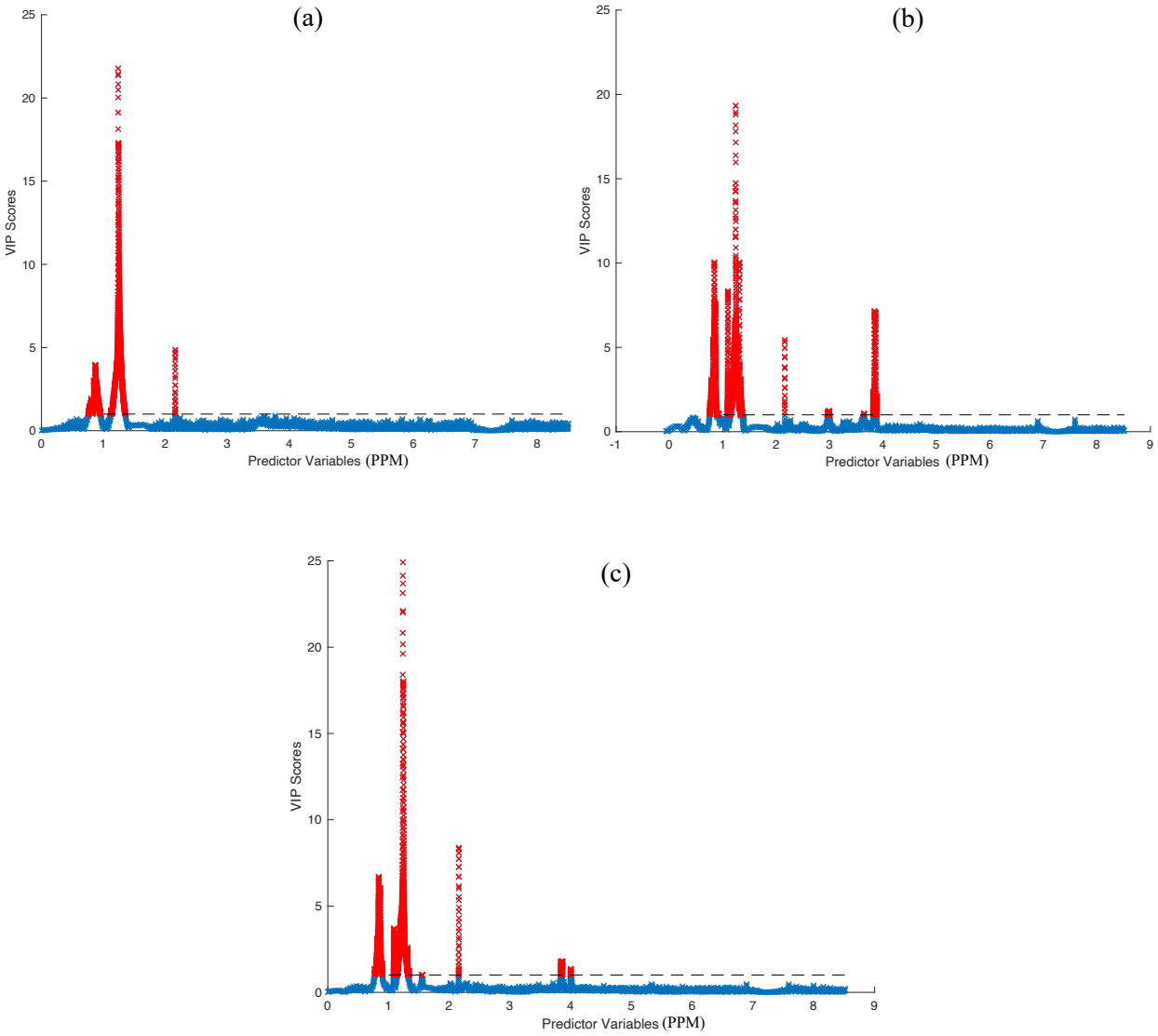


Figure 6.24: VIP Score Plots for (a) RAP-Virgin-Rejuvenator (b) ZDC and (c) Vit. C Blends obtained from NMR.

6.4. Conclusions

This chapter provides an overview of the effects of two types of aging—thermo-oxidative and UV—on the rheological and chemical properties of asphalt binders, both unmodified and with two anti-aging additives at varying concentrations. The anti-aging additives studied were ascorbic acid (Vit. C) at concentrations of 1%, 2%, and 3%, and zinc diethyldithiocarbamate (ZDC) at concentrations of 3%, 4%, and 5%. The chapter also outlines the development and challenges involved in the construction of a UV aging chamber for asphalt binders, featuring water spraying cycles at an elevated temperature of 70°C. All binder blends underwent thermo-oxidative aging in the Pressure Aging Vessel (PAV) and UV aging in the custom chamber for varying lengths of time.

Rheological testing was performed using the Dynamic Shear Rheometer (DSR) to assess the high- and intermediate-temperature performance and the Bending Beam Rheometer (BBR) to evaluate low-temperature properties. These results are presented and discussed in this chapter. Chemical testing, including Nuclear Magnetic Resonance (NMR) and Fourier Transform Infrared (FTIR) spectroscopy, was conducted, and the data were analyzed primarily using Principal Component Analysis (PCA) and Partial Least Squares Regression (PLSR) multivariate techniques. The findings and conclusions drawn from these analyses were as follows:

- UV aging in the custom-built aging chamber over a period of 6 days caused less severe effects across all binder blends, as observed through master curves, crossover temperatures, and the ΔTc parameter. When comparing rheological parameters, the ZDC blends exhibited more pronounced signs of aging after 21 days of UV exposure when compared to 40 hours of PAV aging. This behaviour contrasts with the IO base binder and the Rejuvenator B blend, where 21 days of UV aging resulted in less severe aging than 40 hours of PAV exposure. This suggests that while ZDC significantly enhances the resistance of asphalt binder blends to thermo-oxidative aging, its effectiveness in mitigating UV-induced aging is limited. Overall, the ZDC-modified blends maintained their high and low-temperature performance better than other blends, both before and after aging. Interestingly, despite previous literature citing Vit. C as possessing antioxidant properties, it appeared to accelerate the thermo-oxidative aging process while UV exposure.
- Spectroscopic analysis revealed that FTIR produced more distinct clusters in PCA score plots, whereas NMR provided a better model fit and more accurate predictions of rheological parameters, aging levels, and aging methods. Both NMR and FTIR were effective in detecting changes in the asphalt binder when comparing UV aging to PAV aging, even though these differences were not reflected in the rheological tests. The Variable Importance in Projection (VIP) plots also indicated the different regions of both NMR and FTIR spectra that are crucial for differentiating between different aging methods and processes. This result aligns with expectations, as UV and PAV aging operate through different mechanisms, leading to the formation of distinct functional groups and chemical components in the resulting aged binder. This underscores that UV aging induces different changes in the asphalt binder compared to thermo-oxidative aging, leading to distinctly different final aged products. These findings emphasize the importance of using spectroscopic techniques to accurately characterize asphalt binders, whether modified or unmodified, and to better understand the aging processes they undergo.

Chapter 7

Conclusions, Recommendations and Future Work

7.1 Overall Summary

This thesis explored the application of advanced analytical techniques in understanding the chemical, rheological, and performance characteristics of asphalt binders. Each chapter provided detailed insights into specific methodologies and outcomes, culminating in a comprehensive understanding of how these factors interplay to affect asphalt quality and longevity. The multifaceted approach employed throughout this research not only highlights the importance of chemical and physical analysis but also emphasizes the need for standardization and methodological rigor in the study of asphalt materials.

Chapter 4 established a critical foundation by evaluating the efficacy of Attenuated Total Reflection Fourier Transform Infrared (ATR-FTIR) spectroscopy combined with multivariate analysis techniques. This chapter provided robust empirical evidence underscoring the analytical strength of ATR-FTIR in characterizing chemical compositions and distinguishing between binder sources and aging states. The study highlighted the potential of ATR-FTIR, particularly when integrated with techniques such as Principal Component Analysis (PCA) and k-means clustering. However, it also addressed a significant challenge: the lack of standardized sample preparation methods that introduce variability in results. The findings indicate a clear need for establishing standardized protocols to enhance reproducibility and reliability across different studies and laboratories. The comparative analysis of Small Quantity (SQ) and Large Quantity (LQ) sample preparation methods further revealed that the LQ method yielded more consistent results, particularly in spectral indices, highlighting the critical role of preparation techniques in obtaining repeatable and reliable data and results.

In **Chapter 5**, the focus shifted to the effects of Styrene Butadiene Styrene (SBS) modification on asphalt binders, providing crucial insights into the aging behaviour and performance of these materials. By integrating conventional rheological tests with advanced chemical analysis techniques, including Nuclear Magnetic Resonance (NMR) and FTIR spectroscopy, the study offered a meticulous perspective on the molecular interactions and aging mechanisms at play in asphalt binders. Key findings demonstrated that increased SBS content significantly improved high-temperature performance and reduced oxidative aging, suggesting that SBS crosslinking leads to improved strength. Both functional group and multivariate analysis, mainly PCA and Partial Least Square Regression (PLSR), were performed on spectroscopic data for exploring patterns in data, in addition to determining relationships between rheological and chemical characteristics of SBS modified binders. The chapter verified previous literature while also paving the way for future investigations into optimal SBS concentrations and the compatibility of different SBS types with various binder sources.

Chapter 6 examined the comparative effects of thermo-oxidative and UV aging on both modified and unmodified asphalt binders. This chapter was particularly noteworthy for the development of a novel UV aging chamber, which allowed for realistic simulation of environmental conditions faced by pavements. The findings underscored the distinct aging mechanisms induced by different environmental factors, highlighting the performance of anti-aging additives namely Zinc Diethyldithiocarbamate (ZDC) and Ascorbic Acid and (Vit. C), which appeared to affect the aging process differently. This section of the research not only contributes to the understanding of how various factors influence asphalt binder longevity but also emphasizes the importance of targeted strategies in formulating effective anti-aging agents.

In conclusion, this thesis underscores significant advancements made in the characterization of asphalt binders through the use of chemo-rheological analytical techniques. The findings not only validate existing literature but also present new avenues for research and practical applications in asphalt technology. The integration of multiple methodologies throughout the study exemplifies the complexity of asphalt materials and the need for interdisciplinary approaches to understand and enhance performance and sustainability.

7.2 Conclusions

The research presented in this thesis leads to several important conclusions regarding asphalt binder characterization and modification, each of which holds implications for both academic and practical application:

1. **ATR-FTIR Spectroscopy Efficacy**: This study confirms that ATR-FTIR spectroscopy, when combined with multivariate analysis techniques, is an exceptionally powerful tool for characterizing the chemical composition and aging states of asphalt binders. The ability to distinguish between different crude binder sources and aging processes using this method is a significant contribution to the field. However, the variability introduced by non-standardized sample preparation methods poses a critical limitation that must be addressed for broader applicability. The large quantity (LQ) method was also found to yield more repeatable ATR-FTIR spectral results when compare to the small quantity (SQ) method indicating that LQ should be used for future standardization efforts. Principal Component Analysis (PCA) uncovers subtle but significant chemical differences between binder sources and aging states that are often missed by conventional FTIR indices, paving the way for more advanced, data-driven binder evaluation techniques.
2. **Role of SBS in Aging Resistance and Relationships between Rheological and Spectroscopic Data**: The findings indicate that SBS concentration and degradation can be quantified using NMR and FTIR spectroscopic testing. SBS polymers exhibit sacrificial aging behavior, protecting the base binder from oxidative damage by preferentially degrading themselves. This highlights the dual

role that SBS plays as a performance enhancer and an aging-resistant modifier in polymer-modified asphalt binders. The unique molecular structure of SBS, which facilitates better intermolecular interactions contributes to the overall elasticity and durability of the binder. The study suggests that the precise concentration of SBS is crucial for optimizing performance. Moreover, strong correlations were identified between spectroscopic data and rheological properties. PCA applied to ATR-FTIR proved more effective for clustering similar binder types, ageing states, and additives, compared to NMR. However, NMR was more advantageous for PLSR applications, particularly in predicting rheological parameters and ageing states. For the first time, this research establishes strong correlations between molecular-level changes (quantified by NMR and FTIR) and rheological properties, such as crossover temperature and ΔT_c, enabling better predictions of binder performance.

3. **Aging Mechanisms**: The research clearly outlines the differences in aging behaviour induced by thermo-oxidative versus UV exposure. Different functional groups and molecular interactions were found to result from each aging type. The findings reveal that while ZDC exhibited effectiveness against thermo-oxidative aging, its impact on UV-induced aging was notably less pronounced. This suggests that specific anti-aging strategies must be developed based on the predominant aging mechanisms encountered in particular environments. Moreover, the unexpected adverse effects of Vit. C, which appeared to accelerate aging rather than mitigate it, highlight the complexities involved in selecting appropriate anti-aging additives. The use of methods like PCA and PLSR were also found to highlight the key differences between UV and thermo-oxidative aging, providing effective tools for understanding changes and predicting rheological parameters from spectroscopic data.

Overall, these conclusions contribute to a more nuanced understanding of asphalt binder behaviour, emphasizing the importance of methodical analysis and the need for continued refinement of analytical protocols and materials. The integration of advanced technologies and methodologies offers promising avenues for improving asphalt binder performance and longevity in real-world applications.

7.3 Recommendations and Future Work

Based on the insights gained from this research, several recommendations for future work can be articulated, each of which addresses critical gaps and challenges identified throughout the study:

1. **Standardization of Methodologies**: Establishing standardized protocols using the LQ method for sample preparation and testing in NMR and ATR-FTIR analysis is crucial for the advancement of asphalt binder research. Future studies should aim to develop comprehensive guidelines that can be universally adopted, minimizing variability and enhancing reproducibility across different research environments, instruments, and operators. Collaborative efforts among researchers,

industry professionals, and standardization organizations could facilitate the establishment of these protocols, leading to a more unified approach in asphalt technology.

2. **Expanded Study of SBS Modifications**: Further research should investigate the impacts of varying SBS types and concentrations in diverse asphalt binder formulations. This can include exploring the compatibility of different SBS types with various binder sources to optimize performance. Additionally, studies should focus on the long-term performance of SBS-modified binders under real-world conditions, assessing how environmental factors and aging influence their durability over time. Understanding the molecular interactions at play will be essential for developing innovative formulations that maximize the benefits of polymer modification.
3. **Investigation of Alternative Anti-Aging Additives**: Given the unexpected outcomes observed with Vit. C, shown to be an anti-oxidant in previous literature, additional studies should focus on identifying and testing new anti-aging additives that can effectively mitigate both thermo-oxidative and UV aging effects. Understanding the mechanisms of these additives will be essential for developing more effective solutions. Research should also explore the potential for synergistic effects when combining multiple anti-aging agents, allowing for targeted formulations that enhance binder longevity.
4. **Integration of Multivariate Techniques**: Continued exploration of multivariate analysis methods, such as PCA and PLSR, in conjunction with advanced spectroscopic techniques can enhance understanding about similarity and differences between different binder sources and ageing states in addition to predictive modeling of asphalt binder performance. This integrative approach can provide a more holistic view of binder behaviour under varying conditions, leading to more accurate assessments of performance, rheological properties and durability. Future studies should prioritize the development of robust predictive models that can be employed in practical applications.
5. **Environmental Impact Assessments**: Future work should consider the environmental implications of using different additives and materials in asphalt technology. Conducting life-cycle assessments of various asphalt formulations can help determine the sustainability of different approaches, guiding the selection of materials that minimize ecological footprints. Additionally, research should explore the potential for incorporating recycled materials and bio-based additives in asphalt formulations to enhance sustainability and reduce waste and maintain or improve overall performance of asphalt mixes.
6. **Utilization of Machine Learning and AI for Data Analysis**: Future research should explore the application of machine learning (ML) and artificial intelligence (AI) algorithms for characterizing asphalt binders, predicting performance, and understanding relationships between spectroscopic

and rheological data. By leveraging these technologies, it may be possible to predict binder performance based solely on spectroscopic data, potentially reducing the need for extensive rheological testing. AI-driven models could also uncover complex patterns and relationships between chemical composition and mechanical properties, enabling faster, more accurate assessments of binder quality and longevity. Developing such predictive frameworks would enhance both the efficiency and accuracy of asphalt binder characterization in research and practical applications.

In summary, this thesis opens several avenues for future exploration and improvement in asphalt binder research, emphasizing the importance of integrating advanced analytical techniques with rheological testing, optimizing material formulations, and addressing standardization challenges in the pursuit of sustainable and high-performance asphalt technologies. The insights gathered from this work not only contribute to the academic understanding of asphalt materials but also offer practical guidance for industry applications aimed at enhancing the longevity and performance of pavement structures. Through continued collaboration and innovation, the asphalt industry can strive toward more sustainable and effective solutions that meet the evolving demands of infrastructure development.

References

AASHTO R 28. (2022). Standard Practice for Accelerated Aging of Asphalt Binder Using a Pressurized Aging Vessel (PAV). In *AASHTO* (Issue January).

AASHTO, Standard Method of Test for Determining the Flexural Creep Stiffness of Asphalt Binder Using the Bending Beam Rheometer (BBR) (2022).

AASHTO T 240. (2013). Standard Method of Test for Effect of Heat and Air on a Moving Film of Asphalt Binder (Rolling Thin-Film Oven Test). In *American Association of State Highway and Transportation Officials*.

Abdi, H. (n.d.). *Partial Least Squares (PLS) Regression*. Retrieved October 8, 2024, from http://www.utdallas.edu/

Adams, J. J., Schabron, J. F., & Boysen, R. (2015). Quantitative vacuum distillation of crude oils to give residues amenable to the asphaltene determinator coupled with saturates, aromatics, and resins separation characterization. *Energy and Fuels*, *29*(5). https://doi.org/10.1021/ef502829t

Adwani, D., Sreeram, A., Pipintakos, G., Mirwald, J., Wang, Y., Hajj, R., Jing, R., & Bhasin, A. (2023). Interpreting the effectiveness of antioxidants to increase the resilience of asphalt binders: A global interlaboratory study. *Construction and Building Materials*, *366*. https://doi.org/10.1016/j.conbuildmat.2022.130231

Aftgelt, K. H., & Harle, O. L. (1975). The Effect of Asphaltenes on Asphalt Viscosity. *Industrial and Engineering Chemistry Product Research and Development*, *14*(4), 240–246. https://doi.org/10.1021/i360056a005

Ahmed, R. Bin, & Hossain, K. (2021a). Characterization of Rejuvenated Asphalt Binders Using FTIR and AFM Techniques. In *RILEM, Bookseries* (pp. 355–361). https://doi.org/10.1007/978-3-030-46455-4_45

Ahmed, R. Bin, & Hossain, K. (2021b). Characterization of Rejuvenated Asphalt Binders Using FTIR and AFM Techniques. In *RILEM, Bookseries* (pp. 355–361). https://doi.org/10.1007/978-3-030-46455-4_45

Airey, G. D. (2003). State of the Art Report on Ageing Test Methods for Bituminous Pavement Materials. In *International Journal of Pavement Engineering* (Vol. 4, Issue 3, pp. 165–176). https://doi.org/10.1080/1029843042000198568

Ali, A. H., Mashaan, N. S., & Karim, M. R. (2013). Investigations of physical and rheological properties of aged rubberised bitumen. *Advances in Materials Science and Engineering*, *2013*. https://doi.org/10.1155/2013/239036

Ali, M. F., & Siddiqui, M. N. (2001). CHANGES IN ASPHALT CHEMISTRY AND DURABILITY DURING OXIDATION AND POLYMER MODIFICATION. *Petroleum Science and Technology*, *19*(9–10), 1229–1249. https://doi.org/10.1081/LFT-100108305

Anderson, R. M., King, G. N., Hanson, D. I., & Blankenship, P. B. (2011). Evaluation of the relationship between asphalt binder properties and non-load related cracking. *Asphalt Paving Technology: Association of Asphalt Paving Technologists-Proceedings of the Technical Sessions*, *80*.

Anne, D., Ziyani, L., Drouadaine, I., Pouget, S., Faucon-Dumont, S., Simard, D., Mouillet, V., Poirier, J. E., Gabet, T., Boulange, L., Nicolai, A., & Gueit, C. (2017). *MURE National Project: FTIR spectroscopy study to assess ageing of asphalt mixtures*. https://doi.org/10.14311/ee.2016.154

Apeagyei, A. K. (2011). Laboratory evaluation of antioxidants for asphalt binders. *Construction and Building Materials*, *25*(1), 47–53. https://doi.org/10.1016/j.conbuildmat.2010.06.058

Apostolidis, P., Liu, X., Kasbergen, C., & Scarpas, A. T. (2017). Synthesis of asphalt binder aging and the state of the art of antiaging technologies. *Transportation Research Record*, *2633*(1), 147–153. https://doi.org/10.3141/2633-17

Arafat, S., Kumar, N., Wasiuddin, N. M., Owhe, E. O., & Lynam, J. G. (2019). Sustainable lignin to enhance asphalt binder oxidative aging properties and mix properties. *Journal of Cleaner Production*, *217*, 456–468. https://doi.org/10.1016/j.jclepro.2019.01.238

ASTM. (2000). *Standard Test Method for Accelerated Weathering Test Conditions and Procedures for Bituminous Materials (Fluorescent UV and Condensation*. *04*(March 2000), 1–2.

ASTM. (2016). *Standard Practice for Accelerated Weathering Test Conditions and Procedures for Bituminous Materials (Xenon-Arc Method)*. *04*, 3–5.

ASTM. (2022). D6521: Standard Practice for Accelerated Aging of Asphalt Binder Using a Pressurized Aging Vessel (PAV). In *ASTM International: West Conshohocken, United States, 9p.* (Issue January).

ASTM D 7175-08. (2008). Standard Test Method for Determining the Rheological Properties of Asphalt Binder Using a Dynamic Shear Rheometer. *ASTM Interanational*, *3*(August).

ASTM D4124-97. (1997). *Standard test methods for separation of asphalt into four fractions*. 1–8. https://www.astm.org/d4124-09r18.html

Aurilio, M., Tavassoti, P., & Baaj, H. (2020a). Comparing the Ability of Different Tests and Rheological Indices to Evaluate the Cracking Resistance of Polymer Modified Asphalt Binders. In *researchgate.net*. Canadian Technical Asphalt Association.

Aurilio, M., Tavassoti, P., & Baaj, H. (2020b). Comparing the Ability of Different Tests and Rheological Indices to Evaluate the Cracking Resistance of Polymer Modified Asphalt Binders Observation of Asphalt Binder Microstructure with ESEM View project Literature Review on Extraction and Recovery of As. In *researchgate.net*. https://www.researchgate.net/publication/346088778

Aurilio, M., Tavassoti, P., Elwardany, M., & Baaj, H. (2023). Characterization of styrene-butadiene-styrene (SBS)-modified asphalt binders using the bending beam rheometer and the asphalt binder cracking device. *Canadian Journal of Civil Engineering*, *50*(8), 681–687. https://doi.org/10.1139/cjce-2022-0319

Azimi Alamdary, Y., Singh, S., & Baaj, H. (2019a). Laboratory simulation of the impact of solar radiation and moisture on long-term age conditioning of asphalt mixes. *Road Materials and Pavement Design*, *20*(sup1). https://doi.org/10.1080/14680629.2019.1587496

Azimi Alamdary, Y., Singh, S., & Baaj, H. (2019b). Laboratory simulation of the impact of solar radiation and moisture on long-term age conditioning of asphalt mixes. *Road Materials and Pavement Design*, *20*(sup1). https://doi.org/10.1080/14680629.2019.1587496

Azimi Alamdary, Y., Singh, S., & Baaj, H. (2022a). Toward a realistic asphalt mix ageing protocol. *Road Materials and Pavement Design*, *23*(10), 2317–2333. https://doi.org/10.1080/14680629.2021.1987303

Azimi Alamdary, Y., Singh, S., & Baaj, H. (2022b). Toward a realistic asphalt mix ageing protocol. *Road Materials and Pavement Design*, *23*(10), 2317–2333. https://doi.org/10.1080/14680629.2021.1987303

Baghaee Moghaddam, T., & Baaj, H. (2016). The use of rejuvenating agents in production of recycled hot mix asphalt: A systematic review. *Construction and Building Materials*, *114*, 805–816. https://doi.org/10.1016/j.conbuildmat.2016.04.015

Baldi-Sevilla, A., Montero, M. L., Aguiar, J. P., & Loría, L. G. (2016). Influence of nanosilica and diatomite on the physicochemical and mechanical properties of binder at unaged and oxidized conditions. *Construction and Building Materials*, *127*, 176–182. https://doi.org/10.1016/j.conbuildmat.2016.09.140

Baqersad, M., & Ali, H. (2019). Rheological and chemical characteristics of asphalt binders recycled using different recycling agents. *Construction and Building Materials*, *228*. https://doi.org/10.1016/j.conbuildmat.2019.116738

Bartholomew, D. J. (2009). Principal Components Analysis. In *International Encyclopedia of Education, Third Edition* (pp. 374–377). https://doi.org/10.1016/B978-0-08-044894-7.01358-0

Beattie, J. R., & Esmonde-White, F. W. L. (2021). Exploration of Principal Component Analysis: Deriving Principal Component Analysis Visually Using Spectra. In *Applied Spectroscopy* (Vol. 75, Issue 4, pp. 361–375). https://doi.org/10.1177/0003702820987847

Behnood, A. (2019a). Application of rejuvenators to improve the rheological and mechanical properties of asphalt binders and mixtures: A review. *Journal of Cleaner Production*, *231*. https://doi.org/10.1016/j.jclepro.2019.05.209

Behnood, A. (2019b). Application of rejuvenators to improve the rheological and mechanical properties of asphalt binders and mixtures: A review. *Journal of Cleaner Production*, *231*, 171–182. https://doi.org/10.1016/j.jclepro.2019.05.209

Behnood, A., & Modiri Gharehveran, M. (2019). Morphology, rheology, and physical properties of polymer-modified asphalt binders. In *European Polymer Journal* (Vol. 112, pp. 766–791). https://doi.org/10.1016/j.eurpolymj.2018.10.049

Bell, C. A., Abwahab, Y., Cristi, M. E., & Sosnovske, D. (1994). *Selection of Laboratory Aging Procedures for Asphalt-Aggregate Mixtures*. 92.

Betancourt Cardozo, F., Avella Moreno, E., & Trujillo, C. A. (2016). Structural Characterization of Unfractionated Asphalts by 1 H NMR and 13 C NMR. *Energy & Fuels*, *30*(4), 2729–2740. https://doi.org/10.1021/acs.energyfuels.5b02941

Borghi, A., Jiménez del Barco Carrión, A., Lo Presti, D., & Giustozzi, F. (2017). Effects of Laboratory Aging on Properties of Biorejuvenated Asphalt Binders. *Journal of Materials in Civil Engineering*, *29*(10). https://doi.org/10.1061/(asce)mt.1943-5533.0001995

Buisine, J. M., Joly, G., Eladlani, A., Such, C., Farcas, F., Ramond, G., Claudy, P., Letoffe, J. M., King, G. N., Planche, J. P., & Germanaud, L. (1993). Thermodynamic Behavior and Physicochemical Analysis of Eight SHRP Bitumens. *Transportation Research Record*, *1386*.

Bunn, C. W., & Holmes, D. R. (1958). Chain configurations in crystals of simple linear polymers. In *Discussions of the Faraday Society* (Vol. 25). https://doi.org/10.1039/DF9582500095

Camargo, I. G. do N., Dhia, T. Ben, Loulizi, A., Hofko, B., & Mirwald, J. (2021). Anti-aging additives: proposed evaluation process based on literature review. *Road Materials and Pavement Design*, *22*(S1). https://doi.org/10.1080/14680629.2021.1906738

Carpenter, S. H., & Wolosick, J. R. (1980). Modifier Influence in the Characterization of Hot-Mix Recycled Material. In *Transportation Research Record (TRB) 777* (Issue 777).

Charrié-Duhaut, A., Lemoine, S., Adam, P., Connan, J., & Albrecht, P. (2000). Abiotic oxidation of petroleum bitumens under natural conditions. *Organic Geochemistry*, *31*(10). https://doi.org/10.1016/S0146-6380(00)00109-1

Cháves-Pabón, S. B., Rondón-Quintana, H. A., & Bastidas-Martínez, J. G. (2019a). Aging of asphalt binders and asphalt mixtures. Summary Part I: Effect on physical-chemical properties. *International Journal of Civil Engineering and Technology*, *10*(12), 259–273.

Cháves-Pabón, S. B., Rondón-Quintana, H. A., & Bastidas-Martínez, J. G. (2019b). Aging of asphalt binders and asphalt mixtures. Summary Part I: Effect on physical-chemical properties. *International Journal of Civil Engineering and Technology*, *10*(12), 259–273. http://iaeme.comhttp//iaeme.com

Chen, A., Liu, G., Zhao, Y., Li, J., Pan, Y., & Zhou, J. (2018). Research on the aging and rejuvenation mechanisms of asphalt using atomic force microscopy. *Construction and Building Materials*, *167*, 177–184. https://doi.org/10.1016/j.conbuildmat.2018.02.008

Chen, J.-S., Lee, C.-T., & Lin, Y.-Y. (2018). Characterization of a Recycling Agent for Restoring Aged Bitumen. *Journal of Materials in Civil Engineering*, *30*(8). https://doi.org/10.1061/(asce)mt.1943-5533.0002388

Chen, Z., Zhang, H., & Duan, H. (2020). Investigation of ultraviolet radiation aging gradient in asphalt binder. *Construction and Building Materials*, *246*. https://doi.org/10.1016/j.conbuildmat.2020.118501

Cong, P., Liu, N., Tian, Y., & Zhang, Y. (2016). Effects of long-term aging on the properties of asphalt binder containing diatoms. *Construction and Building Materials*, *123*, 534–540. https://doi.org/10.1016/j.conbuildmat.2016.07.073

Cong, P., Wang, J., Luo, W., & Zhang, Y. (2021). Effects of aging on the properties of SBS modified asphalt binders containing anti-aging agents. *Construction and Building Materials*, *302*. https://doi.org/10.1016/j.conbuildmat.2021.124413

Cong, P., Wang, X., Xu, P., Liu, J., He, R., & Chen, S. (2013a). Investigation on properties of polymer modified asphalt containing various antiaging agents. *Polymer Degradation and Stability*, *98*(12), 2627–2634. https://doi.org/10.1016/j.polymdegradstab.2013.09.024

Cong, P., Wang, X., Xu, P., Liu, J., He, R., & Chen, S. (2013b). Investigation on properties of polymer modified asphalt containing various antiaging agents. *Polymer Degradation and Stability*, *98*(12), 2627–2634. https://doi.org/10.1016/j.polymdegradstab.2013.09.024

Corbett, L. W. (1969). Composition of Asphalt Based on Generic Fractionation, Using Solvent Deasphaltening, Elution-Adsorption Chromatography, and Densimetric Characterization. *Analytical Chemistry*, *41*(4). https://doi.org/10.1021/ac60273a004

Cui, Y., Chen, Q., Li, M., & Zhang, S. (2023). Study on low temperature crack resistance of warm-mixed recycled SBS modified asphalt mixtures. *Construction and Building Materials*, *409*. https://doi.org/10.1016/j.conbuildmat.2023.134120

Das, P. K., Baaj, H., Kringos, N., & Tighe, S. (2015). Coupling of oxidative ageing and moisture damage in asphalt mixtures. *Road Materials and Pavement Design*, *16*, 265–279. https://doi.org/10.1080/14680629.2015.1030835

Das, P. K., Balieu, R., Kringos, N., & Birgisson, B. (2015). On the oxidative ageing mechanism and its effect on asphalt mixtures morphology. *Materials and Structures/Materiaux et Constructions*, *48*(10), 3113–3127. https://doi.org/10.1617/s11527-014-0385-5

Das, P. K., Kringos, N., & Birgisson, B. (2014). Microscale investigation of thin film surface ageing of bitumen. *Journal of Microscopy*, *254*(2), 95–107. https://doi.org/10.1111/jmi.12122

Davidson, T., Nolan, A., & Mehta, Y. (2014). *A Study to Evaluate the Effects of SBS Polymer Modification on the True Grade of an Asphalt Binder*. 27–34. https://doi.org/10.1061/9780784478493.004

De Arimateia Almeida E Silva, J., De Figueirêdo Lopes Lucena, L. C., Rodrigues, J. K. G., Carvalho, M. W., & Costa, D. B. (2015). Use of Micronized Polyethylene Terephthalate (Pet) Waste in Asphalt Binder. *Petroleum Science and Technology*, *33*(15–16), 1508–1515. https://doi.org/10.1080/10916466.2015.1079538

Deef-Allah, E., & Abdelrahman, M. (2022). Evaluating the Low-temperature Properties of Asphalt Binders Extracted from Mixtures Containing Recycled Materials. *Periodica Polytechnica Civil Engineering*, *66*(2), 593–602. https://doi.org/10.3311/PPci.19681

Dessouky, S., Contreras, D., Sanchez, J., Papagiannakis, A. T., & Abbas, A. (2013). Influence of hindered phenol additives on the rheology of aged polymer-modified bitumen. *Construction and Building Materials*, *38*, 214–223. https://doi.org/10.1016/j.conbuildmat.2012.07.089

Dessouky, S., Contreras, D., Sanchez, J., & Park, D. (2015). Anti-oxidants' effect on bitumen rheology and mixes' mechanical performance. *Innovative Materials and Design for Sustainable Transportation Infrastructure - Selected Papers from the International Symposium on Systematic Approaches to Environmental Sustainability in Transportation*, 8–18. https://doi.org/10.1061/9780784479278.002

Ding, X., Chen, L., Ma, T., Ma, H., Gu, L., Chen, T., & Ma, Y. (2019). Laboratory investigation of the recycled asphalt concrete with stable crumb rubber asphalt binder. *Construction and Building Materials*, *203*, 552–557. https://doi.org/10.1016/j.conbuildmat.2019.01.114

Durrieu, F., Farcas, F., & Mouillet, V. (2007). The influence of UV aging of a Styrene/Butadiene/Styrene modified bitumen: Comparison between laboratory and on site aging. *Fuel*, *86*(10–11), 1446–1451. https://doi.org/10.1016/j.fuel.2006.11.024

Dwiggins, C. W. (1965). A small angle X-ray scattering study of the colloidal nature of petroleum. *Journal of Physical Chemistry*, *69*(10). https://doi.org/10.1021/j100894a041

Eberhardsteiner, L., Füssl, J., Hofko, B., Handle, F., Hospodka, M., Blab, R., & Grothe, H. (2015). Influence of asphaltene content on mechanical bitumen behavior: experimental investigation and micromechanical modeling. *Materials and Structures/Materiaux et Constructions*, *48*(10), 3099–3112. https://doi.org/10.1617/s11527-014-0383-7

Ergon, R. (2013). Principal component regression (PCR) and partial least squares regression (PLSR). In *Mathematical and Statistical Methods in Food Science and Technology*. https://doi.org/10.1002/9781118434635.ch08

Eyssautier, J., Levitz, P., Espinat, D., Jestin, J., Gummel, J., Grillo, I., & Barré, L. (2011). Insight into asphaltene nanoaggregate structure inferred by small angle neutron and X-ray scattering. *Journal of Physical Chemistry B*, *115*(21). https://doi.org/10.1021/jp111468d

Feng, Z. G., Wang, S. J., Bian, H. J., Guo, Q. L., & Li, X. J. (2016). FTIR and rheology analysis of aging on different ultraviolet absorber modified bitumens. *Construction and Building Materials*, *115*, 48–53. https://doi.org/10.1016/j.conbuildmat.2016.04.040

Feng, Z. G., Yu, J. Y., Zhang, H. L., Kuang, D. L., & Xue, L. H. (2013). Effect of ultraviolet aging on rheology, chemistry and morphology of ultraviolet absorber modified bitumen. *Materials and Structures/Materiaux et Constructions*, *46*(7), 1123–1132. https://doi.org/10.1617/s11527-012-9958-3

Fernández-Gómez, W. D., Rondón Quintana, H. A., Daza, C. E., & Reyes Lizcano, F. A. (2014). The effects of environmental aging on Colombian asphalts. *Fuel*, *115*, 321–328. https://doi.org/10.1016/j.fuel.2013.07.009

Filippelli, L., Gentile, L., Rossi, C. O., Ranieri, G. A., & Antunes, F. E. (2012). Structural change of bitumen in the recycling process by using rheology and NMR. *Industrial and Engineering Chemistry Research*, *51*(50). https://doi.org/10.1021/ie301899v

Fini, E. H., Buabeng, F. S., Abu-Lebdeh, T., & Awadallah, F. (2016). Effect of introduction of furfural on asphalt binder ageing characteristics. *Road Materials and Pavement Design*, *17*(3), 638–657. https://doi.org/10.1080/14680629.2015.1108219

Fini, E. H., Hajikarimi, P., Rahi, M., & Moghadas Nejad, F. (2016). Physiochemical, Rheological, and Oxidative Aging Characteristics of Asphalt Binder in the Presence of Mesoporous Silica Nanoparticles. *Journal of Materials in Civil Engineering*, *28*(2). https://doi.org/10.1061/(asce)mt.1943-5533.0001423

Garcia Cucalon, L., Kaseer, F., Arámbula-Mercado, E., Epps Martin, A., Morian, N., Pournoman, S., & Hajj, E. (2019). The crossover temperature: significance and application towards engineering balanced recycled binder blends. *Road Materials and Pavement Design*, *20*(6), 1391–1412. https://doi.org/10.1080/14680629.2018.1447504

Gedik, A. (2021). A literature review of bitumen hardening from past to present: Aging mechanism, indicators, test methods, and retarders. *Airfield and Highway Pavements 2021: Pavement Materials and Sustainability - Selected Papers from the International Airfield and Highway Pavements Conference 2021*, 221–233. https://doi.org/10.1061/9780784483510.021

Ghavibazoo, A., Abdelrahman, M., & Ragab, M. (2015). Evaluation of oxidization of crumb rubber-modified asphalt during short-term aging. *Transportation Research Record*, *2505*, 84–91. https://doi.org/10.3141/2505-11

Grossegger, D., Grothe, H., Hofko, B., & Hospodka, M. (2018). Fluorescence spectroscopic investigation of bitumen aged by field exposure respectively modified rolling thin film oven test. *Road Materials and Pavement Design*, *19*(4). https://doi.org/10.1080/14680629.2017.1281833

Gui, W., Wang, L., Guo, R., & Yang, Y. (2023). Effects of aging behavior on macro and micro characterizations of surfactant–crumb rubber asphalt binders. *Construction and Building Materials*, *408*. https://doi.org/10.1016/j.conbuildmat.2023.133535

Gulotta, T. M., Mistretta, M., & Praticò, F. G. (2019). A life cycle scenario analysis of different pavement technologies for urban roads. *Science of the Total Environment*, *673*, 585–593. https://doi.org/10.1016/j.scitotenv.2019.04.046

Guo, M., Liang, M., Fu, Y., Sreeram, A., & Bhasin, A. (2021). Average molecular structure models of unaged asphalt binder fractions. *Materials and Structures/Materiaux et Constructions*, *54*(4). https://doi.org/10.1617/s11527-021-01754-2

Guo, M., Liang, M., Sreeram, A., Bhasin, A., & Luo, D. (2022). Characterisation of rejuvenation of various modified asphalt binders based on simplified chromatographic techniques. *International Journal of Pavement Engineering*, *23*(12). https://doi.org/10.1080/10298436.2021.1943743

Hadole, H. P., Suryawanshi, S. D., Khapne, V. A., & Ranadive, M. S. (2021). Moisture Damage Resistance of Short-Term Aged Pyro-Oil–Modified Bitumen Using Rolling Thin Film Oven by Surface Free Energy Approach. *Journal of Materials in Civil Engineering*, *33*(10). https://doi.org/10.1061/(asce)mt.1943-5533.0003872

Haghshenas, H. F., Rea, R., & Haghshenas, D. F. (2019). Aging resistance of asphalt binders through the use of zinc diethyldithiocarbamate. *Petroleum Science and Technology*, *37*(22), 2275–2282. https://doi.org/10.1080/10916466.2019.1633348

Han, J., Wu, S., Zhang, D., & Liu, X. (2011). Investigation of low temperature properties for ultraviolet radiation aged bitumen and mixture. *Key Engineering Materials*, *467–469*, 1535–1540. https://doi.org/10.4028/www.scientific.net/KEM.467-469.1535

Handle, F., Füssl, J., Neudl, S., Grossegger, D., Eberhardsteiner, L., Hofko, B., Hospodka, M., Blab, R., & Grothe, H. (2016). The bitumen microstructure: a fluorescent approach. *Materials and Structures/Materiaux et Constructions*, *49*(1–2). https://doi.org/10.1617/s11527-014-0484-3

He, B., Yu, J., Du, W., Cao, Z., & Han, X. (2019). Preparation and characterization of lignosulfonate grafted layered double hydroxides and their applications as anti-ultraviolet additives for bitumen. *Construction and Building Materials*, *195*, 432–440. https://doi.org/10.1016/j.conbuildmat.2018.11.100

He, X., Hochstein, D., Ge, Q., Ali, A. W., Chen, F., & Yin, H. (2018a). Accelerated Aging of Asphalt by UV Photo-Oxidation Considering Moisture and Condensation Effects. *Journal of Materials in Civil Engineering*, *30*(1). https://doi.org/10.1061/(asce)mt.1943-5533.0002120

He, X., Hochstein, D., Ge, Q., Ali, A. W., Chen, F., & Yin, H. (2018b). Accelerated Aging of Asphalt by UV Photo-Oxidation Considering Moisture and Condensation Effects. *Journal of Materials in Civil Engineering*, *30*(1). https://doi.org/10.1061/(asce)mt.1943-5533.0002120

Herrington, P. R., Patrick, J. E., & Ball, G. F. A. (1994). Oxidation of Roading Asphalts. *Industrial and Engineering Chemistry Research*, *33*(11). https://doi.org/10.1021/ie00035a033

Hettiarachchi, C., Hou, X., Xiang, Q., Yong, D., & Xiao, F. (2020). A blending efficiency model for virgin and aged binders in recycled asphalt mixtures based on blending temperature and duration. *Resources, Conservation and Recycling*, *161*. https://doi.org/10.1016/j.resconrec.2020.104957

Hintz, C., Velasquez, R., Johnson, C., & Bahia, H. (2011). Modification and validation of linear amplitude sweep test for binder fatigue specification. *Transportation Research Record*, *2207*. https://doi.org/10.3141/2207-13

Hofko, B., Alavi, M. Z., Grothe, H., Jones, D., & Harvey, J. (2017). Repeatability and sensitivity of FTIR ATR spectral analysis methods for bituminous binders. *Materials and Structures/Materiaux et Constructions*, *50*(3). https://doi.org/10.1617/s11527-017-1059-x

Hong, H., Zhang, H., & Zhang, S. (2020). Effect of multi-dimensional nanomaterials on the aging behavior of asphalt by atomic force microscope. *Construction and Building Materials*, *260*. https://doi.org/10.1016/j.conbuildmat.2020.120389

Hossain, R., & Wasiuddin, N. M. (2019). Evaluation of Degradation of SBS Modified Asphalt Binder Because of RTFO, PAV, and UV Aging using a Novel Extensional Deformation Test. *Transportation Research Record*, *2673*(6), 447–457. https://doi.org/10.1177/0361198119847471

Hosseinnezhad, S., Zadshir, M., Yu, X., Yin, H., Sharma, B. K., & Fini, E. (2019). Differential effects of ultraviolet radiation and oxidative aging on bio-modified binders. *Fuel*, *251*, 45–56. https://doi.org/10.1016/j.fuel.2019.04.029

Hou, X., Lv, S., Chen, Z., & Xiao, F. (2018). Applications of Fourier transform infrared spectroscopy technologies on asphalt materials. In *Measurement: Journal of the International Measurement Confederation* (Vol. 121). https://doi.org/10.1016/j.measurement.2018.03.001

Hou, X., Xiao, F., Wang, J., & Amirkhanian, S. (2018). Identification of asphalt aging characterization by spectrophotometry technique. *Fuel*, *226*. https://doi.org/10.1016/j.fuel.2018.04.030

Hu, D., Gu, X., Lyu, L., Wang, G., & Cui, B. (2022). Unraveling oxidative aging behavior of asphaltenes using ab initio molecular dynamics and static density functional theory. *Construction and Building Materials*, *318*. https://doi.org/10.1016/j.conbuildmat.2021.126032

Hu, J., Wu, S., Liu, Q., García Hernández, M. I., Wang, Z., Nie, S., & Zhang, G. (2018). Effect of ultraviolet radiation in different wavebands on bitumen. *Construction and Building Materials*, *159*, 479–485. https://doi.org/10.1016/j.conbuildmat.2017.10.117

Hu, J., Wu, S., Liu, Q., García Hernández, M. I., Zeng, W., & Xie, W. (2017a). Study of Antiultraviolet Asphalt Modifiers and Their Antiageing Effects. *Advances in Materials Science and Engineering*, *2017*. https://doi.org/10.1155/2017/9595239

Hu, J., Wu, S., Liu, Q., García Hernández, M. I., Zeng, W., & Xie, W. (2017b). Study of Antiultraviolet Asphalt Modifiers and Their Antiageing Effects. *Advances in Materials Science and Engineering*, *2017*. https://doi.org/10.1155/2017/9595239

Hu, M., Ma, J., Sun, D., Hofko, B., Mirwald, J., Zheng, Y., & Xu, L. (2022). Quantifying Weathering-Aging Test Parameters of High Viscosity–Modified Asphalt by Establishing a Conversion Relationship with Standard PAV Aging. *Journal of Materials in Civil Engineering*, *34*(6). https://doi.org/10.1061/(asce)mt.1943-5533.0004228

Hu, M., Sun, G., Sun, D., Lu, T., Ma, J., & Deng, Y. (2021). Accelerated weathering simulation on rheological properties and chemical structure of high viscosity modified asphalt: A temperature acceleration effect analysis. *Construction and Building Materials*, *268*. https://doi.org/10.1016/j.conbuildmat.2020.121120

Hu, Y., Si, W., Kang, X., Xue, Y., Wang, H., Parry, T., & Airey, G. D. (2022). State of the art: Multiscale evaluation of bitumen ageing behaviour. In *Fuel* (Vol. 326). https://doi.org/10.1016/j.fuel.2022.125045

Huang, J. (2010). Characterization of asphalt fractions by NMR spectroscopy. *Petroleum Science and Technology*, *28*(6). https://doi.org/10.1080/10916460903073797

Hung, A. M., & Fini, E. H. (2019a). Absorption spectroscopy to determine the extent and mechanisms of aging in bitumen and asphaltenes. *Fuel*, *242*, 408–415. https://doi.org/10.1016/j.fuel.2019.01.085

Hung, A. M., & Fini, E. H. (2019b). Absorption spectroscopy to determine the extent and mechanisms of aging in bitumen and asphaltenes. *Fuel*, *242*, 408–415. https://doi.org/10.1016/j.fuel.2019.01.085

Hung, A. M., Kazembeyki, M., Hoover, C. G., & Fini, E. H. (2019). Evolution of Morphological and Nanomechanical Properties of Bitumen Thin Films as a Result of Compositional Changes Due to Ultraviolet Radiation. *ACS Sustainable Chemistry and Engineering*, *7*(21), 18005–18014. https://doi.org/10.1021/acssuschemeng.9b04846

Hunter, C. A., & Sanders, J. K. M. (1990). The Nature of π-π Interactions. *Journal of the American Chemical Society*, *112*(14), 5525–5534. https://doi.org/10.1021/ja00170a016

Hunter, R., Self, A., & Read, J. (2015). The Shell Bitumen Handbook, 6th edition. In *The Shell Bitumen Handbook, 6th edition*. https://doi.org/10.1680/tsbh.58378

Ibrahim, I. M., Fathy, E. S., El-Shafie, M., & Elnaggar, M. Y. (2015). Impact of incorporated gamma irradiated crumb rubber on the short-term aging resistance and rheological properties of asphalt binder. *Construction and Building Materials*, *81*, 42–46. https://doi.org/10.1016/j.conbuildmat.2015.01.015

Ingrassia, L. P., Lu, X., Ferrotti, G., Conti, C., & Canestrari, F. (2020). Investigating the "circular propensity" of road bio-binders: Effectiveness in hot recycling of reclaimed asphalt and recyclability potential. *Journal of Cleaner Production*, *255*. https://doi.org/10.1016/j.jclepro.2020.120193

Jacobs, G., Margaritis, A., Hernando, D., He, L., Blom, J., & Van den bergh, W. (2021). Influence of soft binder and rejuvenator on the mechanical and chemical properties of bituminous binders. *Journal of Cleaner Production*, *287*. https://doi.org/10.1016/j.jclepro.2020.125596

Jing, R., Varveri, A., Liu, X., Scarpas, A., & Erkens, S. (2020). Rheological, fatigue and relaxation properties of aged bitumen. *International Journal of Pavement Engineering*, *21*(8). https://doi.org/10.1080/10298436.2019.1654609

Kadhim, H. (2019). *Improving Durability of Asphalt Mixes Produced With Reclaimed Asphalt Pavement (Rap) by Enhancing Binder Blending*. University of Waterloo.

Karim, F., Hussain, J., & Hafeez, I. (2021). Estimating the Asphalt Binder Film Thickness Using Scanning Electron Microscope and Energy Dispersive X-Ray Spectroscopy. *Advances in Materials Science and Engineering*, *2021*. https://doi.org/10.1155/2021/8894970

Karlsson, R., & Isacsson, U. (2003). Application of FTIR-ATR to Characterization of Bitumen Rejuvenator Diffusion. *Journal of Materials in Civil Engineering*, *15*(2), 157–165. https://doi.org/10.1061/(asce)0899-1561(2003)15:2(157)

Karnati, S. R., Oldham, D., Fini, E. H., & Zhang, L. (2019). Surface functionalization of silica nanoparticles to enhance aging resistance of asphalt binder. *Construction and Building Materials*, *211*, 1065–1072. https://doi.org/10.1016/j.conbuildmat.2019.03.257

Kaseer, F., Cucalon, L. G., Arámbula-Mercado, E., Martin, A. E., & Epps, J. (2018). Practical tools for optimizing recycled materials content and recycling agent dosage for improved short- and long-term performance of rejuvenated binder blends and mixtures. *Asphalt Paving Technology: Association of Asphalt Paving Technologists-Proceedings of the Technical Sessions*, *87*, 513–555. https://doi.org/10.12783/aapt2018/33816

Kaseer, F., Martin, A. E., & Arámbula-Mercado, E. (2019). Use of recycling agents in asphalt mixtures with high recycled materials contents in the United States: A literature review. In *Construction and Building Materials* (Vol. 211). https://doi.org/10.1016/j.conbuildmat.2019.03.286

Kassem, E., Khan, M. S., Katukuri, S., Sirin, O., Muftah, A., & Bayomy, F. (2019). Retarding aging of asphalt binders using antioxidant additives and copolymers. *International Journal of Pavement Engineering*, *20*(10), 1154–1169. https://doi.org/10.1080/10298436.2017.1394098

Kaya Ozdemir, D., Topal, A., & McNally, T. (2021a). Relationship between microstructure and phase morphology of SBS modified bitumen with processing parameters studied using atomic force microscopy. *Construction and Building Materials*, *268*. https://doi.org/10.1016/j.conbuildmat.2020.121061

Kaya Ozdemir, D., Topal, A., & McNally, T. (2021b). Relationship between microstructure and phase morphology of SBS modified bitumen with processing parameters studied using atomic force microscopy. *Construction and Building Materials*, *268*. https://doi.org/10.1016/j.conbuildmat.2020.121061

Kemp, G. R., & Predoehl, N. H. (1981). A COMPARISON OF FIELD AND LABORATORY ENVIRONMENTS ON ASPHALT DURABILITY. *Conference of Association of Asphalt Paving Technologists*, *50*.

Khavandi Khiavi, A., Ghanbari, A., & Ahmadi, E. (2021a). Evaluation of Poly 2-Hydroxyethyl Methacrylate—Modified Bitumen Aging Using NMR and FTIR Techniques. *Journal of Transportation Engineering, Part B: Pavements*, *147*(1). https://doi.org/10.1061/jpeodx.0000228

Khavandi Khiavi, A., Ghanbari, A., & Ahmadi, E. (2021b). Evaluation of Poly 2-Hydroxyethyl Methacrylate—Modified Bitumen Aging Using NMR and FTIR Techniques. *Journal of Transportation Engineering, Part B: Pavements*, *147*(1). https://doi.org/10.1061/jpeodx.0000228

Kherif, F., & Latypova, A. (2019). Principal component analysis. In *Machine Learning: Methods and Applications to Brain Disorders* (pp. 209–225). https://doi.org/10.1016/B978-0-12-815739-8.00012-2

Kim, K. W., & Burati, J. L. (1993). Use of GPC Chromatograms to Characterize Aged Asphalt Cements. *Journal of Materials in Civil Engineering*, *5*(1). https://doi.org/10.1061/(asce)0899-1561(1993)5:1(41)

Koots, J. A., & Speight, J. G. (1975). Relation of petroleum resins to asphaltenes. *Fuel*, *54*(3), 179–184. https://doi.org/10.1016/0016-2361(75)90007-1

Kuang, D., Yu, J., Feng, Z., Li, R., Chen, H., Guan, Y., & Zhang, Z. (2014). Performance evaluation and preventive measures for aging of different bitumens. *Construction and Building Materials*, *66*, 209–213. https://doi.org/10.1016/j.conbuildmat.2014.04.016

Lamontagne, J., Dumas, P., Mouillet, V., & Kister, J. (2001). Comparison by Fourier transform infrared (FTIR) spectroscopy of different ageing techniques: Application to road bitumens. *Fuel*, *80*(4). https://doi.org/10.1016/S0016-2361(00)00121-6

Lamontagne, J., Durrieu, F., Planche, J. P., Mouillet, V., & Kister, J. (2001). Direct and continuous methodological approach to study the ageing of fossil organic material by infrared microspectrometry imaging: Application to polymer modified bitumen. *Analytica Chimica Acta*, *444*(2). https://doi.org/10.1016/S0003-2670(01)01235-1

Lee, S. J., Hu, J., Kim, H., Amirkhanian, S. N., & Jeong, K. D. (2011). Aging analysis of rubberized asphalt binders and mixes using gel permeation chromatography. *Construction and Building Materials*, *25*(3). https://doi.org/10.1016/j.conbuildmat.2010.08.004

Lesueur, D. (2009a). The colloidal structure of bitumen: Consequences on the rheology and on the mechanisms of bitumen modification. In *Advances in Colloid and Interface Science* (Vol. 145, Issues 1–2, pp. 42–82). https://doi.org/10.1016/j.cis.2008.08.011

Lesueur, D. (2009b). The colloidal structure of bitumen: Consequences on the rheology and on the mechanisms of bitumen modification. In *Advances in Colloid and Interface Science* (Vol. 145, Issues 1–2, pp. 42–82). https://doi.org/10.1016/j.cis.2008.08.011

Lesueur, D., Teixeira, A., Lázaro, M. M., Andaluz, D., & Ruiz, A. (2016). A simple test method in order to assess the effect of mineral fillers on bitumen ageing. *Construction and Building Materials*, *117*, 182–189. https://doi.org/10.1016/j.conbuildmat.2016.05.003

Li, B., Li, X., Kundwa, M. J., Li, Z., & Wei, D. (2021). Evaluation of the adhesion characteristics of material composition for polyphosphoric acid and SBS modified bitumen based on surface free energy theory. *Construction and Building Materials*, *266*. https://doi.org/10.1016/j.conbuildmat.2020.121022

Li, C., Wu, S., Chen, Z., Shu, B., Li, Y., Xiao, Y., & Liu, Q. (2019). Synthesis of Fe3O4-decorated Mg-Al layered double hydroxides magnetic nanosheets to improve anti-ultraviolet aging and microwave absorption properties used in asphalt materials. *Construction and Building Materials*, *220*, 320–328. https://doi.org/10.1016/j.conbuildmat.2019.06.032

Li, Y., Feng, J., Wu, S., Chen, A., Kuang, D., Bai, T., Gao, Y., Zhang, J., Li, L., Wan, L., Liu, Q., Chen, Z., & Gu, D. (2022a). Review of ultraviolet ageing mechanisms and anti-ageing methods for asphalt binders. In *Journal of Road Engineering* (Vol. 2, Issue 2, pp. 137–155). https://doi.org/10.1016/j.jreng.2022.04.002

Li, Y., Feng, J., Wu, S., Chen, A., Kuang, D., Bai, T., Gao, Y., Zhang, J., Li, L., Wan, L., Liu, Q., Chen, Z., & Gu, D. (2022b). Review of ultraviolet ageing mechanisms and anti-ageing methods for asphalt binders. In *Journal of Road Engineering* (Vol. 2, Issue 2, pp. 137–155). https://doi.org/10.1016/j.jreng.2022.04.002

Li, Y., Feng, J., Yang, F., Wu, S., Liu, Q., Bai, T., Liu, Z., Li, C., Gu, D., Chen, A., & Jin, Y. (2021). Gradient aging behaviors of asphalt aged by ultraviolet lights with various intensities. *Construction and Building Materials*, *295*. https://doi.org/10.1016/j.conbuildmat.2021.123618

Li, Y., Li, H., Nie, S., Wu, S., Liu, Q., Li, C., Shu, B., Li, C., Song, W., Zou, Y., & Pang, L. (2020). Negative impacts of environmental factors (UV radiation, water and different solutions) on bitumen and its mechanism. *Construction and Building Materials*, *265*. https://doi.org/10.1016/j.conbuildmat.2020.120288

Li, Y., Wu, S., Dai, Y., Li, C., Song, W., Li, H., Li, C., & Shu, B. (2020a). Transitions of component, physical, rheological and self-healing properties of petroleum bitumen from the loose bituminous mixture after UV irradiation. *Fuel*, *262*. https://doi.org/10.1016/j.fuel.2019.116507

Li, Y., Wu, S., Dai, Y., Li, C., Song, W., Li, H., Li, C., & Shu, B. (2020b). Transitions of component, physical, rheological and self-healing properties of petroleum bitumen from the loose bituminous mixture after UV irradiation. *Fuel*, *262*. https://doi.org/10.1016/j.fuel.2019.116507

Li, Y., Wu, S., Liu, Q., Xie, J., Li, H., Dai, Y., Li, C., Nie, S., & Song, W. (2019). Aging effects of ultraviolet lights with same dominant wavelength and different wavelength ranges on a hydrocarbon-based polymer (asphalt). *Polymer Testing*, *75*, 64–75. https://doi.org/10.1016/j.polymertesting.2019.01.025

Lin, P., Yan, C., Huang, W., Li, Y., Zhou, L., Tang, N., Xiao, F., Zhang, Y., & Lv, Q. (2019). Rheological, chemical and aging characteristics of high content polymer modified asphalt. *Construction and Building Materials*, *207*. https://doi.org/10.1016/j.conbuildmat.2019.02.086

Lins, V. F. C., Araújo, M. F. A. S., Yoshida, M. I., Ferraz, V. P., Andrada, D. M., & Lameiras, F. S. (2008). Photodegradation of hot-mix asphalt. *Fuel*, *87*(15–16), 3254–3261. https://doi.org/10.1016/j.fuel.2008.04.039

Liu, S. (2013). Laboratory study on photo-oxidative aging of asphalt. *Asian Journal of Chemistry*, *25*(11), 6164–6166. https://doi.org/10.14233/ajchem.2013.14298

Liu, X., Wu, S., Liu, G., & Li, L. (2015). Effect of ultraviolet aging on rheology and chemistry of LDH-modified bitumen. *Materials*, *8*(8), 5238–5249. https://doi.org/10.3390/ma8085238

Lo Presti, D., Vasconcelos, K., Orešković, M., Pires, G. M., & Bressi, S. (2020). On the degree of binder activity of reclaimed asphalt and degree of blending with recycling agents. *Road Materials and Pavement Design*, *21*(8). https://doi.org/10.1080/14680629.2019.1607537

Lu, X., & Isacsson, U. (2002). Effect of ageing on bitumen chemistry and rheology. *Construction and Building Materials*, *16*(1), 15–22. https://doi.org/10.1016/S0950-0618(01)00033-2

Lu, X., Soenen, H., Sjövall, P., & Pipintakos, G. (2021). Analysis of asphaltenes and maltenes before and after long-term aging of bitumen. *Fuel*, *304*. https://doi.org/10.1016/j.fuel.2021.121426

Luo, S., Tian, J., Liu, Z., Lu, Q., Zhong, K., & Yang, X. (2020). Rapid determination of styrene-butadiene-styrene (SBS) content in modified asphalt based on Fourier transform infrared (FTIR) spectrometer and linear regression analysis. *Measurement: Journal of the International Measurement Confederation*, *151*. https://doi.org/10.1016/j.measurement.2019.107204

Ma, L., Li, Z., & Huang, J. (2011a). Investigation of Chemistry by FTIR and NMR during the Natural Exposure Aging of Asphalt. *Pavements and Materials*, 150–157. https://doi.org/10.1061/47623(402)18

Ma, L., Li, Z., & Huang, J. (2011b). Investigation of Chemistry by FTIR and NMR during the Natural Exposure Aging of Asphalt. *Pavements and Materials*, 150–157. https://doi.org/10.1061/47623(402)18

Ma, L., Varveri, A., Jing, R., & Erkens, S. (2023). Chemical characterisation of bitumen type and ageing state based on FTIR spectroscopy and discriminant analysis integrated with variable selection methods. *Road Materials and Pavement Design*, *24*(S1). https://doi.org/10.1080/14680629.2023.2181008

Ma, T., Huang, X., Zhao, Y., & Yuan, H. (2012a). Aging Behaviour and Mechanism of SBS-Modified Asphalt. *Journal of Testing and Evaluation*, *40*(7). https://doi.org/10.1520/JTE20120150

Ma, T., Huang, X., Zhao, Y., & Yuan, H. (2012b). Aging Behaviour and Mechanism of SBS-Modified Asphalt. *Journal of Testing and Evaluation*, *40*(7). https://doi.org/10.1520/JTE20120150

Ma, Y., Hu, W., Polaczyk, P. A., Han, B., Xiao, R., Zhang, M., & Huang, B. (2020). Rheological and aging characteristics of the recycled asphalt binders with different rejuvenator incorporation methods. *Journal of Cleaner Production*, *262*, 121249. https://doi.org/10.1016/J.JCLEPRO.2020.121249

Margaritis, A., Pipintakos, G., Jacobs, G., Hernando, D., Bruynen, M., Bruurs, J., & Van den bergh, W. (2021). Evaluating the role of recycling rate and rejuvenator on the chemo-rheological properties of reclaimed polymer-modified binders. *Road Materials and Pavement Design*, *22*(S1). https://doi.org/10.1080/14680629.2021.1905700

Margaritis, A., Soenen, H., Fransen, E., Pipintakos, G., Jacobs, G., Blom, J., & Van den bergh, W. (2020). Identification of ageing state clusters of reclaimed asphalt binders using principal component analysis (PCA) and hierarchical cluster analysis (HCA) based on chemo-rheological parameters. *Construction and Building Materials*, *244*. https://doi.org/10.1016/j.conbuildmat.2020.118276

Margaritis, A., Tofani, G., Jacobs, G., Blom, J., Tavernier, S., Vuye, C., & Van den Bergh, W. (2019). On the applicability of ATR-FTIR microscopy to evaluate the blending between neat bitumen and bituminous coating of reclaimed asphalt. *Coatings*, *9*(4). https://doi.org/10.3390/coatings9040240

Maschauer, D., Mirwald, J., & Hofko, B. (2022). Viennese Ageing Procedure (VAPro): adaptions and further development to address low-temperature performance of aged asphalt mixtures. *Road Materials and Pavement Design*, *23*(S1). https://doi.org/10.1080/14680629.2022.2029547

Menapace, I., Nogueira d'Eurydice, M., Galvosas, P., Hunter, M. W., Sirin, O., & Masad, E. (2017a). Aging evaluation of asphalt samples with Low Field Nuclear Magnetic Resonance. *Materials Characterization*, *128*. https://doi.org/10.1016/j.matchar.2017.01.029

Menapace, I., Nogueira d'Eurydice, M., Galvosas, P., Hunter, M. W., Sirin, O., & Masad, E. (2017b). Aging evaluation of asphalt samples with Low Field Nuclear Magnetic Resonance. *Materials Characterization*, *128*. https://doi.org/10.1016/j.matchar.2017.01.029

Michalica, P., Kazatchkov, I. B., Stastna, J., & Zanzotto, L. (2008). Relationship between chemical and rheological properties of two asphalts of different origins. *Fuel*, *87*(15–16), 3247–3253. https://doi.org/10.1016/j.fuel.2008.05.021

Michon, L., Martin, D., Planche, J. P., & Hanquet, B. (1997). Estimation of average structural parameters of bitumens by 13C nuclear magnetic resonance spectroscopy. *Fuel*, *76*(1). https://doi.org/10.1016/S0016-2361(96)00184-6

Mikhailenko, P., Bertron, A., & Ringot, E. (2016). Methods for Analyzing the Chemical Mechanisms of Bitumen Aging and Rejuvenation with FTIR Spectrometry. In *RILEM Bookseries* (Vol. 11, pp. 203–214). https://doi.org/10.1007/978-94-017-7342-3_17

Mirwald, J., Hofko, B., & Grothe, H. (2021). Utilising fluorescence spectroscopy and optical microscopy to investigate bitumen long-term ageing. *Road Materials and Pavement Design*, *22*(S1). https://doi.org/10.1080/14680629.2020.1856170

Mirwald, J., Nura, D., & Hofko, B. (2022a). Recommendations for handling bitumen prior to FTIR spectroscopy. *Materials and Structures/Materiaux et Constructions*, *55*(2). https://doi.org/10.1617/s11527-022-01884-1

Mirwald, J., Nura, D., & Hofko, B. (2022b). Recommendations for handling bitumen prior to FTIR spectroscopy. *Materials and Structures/Materiaux et Constructions*, *55*(2). https://doi.org/10.1617/s11527-022-01884-1

Mirwald, J., Werkovits, S., Camargo, I., Maschauer, D., Hofko, B., & Grothe, H. (2020a). Investigating bitumen long-term-ageing in the laboratory by spectroscopic analysis of the SARA fractions. *Construction and Building Materials*, *258*. https://doi.org/10.1016/j.conbuildmat.2020.119577

Mirwald, J., Werkovits, S., Camargo, I., Maschauer, D., Hofko, B., & Grothe, H. (2020b). Understanding bitumen ageing by investigation of its polarity fractions. *Construction and Building Materials*, *250*. https://doi.org/10.1016/j.conbuildmat.2020.118809

Mirwald, J., Werkovits, S., Camargo, I., Maschauer, D., Hofko, B., & Grothe, H. (2022). Time and Storage Dependent Effects of Bitumen—Comparison of Surface and Bulk. In *RILEM Bookseries* (Vol. 27). https://doi.org/10.1007/978-3-030-46455-4_235

Mouillet, V., Lamontagne, J., Durrieu, F., Planche, J. P., & Lapalu, L. (2008). Infrared microscopy investigation of oxidation and phase evolution in bitumen modified with polymers. *Fuel*, *87*(7). https://doi.org/10.1016/j.fuel.2007.06.029

Mousavi, M., Pahlavan, F., Oldham, D., Hosseinnezhad, S., & Fini, E. H. (2016). Multiscale Investigation of Oxidative Aging in Biomodified Asphalt Binder. *Journal of Physical Chemistry C*, *120*(31). https://doi.org/10.1021/acs.jpcc.6b05004

Nare, K., & Hlangothi, S. P. (2019). Thermorheological Evaluation of Antiaging Behavior of Four Antioxidants in 70/100 Bitumen. *Journal of Materials in Civil Engineering*, *31*(5). https://doi.org/10.1061/(asce)mt.1943-5533.0002658

National Asphalt Pavement Association. (2010). *Reclaimed Asphalt Pavement - Material Description - User Guidelines for Waste and Byproduct Materials in Pavement Construction - FHWA-RD-97-148*.

Nazari, H., Naderi, K., & Moghadas Nejad, F. (2018). Improving aging resistance and fatigue performance of asphalt binders using inorganic nanoparticles. *Construction and Building Materials*, *170*, 591–602. https://doi.org/10.1016/j.conbuildmat.2018.03.107

Oliviero Rossi, C., Caputo, P., De Luca, G., Maiuolo, L., Eskandarsefat, S., & Sangiorgi, C. (2018). 1H-NMR Spectroscopy: A Possible Approach to Advanced Bitumen Characterization for Industrial and Paving Applications. *Applied Sciences*, *8*(2), 229. https://doi.org/10.3390/app8020229

Omairey, E. L., Gu, F., & Zhang, Y. (2021). An equation-based multiphysics modelling framework for oxidative ageing of asphalt pavements. *Journal of Cleaner Production*, *280*. https://doi.org/10.1016/j.jclepro.2020.124401

Omairey, E. L., Zhang, Y., Al-Malaika, S., Sheena, H., & Gu, F. (2019). Impact of anti-ageing compounds on oxidation ageing kinetics of bitumen by infrared spectroscopy analysis. *Construction and Building Materials*, *223*, 755–764. https://doi.org/10.1016/j.conbuildmat.2019.07.021

Omar, H. A., Katman, H. Y., Bilema, M., Ahmed, M. K. A., Milad, A., & Md Yusoff, N. I. (2021). The effect of ageing on chemical and strength characteristics of nanoclay-modified bitumen and asphalt mixture. *Applied Sciences (Switzerland)*, *11*(15). https://doi.org/10.3390/app11156709

Ontario Asphalt Pavement Council. (2017). *The ABCs of RAP*.

Osmari, P. H., Leite, L. F. M., Aragão, F. T. S., Cravo, M. C. C., Dantas, L. N., & Macedo, T. F. (2019a). Cracking resistance evaluation of asphalt binders subjected to different laboratory and field aging conditions. *Road Materials and Pavement Design*, *20*(sup2), S663–S677. https://doi.org/10.1080/14680629.2019.1618530

Osmari, P. H., Leite, L. F. M., Aragão, F. T. S., Cravo, M. C. C., Dantas, L. N., & Macedo, T. F. (2019b). Cracking resistance evaluation of asphalt binders subjected to different laboratory and field aging conditions. *Road Materials and Pavement Design*, *20*(sup2), S663–S677. https://doi.org/10.1080/14680629.2019.1618530

Ouyang, C., Wang, S., Zhang, Y., & Zhang, Y. (2006a). Improving the aging resistance of asphalt by addition of Zinc dialkyldithiophosphate. *Fuel*, *85*(7–8), 1060–1066. https://doi.org/10.1016/j.fuel.2005.08.023

Ouyang, C., Wang, S., Zhang, Y., & Zhang, Y. (2006b). Improving the aging resistance of styrene-butadiene-styrene tri-block copolymer modified asphalt by addition of antioxidants. *Polymer Degradation and Stability*, *91*(4), 795–804. https://doi.org/10.1016/j.polymdegradstab.2005.06.009

Penetration, A. D. (2013). Evaluate Aging Effect of SBS Modified Bitumen. *International Journal of Civil and Environmental Engineering*, *17*(2), 261–264. https://doi.org/10.5281/ZENODO.1055601

Peng, C., Yu, J., Dai, J., & Yin, J. (2015). Effect of Zn/Al layered double hydroxide containing 2-hydroxy-4-n-octoxy-benzophenone on UV aging resistance of asphalt. *Advances in Materials Science and Engineering*, *2015*. https://doi.org/10.1155/2015/739831

Pérez-Ortega, J., Nely Almanza-Ortega, N., Vega-Villalobos, A., Pazos-Rangel, R., Zavala-Díaz, C., & Martínez-Rebollar, A. (2020). The K -Means Algorithm Evolution. In *Introduction to Data Science and Machine Learning*. https://doi.org/10.5772/intechopen.85447

Petersen, J. C. (1975). Quantitative Method Using Differential Infrared Spectrometry for the Determination of Compound Types Absorbing in the Carbonyl Region in Asphalts. *Analytical Chemistry*, *47*(1). https://doi.org/10.1021/ac60351a037

Petersen, J. C. (2009). A Review of the Fundamentals of Asphalt Oxidation (E-C140). *Transportation Research Record: Journal of the Transportation Research Board*, *E-C140*(October).

Petersen, J. C., Barbour, F. A., & Dorrence, S. M. (1975). Identification of Dicarboxylic Anhydrides in Oxidized Asphalts. *Analytical Chemistry*, *47*(1). https://doi.org/10.1021/ac60351a005

Petersen, J. C., Barbour, R. V., Dorrence, S. M., Barbour, F. A., & Helm, R. V. (1971). Molecular Interactions of Asphalt: Tentative Identification of 2-Quinolones in Asphalt and Their Interaction with Carboxylic Acids Present. *Analytical Chemistry*, *43*(11). https://doi.org/10.1021/ac60305a012

Pipintakos, G., Blom, J., Soenen, H., & Van den bergh, W. (2021). Coupling AFM and CLSM to investigate the effect of ageing on the bee structures of bitumen. *Micron*, *151*. https://doi.org/10.1016/j.micron.2021.103149

Pipintakos, G., Soenen, H., Ching, H. Y. V., Velde, C. Vande, Doorslaer, S. Van, Lemière, F., Varveri, A., & Van den bergh, W. (2021a). Exploring the oxidative mechanisms of bitumen after laboratory short- and long-term ageing. *Construction and Building Materials*, *289*, 123–182. https://doi.org/10.1016/j.conbuildmat.2021.123182

Pipintakos, G., Soenen, H., Ching, H. Y. V., Velde, C. Vande, Doorslaer, S. Van, Lemière, F., Varveri, A., & Van den bergh, W. (2021b). Exploring the oxidative mechanisms of bitumen after laboratory short-

and long-term ageing. *Construction and Building Materials*, *289*, 123–182. https://doi.org/10.1016/j.conbuildmat.2021.123182

Pipintakos, G., Sreeram, A., Mirwald, J., & Bhasin, A. (2024). Engineering bitumen for future asphalt pavements: A review of chemistry, structure and rheology. *Materials & Design*, *244*, 113157. https://doi.org/10.1016/J.MATDES.2024.113157

Pipintakos, G., Vincent Ching, H. Y., Soenen, H., Sjövall, P., Mühlich, U., Van Doorslaer, S., Varveri, A., Van den bergh, W., & Lu, X. (2020). Experimental investigation of the oxidative ageing mechanisms in bitumen. *Construction and Building Materials*, *260*. https://doi.org/10.1016/j.conbuildmat.2020.119702

Polacco, G., Muscente, A., Biondi, D., & Santini, S. (2006). Effect of composition on the properties of SEBS modified asphalts. *European Polymer Journal*, *42*(5). https://doi.org/10.1016/j.eurpolymj.2005.11.024

Polo-Mendoza, R., Martinez-Arguelles, G., Walubita, L. F., Moreno-Navarro, F., Giustozzi, F., Fuentes, L., & Navarro-Donado, T. (2022a). Ultraviolet ageing of bituminous materials: A comprehensive literature review from 2011 to 2022. In *Construction and Building Materials* (Vol. 350). https://doi.org/10.1016/j.conbuildmat.2022.128889

Polo-Mendoza, R., Martinez-Arguelles, G., Walubita, L. F., Moreno-Navarro, F., Giustozzi, F., Fuentes, L., & Navarro-Donado, T. (2022b). Ultraviolet ageing of bituminous materials: A comprehensive literature review from 2011 to 2022. In *Construction and Building Materials* (Vol. 350). https://doi.org/10.1016/j.conbuildmat.2022.128889

Porto, M., Angelico, R., Caputo, P., Abe, A. A., Teltayev, B., & Rossi, C. O. (2022). The Structure of Bitumen: Conceptual Models and Experimental Evidences. In *Materials* (Vol. 15, Issue 3). https://doi.org/10.3390/ma15030905

Preciado, J., Gulzar, S., Fried, A., Castorena, C., Underwood, S., Habbouche, J., & Boz, I. (2024). Low-Temperature Performance Evaluation of Recycled Binder Blends for Assessing Recycling Agents' Acceptance. *JOURNAL OF MATERIALS IN CIVIL ENGINEERING*, *36*(9). https://doi.org/10.1061/JMCEE7.MTENG-17661

Primerano, K., Mirwald, J., Lohninger, J., & Hofko, B. (2023). Characterization of long-term aged bitumen with FTIR spectroscopy and multivariate analysis methods. *Construction and Building Materials*, *409*. https://doi.org/10.1016/j.conbuildmat.2023.133956

Prosperi, E., & Bocci, E. (2021). A review on bitumen aging and rejuvenation chemistry: Processes, materials and analyses. In *Sustainability (Switzerland)* (Vol. 13, Issue 12). https://doi.org/10.3390/su13126523

Qian, C., & Fan, W. (2020). Evaluation and characterization of properties of crumb rubber/SBS modified asphalt. *Materials Chemistry and Physics*, *253*. https://doi.org/10.1016/j.matchemphys.2020.123319

Qiu, Y., Yuan, H., Ding, H., Li, R., & Zhou, Z. (2022). Quantification of Recycled Engine Oil Bottoms in Asphalt Binder Using Nuclear Magnetic Resonance Techniques. *Journal of Materials in Civil Engineering*, *34*(12). https://doi.org/10.1061/(ASCE)MT.1943-5533.0004496

Rajib, A. I., Samieadel, A., Zalghout, A., Kaloush, K. E., Sharma, B. K., & Fini, E. H. (2020). Do all rejuvenators improve asphalt performance? *Road Materials and Pavement Design*. https://doi.org/10.1080/14680629.2020.1826348

Rathore, M., & Zaumanis, M. (2020). Impact of laboratory mixing procedure on the properties of reclaimed asphalt pavement mixtures. *Construction and Building Materials*, *264*, 120709. https://doi.org/10.1016/j.conbuildmat.2020.120709

Redelius, P., & Soenen, H. (2015). Relation between bitumen chemistry and performance. *Fuel*, *140*. https://doi.org/10.1016/j.fuel.2014.09.044

Remisova, E., & Briliak, D. (2023a). Evaluation of the Effect of Thermo-Oxidative Aging and UV Radiation on Asphalt Stiffness. *Materials*, *16*(10). https://doi.org/10.3390/ma16103716

Remisova, E., & Briliak, D. (2023b). Evaluation of the Effect of Thermo-Oxidative Aging and UV Radiation on Asphalt Stiffness. *Materials*, *16*(10). https://doi.org/10.3390/ma16103716

Ren, S., Liu, X., Lin, P., Jing, R., & Erkens, S. (2022a). Toward the long-term aging influence and novel reaction kinetics models of bitumen. *International Journal of Pavement Engineering*, *24*(2). https://doi.org/10.1080/10298436.2021.2024188

Ren, S., Liu, X., Lin, P., Jing, R., & Erkens, S. (2022b). Toward the long-term aging influence and novel reaction kinetics models of bitumen. *International Journal of Pavement Engineering*, *24*(2). https://doi.org/10.1080/10298436.2021.2024188

Rossi, C. O., Caputo, P., Ashimova, S., Fabozzi, A., D'Errico, G., & Angelico, R. (2018a). Effects of natural antioxidant agents on the bitumen aging process: An EPR and rheological investigation. *Applied Sciences (Switzerland)*, *8*(8). https://doi.org/10.3390/app8081405

Rossi, C. O., Caputo, P., Ashimova, S., Fabozzi, A., D'Errico, G., & Angelico, R. (2018b). Effects of natural antioxidant agents on the bitumen aging process: An EPR and rheological investigation. *Applied Sciences (Switzerland)*, *8*(8). https://doi.org/10.3390/app8081405

Rossi, C. O., Caputo, P., Loise, V., Ashimova, S., Teltayev, B., & Sangiorgi, C. (2019). A new green rejuvenator: Evaluation of structural changes of aged and recycled bitumens by means of rheology and NMR. In *RILEM Bookseries* (Vol. 20). https://doi.org/10.1007/978-3-030-00476-7_28

Ruby-Figueroa, R. (2015). Partial Least Square Regression (PLSR). In *Encyclopedia of Membranes*. https://doi.org/10.1007/978-3-642-40872-4_2000-1

Sakib, N., & Bhasin, A. (2019). Measuring polarity-based distributions (SARA) of bitumen using simplified chromatographic techniques. *International Journal of Pavement Engineering*, *20*(12). https://doi.org/10.1080/10298436.2018.1428972

Salkind, N. (2013). K-Means Cluster Analysis. In *Encyclopedia of Measurement and Statistics*. https://doi.org/10.4135/9781412952644.n237

Schwettmann, K., Höhne, P., & Stephan, D. (2022). Comparison of column chromatography and solid-phase extraction on virgin and aged bituminous maltene phases. *Materials and Structures/Materiaux et Constructions*, *55*(10). https://doi.org/10.1617/s11527-022-02079-4

Shan, L., Xie, R., Wagner, N. J., He, H., & Liu, Y. (2019). Microstructure of neat and SBS modified asphalt binder by small-angle neutron scattering. *Fuel*, *253*, 1589–1596. https://doi.org/10.1016/j.fuel.2019.05.087

Shen, J., Amirkhanian, S. N., & Lee, S.-J. (2007). HP-GPC Characterization of Rejuvenated Aged CRM Binders. *Journal of Materials in Civil Engineering*, *19*(6). https://doi.org/10.1061/(asce)0899-1561(2007)19:6(515)

Shi, H. (2014). Improvement of Polymers by UV Irradiation: The Research in Ageing and Solidification - Take Polysiloxane-Modified-Polyacrylates and Asphalt as AnExample. *Applied Mechanics and Materials*, *541–542*, 90–94. https://doi.org/10.4028/www.scientific.net/AMM.541-542.90

Siddiqui, M. N. (2010). NMR fingerprinting of chemical changes in asphalt fractions on oxidation. *Petroleum Science and Technology*, *28*(4). https://doi.org/10.1080/10916460903070751

Singh, S. K., Kumar, Y., & Ravindranath, S. S. (2018). Thermal degradation of SBS in bitumen during storage: Influence of temperature, SBS concentration, polymer type and base bitumen. *Polymer Degradation and Stability*, *147*. https://doi.org/10.1016/j.polymdegradstab.2017.11.008

Sirin, O., Paul, D. K., & Kassem, E. (2018). State of the Art Study on Aging of Asphalt Mixtures and Use of Antioxidant Additives. In *Advances in Civil Engineering* (Vol. 2018). https://doi.org/10.1155/2018/3428961

Słowik, M. (2017). Thermorheological Properties of Styrene-Butadiene-Styrene (SBS) Copolymer Modified Road Bitumen. *Procedia Engineering*, *208*, 145–150. https://doi.org/10.1016/j.proeng.2017.11.032

Soenen, H., De Visscher, J., Vanelstraete, A., & Redelius, P. (2006). Influence of thermal history on rheological properties of various bitumen. *Rheologica Acta*, *45*(5). https://doi.org/10.1007/s00397-005-0032-8

Soenen, H., Lu, X., & Laukkanen, O. V. (2016). Oxidation of bitumen: molecular characterization and influence on rheological properties. *Rheologica Acta*, *55*(4). https://doi.org/10.1007/s00397-016-0919-6

Standard Specifications for Transportation Materials and Methods of Sampling and Testing (2022 Edition), and AASHTO Provisional Standards, 42nd Edition - T 315-22 - Determining the Rheological Properties of Asphalt Binder Using a Dynamic Shear Rheometer (DSR) - Knovel. (n.d.). Retrieved October 8, 2024, from https://app.knovel.com/web/view/pdf/show.v/rcid:kpSSTMMS81/cid:kt0136BCT9/viewerType:pdf//root_slug:t-315-22---determining-the-rheological-properties-of-asphalt-binder-using-a-dynamic-shear-rheometer-dsr/url_slug:t-315-22-determining?cid=kt0136BCT9&b-q=Specifications%20AASHTO&b-toc-cid=kpSSTMMS81&b-toc-title=Standard%20Specifications%20for%20Transportation%20Materials%20and%20Methods%20of%20Sampling%20and%20Testing%20%282022%20Edition%29%2C%20and%20AASHTO%20Provisional%20Standards%2C%2042nd%20Edition&b-toc-url-slug=t-315-22-determining&include_synonyms=no

Steiner, D., Hofko, B., Hospodka, M., Handle, F., Grothe, H., Füssl, J., Eberhardsteiner, L., & Blab, R. (2016). Towards an optimised lab procedure for long-term oxidative ageing of asphalt mix specimen. *International Journal of Pavement Engineering*, *17*(6), 471–477. https://doi.org/10.1080/10298436.2014.993204

Stewart, J. E. (1957). Infrared spectra of chromatographically fractionated asphalts. *Journal of Research of the National Bureau of Standards*, *58*(5). https://doi.org/10.6028/jres.058.033

Such, C., Brule, B., & Baluja-Santos, C. (1979). Characterization of a road asphalt by chromatographic techniques (GPC and HPLC). *Journal of Liquid Chromatography*, *2*(3). https://doi.org/10.1080/01483917908060074

Sun, D., Zhang, L., & Zhang, X. (2011). Quantification of SBS content in SBS polymer modified asphalt by FTIR. *Advanced Materials Research*, *287–290*. https://doi.org/10.4028/www.scientific.net/AMR.287-290.953

Sun, X., Qin, X., Liu, Z., Yin, Y., Zou, C., & Jiang, S. (2020). New preparation method of bitumen samples for UV aging behavior investigation. *Construction and Building Materials*, *233*. https://doi.org/10.1016/j.conbuildmat.2019.117278

Sun, X., Yuan, J., Liu, Z., Qin, X., & Yin, Y. (2021). Evaluation and characterization on the segregation and dispersion of anti-UV aging modifying agent in asphalt binder. *Construction and Building Materials*, *289*. https://doi.org/10.1016/j.conbuildmat.2021.123204

Syms, C. (2019). Principal Components Analysis. In *Encyclopedia of Ecology: Volume 1-4, Second Edition* (Vol. 3, pp. 566–573). https://doi.org/10.1016/B978-0-12-409548-9.11152-2

Szerb, E. I., Nicotera, I., Teltayev, B., Vaiana, R., & Rossi, C. O. (2018). Highly stable surfactant-crumb rubber-modified bitumen: NMR and rheological investigation. *Road Materials and Pavement Design*, *19*(5). https://doi.org/10.1080/14680629.2017.1289975

Takahashi, M. M., Vasconcelos, K. L., Cravo, M. C. C., & Bernucci, L. L. B. (2019a). Field Aging Evaluation of Asphalt Binders by Chemical and Rheological Characterization. In *RILEM Bookseries* (Vol. 20, pp. 84–89). https://doi.org/10.1007/978-3-030-00476-7_14

Takahashi, M. M., Vasconcelos, K. L., Cravo, M. C. C., & Bernucci, L. L. B. (2019b). Field Aging Evaluation of Asphalt Binders by Chemical and Rheological Characterization. In *RILEM Bookseries* (Vol. 20, pp. 84–89). https://doi.org/10.1007/978-3-030-00476-7_14

Tammer, M. (2004). G. Sokrates: Infrared and Raman characteristic group frequencies: tables and charts. *Colloid and Polymer Science*, *283*(2). https://doi.org/10.1007/s00396-004-1164-6

Tan, Y., Wang, J., Xue, Z., Feng, Z., & Xu, H. (2008a). Laboratory study on ultraviolet aging behavior of asphalt binder and mixture. *Proceedings of the 7th International Conference of Chinese Transportation Professionals Congress 2007: Plan, Build, and Manage Transportation Infrastructures in China*, 752–759. https://doi.org/10.1061/40952(317)73

Tan, Y., Wang, J., Xue, Z., Feng, Z., & Xu, H. (2008b). Laboratory study on ultraviolet aging behavior of asphalt binder and mixture. *Proceedings of the 7th International Conference of Chinese Transportation Professionals Congress 2007: Plan, Build, and Manage Transportation Infrastructures in China*, 752–759. https://doi.org/10.1061/40952(317)73

Tanzadeh, R., & Shafabakhsh, G. (2020). Surface free energy and adhesion energy evaluation of modified bitumen with recycled carbon black (micro-nano) from gases and petrochemical waste. *Construction and Building Materials*, *245*. https://doi.org/10.1016/j.conbuildmat.2020.118361

Tauste, R., Moreno-Navarro, F., Sol-Sánchez, M., & Rubio-Gámez, M. C. (2018a). Understanding the bitumen ageing phenomenon: A review. *Construction and Building Materials*, *192*, 593–609. https://doi.org/10.1016/j.conbuildmat.2018.10.169

Tauste, R., Moreno-Navarro, F., Sol-Sánchez, M., & Rubio-Gámez, M. C. (2018b). Understanding the bitumen ageing phenomenon: A review. *Construction and Building Materials*, *192*, 593–609. https://doi.org/10.1016/j.conbuildmat.2018.10.169

Traxler, R. N. (1961). Relation between asphalt composition and hardening by volatilization and oxidation. *Proceedings, American Association of Asphalt Paving Technologists*, *30*(1), 359–377.

Vidal, R., Ma, Y., & Sastry, S. S. (2016). Principal component analysis. In *Interdisciplinary Applied Mathematics* (Vol. 40, pp. 25–62). https://doi.org/10.1007/978-0-387-87811-9_2

Vijayan, V., Mantalovas, K., Acuto, F., & Di Mino, G. (2023a). Evaluating the Ageing Sensitivity of the Asphalt Binder via Distinct Ageing Methods. *Infrastructures*, *8*(11). https://doi.org/10.3390/infrastructures8110163

Vijayan, V., Mantalovas, K., Acuto, F., & Di Mino, G. (2023b). Evaluating the Ageing Sensitivity of the Asphalt Binder via Distinct Ageing Methods. *Infrastructures*, *8*(11). https://doi.org/10.3390/infrastructures8110163

Villegas-Villegas, R. E., Baldi-Sevilla, A., Aguiar-Moya, J. P., & Loria-Salazar, L. (2018). Analysis of asphalt oxidation by means of accelerated testing and environmental conditions. *Transportation Research Record*, *2672*(28), 244–255. https://doi.org/10.1177/0361198118777630

Wang, F., Zhang, L., Zhang, X., Li, H., & Wu, S. (2020a). Aging Mechanism and Rejuvenating Possibility of SBS Copolymers in Asphalt Binders. *Polymers*, *12*(1), 92. https://doi.org/10.3390/polym12010092

Wang, F., Zhang, L., Zhang, X., Li, H., & Wu, S. (2020b). Aging Mechanism and Rejuvenating Possibility of SBS Copolymers in Asphalt Binders. *Polymers*, *12*(1), 92. https://doi.org/10.3390/polym12010092

Wang, J., Wu, S., Han, J., & Liu, X. (2012). Study on preparation and UV ageing resistance effect of LDHs modified asphalt. *Key Engineering Materials*, *509*, 194–202. https://doi.org/10.4028/www.scientific.net/KEM.509.194

Wang, K., Yuan, Y., Han, S., & Yang, Y. (2019). Application of FTIR spectroscopy with solvent-cast film and PLS regression for the quantification of SBS content in modified asphalt. *International Journal of Pavement Engineering*, *20*(11), 1336–1341. https://doi.org/10.1080/10298436.2017.1413242

Wang, Z., Li, J., Zhang, Z., Jia, M., & Yang, J. (2020). Formulation of a new warm-mix recycling agent and its rejuvenating effect on aged asphalt. *Construction and Building Materials*, *262*, 120804. https://doi.org/10.1016/j.conbuildmat.2020.120804

Weigel, S., Gehrke, M., Recknagel, C., & Stephan, D. A. (2021). Identification and quantification of additives in bituminous binders based on FTIR spectroscopy and multivariate analysis methods. *Materials and Structures/Materiaux et Constructions*, *54*(4). https://doi.org/10.1617/s11527-021-01763-1

Weigel, S., & Stephan, D. (2017). The prediction of bitumen properties based on FTIR and multivariate analysis methods. *Fuel*, *208*. https://doi.org/10.1016/j.fuel.2017.07.048

Weigel, S., & Stephan, D. (2018a). Differentiation of bitumen according to the refinery and ageing state based on FTIR spectroscopy and multivariate analysis methods. *Materials and Structures/Materiaux et Constructions*, *51*(5). https://doi.org/10.1617/s11527-018-1252-6

Weigel, S., & Stephan, D. (2018b). Relationships between the chemistry and the physical properties of bitumen. *Road Materials and Pavement Design*, *19*(7). https://doi.org/10.1080/14680629.2017.1338189

Werkovits, S., Bacher, M., Mirwald, J., Theiner, J., Rosenau, T., Hofko, B., & Grothe, H. (2023). The impact of field ageing on molecular structure and chemistry of bitumen. *Fuel*, *343*, 127–139. https://doi.org/10.1016/j.fuel.2023.127904

Werkovits, S., Bacher, M., Theiner, J., Rosenau, T., & Grothe, H. (2022). Multi-spectroscopic characterization of bitumen and its polarity-based fractions. *Construction and Building Materials*, *352*. https://doi.org/10.1016/j.conbuildmat.2022.128992

Werkovits, S., Primerano, K., Schöberl, T. R., Hofko, B., & Grothe, H. (2024). How infrared and fluorescence spectroscopy can shed new light on the characterization of bitumen and its ageing processes. *Road Materials and Pavement Design*, *25*(sup1). https://doi.org/10.1080/14680629.2023.2191730

Wheelwright, M., Levine, Z., Garfinkel-Castro, A., Bushman, T., & Brewer, S. C. (2020). PRINCIPAL COMPONENT AND FACTOR ANALYSIS. In *Advanced Quantitative Research Methods for Urban Planners* (pp. 95–120). https://doi.org/10.4324/9780429325038-5

Woods, J. R., Kung, J., Kingston, D., Kotlyar, L., Sparks, B., & McCracken, T. (2008). Canadian crudes: A comparative study of SARA fractions from a modified HPLC separation technique. *Oil and Gas Science and Technology*, *63*(1 SPEC. ISS.). https://doi.org/10.2516/ogst:2007080

Wu, J. (2012). *Cluster Analysis and K-means Clustering: An Introduction* (pp. 1–16). https://doi.org/10.1007/978-3-642-29807-3_1

Wu, S., Han, J., Pang, L., Yu, M., & Wang, T. (2012). Rheological properties for aged bitumen containing ultraviolate light resistant materials. *Construction and Building Materials*, *33*, 133–138. https://doi.org/10.1016/j.conbuildmat.2012.01.019

Wu, S. peng, Pang, L., Mo, L. tong, Chen, Y. chun, & Zhu, G. jun. (2009). Influence of aging on the evolution of structure, morphology and rheology of base and SBS modified bitumen. *Construction and Building Materials*, *23*(2), 1005–1010. https://doi.org/10.1016/j.conbuildmat.2008.05.004

Wu, S., Zhao, Z., Li, Y., Pang, L., Amirkhanian, S., & Riara, M. (2017). Evaluation of aging resistance of Graphene oxide modified asphalt. *Applied Sciences (Switzerland)*, *7*(7). https://doi.org/10.3390/app7070702

Wu, W., Wang, C., Zhao, P., Xiu, L., Fan, L., Bi, F., Song, X., & Zhou, X. (2022). The Fingerprint Identification of Asphalt Aging Based on 1H-NMR and Chemometrics Analysis. *Materials*, *15*(19), 6825. https://doi.org/10.3390/ma15196825

Xu, G., & Wang, H. (2017). Molecular dynamics study of oxidative aging effect on asphalt binder properties. *Fuel*, *188*, 1–10. https://doi.org/10.1016/j.fuel.2016.10.021

Xu, G., Wang, H., & Sun, W. (2018). Molecular dynamics study of rejuvenator effect on RAP binder: Diffusion behavior and molecular structure. *Construction and Building Materials*, *158*, 1046–1054. https://doi.org/10.1016/j.conbuildmat.2017.09.192

Xu, G., Wang, H., & Zhu, H. (2017). Rheological properties and anti-aging performance of asphalt binder modified with wood lignin. *Construction and Building Materials*, *151*, 801–808. https://doi.org/10.1016/j.conbuildmat.2017.06.151

Xu, S., Yu, J., Zhang, C., & Sun, Y. (2015). Effect of ultraviolet aging on rheological properties of organic intercalated layered double hydroxides modified asphalt. *Construction and Building Materials*, *75*, 421–428. https://doi.org/10.1016/j.conbuildmat.2014.11.046

Yamaguchi, K., Sasaki, I., Nishizaki, I., Meiarashi, S., & Moriyoshi, A. (2005). Effects of film thickness, wavelength, and carbon black on photodegradation of asphalt. *Journal of the Japan Petroleum Institute*, *48*(3), 150–155. https://doi.org/10.1627/jpi.48.150

Yan, C., Huang, W., Xiao, F., Wang, L., & Li, Y. (2018). Proposing a new infrared index quantifying the aging extent of SBS-modified asphalt. *Road Materials and Pavement Design*, *19*(6). https://doi.org/10.1080/14680629.2017.1318082

Yan, C., Huang, W., Xu, J., Yang, H., Zhang, Y., & Bahia, H. U. (2022a). Quantification of re-refined engine oil bottoms (REOB) in asphalt binder using ATR-FTIR spectroscopy associated with partial least squares (PLS) regression. *Road Materials and Pavement Design*, *23*(4), 958–972. https://doi.org/10.1080/14680629.2020.1861969

Yan, C., Huang, W., Xu, J., Yang, H., Zhang, Y., & Bahia, H. U. (2022b). Quantification of re-refined engine oil bottoms (REOB) in asphalt binder using ATR-FTIR spectroscopy associated with partial least squares (PLS) regression. *Road Materials and Pavement Design*, *23*(4), 958–972. https://doi.org/10.1080/14680629.2020.1861969

Yang, T., Jia, Y. S., Pan, Y. Y., & Zhao, Y. L. (2022). Evaluation of the Low-Temperature Cracking Performance of Recycled Asphalt Mixture: A Development of Equivalent Fracture Temperature. *BUILDINGS*, *12*(9). https://doi.org/10.3390/buildings12091366

Yao, H., You, Z., Li, L., Lee, C. H., Wingard, D., Yap, Y. K., Shi, X., & Goh, S. W. (2013). Rheological Properties and Chemical Bonding of Asphalt Modified with Nanosilica. *Journal of Materials in Civil Engineering*, *25*(11), 1619–1630. https://doi.org/10.1061/(asce)mt.1943-5533.0000690

Yilmaz, M., & Çeloğlu, M. E. (2013). Effects of SBS and different natural asphalts on the properties of bituminous binders and mixtures. *Construction and Building Materials*, *44*, 533–540. https://doi.org/10.1016/j.conbuildmat.2013.03.036

Yin, J., Wang, S., & Lv, F. (2013). Improving the short-term aging resistance of asphalt by addition of crumb rubber radiated by microwave and impregnated in epoxidized soybean oil. *Construction and Building Materials*, *49*, 712–719. https://doi.org/10.1016/j.conbuildmat.2013.08.067

Yousif, E., & Haddad, R. (2013). Photodegradation and photostabilization of polymers, especially polystyrene: Review. In *SpringerPlus* (Vol. 2, Issue 1). https://doi.org/10.1186/2193-1801-2-398

Yu, H., Bai, X., Qian, G., Wei, H., Gong, X., Jin, J., & Li, Z. (2019). Impact of ultraviolet radiation on the aging properties of SBS-modified asphalt binders. *Polymers*, *11*(7). https://doi.org/10.3390/polym11071111

Yu, J. Y., Feng, P. C., Zhang, H. L., & Wu, S. P. (2009). Effect of organo-montmorillonite on aging properties of asphalt. *Construction and Building Materials*, *23*(7), 2636–2640. https://doi.org/10.1016/j.conbuildmat.2009.01.007

Yu, M., Wu, S., & Chen, M. (2012). Experimental investigation of the volatilization of asphalts under different conditions. *Advanced Materials Research*, *463–464*, 69–75. https://doi.org/10.4028/www.scientific.net/AMR.463-464.69

Yu, S., Shen, S., Zhang, C., Zhang, W., & Jia, X. (2017). Evaluation of the Blending Effectiveness of Reclaimed Asphalt Pavement Binder. *Journal of Materials in Civil Engineering*, *29*(12). https://doi.org/10.1061/(asce)mt.1943-5533.0002095

Yu, X., Zaumanis, M., dos Santos, S., & Poulikakos, L. D. (2014). Rheological, microscopic, and chemical characterization of the rejuvenating effect on asphalt binders. *Fuel*, *135*, 162–171. https://doi.org/10.1016/j.fuel.2014.06.038

Yuan, J., Lu, H., Yin, W., & Wu, Y. (2019). Influences of Naphthenic Oil on SBS-Modified Asphalt Binder. *Journal of Materials in Civil Engineering*, *31*(8). https://doi.org/10.1061/(asce)mt.1943-5533.0002803

Yut, I., & Zofka, A. (2014). Correlation between rheology and chemical composition of aged polymer-modified asphalts. *Construction and Building Materials*, *62*, 109–117. https://doi.org/10.1016/j.conbuildmat.2014.03.043

Zaidullin, I. M., Petrova, L. M., Yakubov, M. R., & Borisov, D. N. (2013). Variation of the composition of asphaltenes in the course of bitumen aging in the presence of antioxidants. *Russian Journal of Applied Chemistry*, *86*(7), 1070–1075. https://doi.org/10.1134/S1070427213070203

Zakirova, L. Y., Vol'Fson, S. I., & Khakimullin, Y. N. (2007). Determination of the surface free energy of thermoelastoplastic-modified bitumen. *Polymer Science - Series C*, *49*(2), 149–151. https://doi.org/10.1134/S1811238207020105

Zaumanis, M., & Mallick, R. B. (2013). Finite Element Modeling of Rejuvenator Diffusion in RAP Binder Film – Simulation of Plant Mixing Process. In *Multi-Scale Modeling and Characterization of Infrastructure Materials* (pp. 407–419). https://doi.org/10.1007/978-94-007-6878-9_30

Zaumanis, M., Mallick, R. B., & Frank, R. (2014). Determining optimum rejuvenator dose for asphalt recycling based on Superpave performance grade specifications. *Construction and Building Materials*, *69*. https://doi.org/10.1016/j.conbuildmat.2014.07.035

Zeng, W., Wu, S., Wen, J., & Chen, Z. (2015a). The temperature effects in aging index of asphalt during UV aging process. *Construction and Building Materials*, *93*, 1125–1131. https://doi.org/10.1016/j.conbuildmat.2015.05.022

Zeng, W., Wu, S., Wen, J., & Chen, Z. (2015b). The temperature effects in aging index of asphalt during UV aging process. *Construction and Building Materials*, *93*, 1125–1131. https://doi.org/10.1016/j.conbuildmat.2015.05.022

Zhang, C., Yu, J., Xu, S., Xue, L., & Cao, Z. (2016). Influence of UV aging on the rheological properties of bitumen modified with surface organic layered double hydroxides. *Construction and Building Materials*, *123*, 574–580. https://doi.org/10.1016/j.conbuildmat.2016.07.048

Zhang, H., Xia, W., Hu, Z., & Xu, T. (2021). Inhibitory effects of developed composite anti-aging agent on microbial degradation of asphalt. *Construction and Building Materials*, *292*. https://doi.org/10.1016/j.conbuildmat.2021.123399

Zhang, H., Yu, J., Wang, H., & Xue, L. (2011). Investigation of microstructures and ultraviolet aging properties of organo-montmorillonite/SBS modified bitumen. *Materials Chemistry and Physics*, *129*(3), 769–776. https://doi.org/10.1016/j.matchemphys.2011.04.078

Zhang, P., Guo, Q., Tao, J., Ma, D., & Wang, Y. (2019). Aging mechanism of a diatomite-modified asphalt binder using Fourier-transform infrared (FTIR) spectroscopy analysis. *Materials*, *12*(6). https://doi.org/10.3390/ma12060988

Zhang, S., Hong, H., Zhang, H., & Chen, Z. (2021). Investigation of anti-aging mechanism of multi-dimensional nanomaterials modified asphalt by FTIR, NMR and GPC. *Construction and Building Materials*, *305*. https://doi.org/10.1016/j.conbuildmat.2021.124809

Zhang, X., Zhang, K., Wu, C., Liu, K., & Jiang, K. (2020). Preparation of bio-oil and its application in asphalt modification and rejuvenation: A review of the properties, practical application and life cycle assessment. *Construction and Building Materials*, *262*, 120528. https://doi.org/10.1016/j.conbuildmat.2020.120528

Zhao, K., & Wang, Y. (2020). Improvements on the use of GPC to measure large-size microstructures in aged asphalt binders. *International Journal of Pavement Engineering*. https://doi.org/10.1080/10298436.2020.1852561

Zhao, X., Wang, S., Wang, Q., & Yao, H. (2016). Rheological and structural evolution of SBS modified asphalts under natural weathering. *Fuel*, *184*. https://doi.org/10.1016/j.fuel.2016.07.018

Zhao, Z. J., Xu, S., Wu, W. F., Yu, J. Y., & Wu, S. P. (2015). The aging resistance of asphalt containing a compound of LDHs and antioxidant. *Petroleum Science and Technology*, *33*(7), 787–793. https://doi.org/10.1080/10916466.2015.1014965

Zhou, T., Cao, L., Fini, E. H., Li, L., Liu, Z., & Dong, Z. (2020). Behaviors of asphalt under certain aging levels and effects of rejuvenation. *Construction and Building Materials*, *249*. https://doi.org/10.1016/j.conbuildmat.2020.118748

Zhou, X., Zhao, G., Wu, S., Tighe, S., Pickel, D., Chen, M., Adhikari, S., & Gao, Y. (2020). Effects of biochar on the chemical changes and phase separation of bio-asphalt under different aging conditions. *Journal of Cleaner Production*, *263*. https://doi.org/10.1016/j.jclepro.2020.121532

Ziari, H., Moniri, A., Bahri, P., & Saghafi, Y. (2019). The effect of rejuvenators on the aging resistance of recycled asphalt mixtures. *Construction and Building Materials*, *224*. https://doi.org/10.1016/j.conbuildmat.2019.06.181

Appendix A

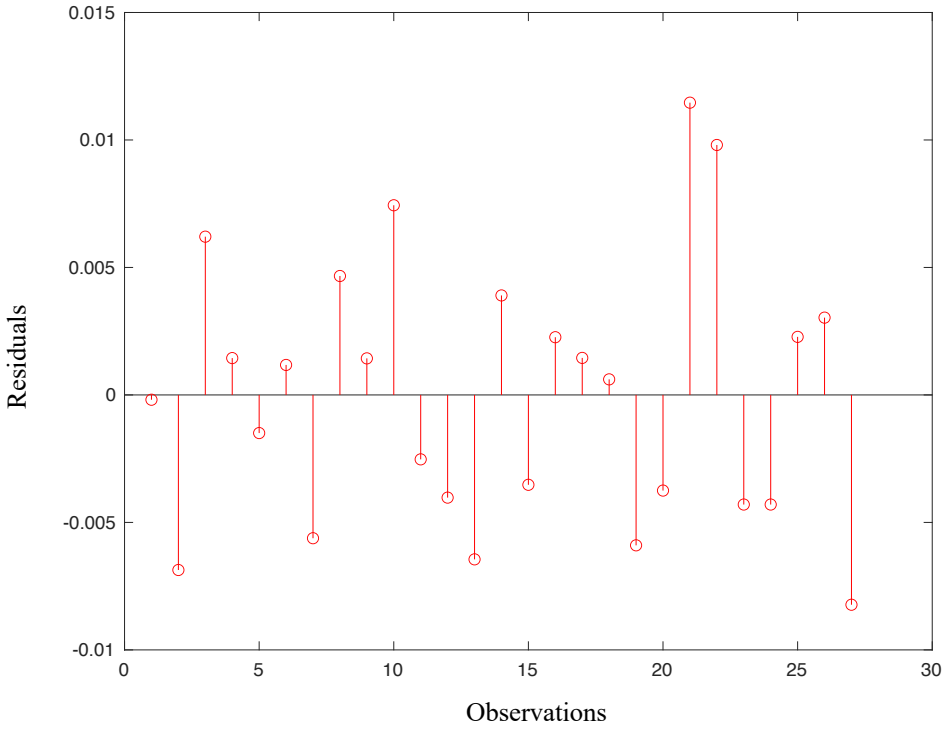


Figure A-1: Residual Plot for aging state obtained from PLSR on NMR data for Binder A only.

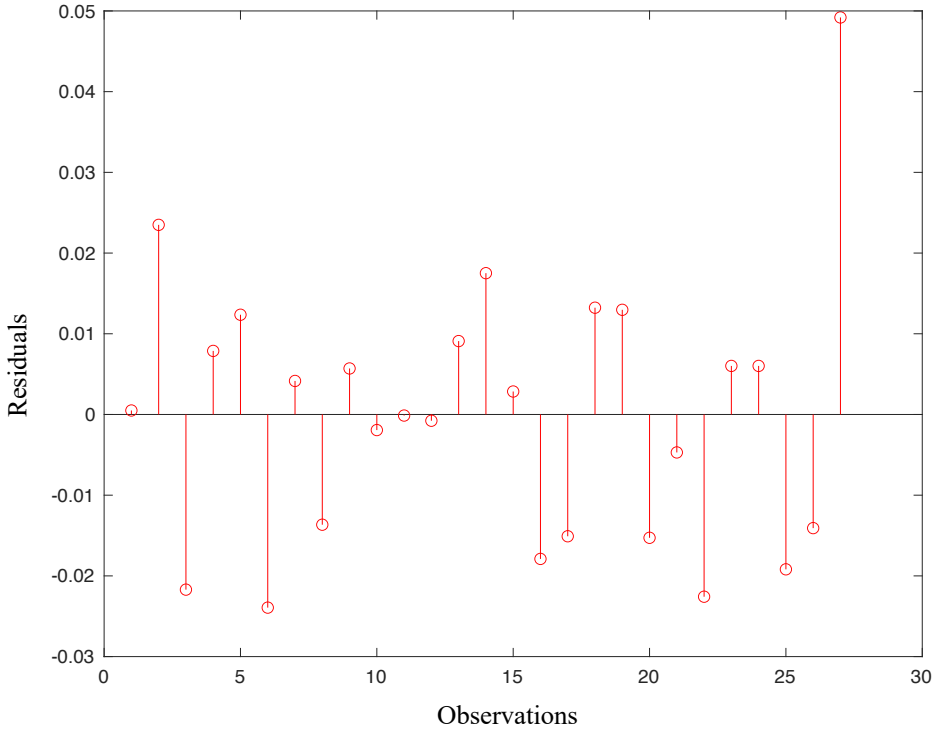


Figure A-2: Residual Plot for SBS Concentration obtained from PLSR on NMR data for Binder A only.

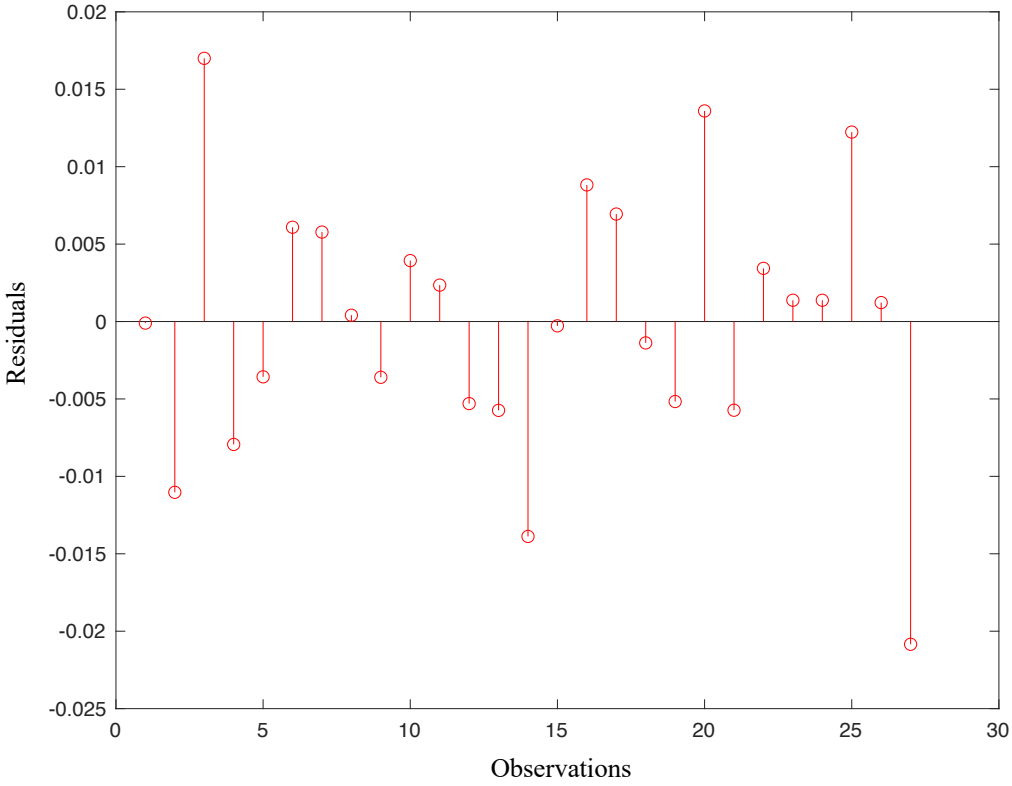


Figure A-3: Residual Plot for ΔTc obtained from PLSR on NMR data for Binder A only.

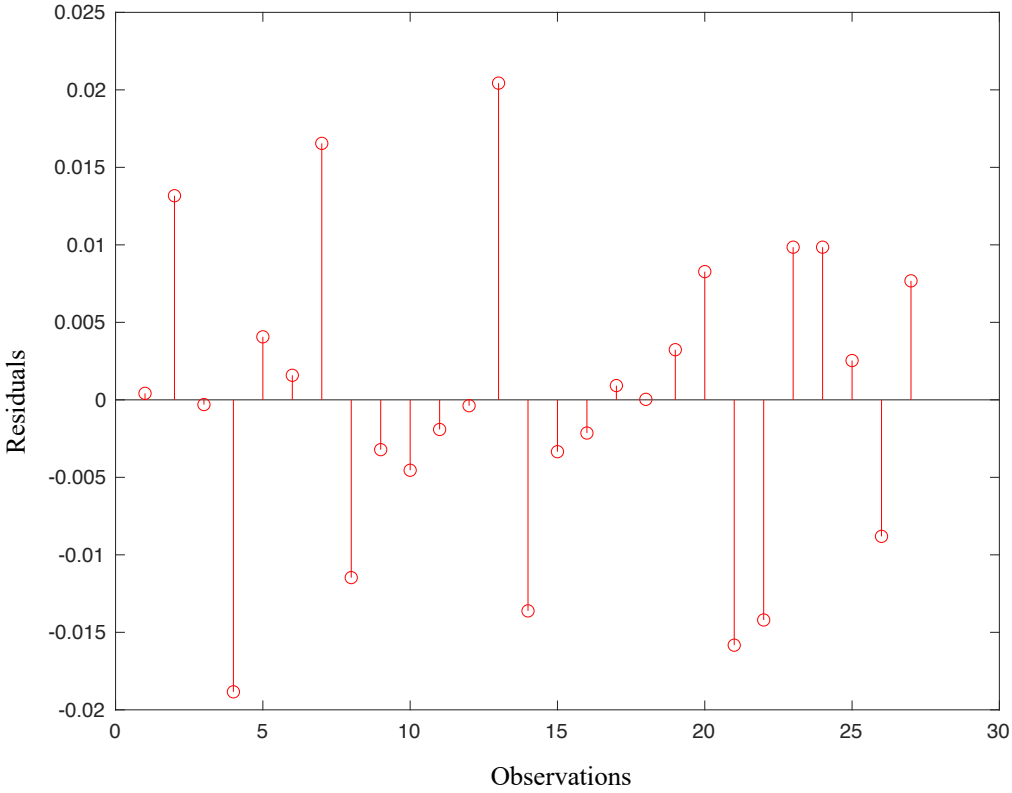


Figure A-4: Residual Plot for Crossover Temperature obtained from PLSR on NMR data for Binder A only.

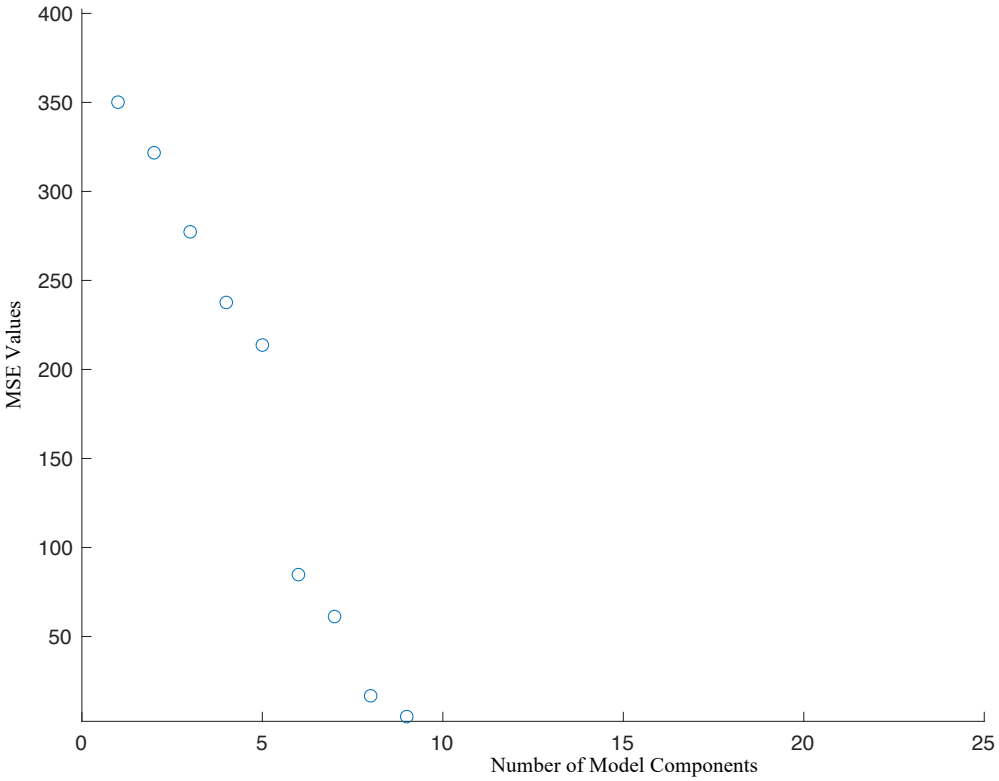


Figure A-5: MSE vs Number of Components in PLSR model using NMR data for Binder A.

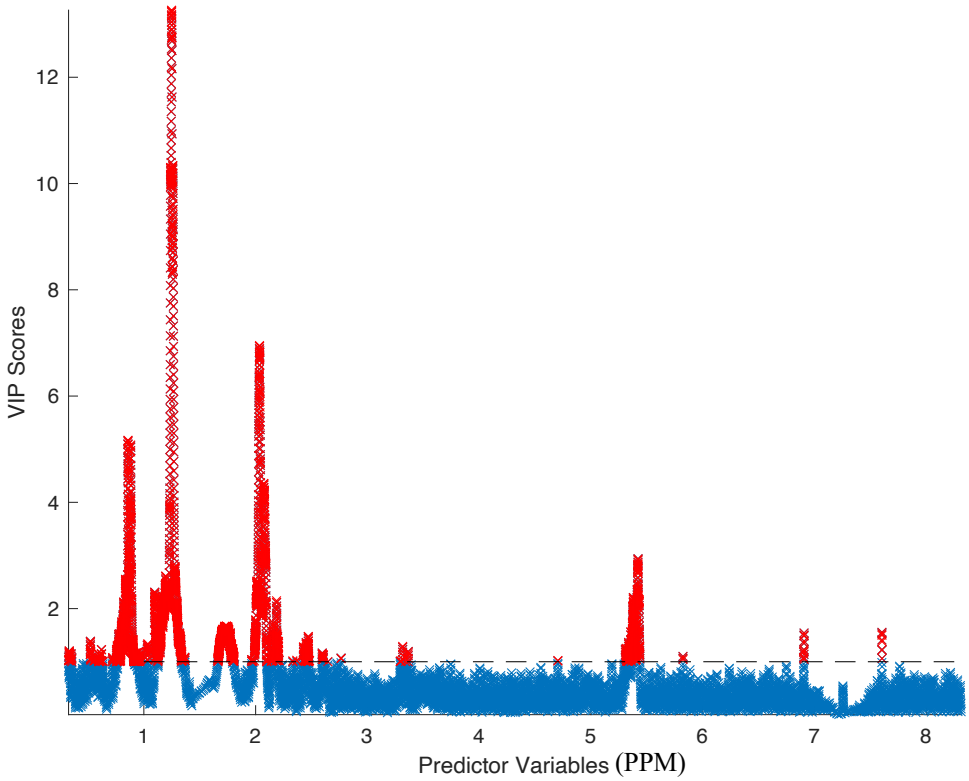


Figure A-6: VIP Score Plot obtained from PLSR on NMR data for Binder A only. (Red points represent VIP > 1).

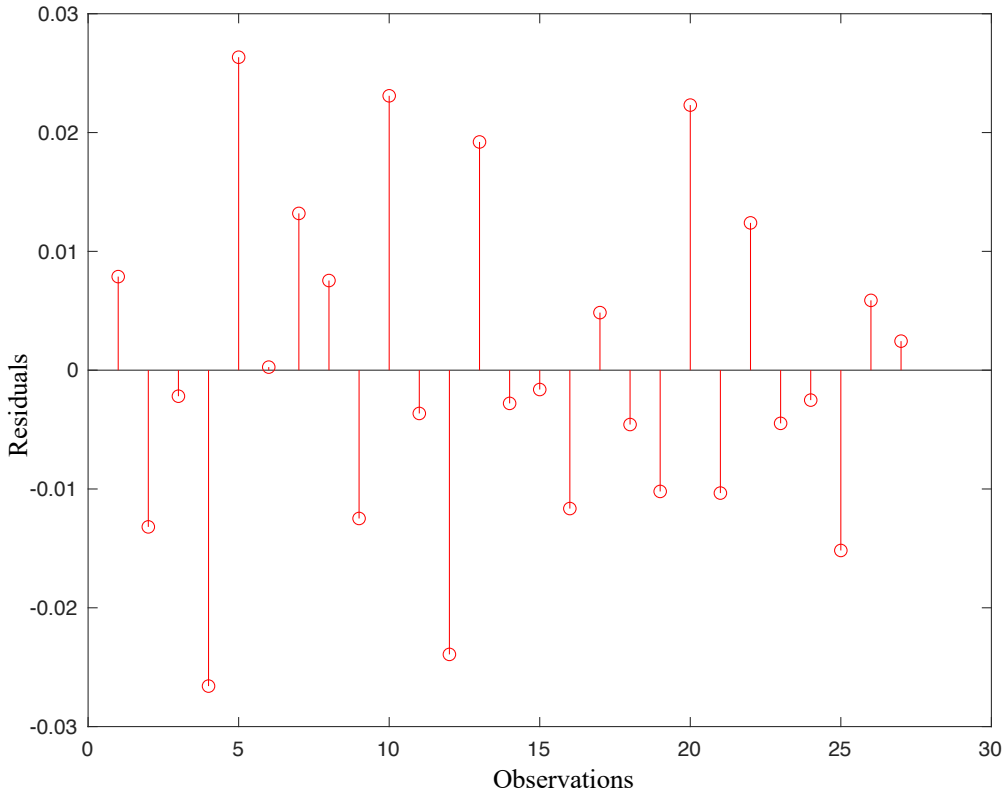


Figure A-7: Residual Plot for aging state obtained from PLSR on NMR data for Binder B only.

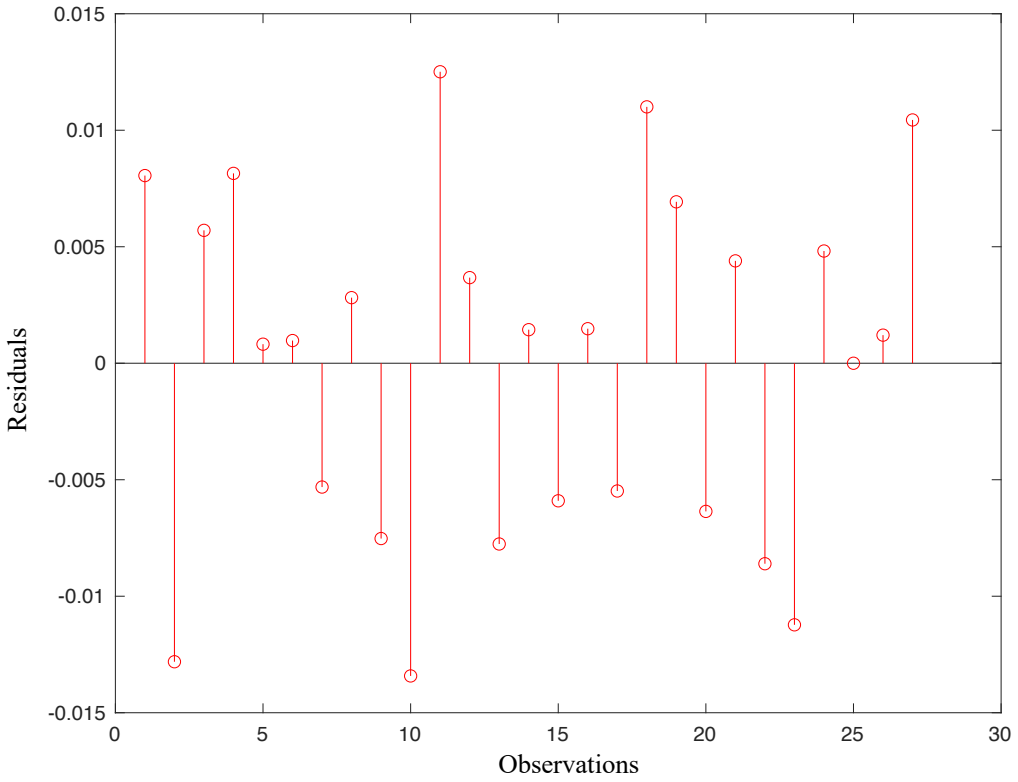


Figure A-8: Residual Plot for SBS concentration obtained from PLSR on NMR data for Binder B only.

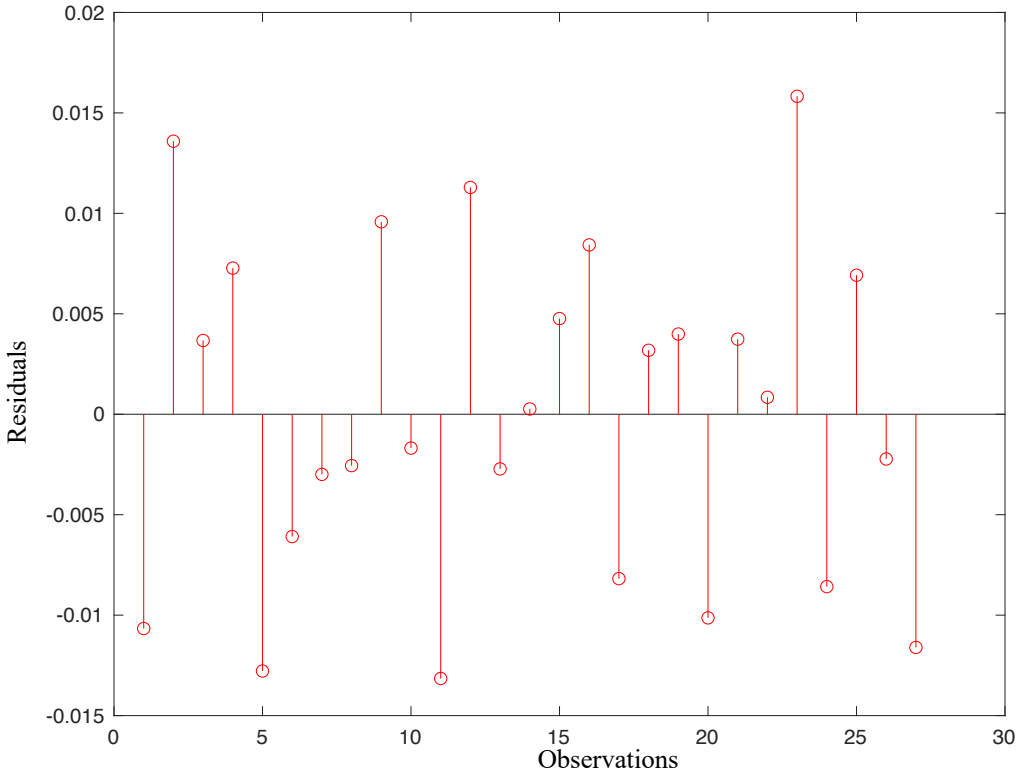


Figure A-9: Residual Plot for ΔTc obtained from PLSR on NMR data for Binder B only.

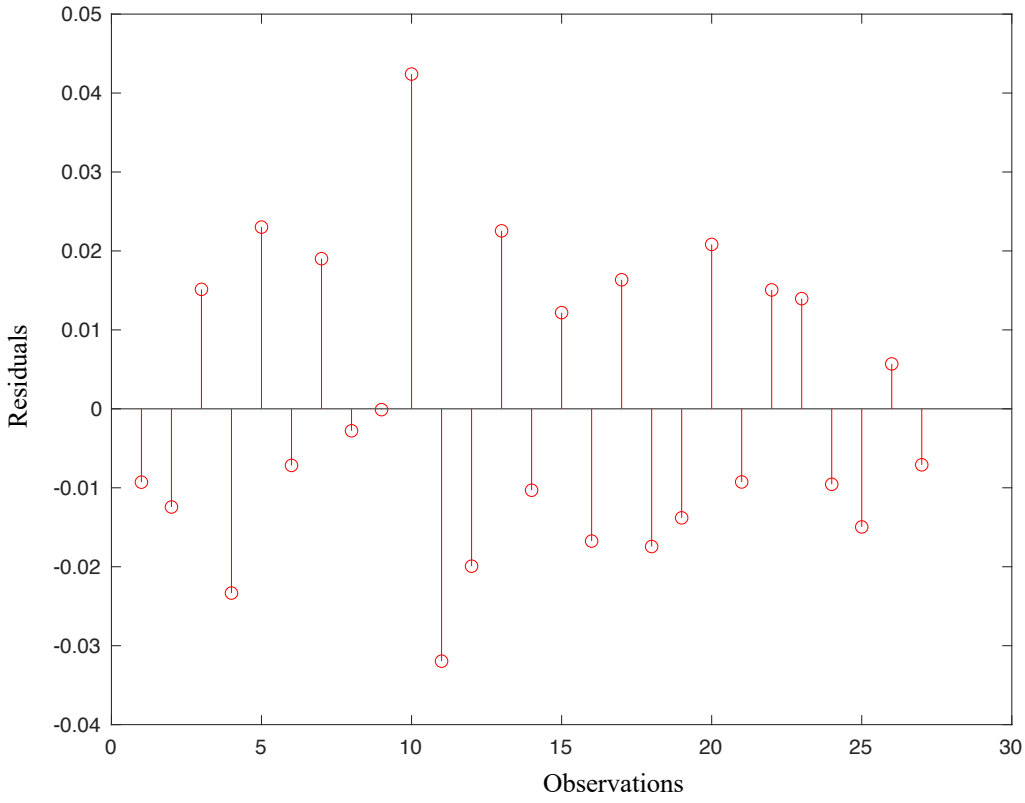


Figure A-10: Residual Plot for Crossover Temperature obtained from PLSR on NMR data for Binder B only.

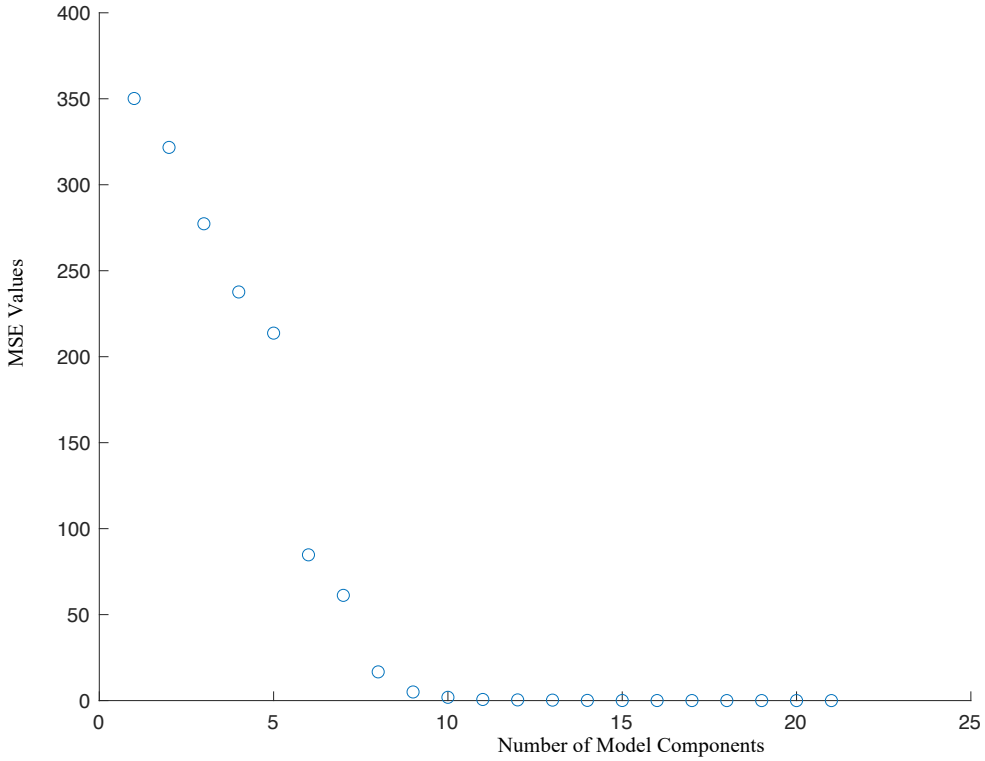


Figure A-11: MSE vs Number of Components in PLSR model using NMR data for Binder B.

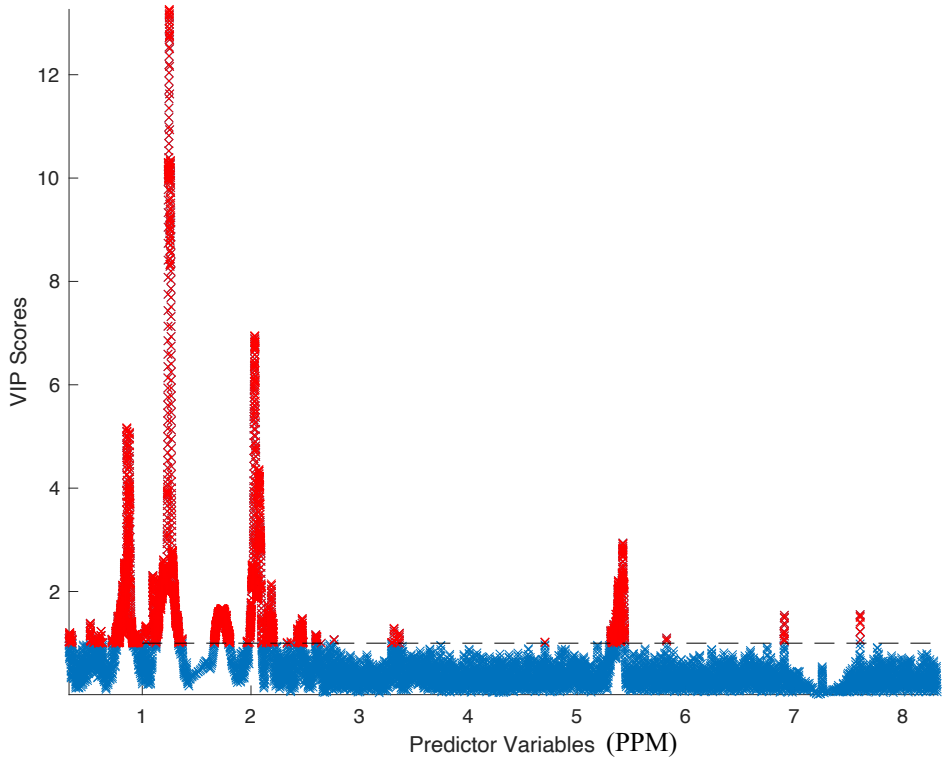


Figure A-12: VIP Score Plot obtained from PLSR on NMR data for Binder B only. (Red points represent VIP > 1).

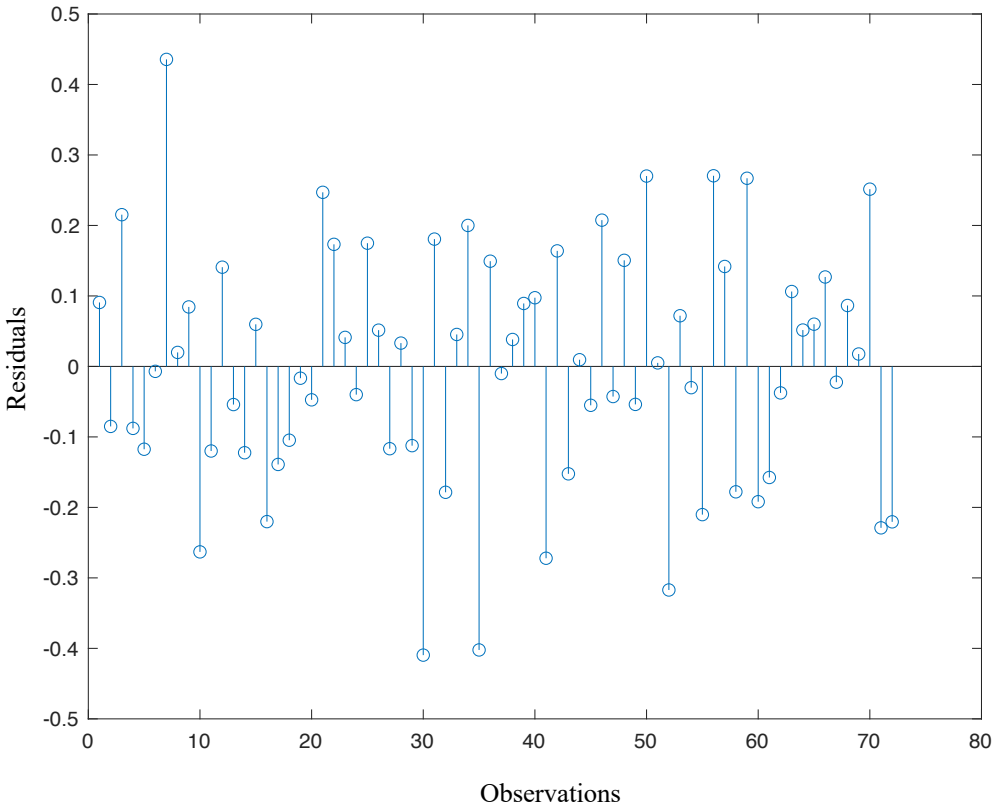


Figure A-13: Residual Plot for aging state obtained from PLSR on FTIR data for Binder A only.

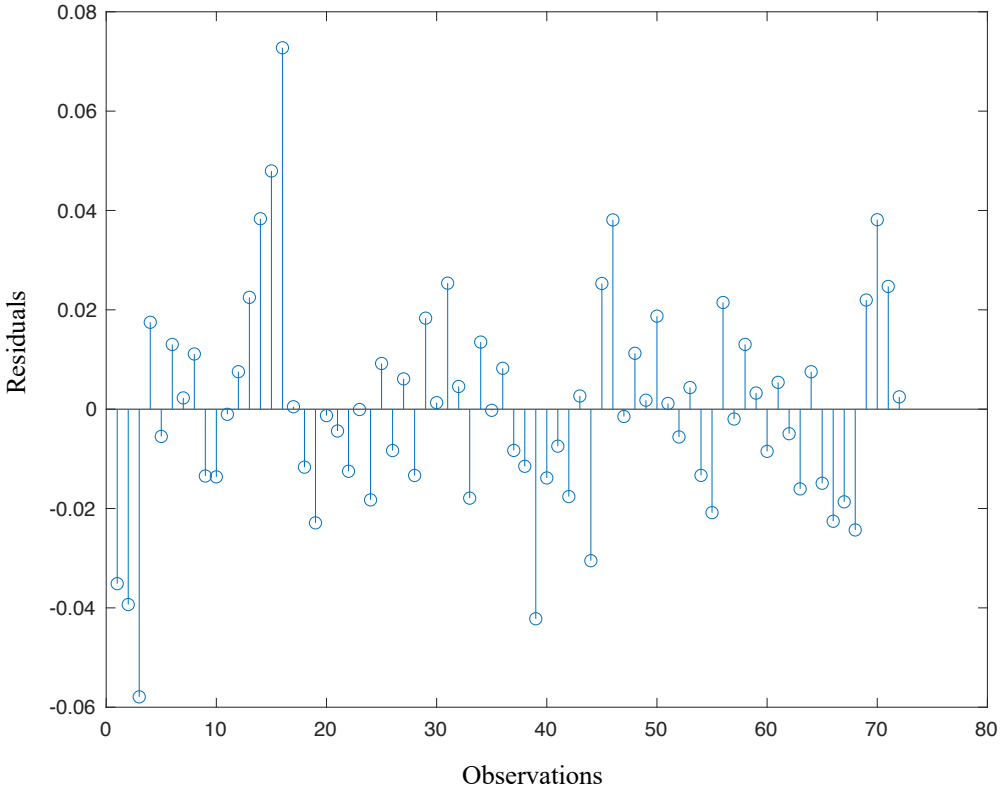


Figure A-14: Residual Plot for SBS concentration obtained from PLSR on FITR data for Binder A only.

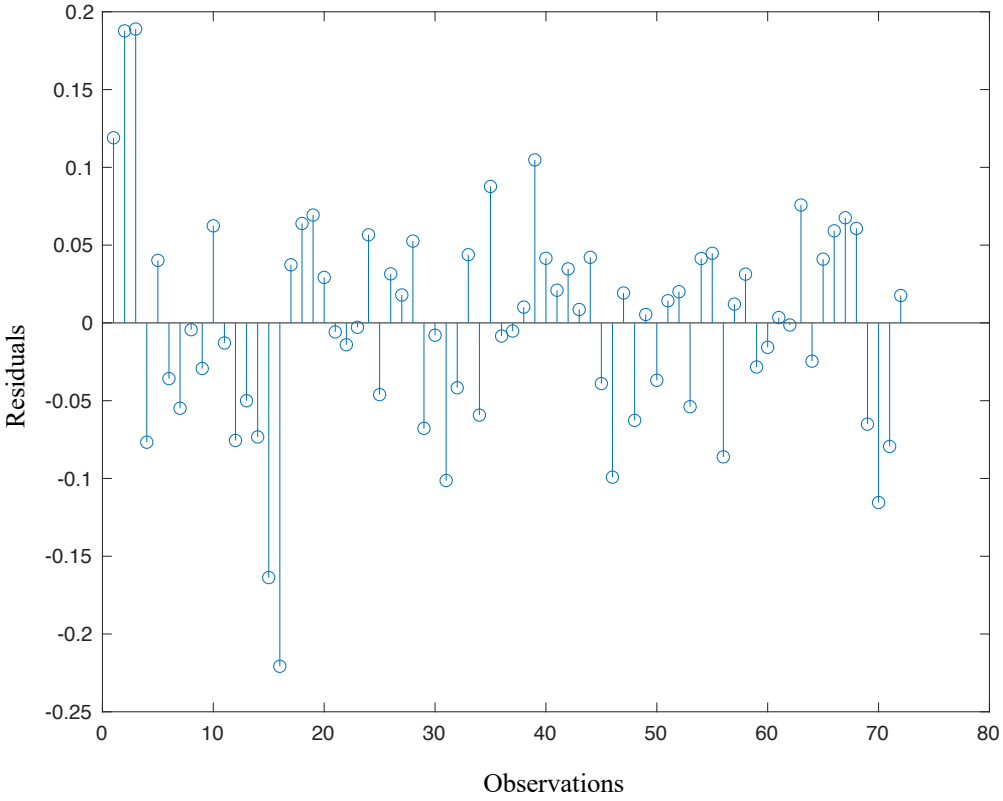


Figure A-15: Residual Plot for ΔTc obtained from PLSR on FTIR data for Binder A only.

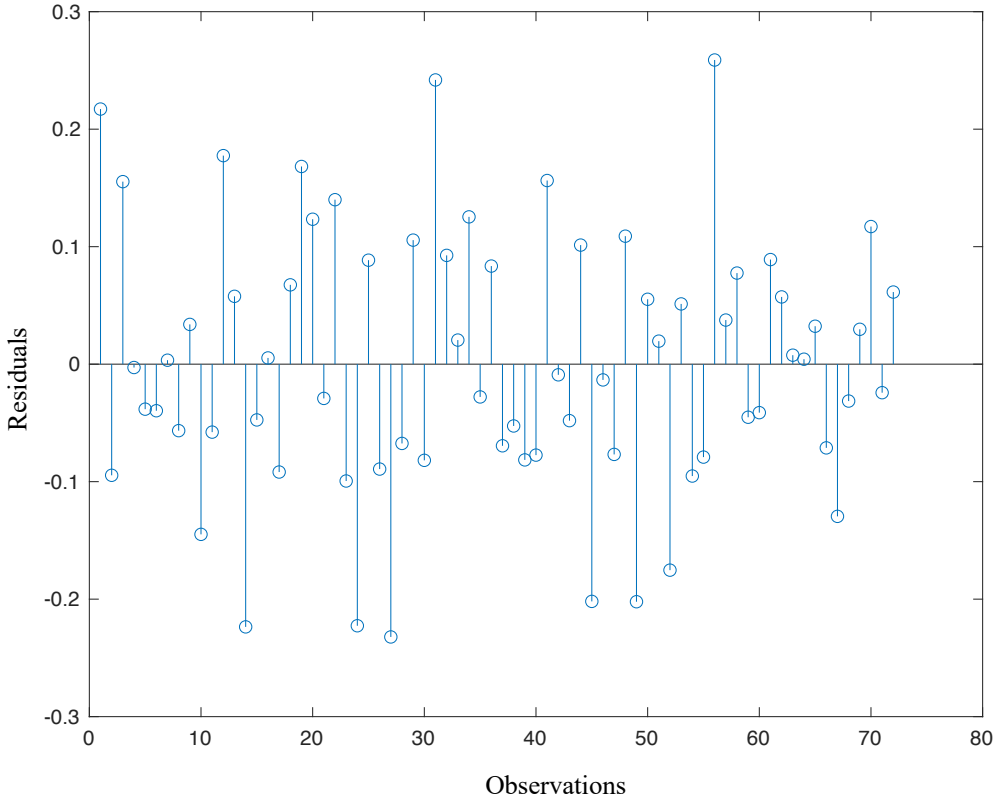


Figure A-16: Residual Plot for Crossover Temperature obtained from PLSR on FTIR data for Binder A only.

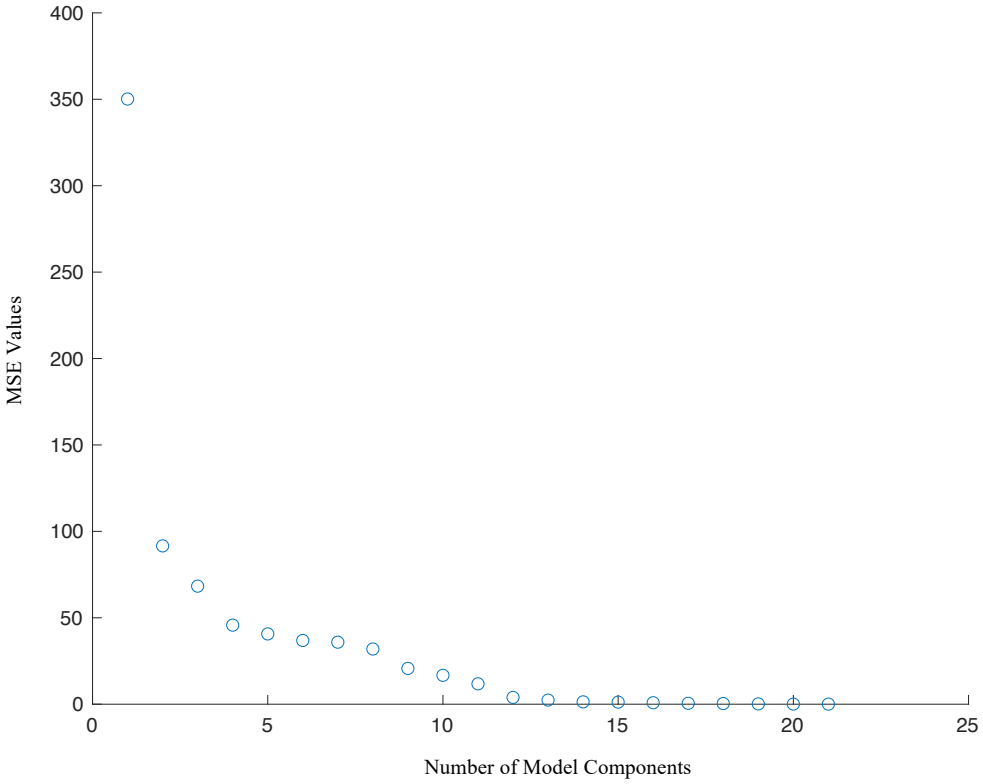


Figure A-17: MSE vs Number of Components in PLSR model using FTIR data for Binder A.

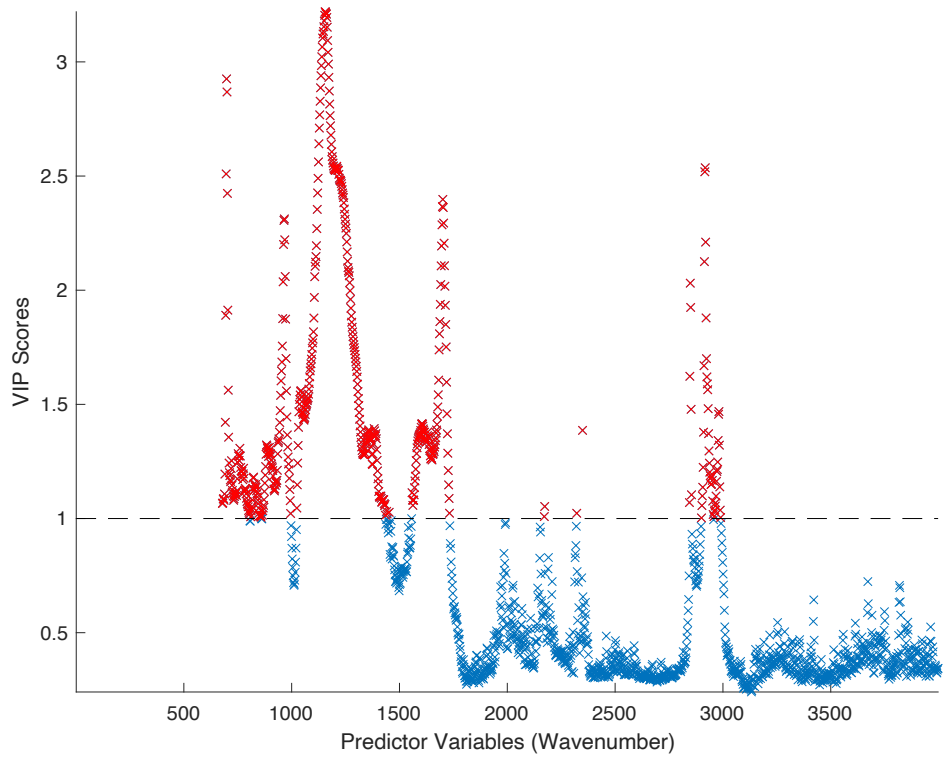


Figure A-18: VIP Score Plot obtained from PLSR on FTIR data for Binder A only. (Red points represent VIP > 1)

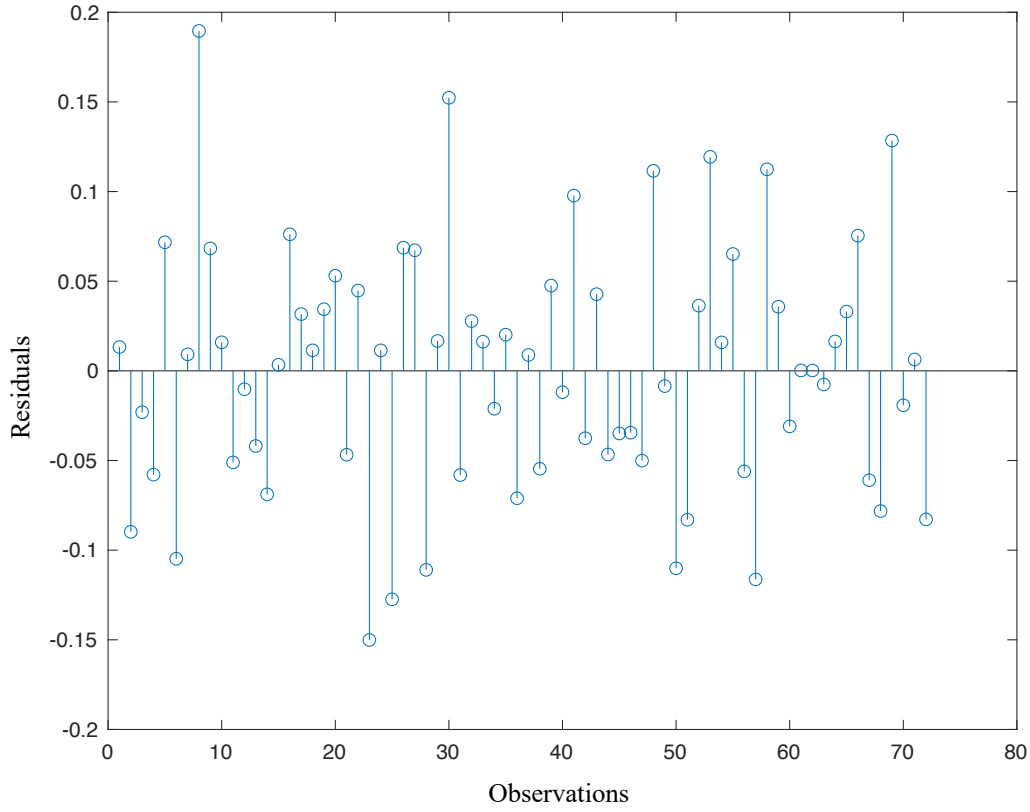


Figure A-19: Residual Plot for aging state obtained from PLSR on FTIR data for Binder B only.

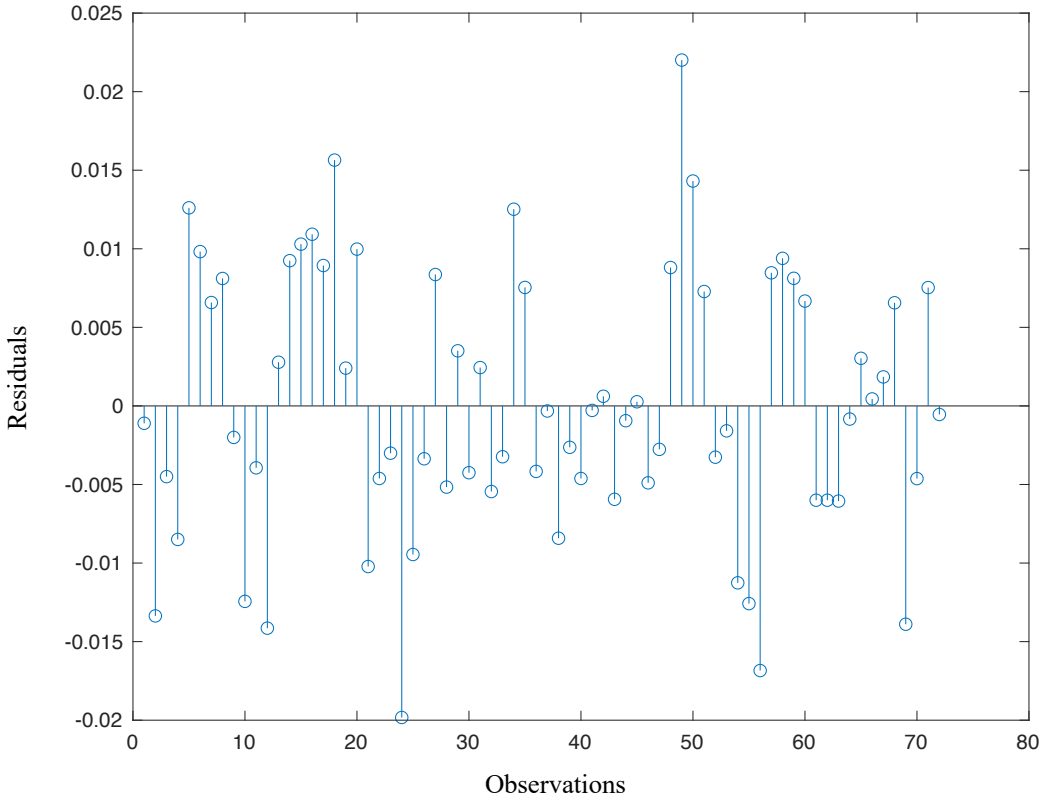


Figure A-20: Residual Plot for SBS concentration obtained from PLSR on FITR data for Binder B only.

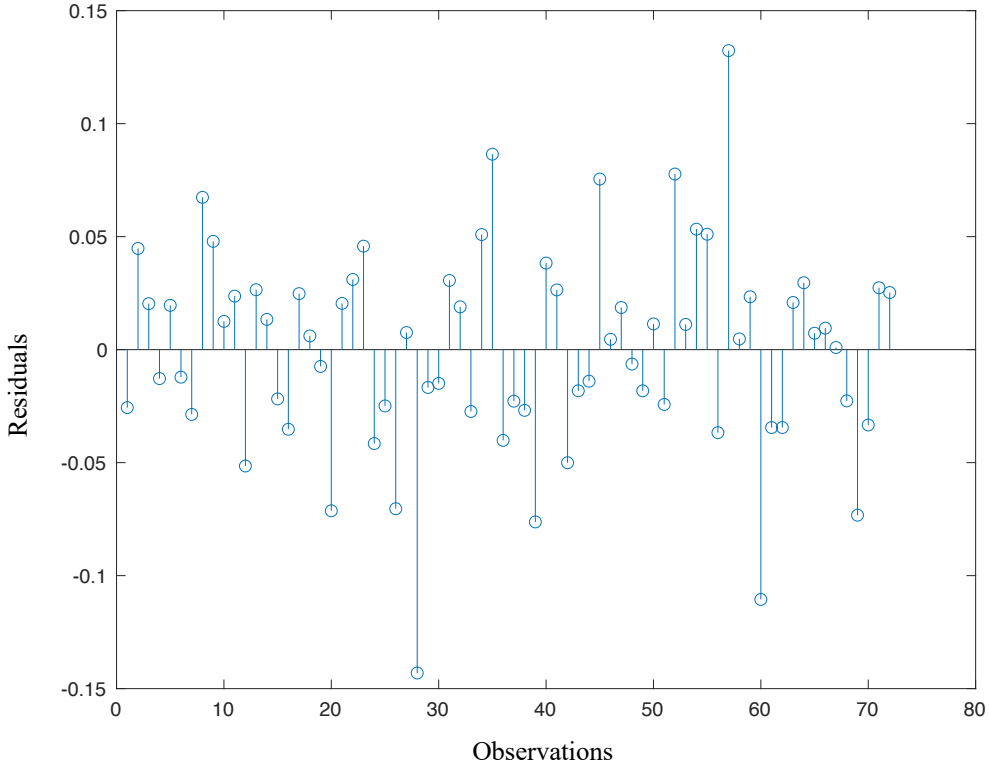


Figure A-21: Residual Plot for ΔTc obtained from PLSR on FTIR data for Binder B only.

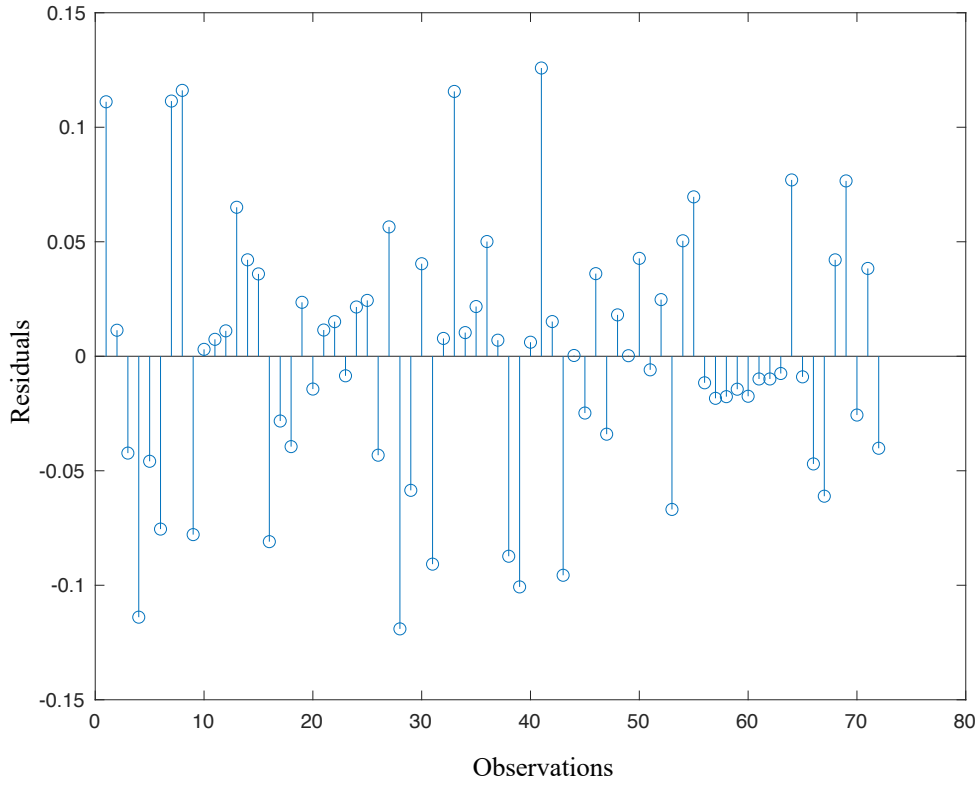


Figure A-22: Residual Plot for Crossover Temperature obtained from PLSR on FTIR data for Binder B only.

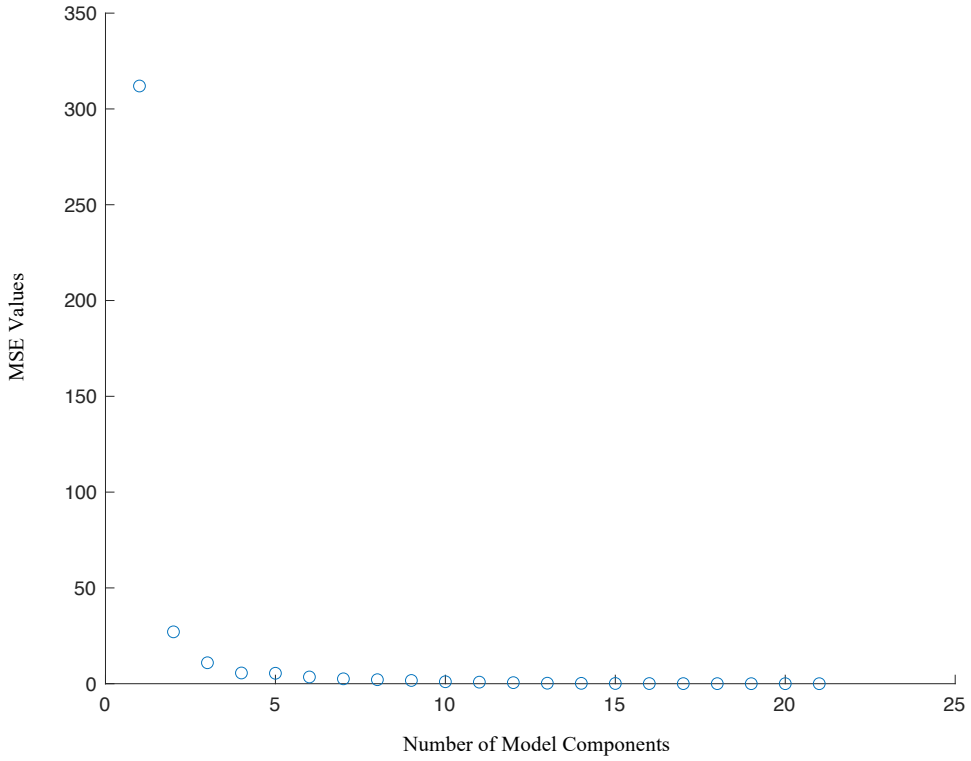


Figure A-23: MSE vs Number of Components in PLSR model using FTIR data for Binder B.

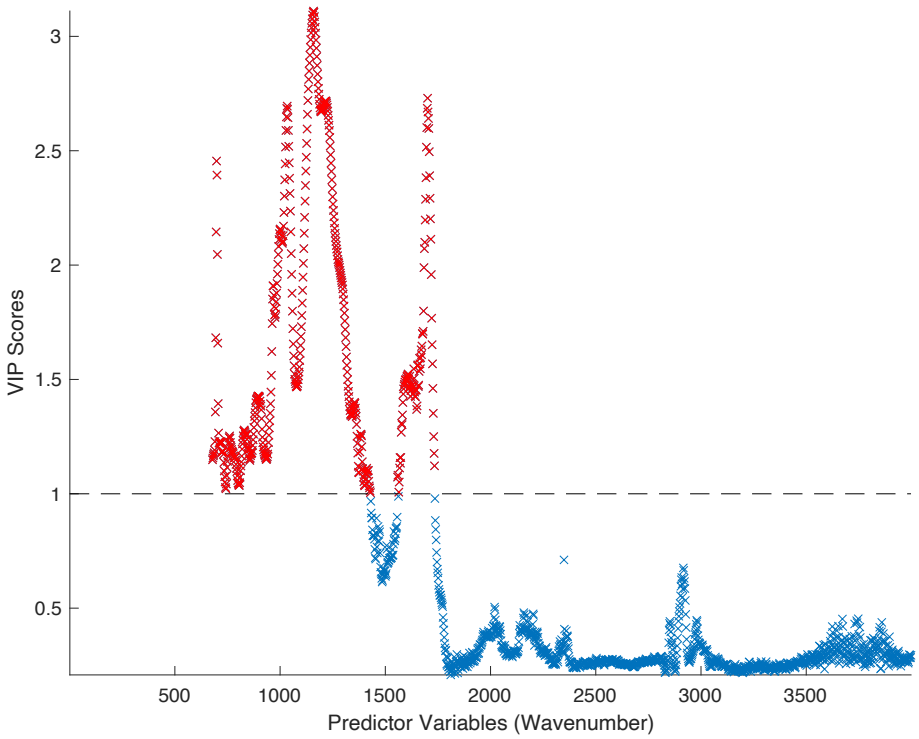


Figure A-24: VIP Score Plot obtained from PLSR on FTIR data for Binder B only. (Red points represent VIP > 1).

Appendix B

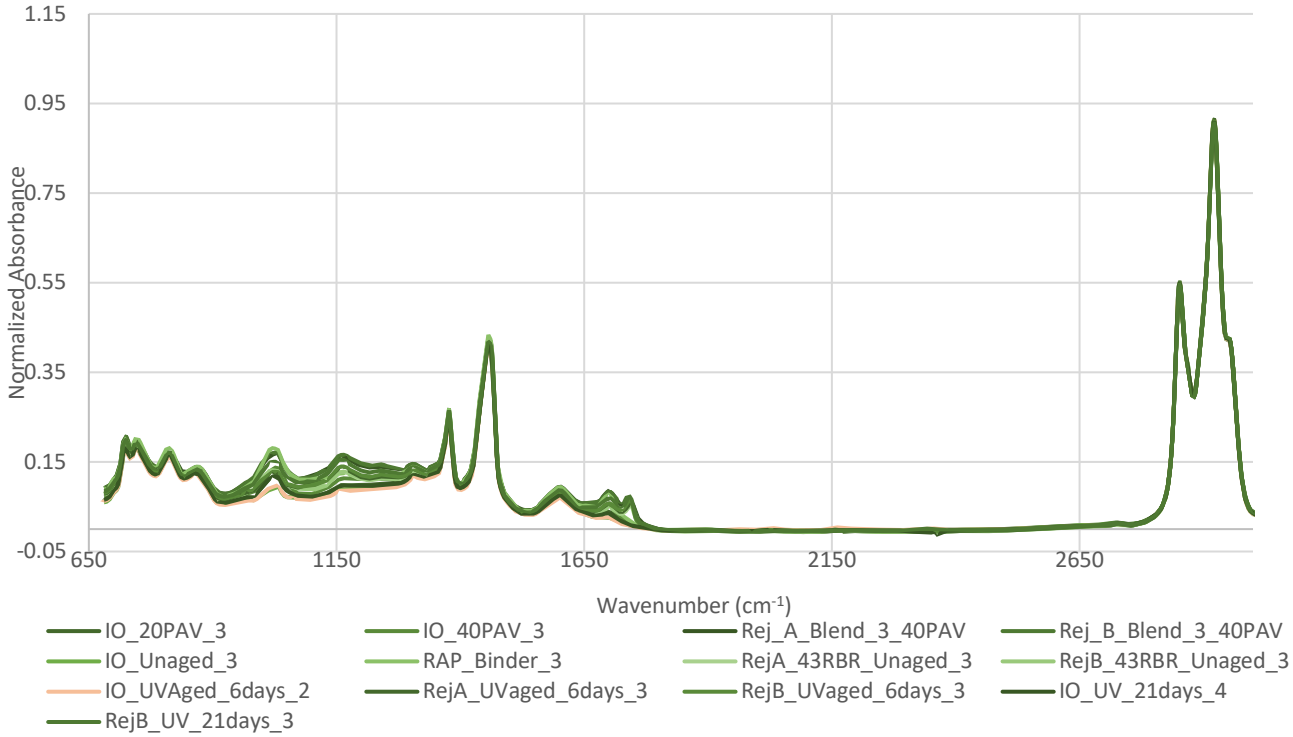


Figure B-1: Normalized FTIR Spectral Data for all RAP-IO-Rejuvenator Blends at all ageing states.

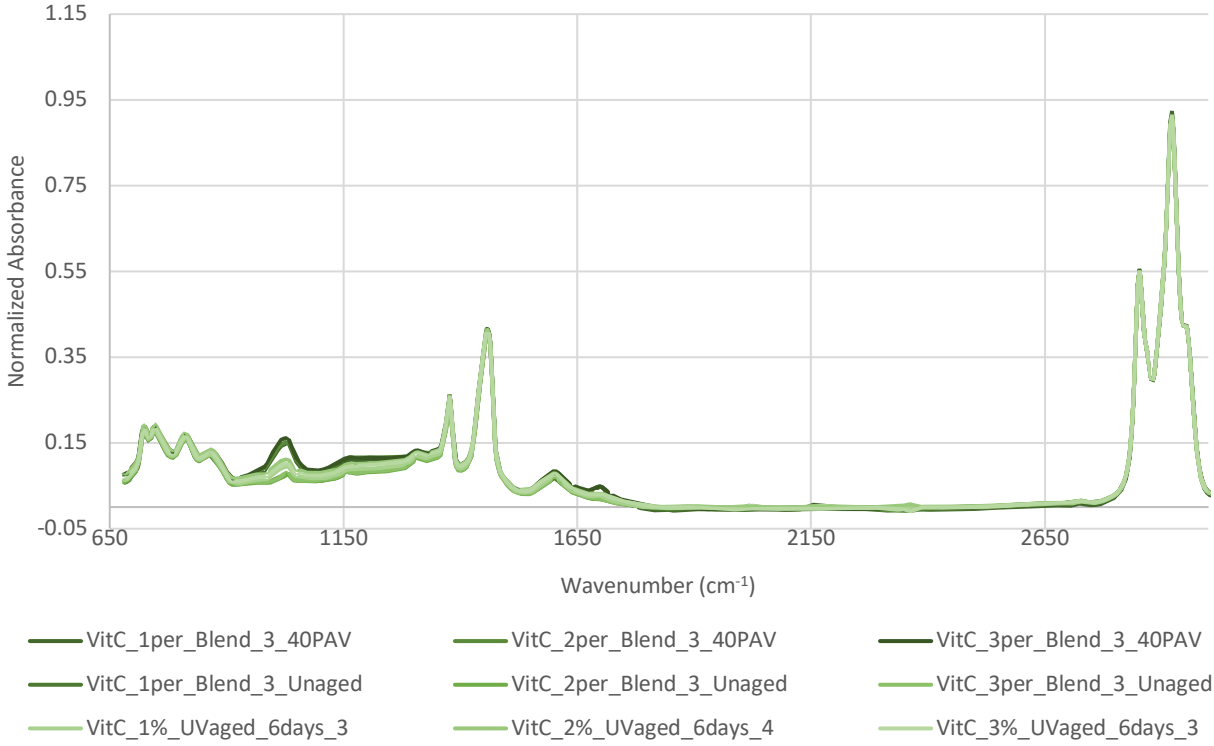


Figure B-2: Normalized FTIR Spectral Data for all Vit. C Blends at all ageing states.

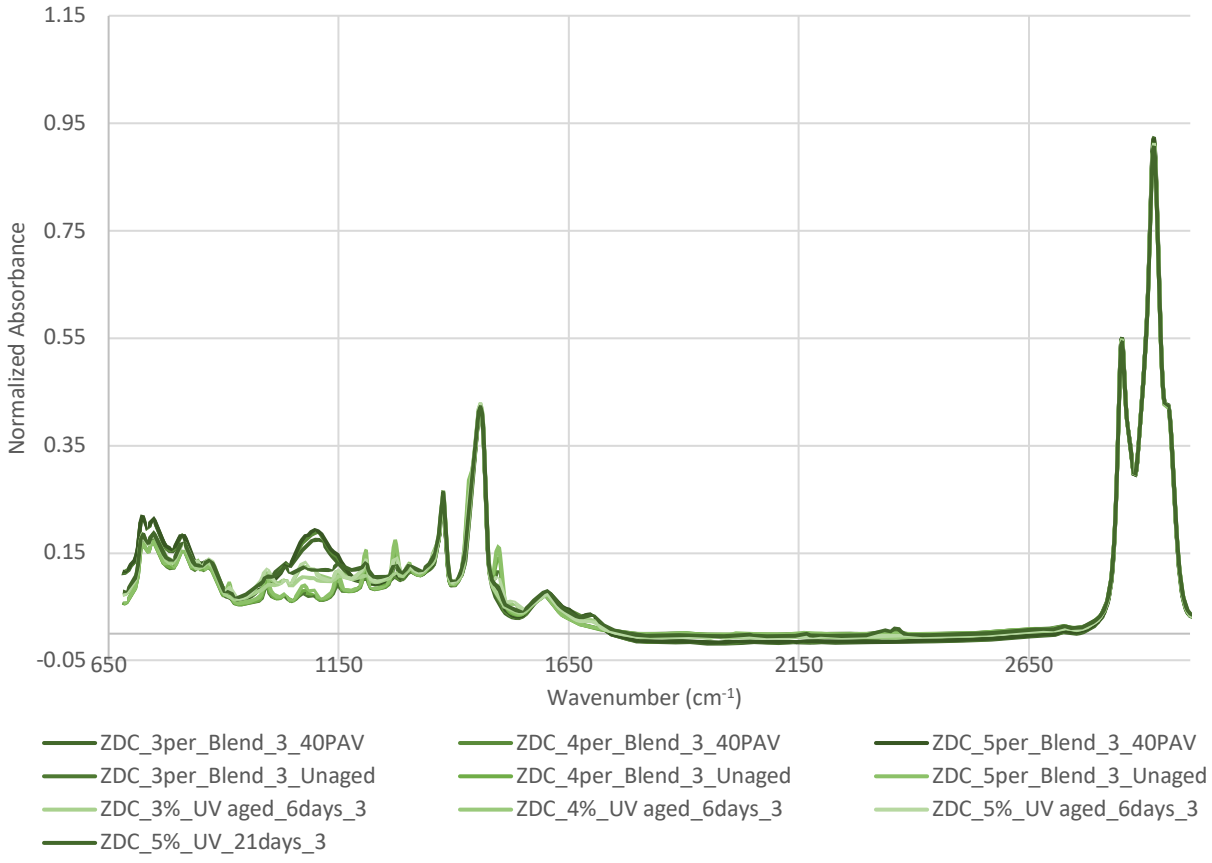


Figure B-3: Normalized FTIR Spectral Data for all ZDC Blends at all ageing states.

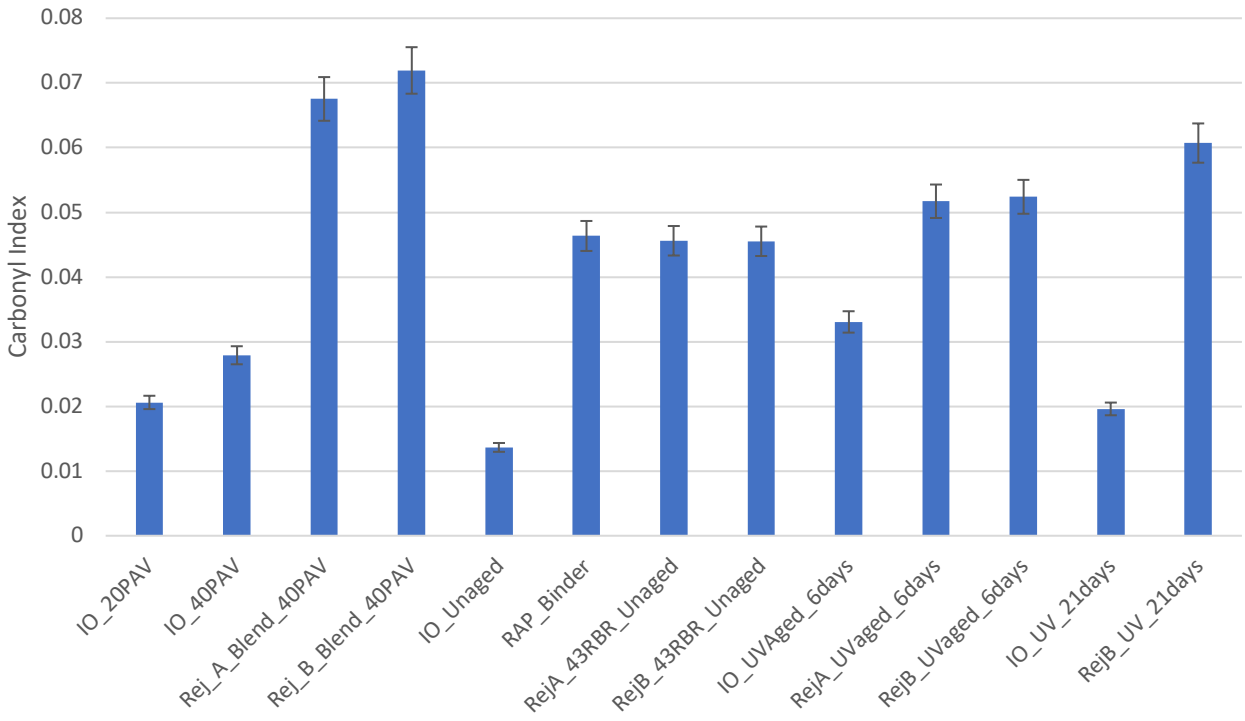


Figure B-4: Carbonyl Indices based on FTIR spectra for RAP-IO-Rejuvenator Blends.

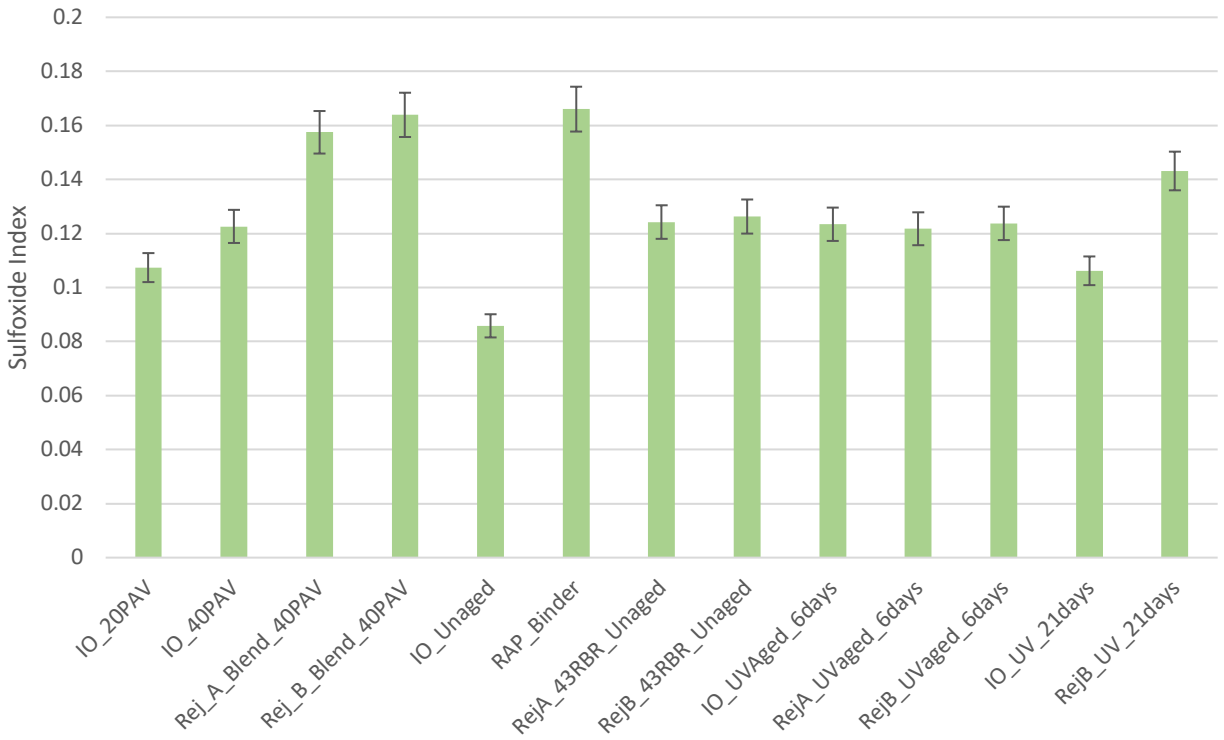


Figure B-5: Sulfoxide Indices based on FTIR spectra for RAP-IO-Rejuvenator Blends.

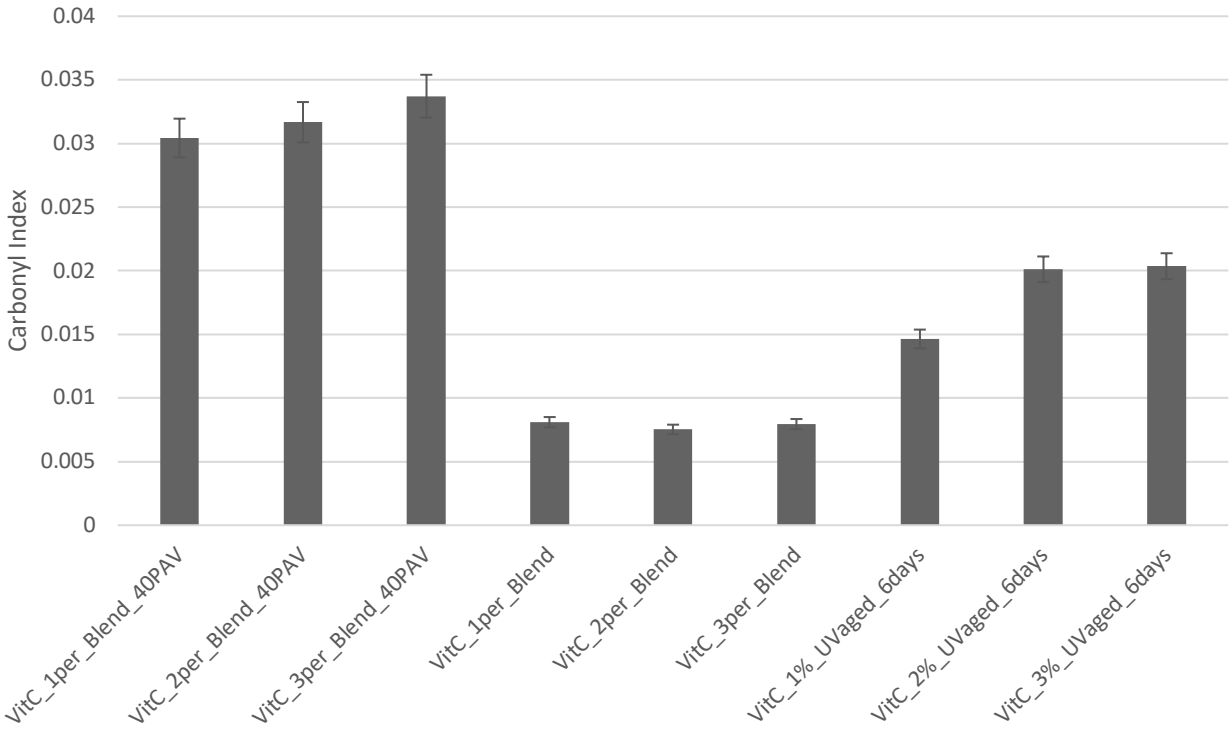


Figure B-6: Carbonyl Indices based on FTIR spectra for Vit C Blends.

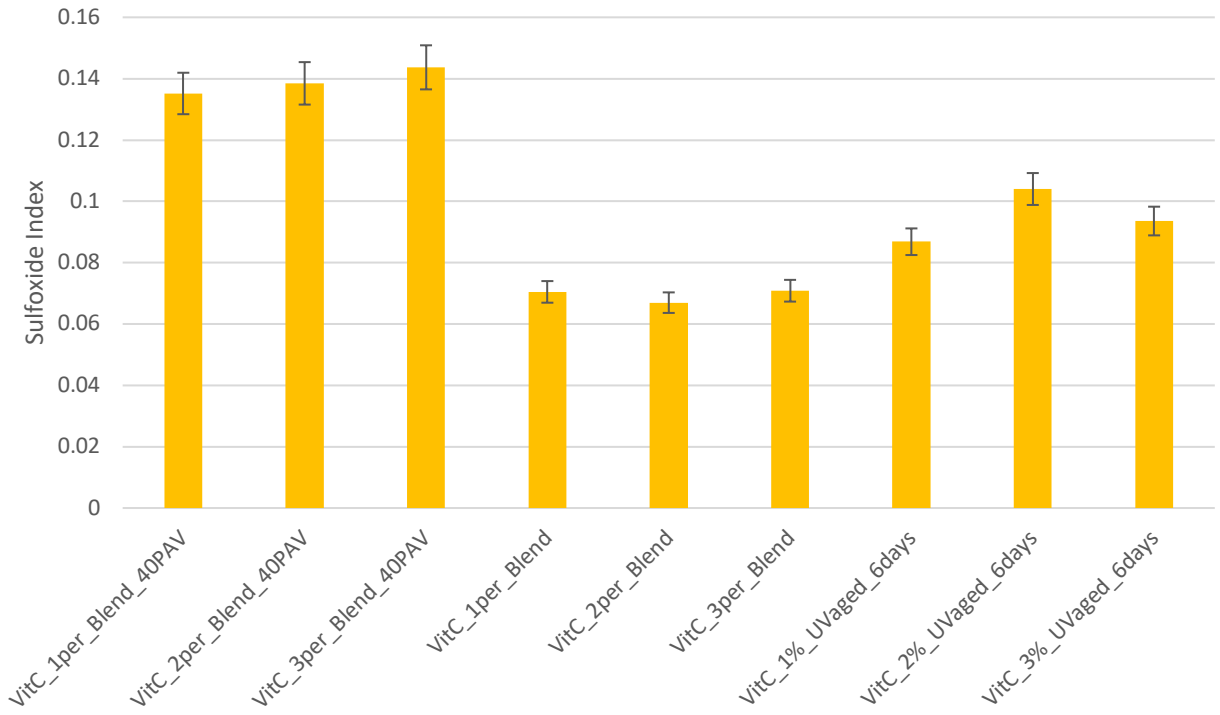


Figure B-7: Sulfoxide Indices based on FTIR spectra for Vit C Blends.

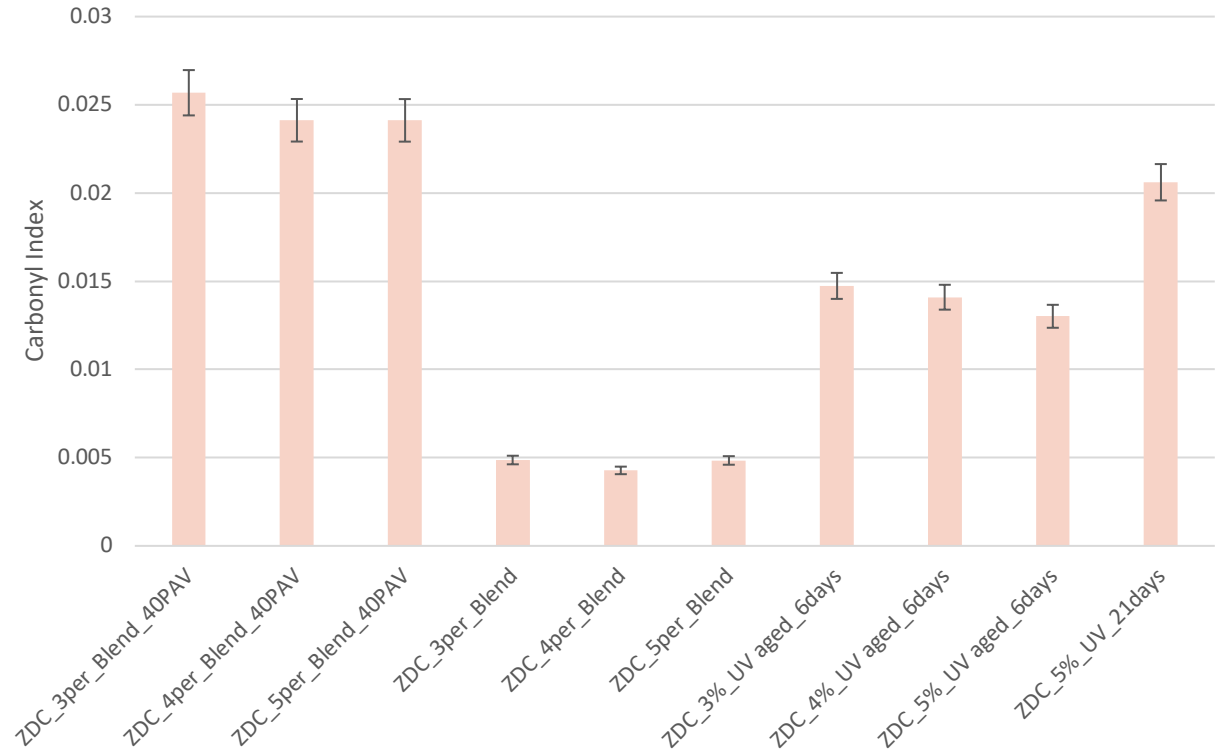


Figure B-8: Carbonyl Indices based on FTIR spectra for ZDC Blends.

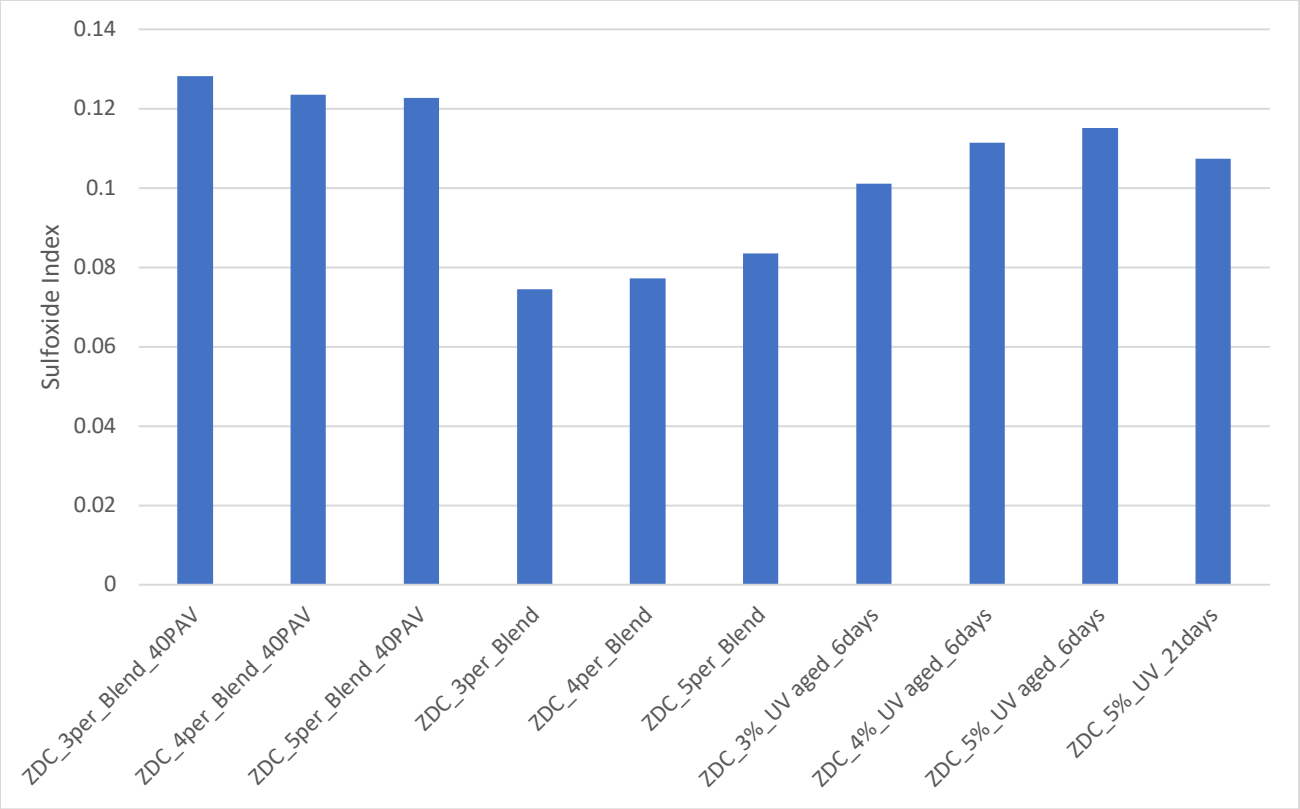


Figure B-9: Sulfoxide Indices based on FTIR spectra for ZDC Blends.

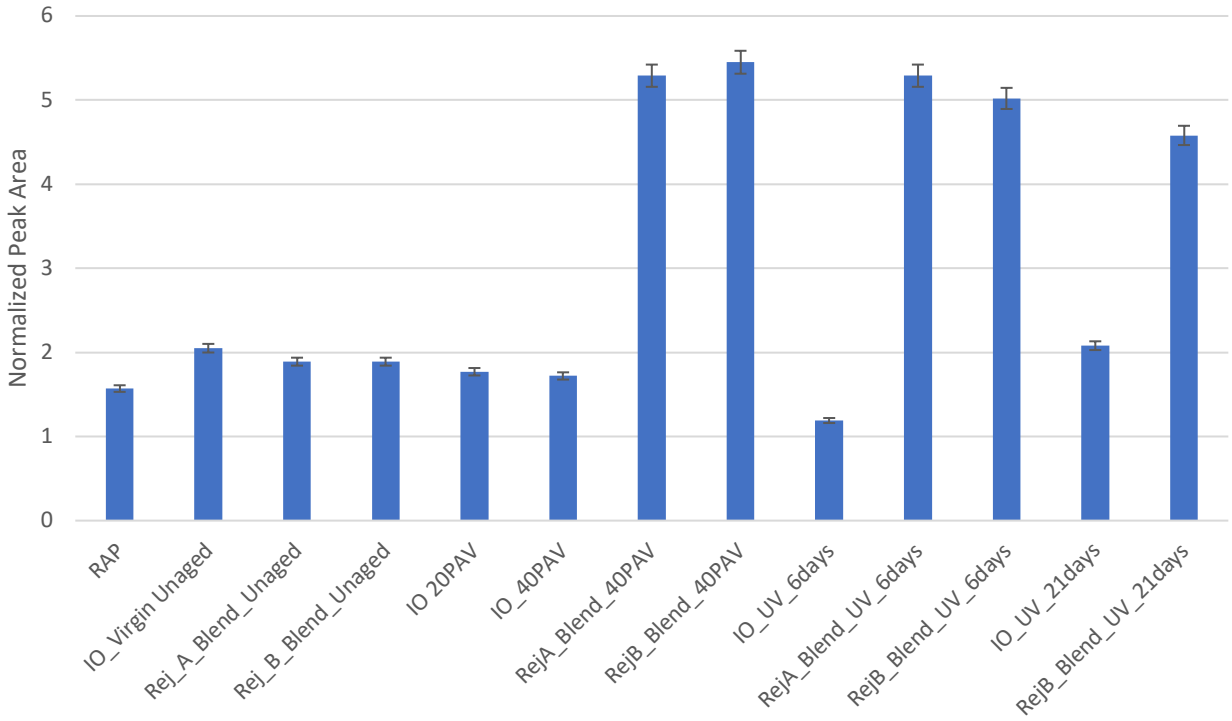


Figure B-10: H_γ normalized peak area based on NMR spectra for RAP-IO-Rejuvenator Blends.

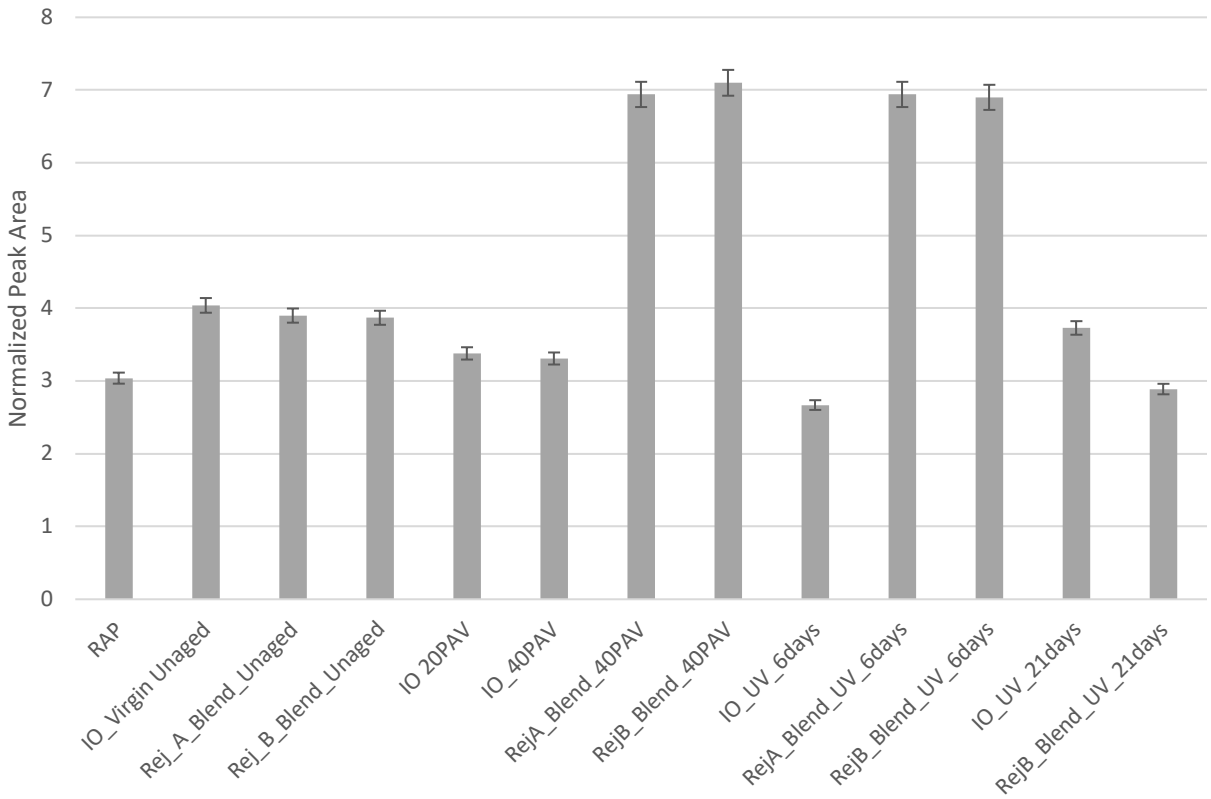


Figure B-11: H_β normalized peak area based on NMR spectra for RAP-IO-Rejuvenator Blends.

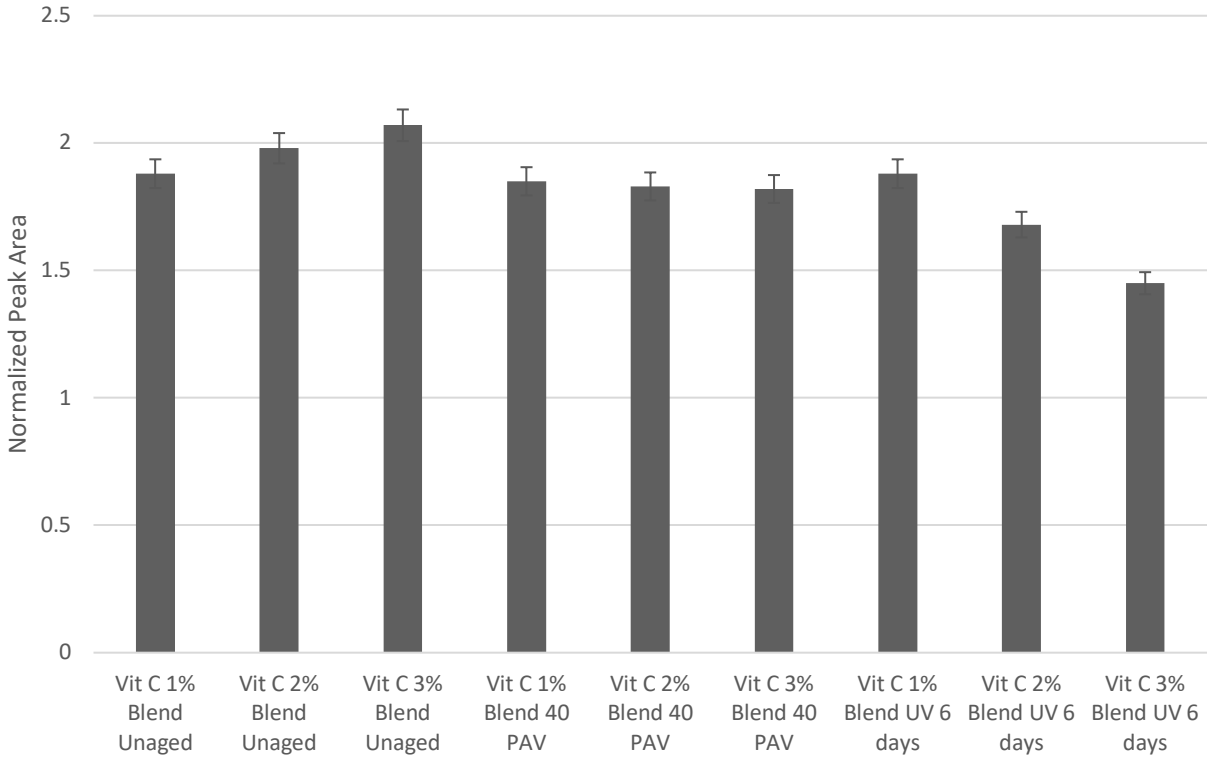


Figure B-12: H_γ normalized peak area based on NMR spectra for Vit. C Blends.

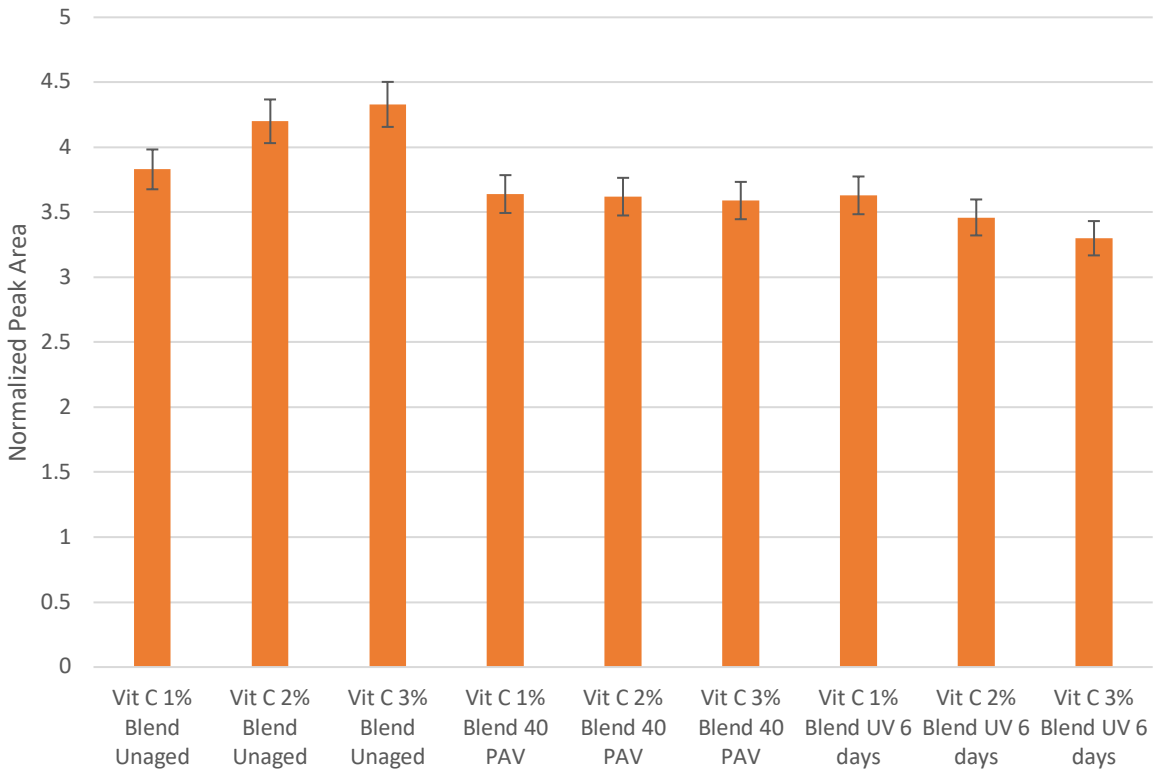


Figure B-13: H_β normalized peak area based on NMR spectra for Vit. C Blends.

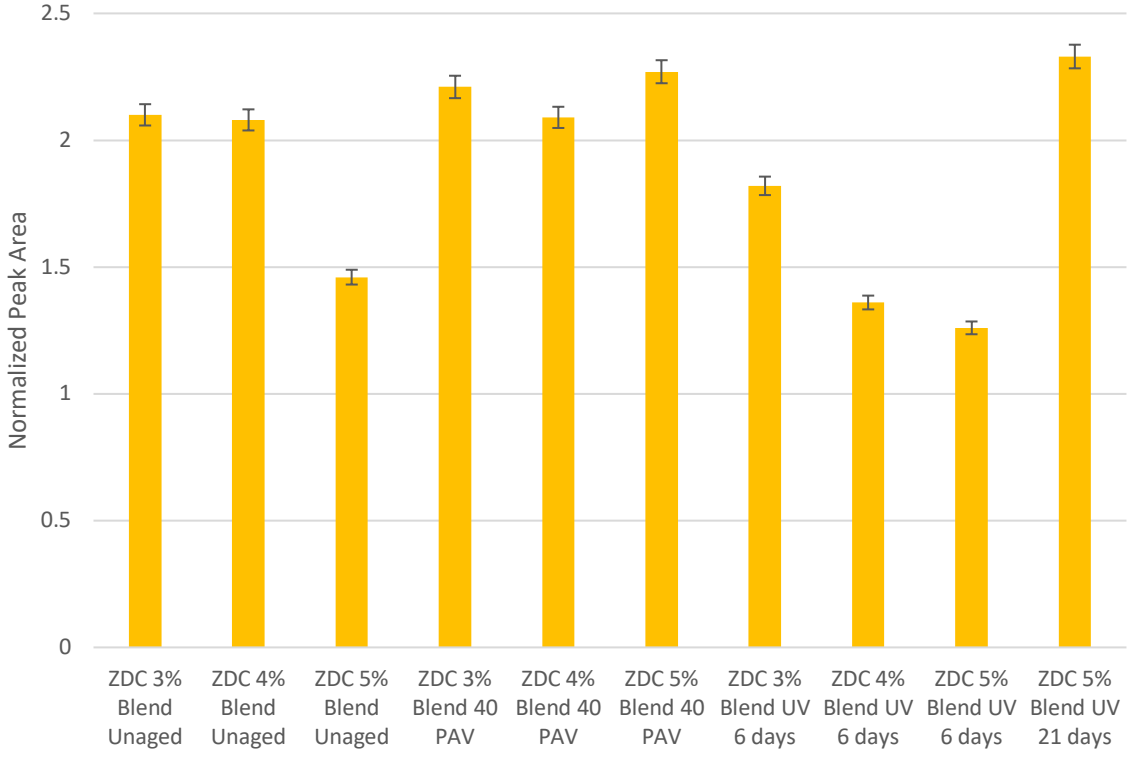


Figure B-14: H_γ normalized peak area based on NMR spectra for ZDC Blends.

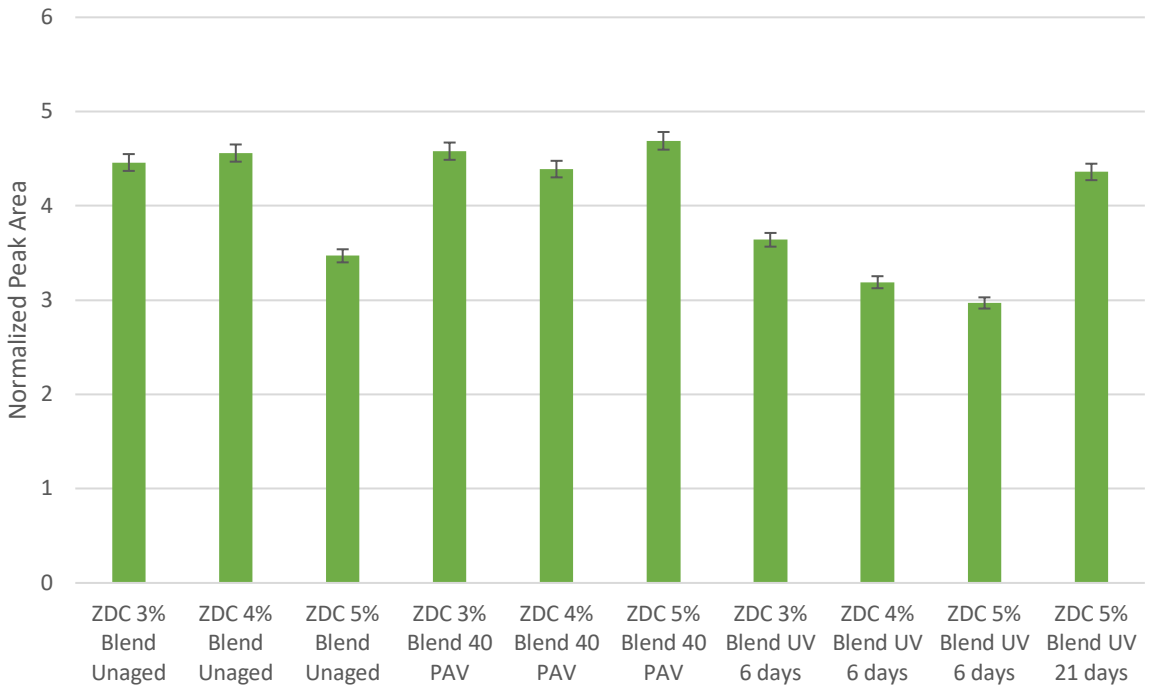


Figure B-15: H_β normalized peak area based on NMR spectra for ZDC Blends.

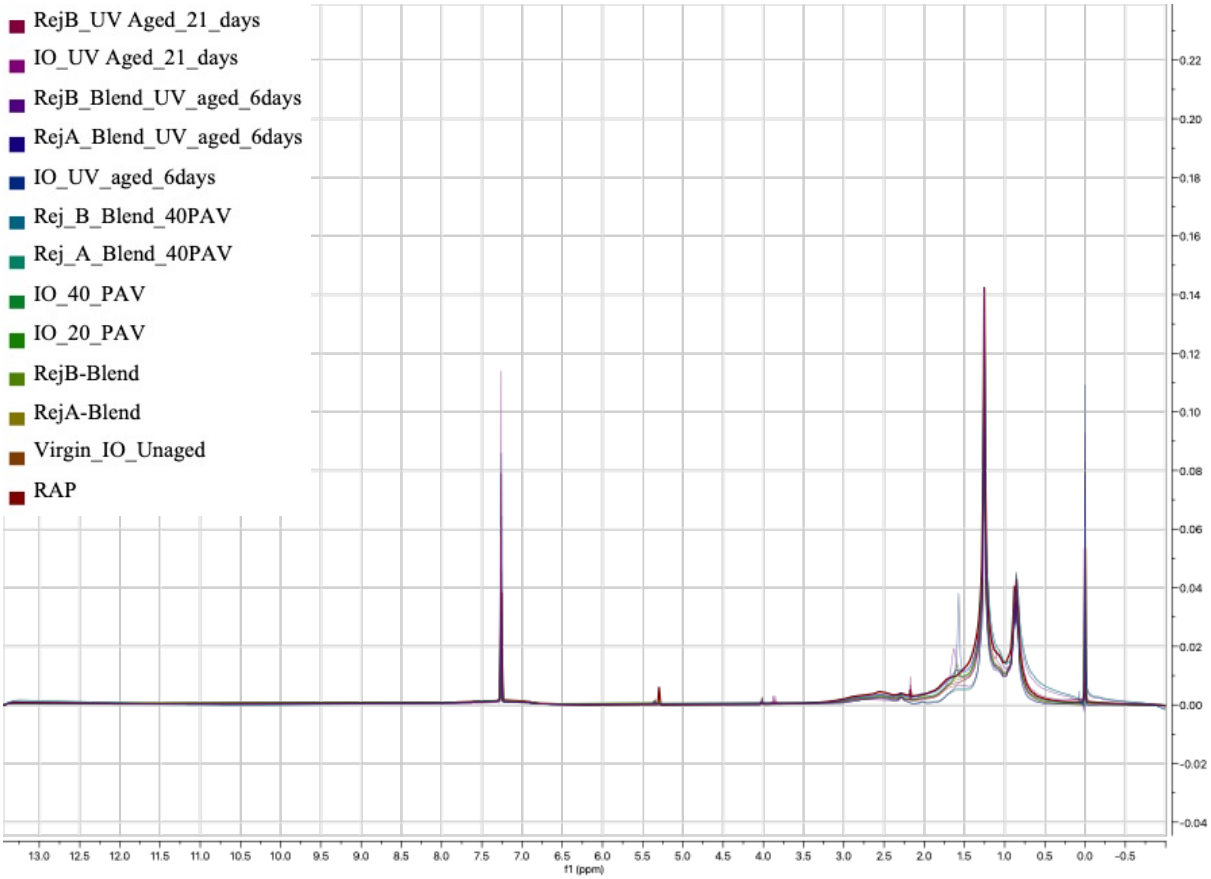


Figure B-16: Normalized NMR Spectral Data for all RAP-IO-Rejuvenator Blends at all ageing states.

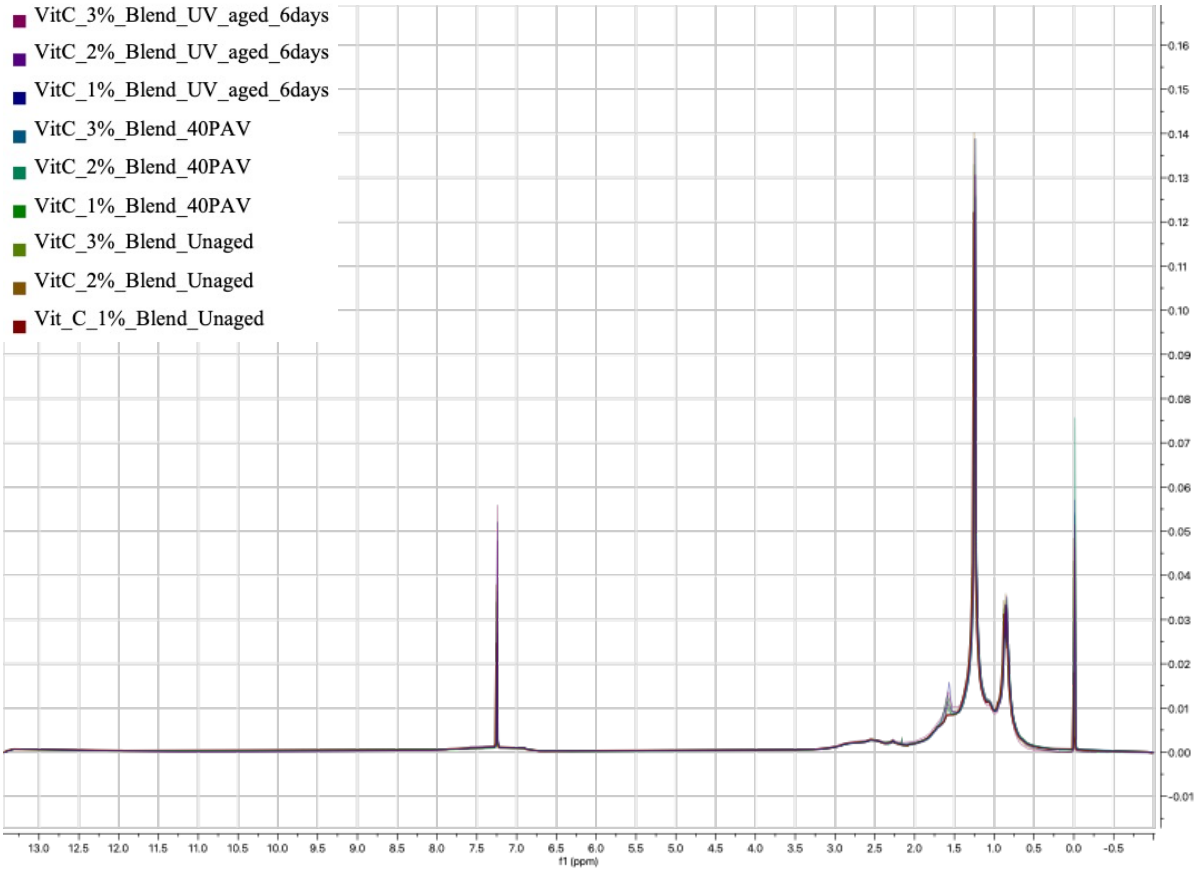


Figure B-17: Normalized NMR Spectral Data for all Vit.C Blends at all ageing states.

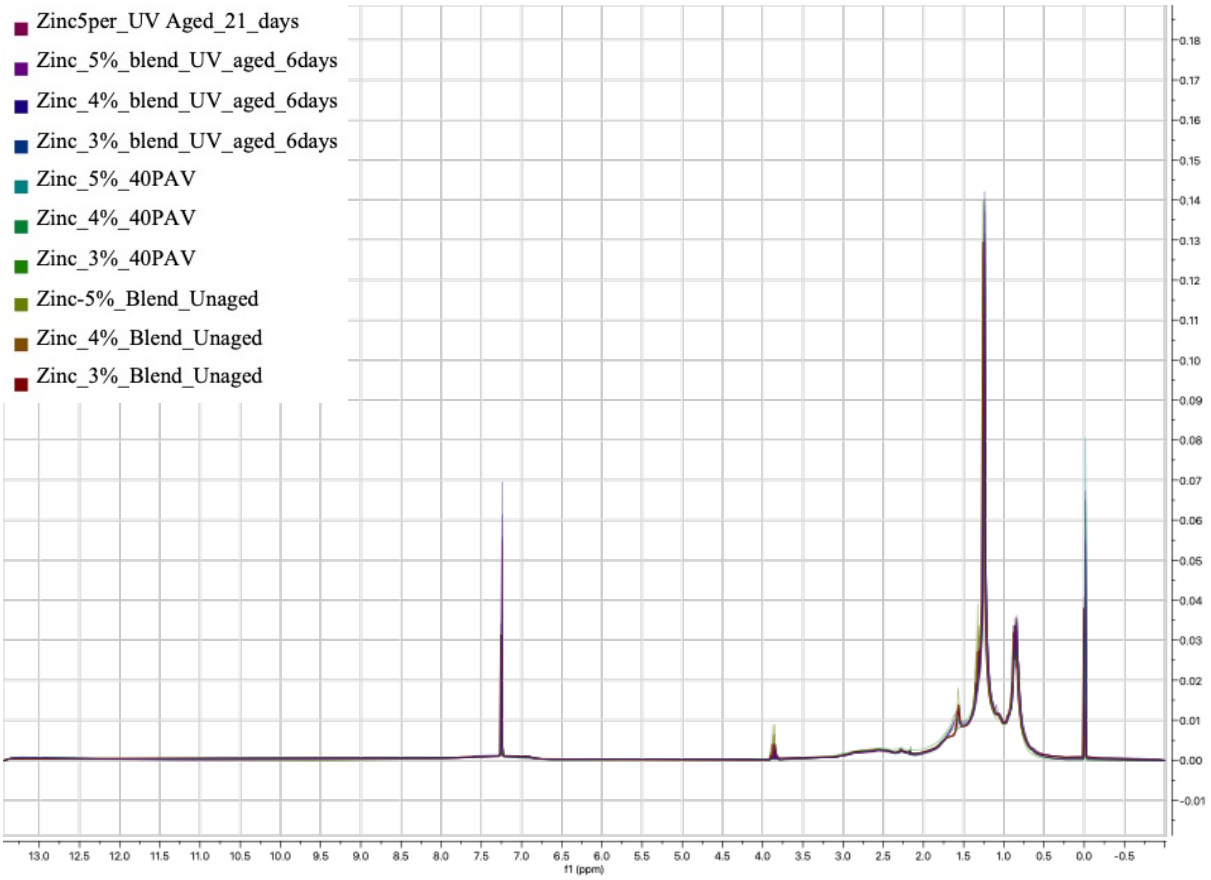


Figure B-18: Normalized NMR Spectral Data for all ZDC Blends at all ageing states.